Coordination Chemistry of Azamacrocycles Functionalised with *N*–pendant Pyridyl, Bipyridyl and Terpyridyl Arms.

Philippa Sheldon

A thesis submitted as part requirement for the degree of

Doctor of Philosophy

Department of Chemistry

University of Warwick

September 1994

Table of Contents

List of Figures

List of Tables

Ligands Discussed in this Thesis

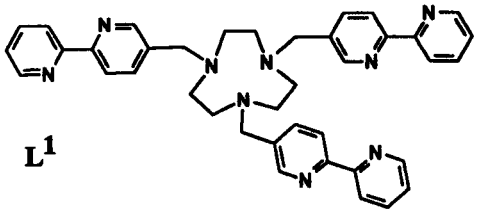

L^1

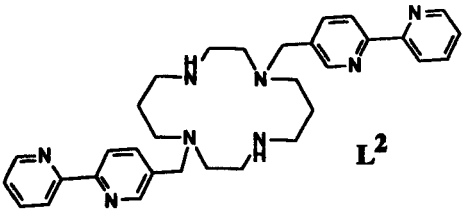

L^2

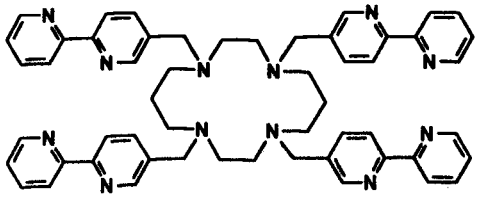

L^3

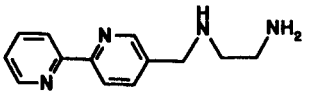

L^4

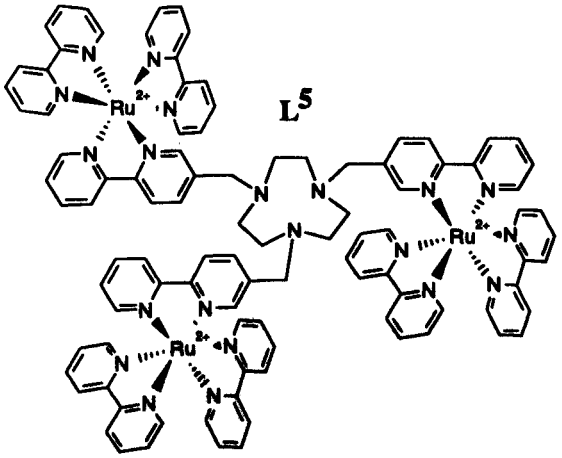

L^5

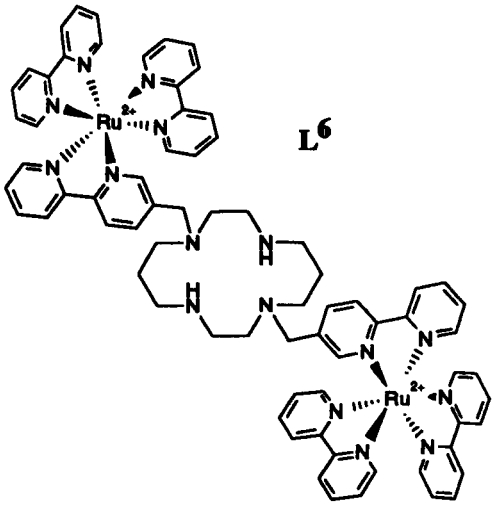

L^6

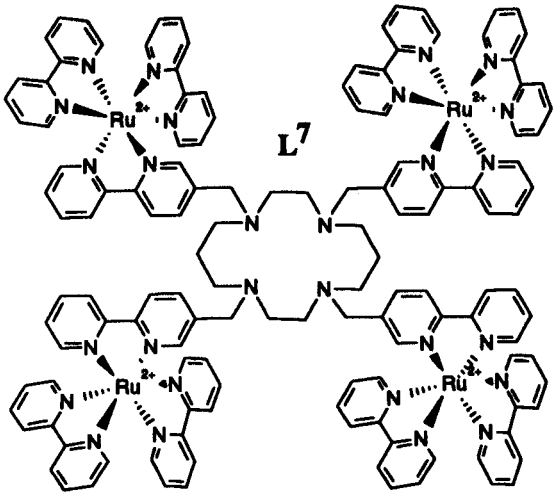

L^7

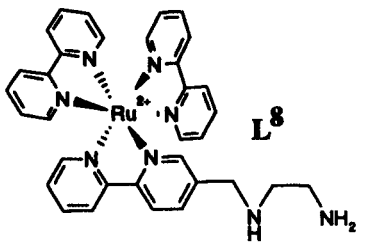

L^8

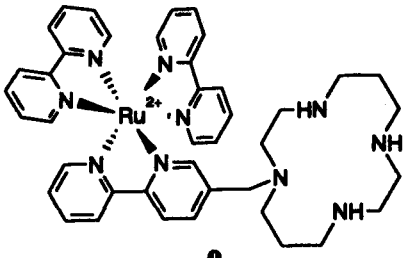

L^9

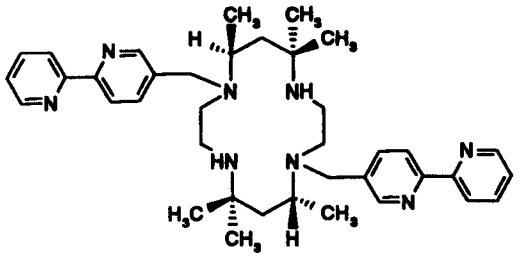

L^{10}

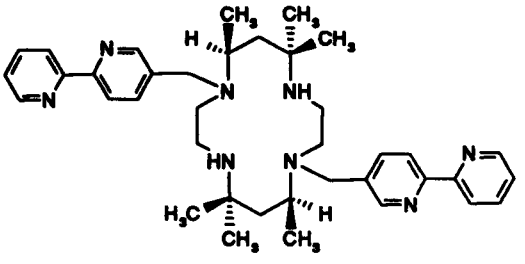

L^{11}

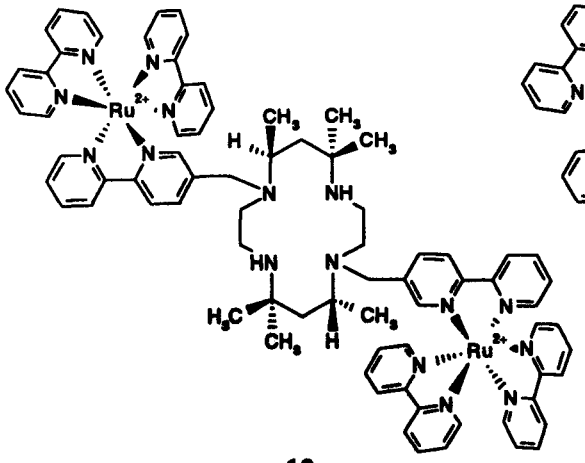

L^{12}

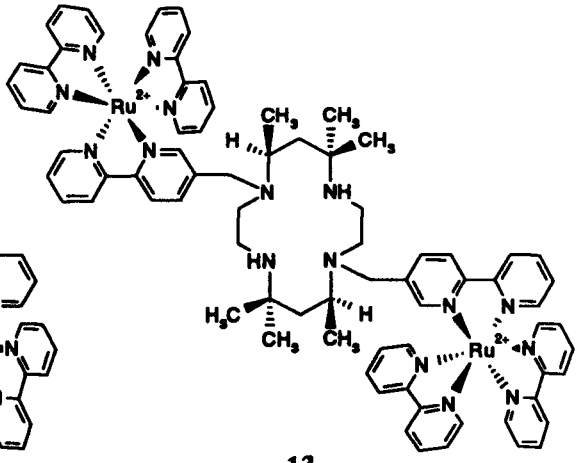

L^{13}

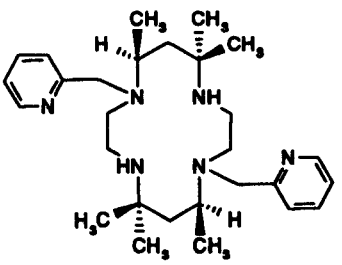

L^{14}

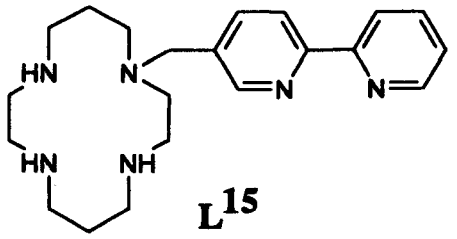

L^{15}

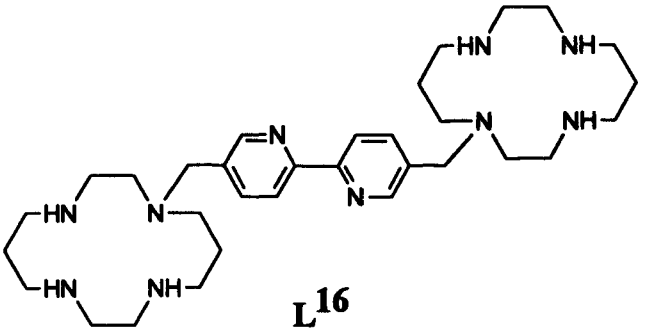

L^{16}

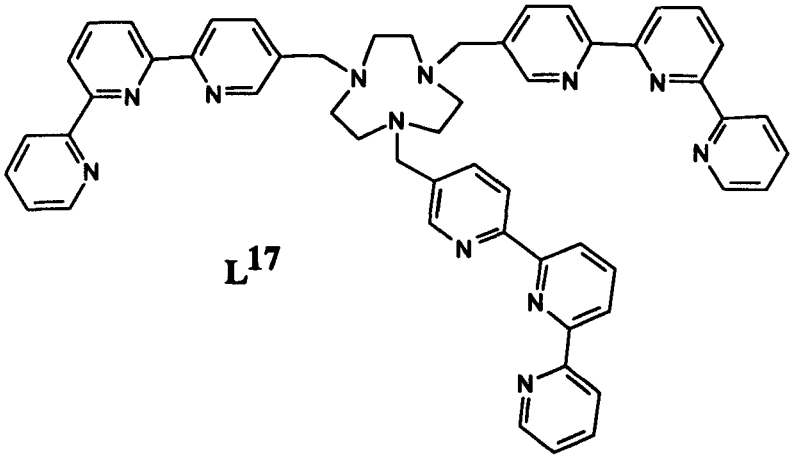

L^{17}

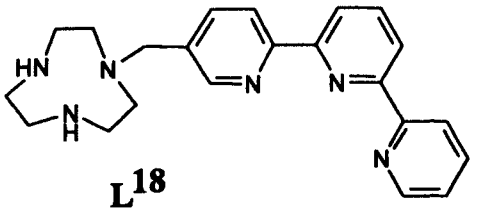

L^{18}

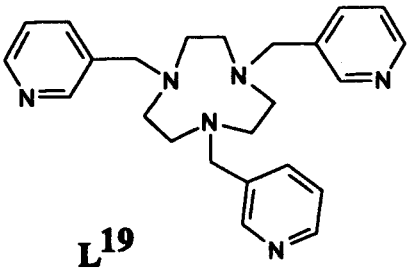

L^{19}

Acknowledgements

I would like to thank the following people for their help during the course of this work:–

Professor Peter Moore for all his advice and encouragement.

Dr O. W. Howarth and Dr J. Hastings for running some of the NMR spectra.

Dr N. W. Alcock and Dr W. Errington for carrying out the X–ray crystal structure determinations.

Mr I. Katal for running the mass spectra.

Mr P. Moore for some of the elemental analyses.

SERC for financial support.

All my family and friends for aiding and some very enjoyable abetting.

Declaration

The work described in this thesis is my own work except where otherwise indicated.

Some of the material has been accepted for publication with the following title:– 1,4,7–Tris(2,2'–bipyridyl–5–ylmethyl)–1,4,7–triazacyclononane (L^1), a Pre-organised Tris–(2,2'–bipyridyl) Chelating Macrocyclic Ligand. X–Ray structure of $[Ru(L^1H)][PF_6]_3$.

P. Sheldon, W. Errington, P. Moore, S. C. Rawle and S. M. Smith, *J. Chem. Soc., Chem. Commun.*, 1994, in press.

P. Sheldon.

Summary

This thesis describes the synthesis and characterisation of a series of new azamacrocyclic ligands (L^1–L^3, L^{10}, L^{11}, L^{14}, L^{16}–L^{19}), which have been N–functionalised with pendant pyridylmethyl– ($pyCH_2$–), bipyridylmethyl– ($bipyCH_2$–) and terpyridylmethyl– ($terpyCH_2$–) arms. Some of the coordination chemistry of these ligands with transition metal ions is reported. A sexidentate tris(2,2'–bipyridyl) chelating ligand, 1,4,7–tris(2,2'–bipyridyl–5'–ylmethyl)–1,4,7–triazacyclononane (L^1) has been developed, and the crystal structures of the mononuclear complexes $[M(L^1H)]^{3+}$ (M = Ru, Cu) are reported. In $[M(L^1H)]^{3+}$, the azamacrocyclic nitrogen atoms are non–coordinating to M, but have a high affinity for a single proton trapped in the macrocyclic cavity. An analogous nonadentate ligand (L^{17}) has been developed based on 9N3 with three N–pendant $terpyCH_2$– arms, and complexes of L^{17} with Eu(III) and La(III) are reported. The complex $[Eu(L^{17}H)](PF_6)_4$ is found to be strongly fluorescent in acetonitrile and methanol / water solution. Ligands with potential use as fluorescent pH and transition metal ion sensors have been developed by reacting the azamacrocyclic N–pendant $bipyCH_2$ arms of L^1–L^3, L^{10} and L^{11} with *cis*–$[Ru(bipy)_2Cl_2]$ to give macrocycles with up to four attached $[Ru(bipy)_3]^{2+}$ groups (L^5–L^7, L^{12}, L^{13}).

Abbreviations

9N3	1,4,7–triazacyclononane
14N4, cyclam	1,4,8,11–tetraazacyclotetradecane
Å	angstrom (10^{-10} m)
bipy	2,2'–bipyridine
br	broad
CI	chemical ionisation
COSY	proton – 2D correlation spectrum
d	doublet
DEPT	distortionless enhancement by polarisation transfer
EI	electron impact ionisation
Et	ethyl
FAB	fast atom bombardment
ICP	inductively–coupled plasma spectrometry
m	multiplet
mbzimpy	2,6–bis(1–methylbenzimidazol–2–yl)pyridine
Me	methyl
mer	meridional
MLCT	metal to ligand charge transfer
NMR	nuclear magnetic resonance
NBA	nitrobenzyl alcohol
NOE	nuclear Overhauser enhancement
p.p.m.	parts per million
Pr	propyl
pyterpy	4'–(4'''–pyridyl)–2,2':6',2''–terpyridine
q	quartet
qu	quintet
s	singlet

sh	shoulder
t	triplet
terpy	2,2':6',2"–terpyridine
tet *a*	5,7,7,12,14,14–hexamethyl–1,4,8,11–tetraazacyclotetradecane, isomer *a*
tet *b*	5,7,7,12,14,14–hexamethyl–1,4,8,11–tetraazacyclotetradecane, isomer *b*
THF	tetrahydrofuran
uv	ultra–violet
δ	chemical shift
ε	extinction coefficient
λ	wavelength

CHAPTER 1

Chapter 1

Introduction

1.1 Macrocyclic Ligands.

The study of macrocycles and their compounds has become a major part of coordination chemistry.[1–4] Since the 1960s there has been a rapid growth of interest into all aspects of macrocyclic ligand chemistry, which now has an impact on many wider chemical and biochemical fields.

A macrocycle is a cyclic molecule containing at least nine atoms, a minimum three of which must be donor atoms. Typical examples are shown in **Figure 1.1.** Complexes of these ligands characteristically show high thermodynamic stability, enhanced metal ion selectivity and marked kinetic inertness to the dissociation of the complexes they form.

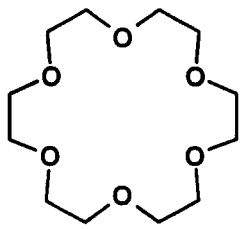

18-crown-6

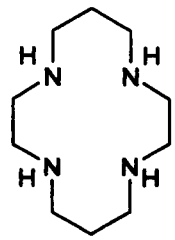

cyclam

Figure 1.1. Two common macrocycles.

Macrocyclic ligand complexes are involved in a number of fundamental biological systems, for example heme, chlorophyll and vitamin B_{12}. The importance of macrocyclic systems in nature and the unusual properties that are associated with them, have provided the impetus for much of the research into this extensive family of ligands.

The idea of cyclic ligands was established in the early literature,[5] but their value and potential was not recognised. It was not until 1967 that Pedersen reported on the formation of stable complexes between macrocyclic polyethers and salts of alkali and alkaline earth metals,[6] and began to appreciate their interesting complexing properties.[7] Since then, the family of macrocyclic ligands has grown and diverged from the original simple monocyclic rings. Macrocycles were taken into the third dimension with the development of cryptands[8, 9] and sepulchrands,[10, 11] which are cage like ligands based on crown ethers and azamacrocycles respectively. Increasingly complex systems are now being synthesised. For example, Sauvage has developed ways of interlocking molecular rings to form catenanes,[12] and has even tied molecular knots (**Figure 1.2**).[13]

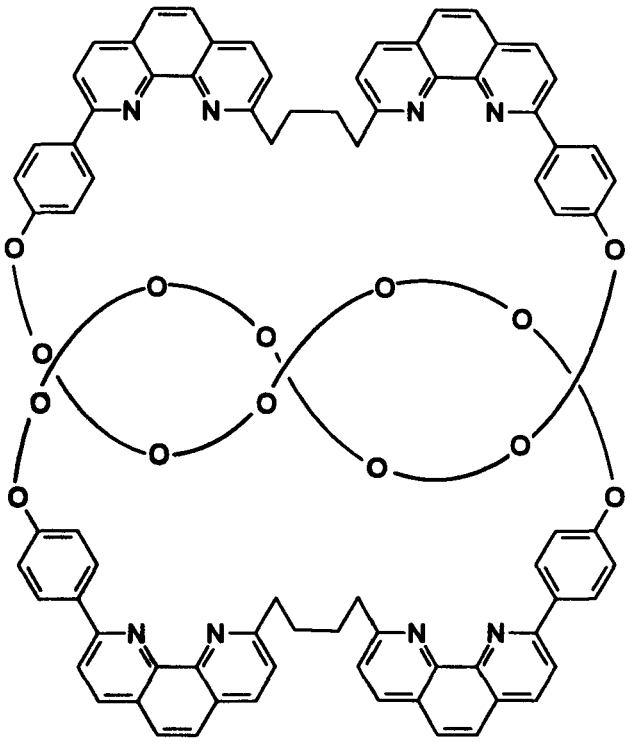

Figure 1.2. A molecular knot.

Stoddart has incorporated macrocycles into rotaxanes, molecules which consist of a linear component encircled by a macrocyclic component.[14, 15] The linear component is stoppered at both ends by large blocking groups, which can also be based on macrocycles.[16, 17]

Current applications of macrocycles are varied. The importance of macrocyclic systems in nature has already been mentioned, and many workers have used them to model biological processes. Recent reviews highlight the use of macrocycles in the development of artificial photosynthesis[18] and in producing advanced models for zinc(II) enzymes.[19] Work in biochemistry is extending the field of macrocyclic chemistry into supramolecular chemistry, which is largely focused on molecular recognition and self-assembly.

Parker[20, 21] has been researching functionalised macrocycles that form stable complexes *in vivo*, for use in therapeutic and diagnostic medicine. Beer[22] has used crown ethers in the development of sensors for group 1 and 2 metal cations. Functionalised azamacrocyclic systems have been used as potential catalysts in the fixation and activation of CO_2,[23-25] which is relevant to natural photosynthesis. As mentioned above, Stoddart[14-16] has used macrocycles in rotaxanes, systems which he is developing as molecular shuttles.

1.2 The Macrocyclic Effect.

The term 'macrocyclic effect' was first used by Cabbiness and Margerum to describe the greater stability observed for the complexes of an *n*-dentate macrocyclic ligand over the most similar *n*-dentate open chain analogue.[26] The macrocyclic effect can be thought of as an extension of the chelate effect, and as with the latter may arise from either entropic or enthalpic contributions, or both.[27] There has been some controversy over the relative importance of these contributions, but in general the macrocyclic effect results from a favourable entropy change, normally aided by a favourable enthalpy change.[28, 29]

Thermodynamic Considerations.

Important contributions to the **entropy change** include:

(i) Changes in the total number of species present.

(ii) Changes in the internal entropy of the ligand. A flexible open chain ligand is expected to lose 'configurational entropy' on coordination, but the more rigid cyclic ligand will undergo a much smaller change in configuration on coordination and so its internal entropy is less affected.

Factors influencing the **enthalpy change** include:

(i) Changes in ligand conformation on complexation. If the ligand is already in the right conformation for complex formation, then little reorganisation energy is required.[30] The ligand is said to be 'preorganised'.[31]

(ii) Different solvation energies of open chain and macrocyclic ligands. Desolvation of cyclic ligands may be easier than of open chain analogues as the former are more compact.

(iii) Dipole – dipole repulsion in macrocyclic ligands. This may lead to a high energy state for the free macrocycle, which is relieved on complex formation.

Kinetic Considerations.

The **rate of formation** of a macrocyclic complex from ligand and metal ion may be slower than that for the related open chain polydentate ligand, the additional steric constraints of the macrocycle hindering the formation pathways. **Dissociation rates** of macrocyclic complexes can be extremely slow relative to the corresponding open chain analogue.[32, 33] The open chain ligand may dissociate *via* a step–wise route which is more difficult for the macrocycle, as the latter has no free end. Macrocycles may have to undergo unfavourable rearrangements such as folding before they can dissociate from the coordination sphere. The slowness of dissociation of macrocyclic ligand from metal ion more than compensates for the slow formation of complexes, and reflects the enhanced thermodynamic stabilities of macrocyclic complexes.[28]

1.3 Size–Match Selectivity.

A close match between metal ion radius and cavity size in the macrocyclic ligand will tend to enhance the stability of the resultant complex. This effect is more pronounced in certain classes of macrocycle. For example, small ring crown ethers may exhibit remarkable selectivity for particular alkaline earth metals, apparently discriminating purely by metal ion size. 18–Crown–6 (**Figure 1.1**) is selective for potassium ion; cavity size radius of ligand and ionic radius of metal have both been estimated at 1.38 Å.[34] Molecular mechanics calculations have been used to investigate metal ion selectivity, and to explore the consequences of a mis–match between metal ion and ligand cavity size.[35] A good fit between cavity size and target ion size does not always indicate high selectivity. When a mis–match occurs, many macrocycles are able to fold, or to coordinate to the metal out of plane of the ring (**Figure 1.3**). Tetraazamacrocycles are found to be especially flexible in this respect[36] and so do not show a selectivity based on size of ion.

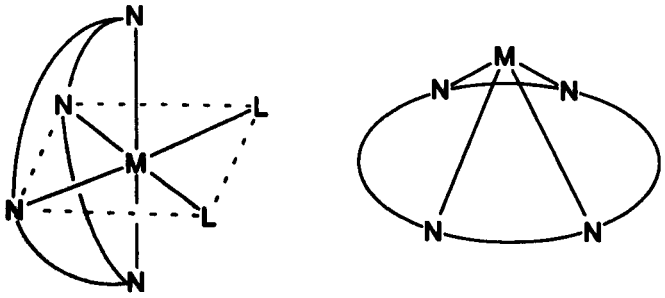

Figure 1.3. Two ways of accommodating a metal of non–ideal size. L indicates coordination sites occupied by other unidentate ligands, such as solvent molecules. In this way, a metal ion that is too large to fit into the macrocyclic ring can still be coordinated strongly to the macrocycle.

Rigid ligands such as porphyrins are unable to compensate for a mis–match in metal ion and cavity size.[37] Introducing unsaturation into the cyclic backbone, or going from a monocyclic ligand to a '3D' cage ligand or cryptand (shown below) will reduce the flexibility.

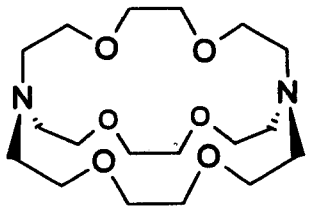

[2.2.2] cryptand

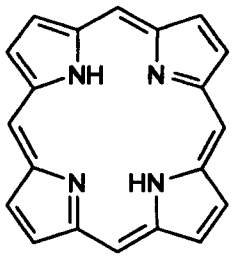

porphine

The ability of macrocycles to bind specific cations does not depend entirely on cavity size. Changing the number and type of donor atoms, adjusting the size of chelate rings formed on complexation and adding substituents to the macrocyclic ring can all modify the selectivity. In addition, responsive macrocycles have been developed whose selectivity and / or strength of binding can be influenced by change in pH, or an input of electrochemical, photochemical or thermal energy.[38]

1.4 Pendant Arm Macrocycles.

Macrocycles functionalised with pendant coordinating arms are receiving considerable attention. This is stimulated by their general coordination chemistry and possible relevance as model ligands for metal enzymes, metal ion selective reagents and metal binding ligands for medical applications.[21, 39–43] Such ligands can be designed so that metal ion coordination will occur at both the macrocyclic and pendant arm sites,[23, 44, 45] or just at the pendant arms.[46] Recently, pendant arm macrocycles (such as **A**) have been used in the self assembly of helicate systems,[47] and as catalysts in the electrochemical reduction of CO_2 (**B**).[48]

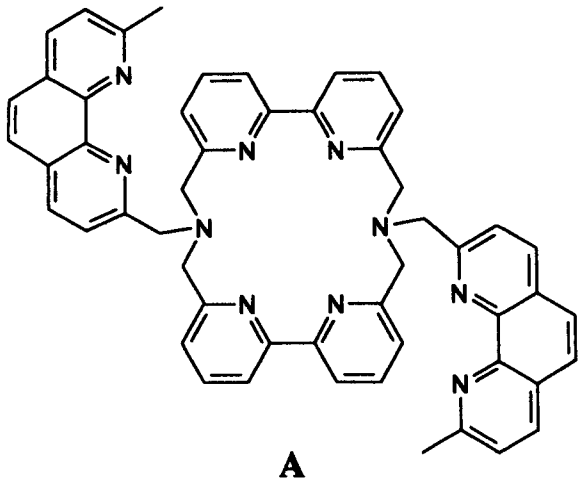

A

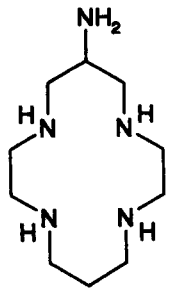

B

Pendant arms may be added for various reasons. Often an increased number of donor atoms is required. Tri–, tetra– and penta–dentate azamacrocycles are widely used as ligands for transition metal ions, but as most of these metals prefer a coordination number of at least six, the above ligands cannot occupy all the coordination sites at once. Filling more of the donor sites will generally increase the stability of the complex. Macrocyclic ligands with increased coordination numbers are required for the formation of polynuclear complexes.[49] An increased coordination number may be achieved by enlarging the ring size and number of donor atoms in that ring, or by attaching one or more pendant arm(s) containing the additional donor atoms. The latter approach has an advantage in that the number of geometric isomers formed on complexation is generally smaller than that formed by analogous unbranched monocyclic relatives.[50] A pendant arm may speed up metal binding rates by chelating to the metal ion before it enters the macrocyclic ring[51] and may lead to novel coordination geometries that are unobtainable using unbranched macrocycles.[52, 53]

Pendant arm macrocycles combine advantages of both open chain and cyclic ligands. The pendant arms allow the coordination flexibility of open chain systems, while the kinetic inertness to dissociation typical of simple macrocyclic ligands is retained. The influence of the pendant arms on complexation depends on the flexibility, length and donor groups of the arms. The effect on the stability of complexes of azacrown ethers with various pendant arms has recently been studied.[54]

The pendant arm can be attached *via* a donor atom of the macrocycle, or *via* an atom in the carbon framework. The former strategy has received greater attention, probably as the syntheses involved are easier, but there can be drawbacks. For instance, functionalisation of nitrogen donors converts a secondary amine into a tertiary amine, a poorer donor for steric reasons. In addition, a metal bound at the macrocyclic cavity may experience an unwanted inductive effect from the nearby pendant arm.

Pendant arm ligands may be designed so that *simultaneous* coordination of a single metal ion at the arm and at the macrocyclic cavity is either encouraged[45] or disallowed[55] (**Figure 1.4**).

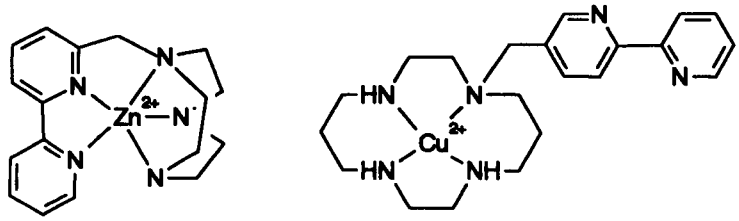

Figure 1.4. Left: Attaching the bipyridyl (bipy) pendant arm *via* the 6 position of the bipyridine means that a single metal ion may coordinate to the bipy unit and the macrocyclic unit simultaneously, as shown. **Right:** With the pendant arm attached to the 5 position, the bipy and macrocyclic units cannot bind to the same metal ion. In this example the bipy arm is left free to coordinate to a second metal ion, and the ligand is therefore suitable for the preparation of polymetallic complexes. Polymetallic complexes are of interest for their possible use in catalysis and multi redox systems.[25, 38]

1.5 Bipyridine and Terpyridine.

2,2'–Bipyridine, 2,2':6',2"–terpyridine (terpy) and related ligands have been used extensively for many years.[56, 57] Recent interest has been stimulated by the attractive photochemical and photophysical properties of bipy.[58–60]

2,2'–Bipyridine is a strong field ligand which forms relatively stable complexes, generally of the form $[M(bipy)_2]^{n+}$ or $[M(bipy)_3]^{n+}$. The free ligand adopts a near planar *trans* arrangement in the solid state, a *cis* arrangement is required on chelation (**Figure 1.5**).

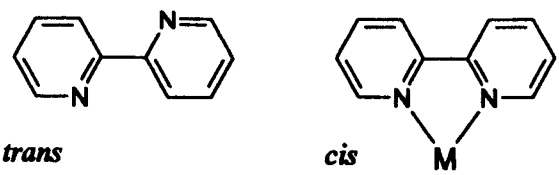

Figure 1.5. *Cis*- and *trans*- 2,2'–bipyridine (bipy).

As an analogue to bipy, terpy has been the subject of a number of studies involving a wide variety of metal centres. Its terdentate nature means that it can occupy three meridonal sites of a metal centre and so can be used to direct the reactivity of a metal centre. The essentially planar terpy ligand adopts a *cis, cis* configuration on chelation to a metal centre. For terpy to act as an efficient terdentate ligand, distortion occurs (**Figure 1.6.**)[57]

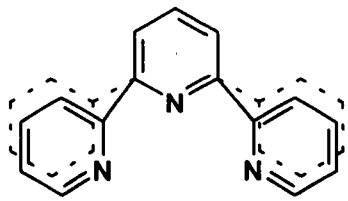

Figure 1.6. Distortion of terpy on coordination. Dashed lines represent the position of the ligand prior to coordination.

When an extreme mis-match between metal ion and ligand geometry occurs, terpy may act as a bidentate ligand, one pyridine ring being left uncoordinated. The uncoordinated pyridine ring may undergo an oscillatory fluxional motion.[61]

The attractive photochemical and photophysical properties of bipyridine have prompted its inclusion into a number of macrocyclic ligands. Terpyridine fragments have also been included, although to a lesser extent. The polypyridine units may form part of the cyclic backbone[62-64] or may be attached as pendant arms.[46, 55, 65, 66]

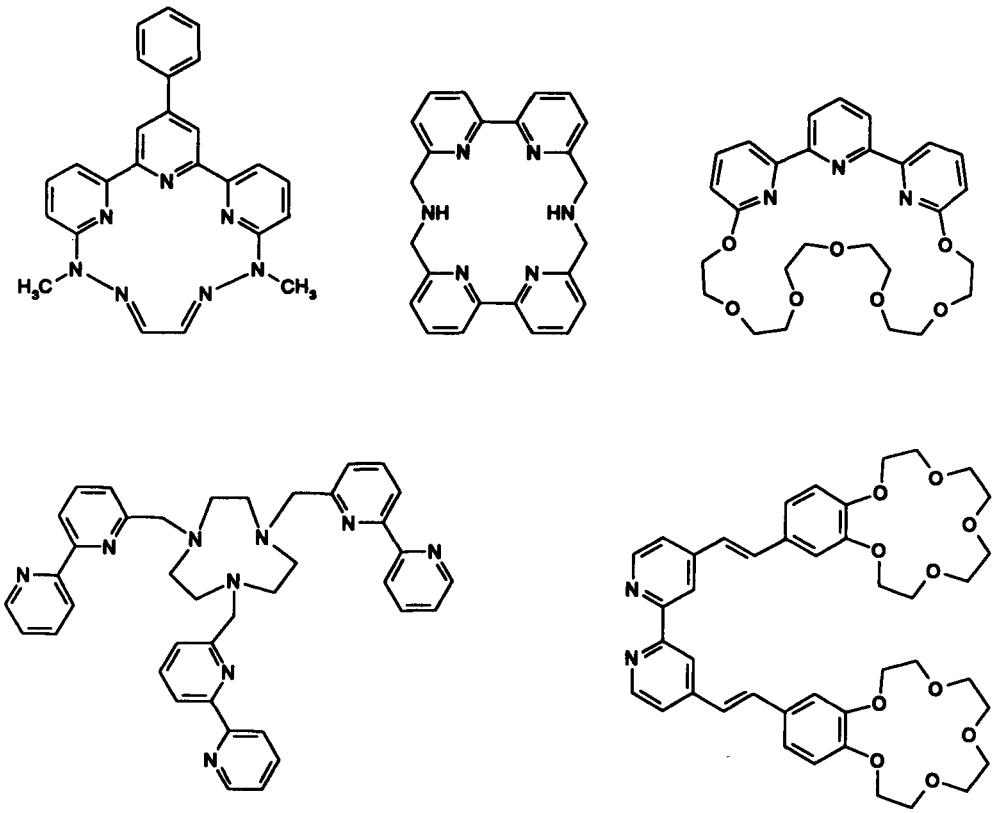

Figure 1.7. Some examples of macrocycles that contain bipy or terpy units.

1.6 Fluorescent Sensors.

Molecular fluorescence is a powerful phenomenon in photophysics and photochemistry. The measurement of fluorescence intensity can be a highly sensitive technique, meaning that only a very low concentration of active molecules is required. This is a significant advantage if biological systems are to be monitored as use of low concentrations of active molecules should reduce the risk of poisoning the host.

A fluorescent sensor for detecting ions contains a fluorescent reporter group and an ion receptor. In the current generation of sensors, the reporter and receptor groups are distinct units separated by a σ bonded spacer or linker group.[67]

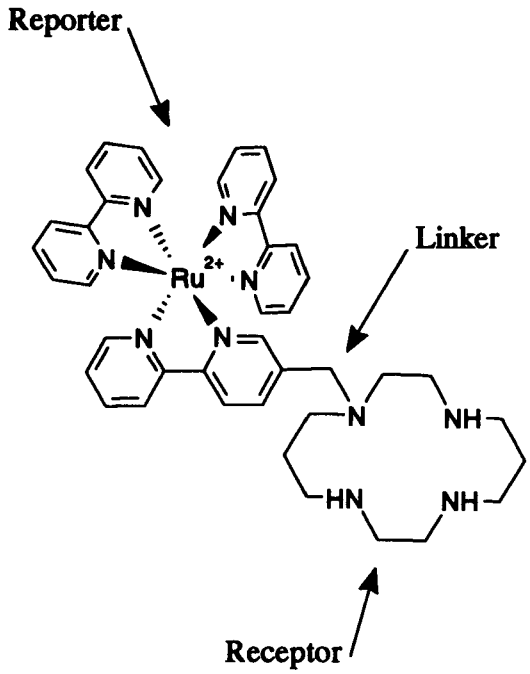

Figure 1.8. The structure of a typical sensor.[55]

Sensors such as that shown in **Figure 1.8** fluoresce as normal until a proton or an appropriate metal ion is bound in the macrocyclic cavity. The fluorescence of the $[Ru(bipy)_3]^{2+}$ group is then quenched; thus the molecule reports the presence of the incoming ion.

The Receptor

The receptor group should bind the target ion selectively, strongly and quickly. Target ion selectivity and the exceptional stability of their complexes have already been noted as features of macrocycles, so such ligands can be expected to perform well as receptors. It should be noted that problems may occur where the metal ion is not fully incorporated into the macrocyclic cavity, remaining above the plane of the macrocycle. Rapid formation of an intermediate where the metal ion is out of plane, followed by slow rearrangement to form a product with the metal ion in the centre of the cavity is also possible.[68]

Several groups have capitalised on the target ion selectivity of the small ring crown ethers, incorporating them into sensors for group 1 and 2 metal cations. An example

of such a sensor is shown in **Figure 1.9**, this and related molecules can be electropolymerised onto platinum to form an electroactive film.[22, 69]

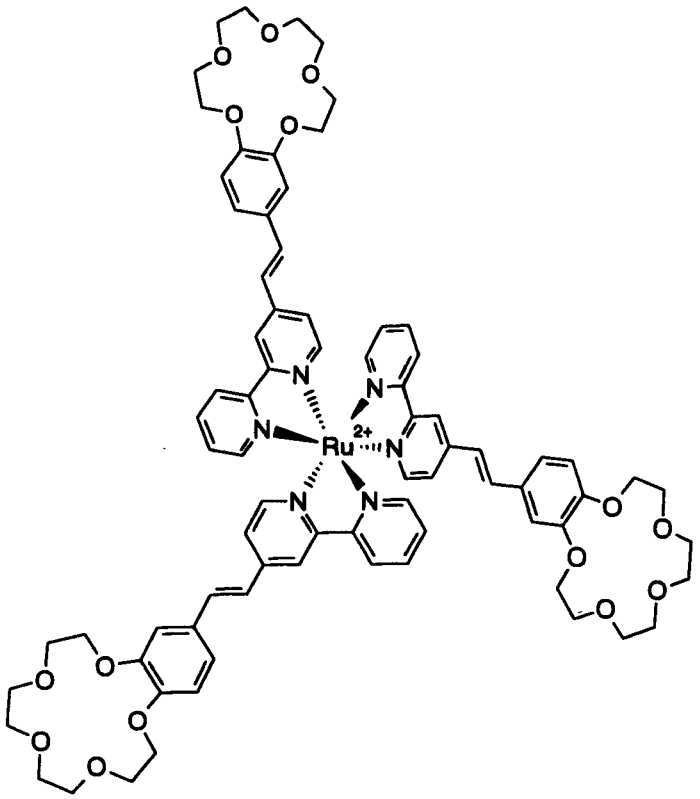

Figure 1.9. A fluorescent sensor for group 1 and 2 metal cations.

The Linker

The linker group in a sensor (**Figure 1.8**) is usually short so that fluorescence of the reporter group is significantly quenched once binding of a metal in the receptor has occurred. Longer links tend to decrease the response of the fluorescent reporter,[70] but it should be noted that whilst the use of excessively short links may promote a very rapid and complete response, they carry the inherent danger of affecting the receptor site through charge and steric effects. In addition to the length of the linking group, its position is also important. The two molecules in **Figure 1.10** should be compared. That on the left has its pendant arm attached *via* the 6 position of the bipy and is reported not to fluoresce at room temperature,[71] the molecule on the right has its pendant arm attached *via* the 5 position and the $[Ru(bipy)_3]^{2+}$ fluoresces as normal.[55]

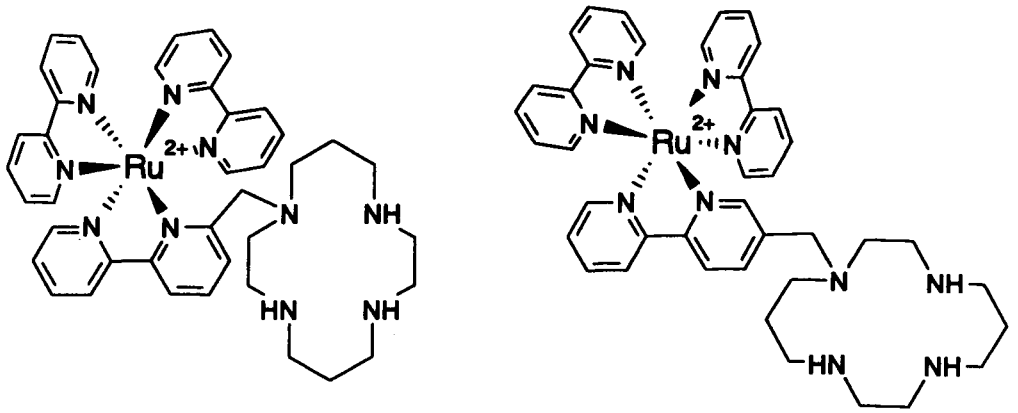

Figure 1.10. Left: Non–fluorescent. **Right:** Fluorescent.

The substituent in the 6 position of the bipy causes a distortion in the RuN_6 coordination sphere.[72] This kind of distortion lowers the energy of the d–d excited states [^{3}MC (triplet metal centred) levels] towards that of the luminescent ^{3}MLCT (triplet metal to ligand charge transfer) state, providing a ready radiationless decay pathway.

The Reporter

The fluorescent reporter group in an ion sensor may be an organic unit such as anthracene, or a transition metal complex like $[Ru(bipy)_3]^{2+}$. This thesis concentrates on molecules that contain the strongly fluorescent $[Ru(bipy)_3]^{2+}$ chromophore. The $[Ru(bipy)_3]^{2+}$ unit has been extensively studied, and features repeatedly in schemes for the conversion of light energy into chemical energy. The photophysical and photochemical properties of complexes like $[Ru(bipy)_3]^{2+}$ are thoroughly documented, and the room temperature emitting character of such compounds has been well established.[58, 64, 73] Workers have been attracted to $[Ru(bipy)_3]^{2+}$ by its chemical stability, redox properties, excited state reactivity, excited state lifetime and luminescence emission. Many derivatives of $[Ru(bipy)_3]^{2+}$ have been synthesised in order to modify ground and excited state properties.[74] These derivatives have substituents added to the bipy rings and / or one or more bipy replaced with another polypyridine ligand. Ruthenium(II)–polypyridine complexes can be used in the

synthesis of luminescent and redox active polynuclear compounds which use light to initiate energy and / or electron transfer processes.

Absorption of a photon by a molecule of $[Ru(bipy)_3]^{2+}$ takes that molecule to an excited electronic state, a high energy unstable species which must loose energy. Energy can be lost from the excited state in a number of ways; by photochemical reaction, luminescence, degradation of the excess energy into heat or *via* a quenching process where it interacts with other species present in solution. The Jablonski diagram (**Figure 1.11**) shows these various deactivation processes.

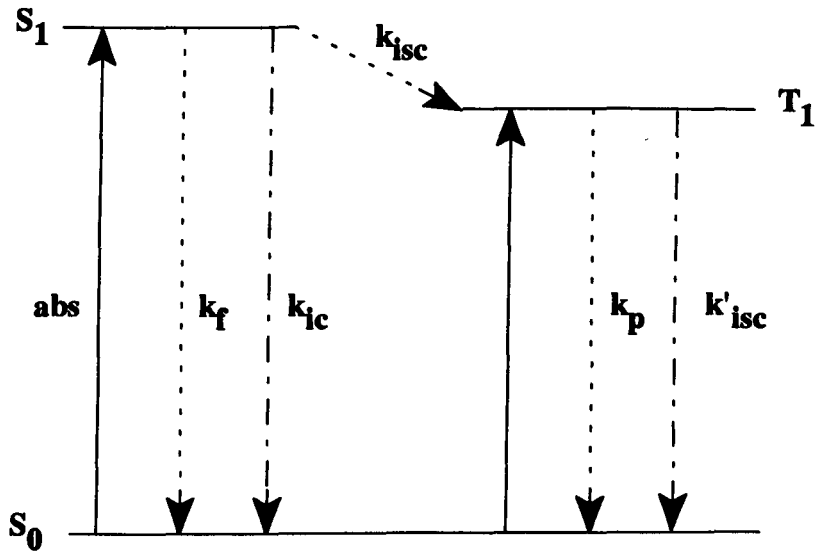

Figure 1.11. Schematic Jablonski diagram[60] showing the various deactivation processes. k_f, k_{ic}, k_{isc}, k_p, And k'_{isc} are the unimolecular rate constants for fluorescence, internal conversion, $S_1 \rightarrow T_1$ intersystem crossing, phosphorescence and $T_1 \rightarrow S_0$ intersystem crossing, respectively.

$[Ru(bipy)_3]^{2+}$ has several advantages as a reporter group. It has a long lived (300-600 ns) luminescence, due to emission from a triplet metal to ligand charge transfer (^{3}MLCT) state.[75] The long lifetime of the excited state provides the opportunity for reactions to occur before deactivation takes place. In a large number

of systems $[Ru(bipy)_3]^{2+}$ is directly attached to the reaction site. It is hoped that this allows the most efficient use of energy or electrons transferred from $[Ru(bipy)_3]^{2+}$. When $[Ru(bipy)_3]^{2+}$ is intramolecularly linked to certain macrocyclic complexes, the ^{3}MLCT is quenched.[71, 76, 77]

Quenching of $*[Ru(bipy)_3]^{2+}$.

There are two routes for quenching; energy transfer (Eqn. 1.1) or electron transfer. Since $*[Ru(bipy)_3]^{2+}$ (* denotes an excited state) is both a good electron donor and a good electron acceptor, quenching by electron transfer can be divided into oxidative quenching (Eqn. 1.2), and reductive quenching (Eqn. 1.3).[60]

$$*[Ru(bipy)_3]^{2+} + Q \rightarrow [Ru(bipy)_3]^{2+} + *Q \quad \text{energy transfer} \qquad \text{(Eqn. 1.1)}$$

$$*[Ru(bipy)_3]^{2+} + Q \rightarrow [Ru(bipy)_3]^{3+} + Q^- \quad \text{oxidative quenching} \qquad \text{(Eqn. 1.2)}$$

$$*[Ru(bipy)_3]^{2+} + Q \rightarrow [Ru(bipy)_3]^{+} + Q^+ \quad \text{reductive quenching} \qquad \text{(Eqn. 1.3)}$$

(Q = quencher)

Redox products have been directly observed in flash photolysis experiments, good evidence to support electron transfer quenching. Energy transfer quenching of $*[Ru(bipy)_3]^{2+}$ is thought to be less common, but has been demonstrated in a few cases.

Luminescent pH Sensors.

Fluorescent sensors have been developed for cations, anions and neutral molecules. $[Ru(bipy)_3]^{2+}$ has been incorporated into sensors for both cations[22, 55, 78] and anions.[79] Closely related to the development of cation sensors is the development of luminescent pH sensors. Most of these molecules consist of aromatic hydrocarbon–amine systems,[80, 81] however pH sensors with metal complex reporters have recently

emerged. These sensors contain a tin(IV)–porphryn unit[82] or the $[Ru(bipy)_3]^{2+}$ core (**Figure 1.12**).[83, 84]

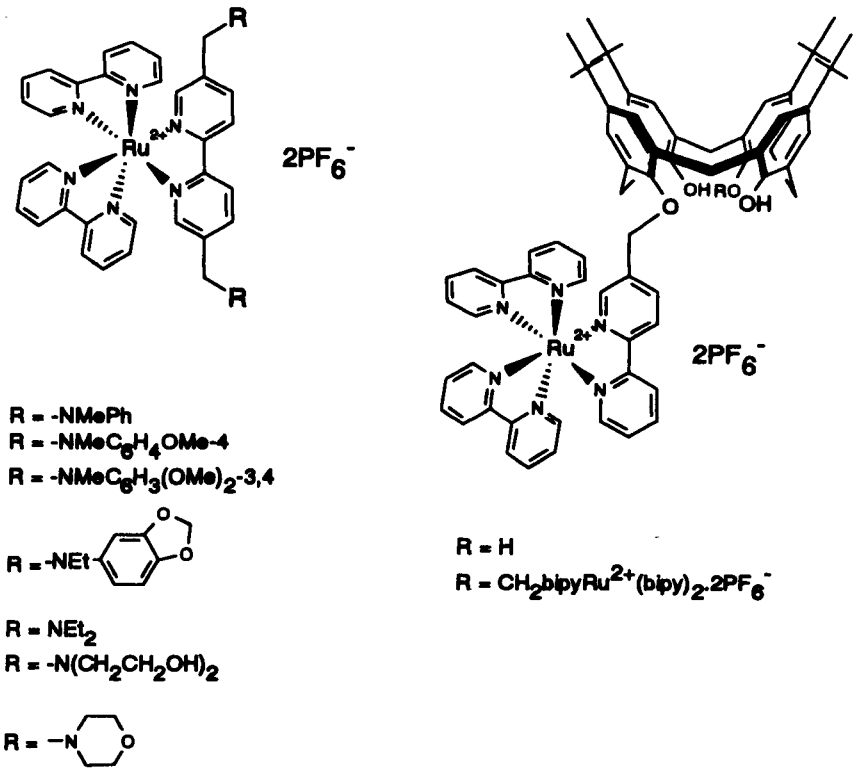

Figure 1.12. Luminescent pH Sensors containing $[Ru(bipy)_3]^{2+}$.

Desirable characteristics common to these sensors are:

(i) $pK_a^* \approx pK_a$ (* denotes an excited state)

(ii) Spectral parameters independent of pH (except for fluorescent intensity).

The presence of a methylene spacer helps achieve these characteristics by keeping the receptor and reporter sites separated in space.

Luminescence quenching in these systems seems to occur in two ways. Depending upon the molecule, photo–induced electron transfer can be responsible for proton assisted quenching of luminescence and proton assisted retrieval of luminescence. In certain systems, the presence of positive charge on side chains close to the

$[Ru(bipy)_3]^{2+}$ can cause photo-cleavage of a Ru–N bond, eventually leading to reformation of the original tris bipyridyl coordination in the ground state.[83] A mechanism for the ligand photodissociation has been proposed, and is discussed below (Section 1.8).

1.7 Other Applications of Cyclam–$[Ru(bipy)_3]^{2+}$ systems.

The use of cyclam–$[Ru(bipy)_3]^{2+}$ and derivatives is not limited to proton or metal ion detection. A Ni(II)–cyclam complex has been shown to act as a catalyst for the reduction of CO_2 to CO,[85, 86] and has been used for this purpose in conjunction with $[Ru(bipy)_3]^{2+}$.[87] Molecules containing both of these groups have been synthesised (**Figure 1.13**). It is hoped that covalently linking the two functionalities together will improve the efficiency of electron transfer between the photoexcited $[Ru(bipy)_3]^{2+}$ to the catalytic site.[23, 65, 71, 88]

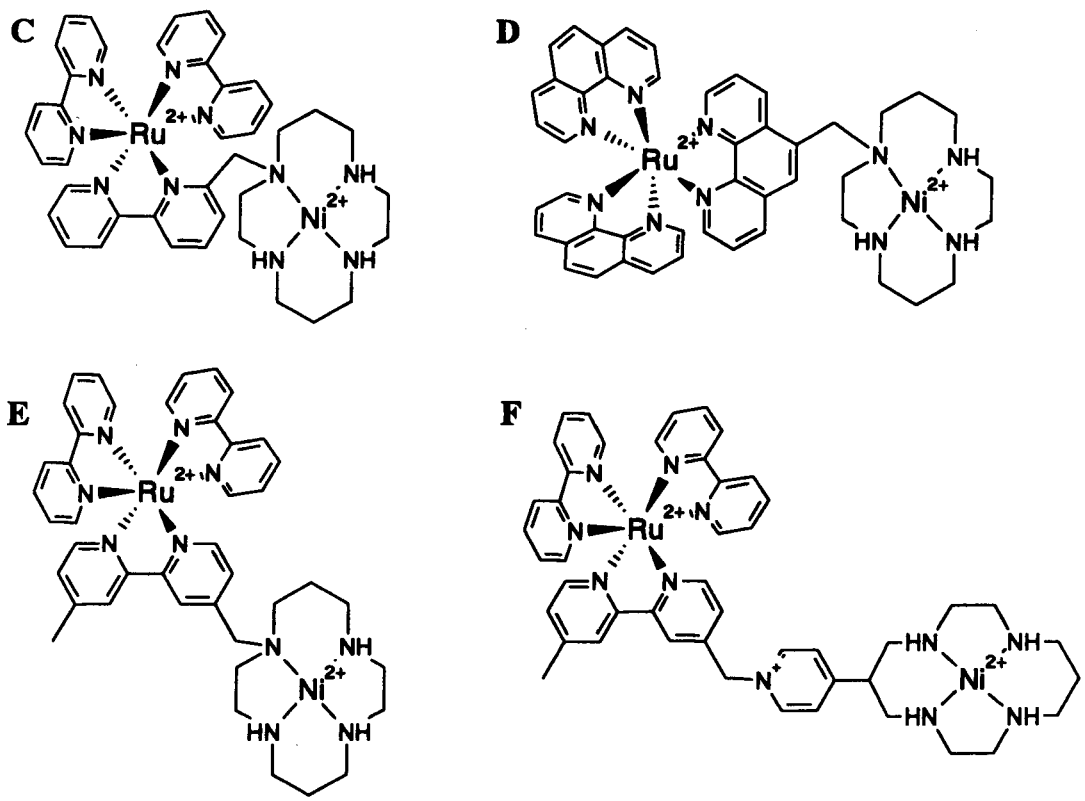

Figure 1.13. Cyclam–$[Ru(polypyridine)_3]^{2+}$ systems.

C does not exhibit much catalytic activity. This was attributed in part to the position of the $-CH_2-$ linker between Ni(II)–cyclam and $[Ru(bipy)_3]^{2+}$ units which is attached *via* the 6 position of the bipy. This causes distortion of the RuN_6 octahedron and reduced photochemical stability.[71] **D** shows improved photochemical stability over **C**, however the emission lifetime of $[Ru(phen)_3]^{2+}$ (phen = 1,10–phenanthrolene) is too short to allow the energy of the excited state to be used effectively by the attached catalytic site.[23] **E** and **F** incorporate $[Ru(bipy)_3]^{2+}$, preferred because of its longer emission lifetime, and the catalytic Ni(II)–cyclam site without steric crowding of either the ruthenium or nickel subunits. Electrochemical studies show that the absence of *N*–alkyl substitution in **F** allows the Ni(II)–cyclam moiety to retain greater similarity to free Ni(II)–cyclam than in **C**–**E**.[23, 65]

1.8 Ligand Photodissociation

The occurrence of ligand photodissociation processes may be a positive mechanism of quenching in some luminescent pH sensors,[83] but is a major drawback to the use of $[Ru(bipy)_3]^{2+}$ in photochemical processes. A detailed mechanism for the ligand photodissociation has been proposed (**Figure 1.14**).[89] It is thought to proceed *via* thermal population of a metal centred (d–d) excited state (^3MC), with subsequent cleavage of one Ru–N bond. Once formed, this monodentate bipy species can either undergo loss of bipy to give $[Ru(bipy)_2X_2]$, or chelate ring closure to reform $[Ru(bipy)_3]^{2+}$. Significant ligand dissociation from the distorted d–d state occurs, particularly in solvents of low dielectric constant and in the presence of coordinating anions.[89] An intermediate of the photosubstitution of $[Ru(bipy)_2(dmbipy)]^{2+}$ (dmbipy = 3,3'–dimethyl–2,2'–bipyridine) containing a monodentate dmbipy ligand has recently been reported.[90, 91]

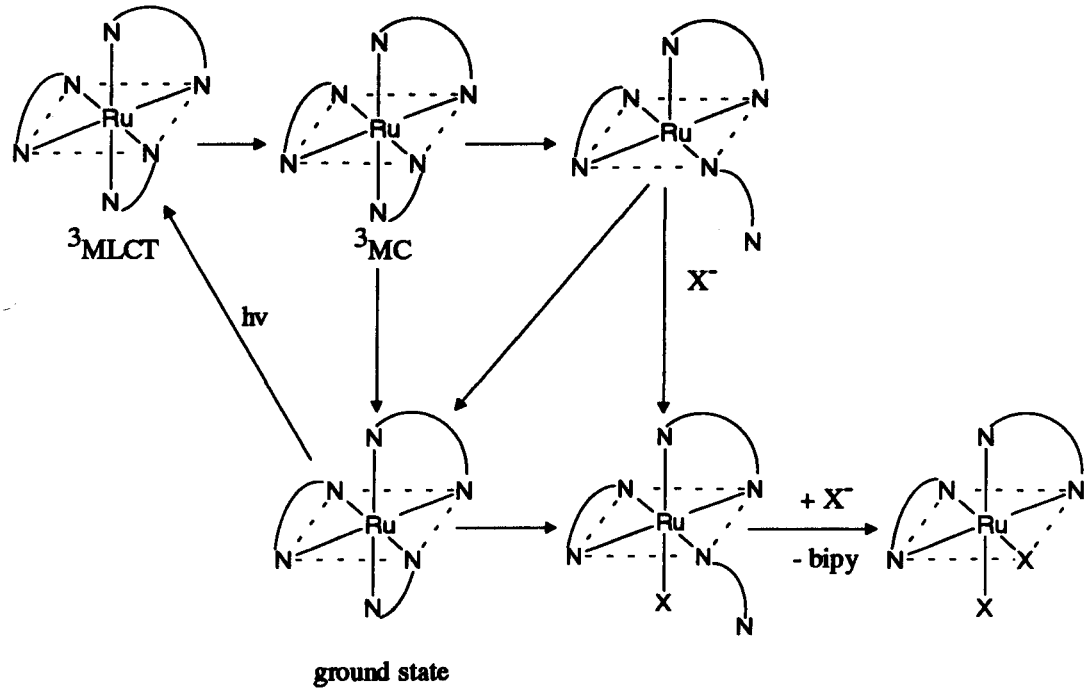

Figure 1.14. Schematic representation of the proposed mechanism of ligand photosubstitution reactions of $[Ru(bipy)_3]^{2+}$.[89]

One way to prevent ligand photodissociation is to form a cage structure around the metal by linking together the bipy ligands with suitable bridges (**Figure 1.15**).[92, 93]

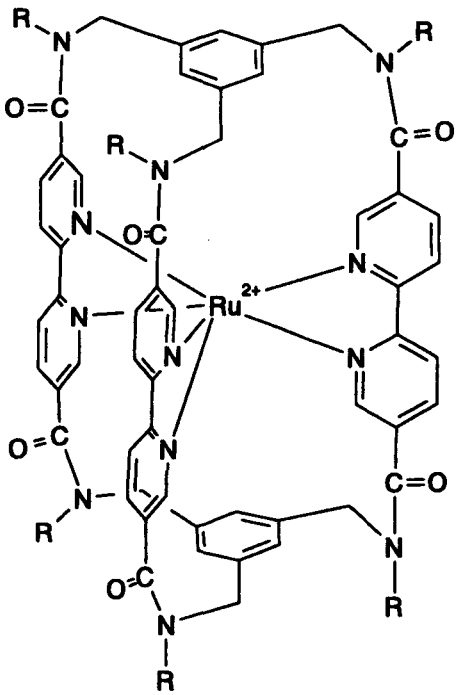

Figure 1.15. Cage complex incorporating the $[Ru(bipy)_3]^{2+}$ core.

The caged complex shown in **Figure 1.15** exhibits comparable luminescent properties to the parent $[Ru(bipy)_3]^{2+}$ complex, but has an approximately 10^4 times higher stability towards ligand photodissociation. Other cage type polypyridine ligands have been prepared,[94] although the ruthenium complexes appear not to have been synthesised to date.

1.9 Polybipyridine Tripod Ligands

Tripod polybipyridine ligands have been synthesised for Ru(II). As with the cage complex in **Figure 1.15**, a major driving force behind their synthesis was to produce complexes containing the $[Ru(bipy)_3]^{2+}$ core which have very low quantum yields for photodecomposition. A single nitrogen atom,[46, 95, 96] a 1, 3, 5–trisubstituted benzene[97] and 1,4,7–triazacyclononane[46, 42, 98] have been used to anchor the bipy arms (**Figure 1.16**).

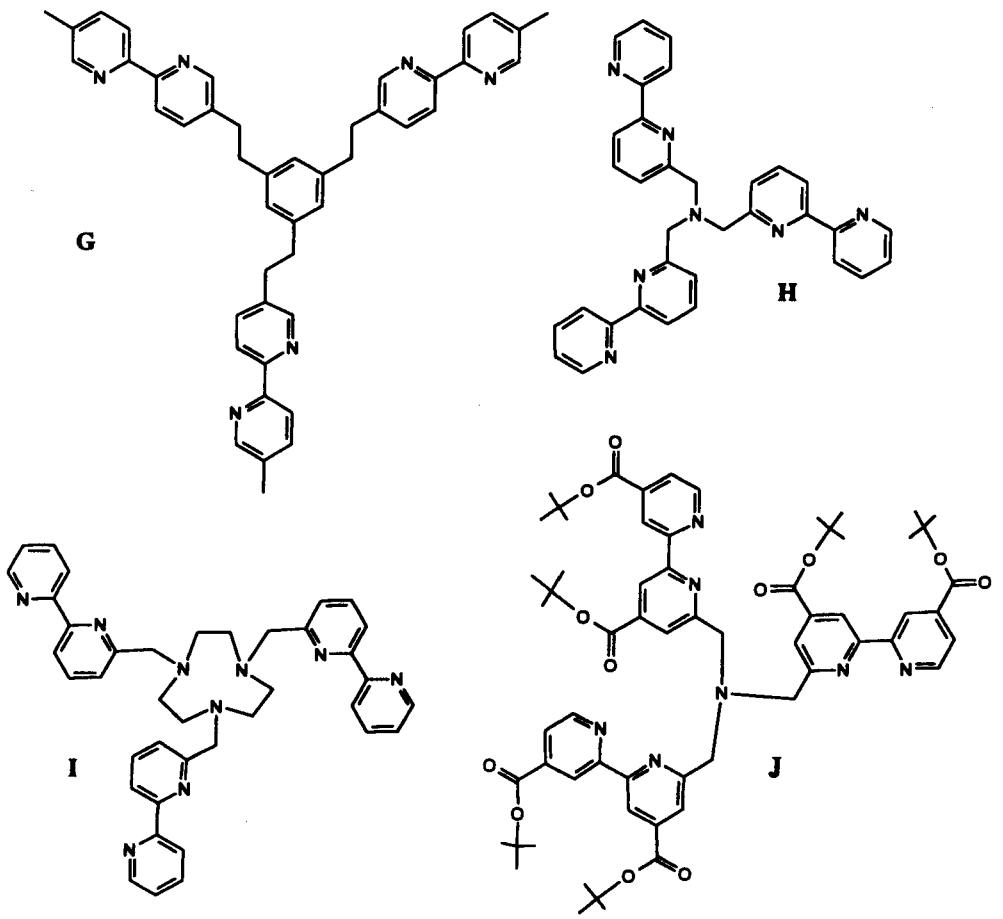

Figure 1.16. Polybipyridine tripod ligands.

Mononuclear Ru(II) hemicaged complexes of the form $[Ru(ligand)]^{2+}$ have been reported for ligands **G** and **H**. $[Ru(G)](PF_6)_2$ has redox and absorption properties very similar to the parent $[Ru(bipy)_3]^{2+}$ complex, but the room temperature lifetime and emission quantum yields of $[Ru(G)](PF_6)_2$ are increased by a factor of 10 compared to the parent complex.[97] No luminescence could be detected for the mononuclear Ru(II) complex of **H**.[46] This could be attributed to steric hindrance at the metal centre, distortion of the RuN_6 coordination octahedron and / or rapid internal quenching by the electron pair on the anchoring N atom. **I** appears to be sterically constrained against octahedral coordination of the three bipy arms around a single metal ion.[46] Reaction of tripods **H** and **I** with Fe(II) should be compared: $[Fe(H)]^{2+}$ was readily prepared by following the synthesis of $[Fe(bipy)_3]^{2+}$. Following the same method, **I** appeared to form a tris(bipy) species but this decomposed whilst still in solution and $[Fe(I)]^{2+}$ could not be isolated.[46]

1.10 Ruthenium(II)–Terpyridine Systems

As discussed above, whereas luminescent $[Ru(bipy)_3]^{2+}$ and derivatives have been well researched and documented, much less interest has been focused on complexes containing 2',2':6',2"–terpyridine (terpy) and analogues. A recent review summarises much of the work in this area.[99] The incorporation of terpy moieties into multidentate ligands is synthetically more difficult than with 2,2'–bipyridine, which probably goes some way to explaining its rather sparse use. In addition, $[Ru(terpy)_2]^{2+}$ would seem to be less useful than $[Ru(bipy)_3]^{2+}$ as it becomes luminescent only at low temperatures. Workers have directly linked the $[Ru(terpy)_2]^{2+}$ moiety to ferrocene[100] and a bis–terpy catenate has been produced.[101] A few derivatives of $[Ru(terpy)_2]^{2+}$ that are luminescent at room temperature have been synthesised.[102, 103] Ruthenium chromophores containing terpy and polyazine bridging ligands are also under investigation.[104]

Advantages of Ru(II)–terpy systems

Ru(II)–terpy systems may be desirable as the geometry of bis–terpy complexes allows the design of supramolecular species where electron donor and acceptor groups may be placed in opposite directions with respect to the light absorber (**Figure 1.17**).[105] This is in contrast to the Ru(II)–bipy systems, where substituents attached to the $[Ru(bipy)_3]^{2+}$ chromophore are close to each other.

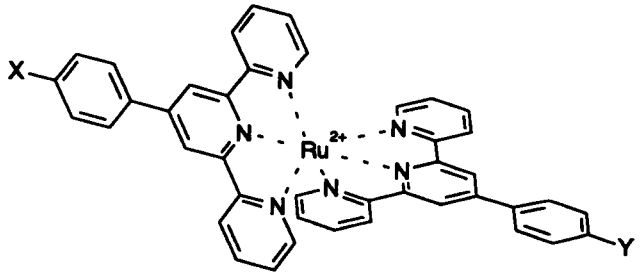

Figure 1.17. Ru(II)–terpy systems can allow substituents such as X and Y to be placed in opposite directions to each other.

Rigid rod–like binuclear Ru(II)–Os(II) terpy complexes have been synthesised,[106] and their luminescence properties studied. $[Ru(terpy)_2]^{2+}$ complexes that have substituents in the 4'-positions do not generate isomeric mixtures, unlike mono–substituted $[Ru(bipy)_3]^{2+}$ systems.

1.11 Lanthanide Complexes of Polybipyridine Ligands.

As discussed above, luminescent molecular systems are of interest because of their potential use for a variety of applications. Some lanthanide ions (particularly Eu^{3+}) have strongly emissive and long–lived excited states. Considerable effort has been focused towards making stable, strongly luminescent complexes of Eu(III) and other appropriate lanthanide ions.[107] The main application for such systems has focused on the use of Eu^{3+} and Tb^{3+} complexes to make luminescent and fluorescent probes. Lanthanide ions lack intense metal–centred absorption bands, so to make use of their emitting properties coordinated ligands are required which absorb light. Energy is

then transferred from ligand excited states to the metal ion, and is emitted as metal centred luminescence. This light conversion process is known as the 'antenna effect'.[107-109] 2,2'-Bipyridine is a suitable ligand, but as Eu^{3+} coordinates more strongly to H_2O than to bipy, two or more bipy units need to be linked together to form a preorganised multidentate ligand. Luminescent lanthanide complexes have been formed with bipyridyl–containing macrocycles,[66, 110] cage like ligands,[108, 109, 111] and podand type ligands[96, 98, 112] (**Figure 1.18**). Lanthanide complexes have also been formed with ligands **H** and **I** (**Figure 1.16**).

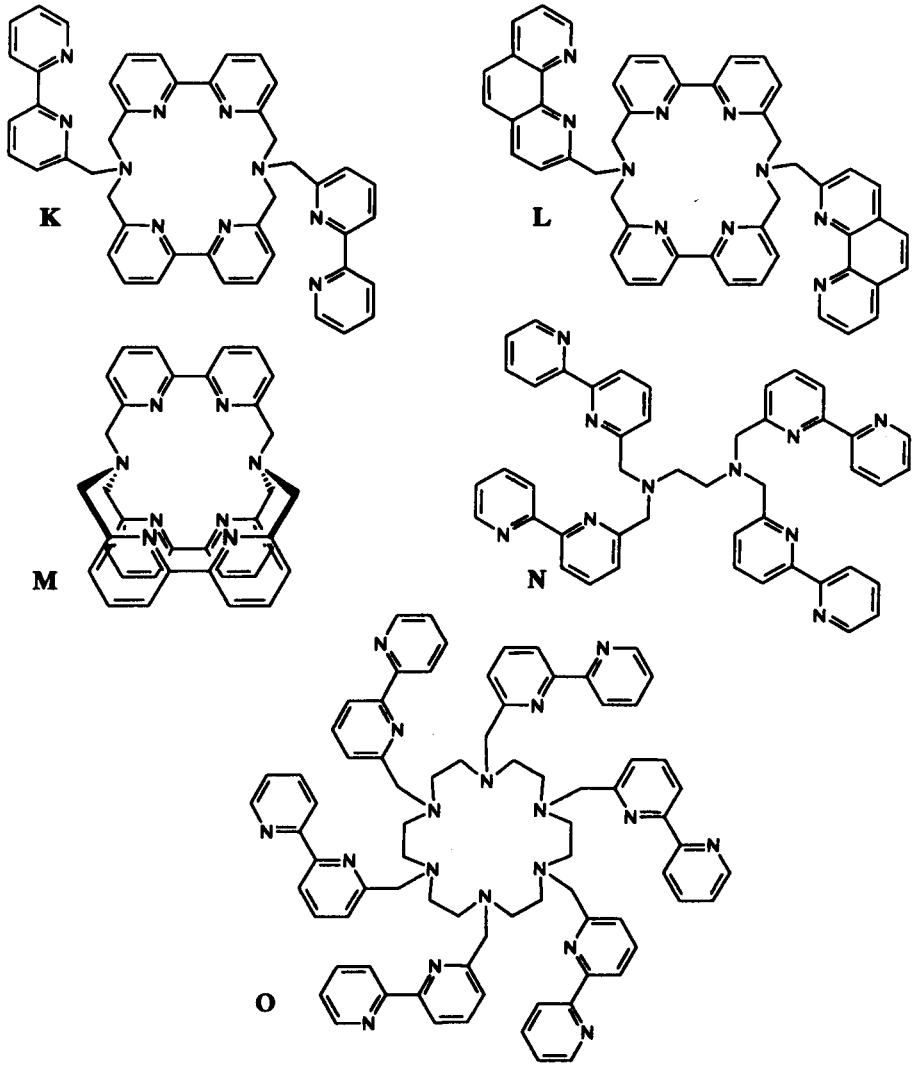

Figure 1.18. Ligands suitable for the formation of luminescent lanthanide complexes.

Eu^{3+} Complexes of tri– and tetrapod ligands undergo dissociation in H_2O,[96] indicating that cryptate or rigid encapsulating macrocyclic ligands are required for the formation

of really stable complexes. Lanthanide complexes of **L** do not decompose in water, unlike those of the related ligand **K**. This is possibly due to the rigidity of the phenanthroline arms.[66] The extent to which the ligand shields the included cation from interactions with solvent molecules is of interest, as coordinated H_2O and CH_3OH molecules assist radiationless decay.[96, 98] As well as being thermodynamically and kinetically stable, lanthanide cryptate complexes provide protection from solvent interactions and promote efficient energy transfer from the ligand to the luminescent metal ion.[109]

Lanthanide 2,2':6',2''–terpyridine complexes have also been studied, although as with the ruthenium systems, the use of terpy has been restricted due to synthetic difficulties with incorporating terpy units into preorganised ligands. Terpy readily forms 1:1 complexes with the lanthanides, 2:1 and 3:1 complexes being less common, the latter forming in the absence of coordinating anions. Terpy analogues have been developed, which are easier to derivatise than terpy itself.[113–115] Some lanthanide complexes with the planar nitrogen ligand mbzimpy (2,6–bis(1–methylbenzimidazol–2–yl)pyridine), which is analogous to terpy, show very efficient light conversion.[116]

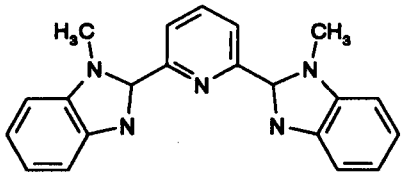

mbzimpy

Terpy derivatives are of interest as ligands for the lanthanides because of the stereochemical preference of these ions for high coordination numbers. Such derivatives have been incorporated into multidentate ligands, which are then used in the development of luminescent triple–helical structures.[117–119]

In this thesis, some new ligands based on azamacrocycles incorporating bipy– and terpy– arms are described.

CHAPTER 2

Chapter 2

1,4,7–Tris(2,2'–bipyridyl–5–ylmethyl)–1,4,7–triazacyclononane, a Sexidentate Ligand Containing Three Pendant Coordinating 2,2'–Bipyridyl Groups.

Polyaza macrocyclic ligands incorporating up to six *N*–functionalised pendant bipyridyl arms are well known.[46, 55, 71, 95 - 98, 112] Such ligands have received considerable attention for the synthesis of photoactive metal complexes, one goal being to produce species of metal ions such as ruthenium(II)[46] and several lanthanides,[98, 112] in which the quantum yields for photodecomposition are very low. In the majority of these ligands, the bipyridyl arms are attached at the 6–position of the bipyridine, and only recently has attachment at the 5–position been developed.[55, 97] The single pendant bipyridyl–arm macrocycle **A**, in which the pendant–arm is attached at the 5–position of the bipyridine, has been shown to be useful for the formation of polynuclear metal complexes in a controlled and systematic fashion.[55] It seemed likely that attaching a bipyridyl arm, at the 5–position of each bipyridine, to all three N–atoms of 9N3 would give a powerful new macrocycle, L^1.

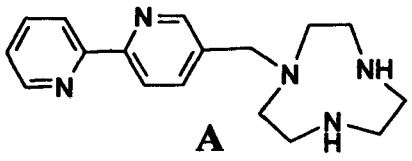

A

It was anticipated that L^1 would be able to coordinate octahedrally to metal ions using all three bipyridyl units rather more readily than **B**, where the three pendant arms are attached at the 6–position of each bipyridine.

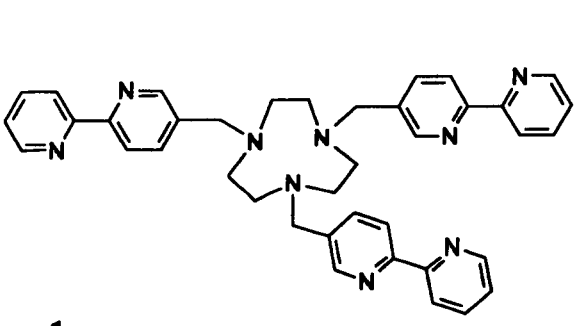

L^1

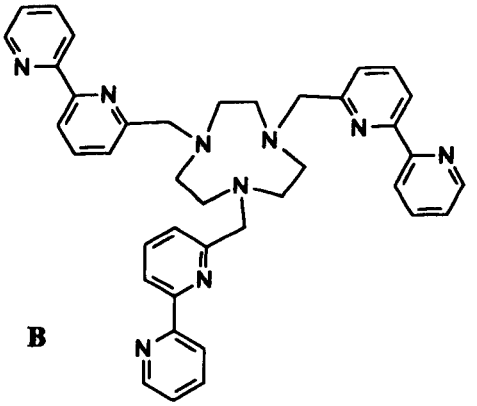

B

The synthesis of L^1 is described, together with the isolation and characterisation of its monomeric Fe(II), Co(II), Ni(II), Cu(II), Zn(II), Ru(II) and Co(III) complexes, and a dimeric Ru(II) compound. The crystal structures of $[M(L^1H)]^{3+}$ (M = Cu, Ru) are also reported.

Results and Discussion.

Synthesis.– L^1 is obtained in good yield from the parent macrocycle 1,4,7–triazacyclononane (9N3) by reaction with three equivalents of 5–(bromomethyl)–2,2'–bipyridine in the presence of a slight excess of triethylamine. The ligand is characterised by its proton and ^{13}C NMR spectra, and by a FAB mass spectrum. In the ^{13}C NMR spectrum in $CDCl_3$, all of the C atoms of the 9N3 ring are equivalent, as are the three methylene carbons of the three pendant arms. There are 10 aromatic carbon resonances, with two overlapping at δ 120.6 p.p.m.

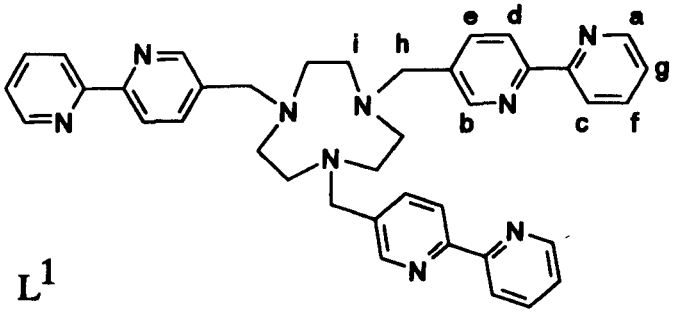

L^1

Figure 2.1. L^1: a – i are the assignments shown in the proton NMR spectrum below (Figure 2.2).

Complexes of L^1.– L^1 reacts with equimolar amounts of labile metal ions such as aqueous or methanolic iron(II), cobalt(II), nickel(II), copper(II) and zinc(II) to give mononuclear complexes of the type $[M(L^1H)]^{3+}$ (M = Fe, Co, Ni, Cu and Zn) in which the macrocycle is monoprotonated and non–coordinating, and all three bipyridyl arms are coordinated (**Figure 2.3**). This is supported by two crystal structures, the FAB mass spectroscopy, NMR studies of the diamagnetic complexes, and by the elemental analyses. Reaction of L^1 with $[Ru\{(CH_3)_2SO\}_4Cl_2]$ gave mononuclear and dinuclear complexes.

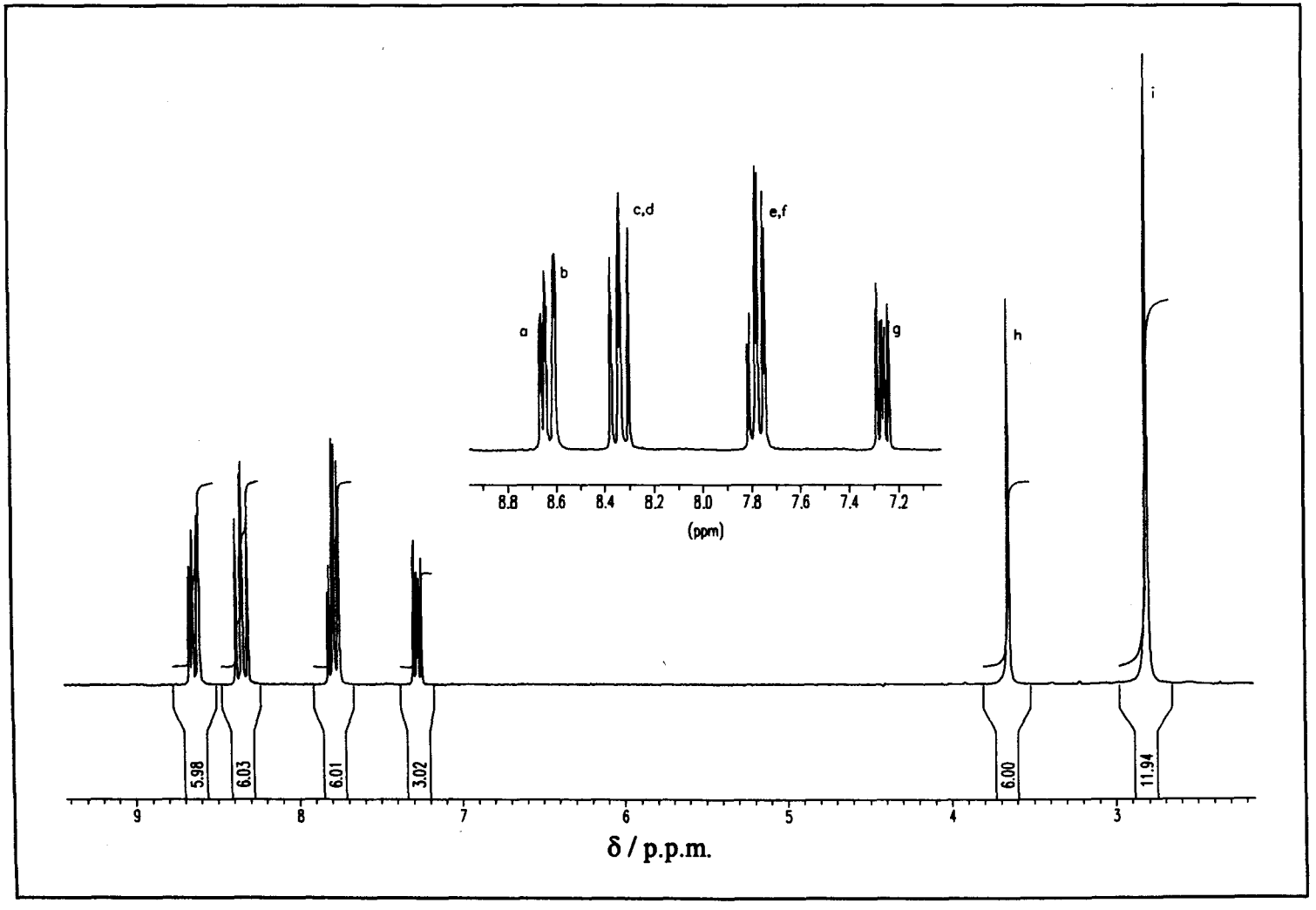

Figure 2.2. Proton NMR Spectrum of L^1 in $CDCl_3$.

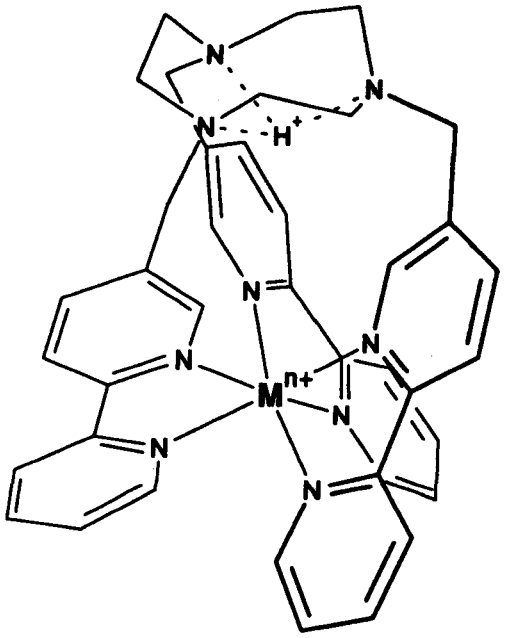

Figure 2.3. Structure of the monomeric complexes of the type $[M(L^1H)]^{n+}$, (M = Fe, Co, Ni, Cu, Zn and Ru).

$[Fe(L^1H)](PF_6)_3$ is obtained as a red crystalline solid. The uv–visible spectrum shows a band with λ_{max} = 520 nm, ε = 7140 $dm^3\ mol^{-1}\ cm^{-1}$, which is similar to that of the $[Fe(bipy)_3]^{2+}$ unit (λ_{max} = 520 nm, ε = 8 650 $dm^3\ mol^{-1}\ cm^{-1}$).[120]

As expected, there are significant differences between the NMR spectra of L^1 and that of its Fe(II) complex. On complexation, the six C atoms of the 9N3 ring split into two groups of three equivalent carbons. In the proton NMR spectrum (**Figure 2.4**), a single acidic proton can be identified as associated with all three N–atoms of the 9N3 ring. The shift of this resonance is temperature dependant, moving from δ 7.79 p.p.m. at 253 K to 7.90 p.p.m. at 315 K. It can just be seen in the 250 MHz proton NMR spectrum (298 K) at δ 7.85 p.p.m. (**Figure 2.4**, inset, left). The two protons of each pendant arm methylene group are non–equivalent and appear as an AB quartet in the room temperature proton NMR spectrum (^2J = –13.5 Hz).

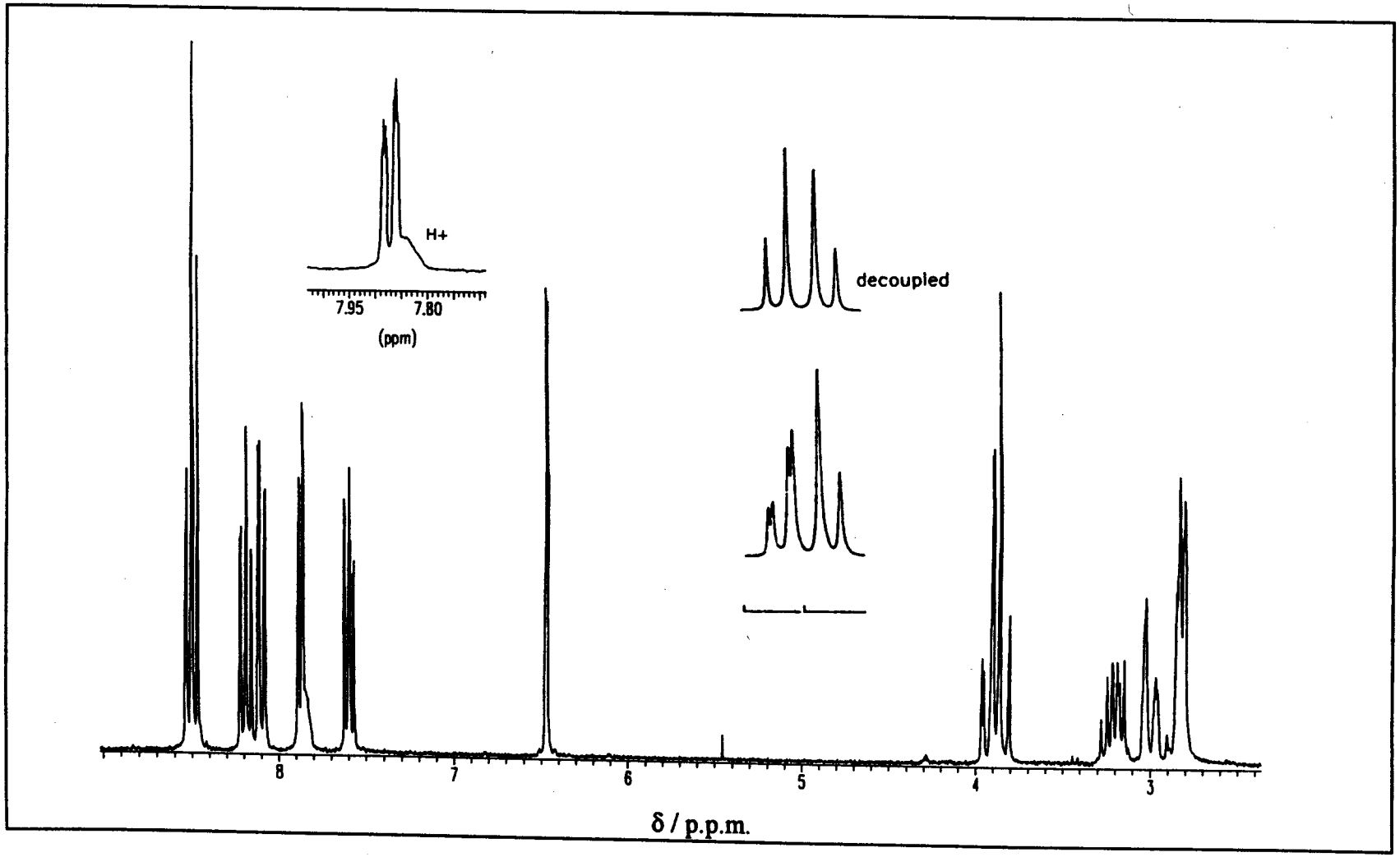

Figure 2.4. Proton NMR Spectrum of $[Fe(L^1H)](PF_6)_3$ in CD_3CN.

This indicates a chiral structure, with slow inter conversion between the two chiral forms, by a trigonal twist process about the C_3 axis. One of the resonances of the AB quartet is split further due to '*trans*' coupling (^3J = 2.9 Hz) to the NH^+ proton of the protonated 9N3 ring. Splitting of the other resonance is less than the line–width of the spectrum. This is because of the smaller coupling to the NH^+ proton when in a '*cis*'–position (as expected from the Karplus relationship). The '*cis*' coupling was calculated for the analogous Ru and Zn complexes, and is detailed below. Decoupling experiments support the assignment of the observed splitting of the AB quartet to the NH^+ proton of the 9N3 ring. When the broad resonance at 7.85 p.p.m. (due to the NH^+ proton of the protonated ring) is irradiated, the split AB quartet at 3.93 p.p.m. becomes a simple quartet – additional coupling having disappeared (**Figure 2.4**, inset, right). The aromatic proton in the 6' position of the bipy ring (H_g, **Figure 2.5**) which appears at δ 8.6 p.p.m. in the free ligand is shifted upfield to δ = 6.5 p.p.m. in the Fe^{2+} complex, a shift of over 2 p.p.m.. This is due to the octahedral geometry adopted on complexation in which H_g lies above the ring current of another pyridine ring. Shifts of a comparable magnitude are observed in the ^1H NMR of the Co(III), Zn(II), monomeric and dimeric Ru(II) complexes. Similar behaviour has also been observed for Ru^{2+} complexes containing tris-2,2'-bipyridyl units.[46, 121] An upfield shift of approximately 1 p.p.m. is observed in $[M(bipy)_3]^{2+}$ complexes.[121]

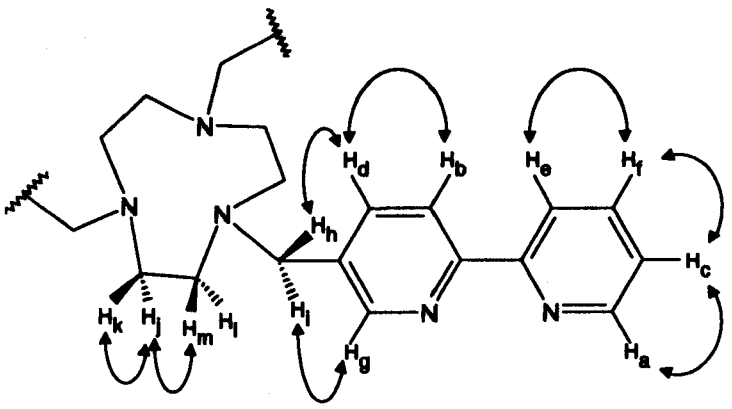

Figure 2.5. Part of the structure of $[Fe(L^1H)](PF_6)_3$ showing observed NOE signals.

Figure 2.5 shows the proximal protons that were established by NOE difference experiments. Also observed were signals between H_e–H_g, and H_k–H_i. It is thought that these interactions were between protons on adjacent bipyridyl arms. NOE effects were not observed between H_b–H_e. It is interesting that in the crystal structures of $[Ru(L^1H)](PF_6)_3$ and $[Cu(L^1H)](ClO_4)_3$, a twist is observed between the pyridyl rings (**Figure 2.6**). If a similar twisting occurs in $[Fe(L^1H)](PF_6)_3$, this would increased the distance between H_b and H_e. This may account for the lack of observed coupling.

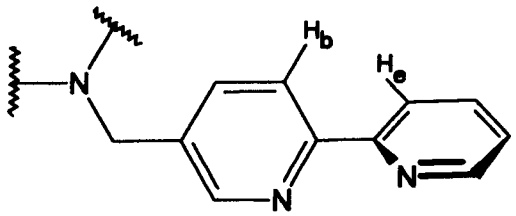

Figure 2.6. Representation of the twisting within bipyridyl arms as observed in the crystal structure of $[Cu(L^1H)](ClO_4)_3$, and to a lesser extent in $[Ru(L^1H)](PF_6)_3$.

Proton NMR spectra of $[Fe(L^1H)](PF_6)_3$ were recorded at four temperatures, 253, 295, 313 and 378 K. At 378 K broadening of all resonances can be seen, possibly indicating that the molecule is interchanging between the two optical isomers. Rapid inter conversion is not occurring at this temperature, as this would probably involve

passing through a trigonal structure in which the bridging CH_2 units and 9N3 ring protons would become equivalent, and so should collapse to form two singlets.

Isolation of the analogous compound $[Fe(B)](PF_6)_2$ has not been achieved to date.[46] It is suggested that the complex forms then decomposes readily in aqueous solution.

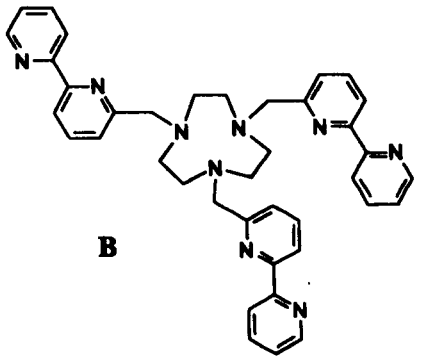

B

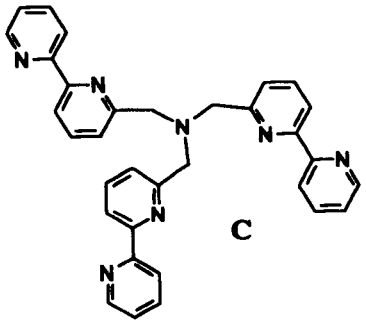

C

The instability of this complex is attributed to the steric constraints of **B** which are against octahedral complexation of the three bipy arms around a single Fe(II) cation. **C**, a less constrained ligand, does form a stable complex with Fe(II).[46]

Reaction of L^1 with $[Ru\{(CH_3)_2SO\}_4Cl_2]$ gave an orange powder, which based on elemental analyses and NMR spectra is tentatively assigned a dimeric structure with the formula $[Ru_2L^1{}_2H](PF_6)_5.2H_2O$. The likely structure is shown in **Figure 2.7.**

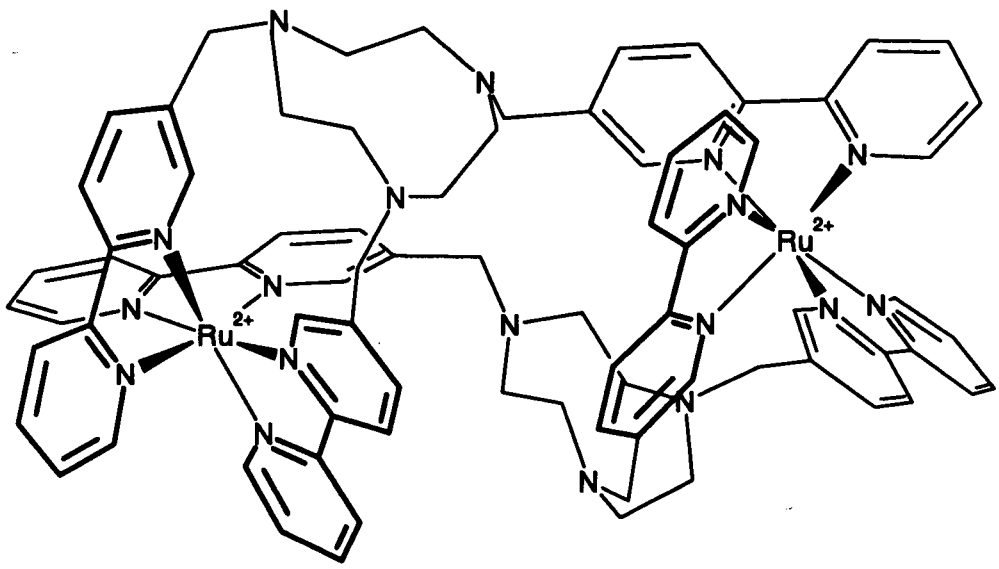

Figure 2.7. Proposed structure of $[Ru_2L^1{}_2H]^{5+}$.

This is supported by elemental analysis. The ^{13}C NMR spectrum (summarized with the elemental analyses in **Table 2.1**) shows 20 upfield (aromatic) resonances, 10 of which are at approximately half the height of the other resonances. Only 10 resonances in this region would be expected for a monomeric complex. There are 3 resonances for the 9N3 ring, two would be expected for a monomeric complex. There are also two resonances for the linking methylene protons, one at half height. The proton NMR spectrum (**Figure 2.8**) is also consistent with formation of a dimeric complex. The linking methylene protons (**Figure 2.9**) split into two groups, one group appears as an AB quartet centred at 4.02 p.p.m. The total integral value of the quartet is 8H. Coinciding in the middle of this quartet is a singlet (δ 4.05 p.p.m.) with a relative integral of 4H.

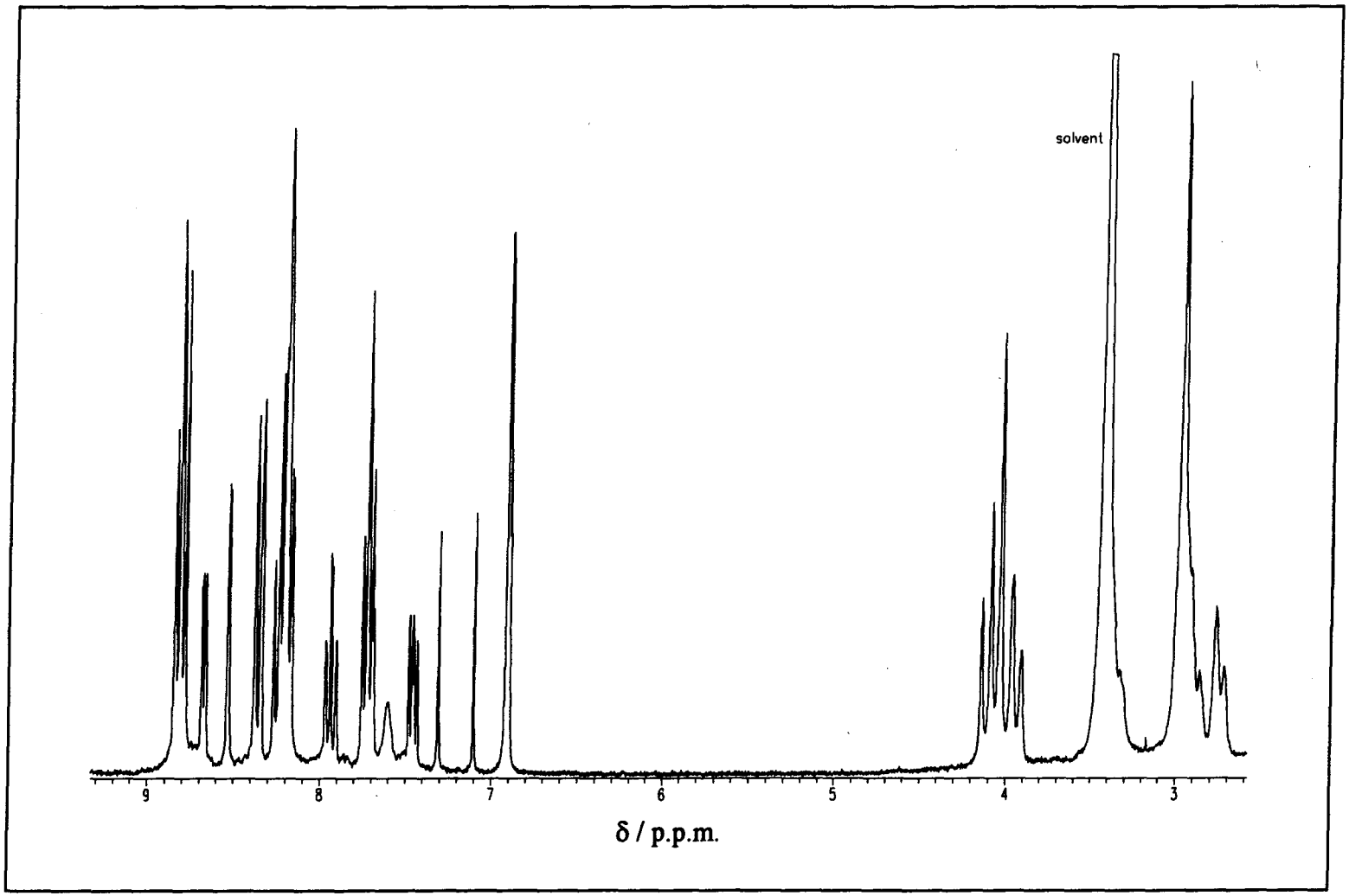

Figure 2.8. Proton NMR Spectrum of $[Ru_2(L^1{}_2H)](PF_6)_5.2H_2O$ in $(CD_3)_2SO$.

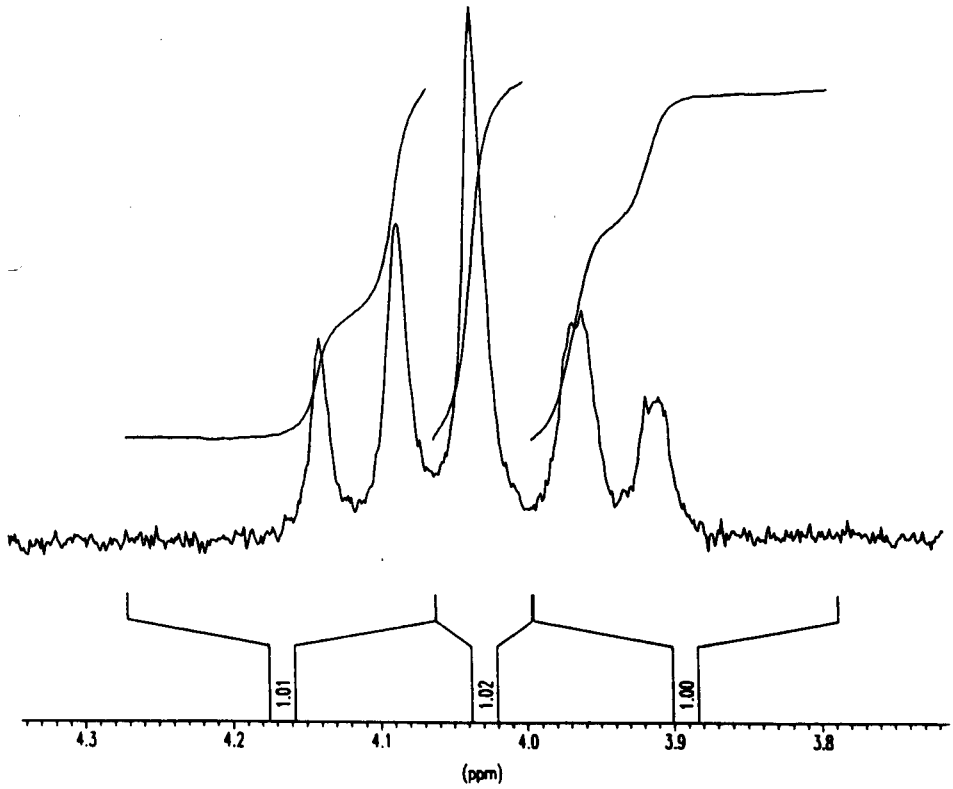

Figure 2.9. Expansion of the proton NMR spectrum of $[Ru_2L^1{}_2H](PF_6)_5.2H_2O$. in $(CD_3)_2SO$ showing resonances assigned to the linking methylene protons.

Curiously, recrystallisation of $[Ru_2L^1{}_2H](PF_6)_5.2H_2O$. from CH_3NO_2 / Et_2O gives red needle crystals of a monomer, $[Ru(L^1H)](PF_6)_3$. Elemental analysis, a FAB mass spectrum, plus proton and ^{13}C NMR spectra confirmed this formulation. It is thought that a slow inter conversion from dimer to monomer occurs in solution. The proton NMR spectrum of the monomeric form is shown below (**Figure 2.10**).

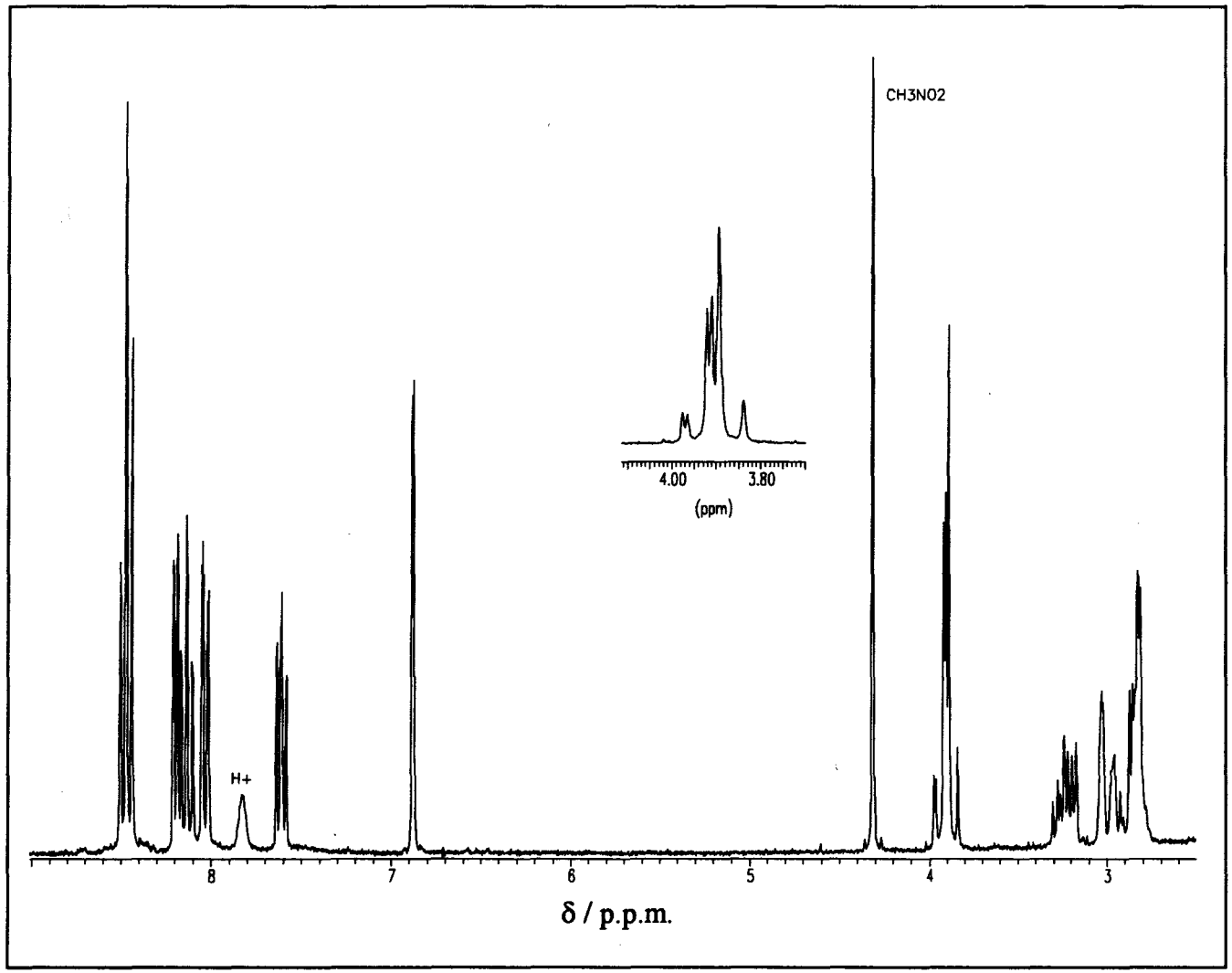

Figure 2.10. Proton NMR Spectrum of $[Ru(L^1H)](PF_6)_3$ in CD_3NO_2.

As expected, the proton NMR spectrum of $[Ru(L^1H)](PF_6)_3$ is similar to that of the analogous Fe(II) complex shown above (**Figure 2.4**). $[Ru(L^1H)](PF_6)_3$ is symmetric (all three bipy arms are equivalent). The two protons of each pendant-arm methylene group are non-equivalent and appear as a single split AB quartet ($^2J = -13.7$ Hz) centred at δ 3.90 p.p.m. As with $[Fe(L^1H)](PF_6)_3$, the single N–H^+ proton shows a strong '*trans*' ^3J coupling to one of each of the CH_2 linking protons ($^3J = 2.9$ Hz) and a weaker '*cis*' coupling to each of the other CH_2 protons ($^3J = 0.47$ Hz). All three coupling constants were calculated from a simulation of the AB quartet. **Figure 2.11** shows the simulated and observed proton NMR spectra.

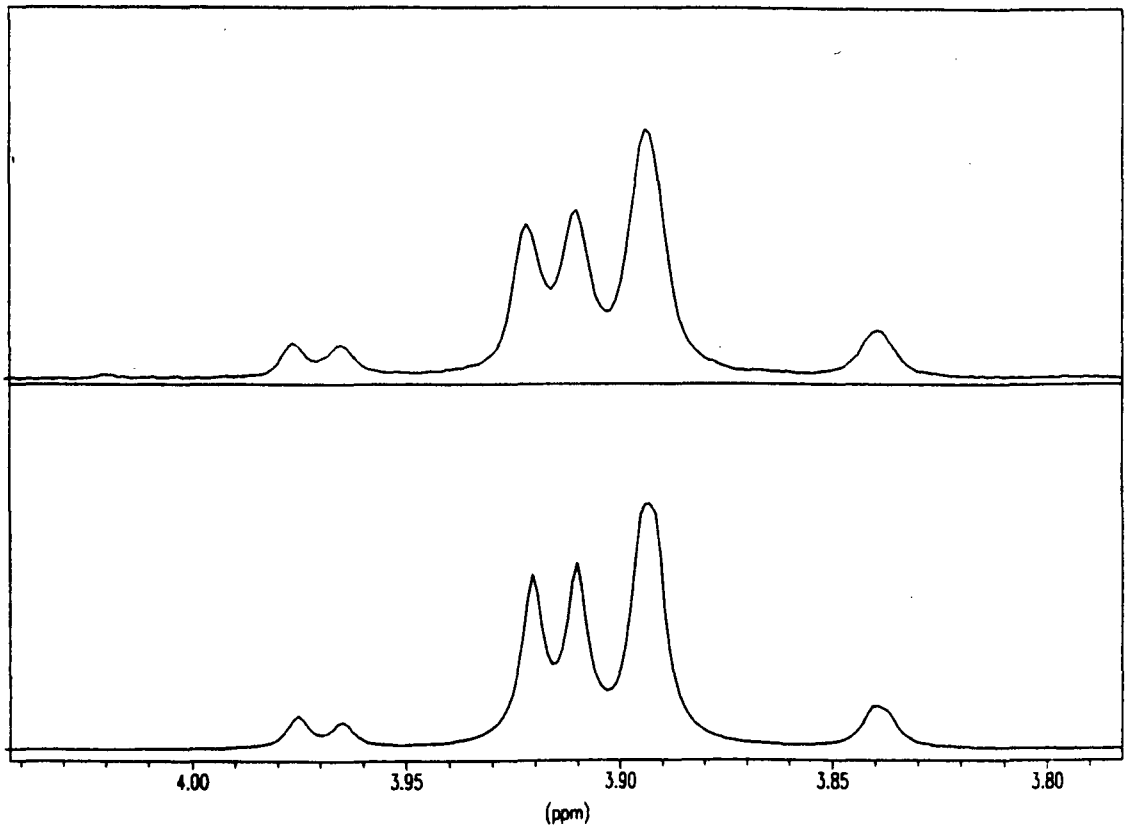

Figure 2.11. Comparison of the observed split AB quartet from the proton NMR resonances of the pendent CH_2 groups of $[RuL^1H]^{3+}$ in CD_3NO_2 (*upper trace*) with that calculated using the Bruker simulation program WINDAISY (*lower trace*).

	monomer	dimer
formula	$C_{39}H_{40}F_{18}N_9P_3Ru$	$C_{78}H_{79}F_{30}N_{18}P_5Ru_2.2H_2O$
found **calculated**	C, 39.95, H, 3.72, N, 10.74, C, 40.01, H, 3.44, N, 10.77 %.	C, 41.55, H, 3.75, N, 11.36, C, 41.98, H, 3.75, N, 11.30 %.
^{13}C NMR (100.62 MHz, $(CD_3)_2SO$), δ / p.p.m. (relative populations in parentheses).	156.71 (3), 156.68 (3), 151.9 (3), 151.6 (3), 139.3 (3), 138.2 (3), 136.9 (3), 128.3 (3), 125.0 (3), 124.5 (3), 56.3 (3), 49.5 (3), 48.6 (3).	156.6 (4), 156.5 (4), 155.1 (2), 154.6 (2), 151.7 (4), 151.4 (4), 150.1 (2), 149.0 (2), 139.1 (4), 138.3 (2), 137.9 (4), 137.1 (2), 136.6 (4), 130.9 (2), 128.0 (4), 124.7 (4), 124.3 (4), 124.1 (2), 120.5 (2), 120.3 (2), 56.3 (4), 55.9 (2), 49.3 (4), 49.1 (4), 48.5 (4).

Table 2.1. Comparison of the ^{13}C NMR spectra and elemental analysis results for $[Ru(L^1H)](PF_6)_3$ and $[Ru_2L^1{}_2H](PF_6)_5.2H_2O$.

For the monomeric complex, elemental analysis confirms the presence of a single proton coupled to all three N atoms of the 9N3 ring (supported by the proton NMR spectrum). The proton is firmly held in the cavity between metal ion and 9N3 ring. Strong base was added in an attempt to see the effect of removing the trapped proton on the fluorescence of the ruthenium complex. However, a proton NMR spectrum showed there to be no evidence for loss of this proton, or for H–D exchange after heating in D_2O / NaOD (pH 14) at 70 °C for 1 h.

$[Ru(L^1H)](PF_6)_3$ is fluorescent, an aqueous solution of this complex emits light centred on 607 nm when excited at 450 nm, which is characteristic of the $[Ru(bipy)_3]^{2+}$ unit.[122] The intensity of this fluorescence is much reduced when compared to that of the parent $[Ru(bipy)_3]^{2+}$ chromophore. The fluorescence intensity of an aqueous solution of $[Ru(L^1H)](PF_6)_3$ (2×10^{-6} mol dm^{-3}) was found to be only 13 % of that of an aqueous solution of $[Ru(bipy)_3]^{2+}$ at the same concentration. Two possible reasons for this are suggested; firstly the geometry around the Ru cation is somewhat strained. Secondly the presence of the proton trapped close to the $[Ru(bipy)_3]^{2+}$ unit may cause some fluorescence quenching. Azamacrocyclic ligands containing $[Ru(bipy)_3]^{2+}$ unit(s) discussed below (Chapter 3) were found to show a much reduced fluorescence intensity in acidic solution, compared to basic solutions of the same concentrations. No luminescence was found for the mononuclear complex $[Ru(C)]^{2+}$ (C is shown on Page 33) at room temperature in various solvents.[46] This lack of luminescence was partially attributed to steric hindrance at the Ru centre, and to distortion of the coordination octahedron.

A single crystal of $[Ru(L^1H)](PF_6)_3$ was investigated by X–ray crystallography. As expected, this shows the ruthenium atom to be in an octahedral environment, coordinated to all three bipy arms (**Figure 2.12**). Three uncomplexed $[PF_6]^-$ groups were located in the lattice confirming the analytical data and the presence of a protonated ligand complex. Selected bond lengths and angles are collected below (**Table 2.2**), together with values reported for $[Ru(bipy)_3]^{2+}$ for comparison.[123, 124, 125] It can be seen that anchoring the three bipy groups to 9N3 results in a geometry that is similar to that found in the $[Ru(bipy)_3]^{2+}$ ion, although in water the visible spectrum of $[Ru(bipy)_3]^{2+}$ (λ_{max} = 452 nm, ε = 14 600 dm^3 mol^{-1} cm^{-1})[122] is somewhat different to that of $[Ru(L^1H)]^{3+}$ (λ_{max} = 468 nm, ε = 9 500 dm^3 mol^{-1} cm^{-1}). From the crystal structure, the trapped NH^+ proton is calculated to be 4.8–4.9 Å away from the Ru centre, and thus too far away to form a hydride bond.

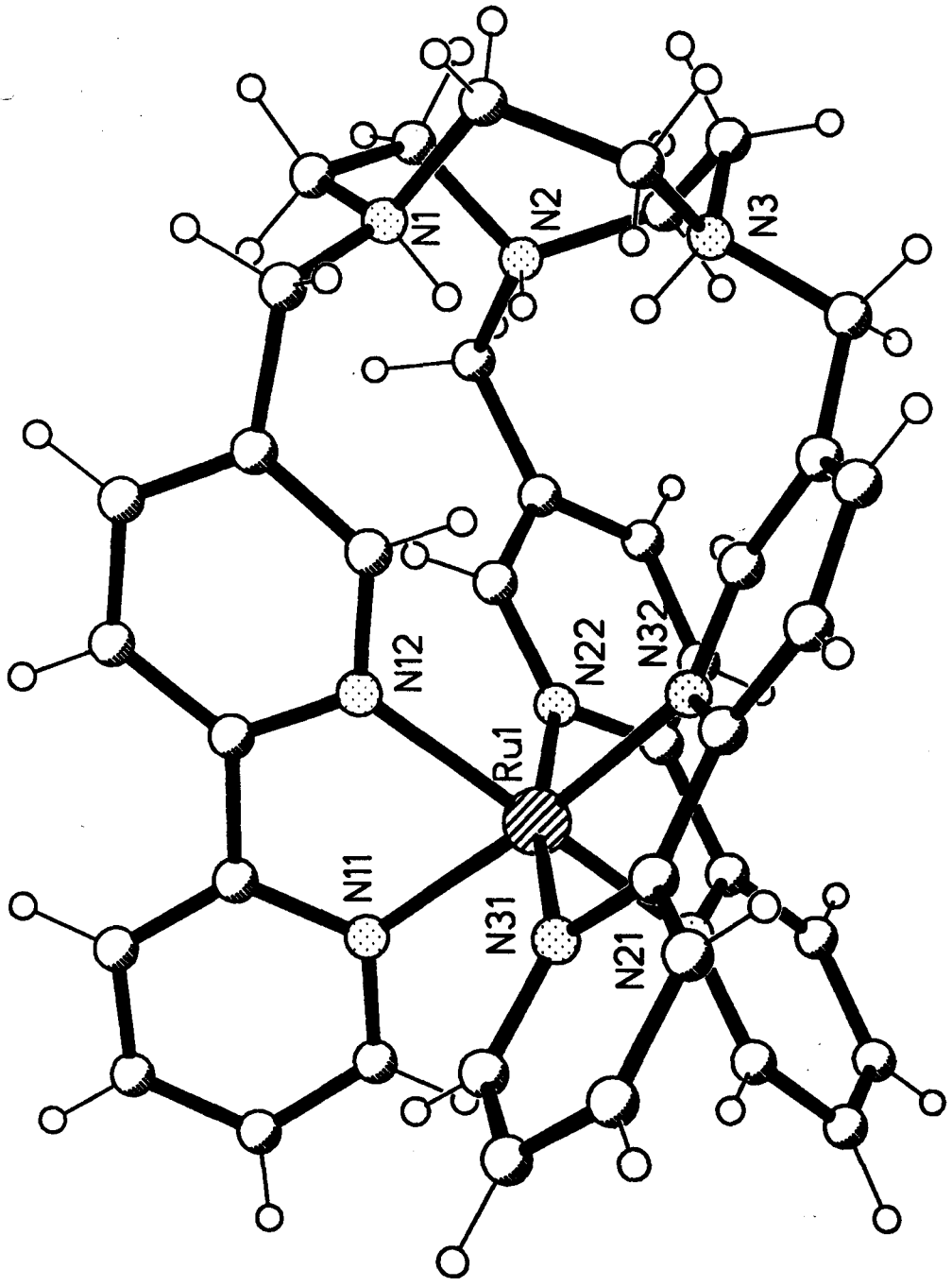

Figure 2.12. The molecular structure of the $[Ru(L^1H)]^{3+}$ ion from the X-ray structure determination, showing the atomic numbering.

Ru1	Distance / Å	Angles / °				
N32	2.036(6) *2.053(2)*					
N21	2.039(6) *2.053(2)*	93.6(2) *89.4(2)*				
N22	2.040(6) *2.053(2)*	92.0(2) *95.7(1)*	79.1(2) *78.6(2)*			
N11	2.041(6) *2.053(2)*	169.3(2) *172.6(2)*	96.0(2) *95.7(1)*	94.4(2) *89.4(2)*		
N12	2.048(6) *2.053(2)*	92.5(2) *95.7(12)*	168.7(2) *172.6(2)*	91.3(2) *95.7(1)*	78.9(2) *78.6(2)*	
N31	2.051(6) *2.053(2)*	78.6(2) *78.6(2)*	96.6(2) *95.7(1)*	169.4(2) *172.6(2)*	95.6(2) *95.7(12)*	93.9(2) *89.4(2)*
	Ru1	**N32**	**N21**	**N22**	**N11**	**N12**

Table 2.2. Comparison of selected bond lengths and angles in the complex $[Ru(L^1H)]^{3+}$ at 225 K with those in $[Ru(bipy)_3]^{2+}$ at 105 K (from ref. 123, in *italics*). Standard deviations are in parentheses.

Attempts were made to investigate the conversion from dimer to monomer by proton NMR. Proton NMR spectra of a sample of $[Ru_2L^1{}_2H](PF_6)_5.2H_2O$ in CD_3NO_2 were recorded after lengthening time intervals (0.5, 1, 2, 5 and 24 h) but no sign of conversion was observed. The same sample was then placed under an atmosphere of Et_2O, fine red needles grew from the resulting Et_2O / CD_3NO_2 solution over three to four days. Proton NMR showed these to be the monomeric $[Ru(L^1H)](PF_6)_3$.

Reaction of L^1 with aqueous Co(II), Ni(II), Cu(II) and Zn(II) also gave monomeric complexes of the form $[M(L^1H)](PF_6)_3$. Treatment of a solution of L^1 and Co(II) gave a Co(III) complex. Proton NMR spectra of the Co(III) and Zn(II) complexes are analogous to the spectrum of $[FeL^1H](PF_6)_3$ already described. The proton NMR spectrum of the Zn(II) complex is shown below (**Figure 2.14**) as it clearly shows the broad singlet at δ = 8.13 p.p.m. which is attributed to the NH^+ proton of the protonated 9N3 ring. As in the proton NMR spectra of the other diamagnetic comlexes of the form $[M(L^1H)]^{3+}$, the two protons of each pendant–arm methylene group are non-equivalent and appear as a split AB quartet. Simulation of this quartet allowed three coupling constants to be calculated; ^2J = –13.6 Hz, ^3J = 3.3 Hz ('*trans*'), ^3J = 0.65 Hz ('*cis*'). **Figure 2.13** shows the simulated and observed spectra.

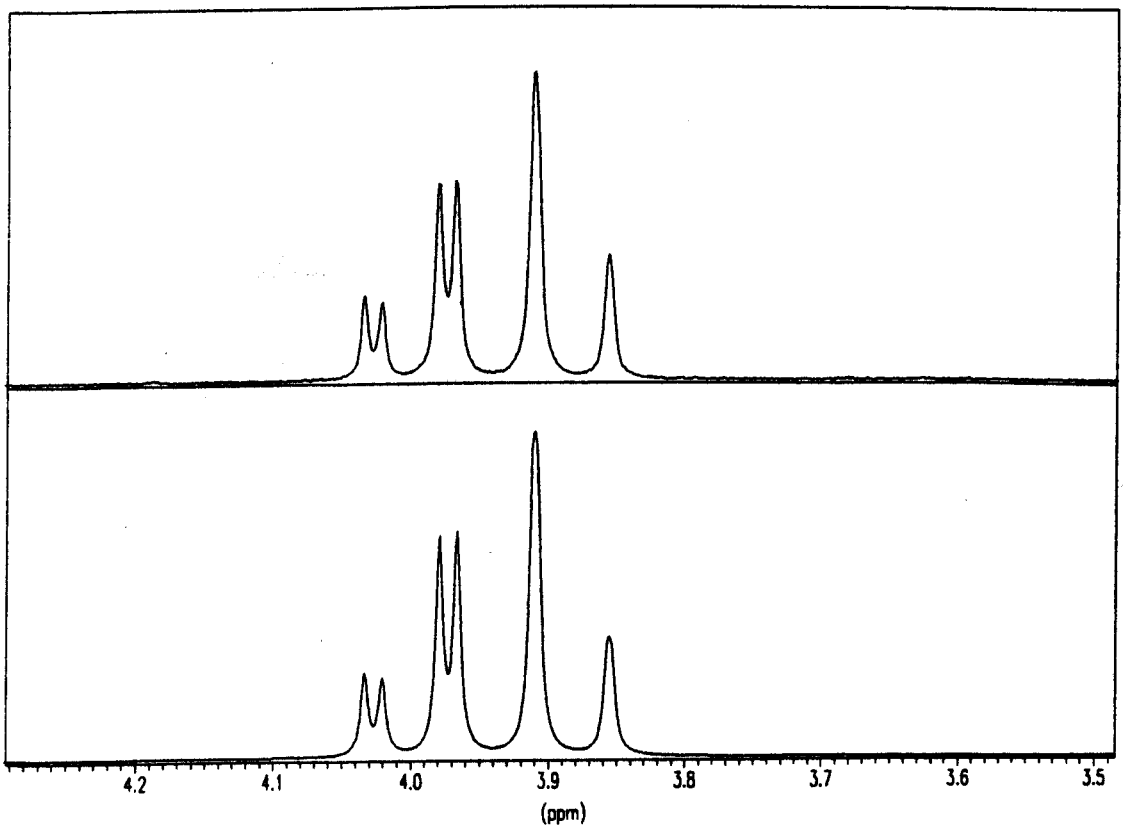

Figure 2.13. *Upper trace*: Observed split AB quartet in the proton NMR spectrum of $[Zn(L^1H)](PF_6)_3$. *Lower trace*: Simulated spectrum.

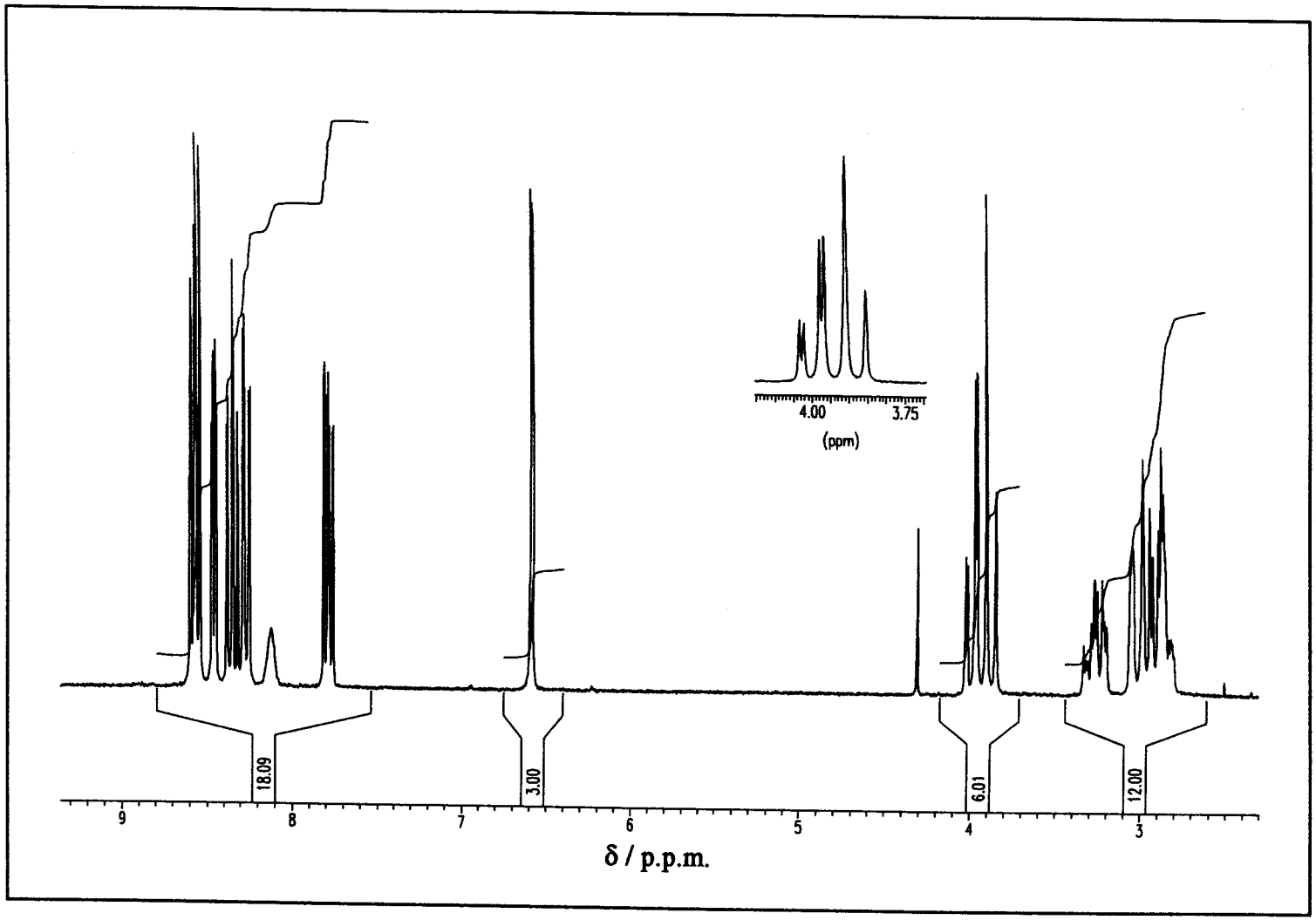

Figure 2.14. Proton NMR spectrum of $[Zn(L^1H)](PF_6)_3$ in CD_3CN

The proton NMR spectrum of the paramagnetic Co(II) complex was obtained (**Figure 2.15**). As expected, this shows fourteen resonances with a total integral value of 40. There are 7 resonances associated with the bipy arms (21H), 2 resonances associated with the bridging protons, (6H, axial and equatorial protons being non-equivalent), 4 resonances associated with the 9N3 ring (2 different types of C atoms, axial and equatorial protons on each), and a single resonance associated with the proton attached to the nitrogen atoms of the 9N3 ring, (1H). Close examination of the spectrum reveals further splitting of the resonances at δ = 9.9, –2.2, –3.3 and -3.9 p.p.m., with coupling constants of 12.5 and 13.9 Hz. Like $[Co(bipy)_3]^{2+}$, $[Co(L^1H)][PF_6]_3$ is a high spin system.

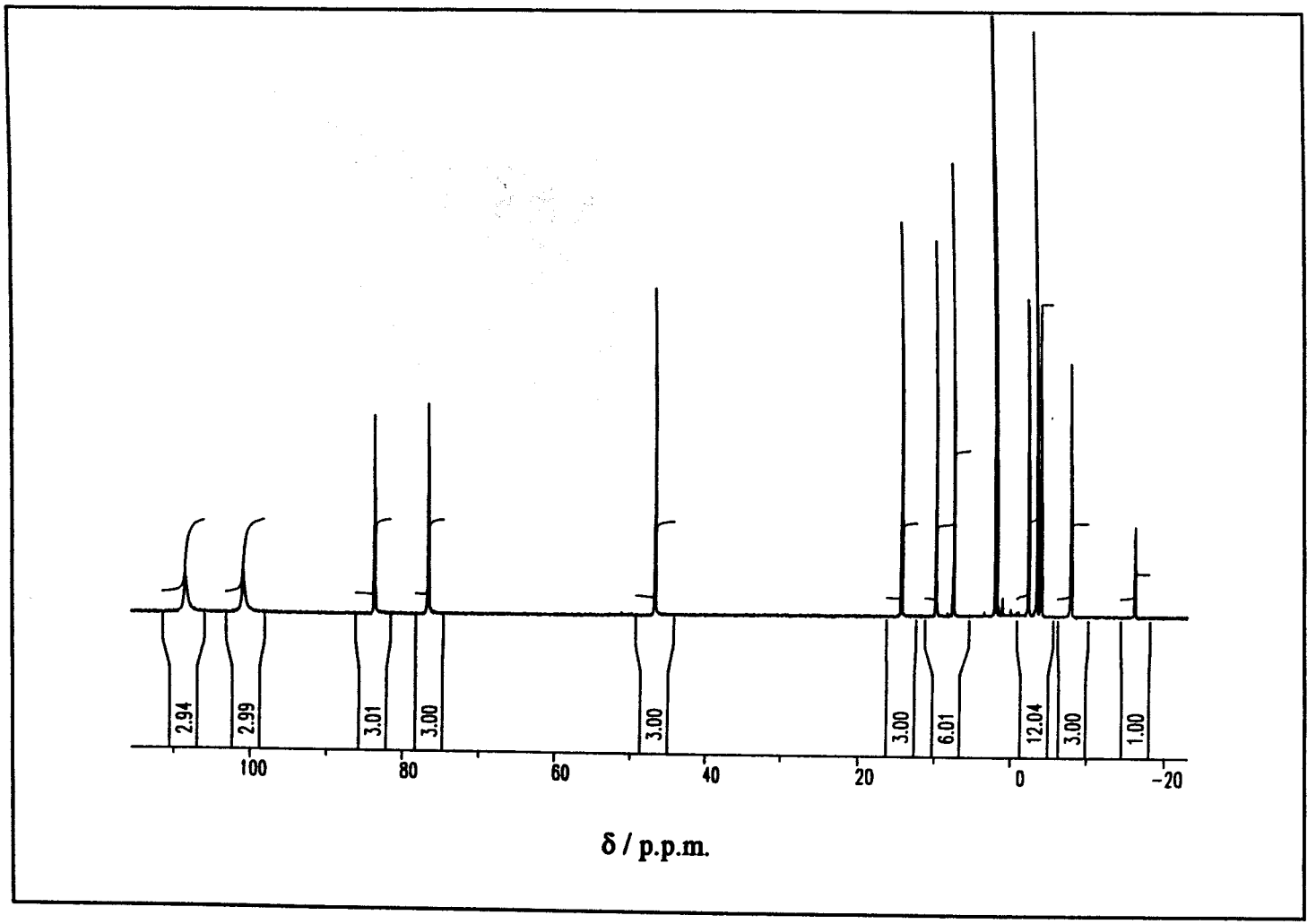

Figure 2.15. Proton NMR Spectrum of $[Co(L^1H)](PF_6)_3$ in CD_3NO_2.

A single crystal of $[Cu(L^1H)](ClO_4)_3$ was investigated by X-ray crystallography. Curiously, this shows two distinct cations, $[Cu^1(L^1H)]^{3+}$ and $[Cu^2(L^1H)]^{3+}$ (**Figures 2.16** and **2.17** respectively). As with the $[Ru(L^1H)]^{3+}$ structure, both Cu^1 and Cu^2 are six coordinate and in an octahedral environment, coordinated to all three bipyridyl arms of L^1. Selected bond lengths and angles are shown in **Tables 2.3** and **2.4.**

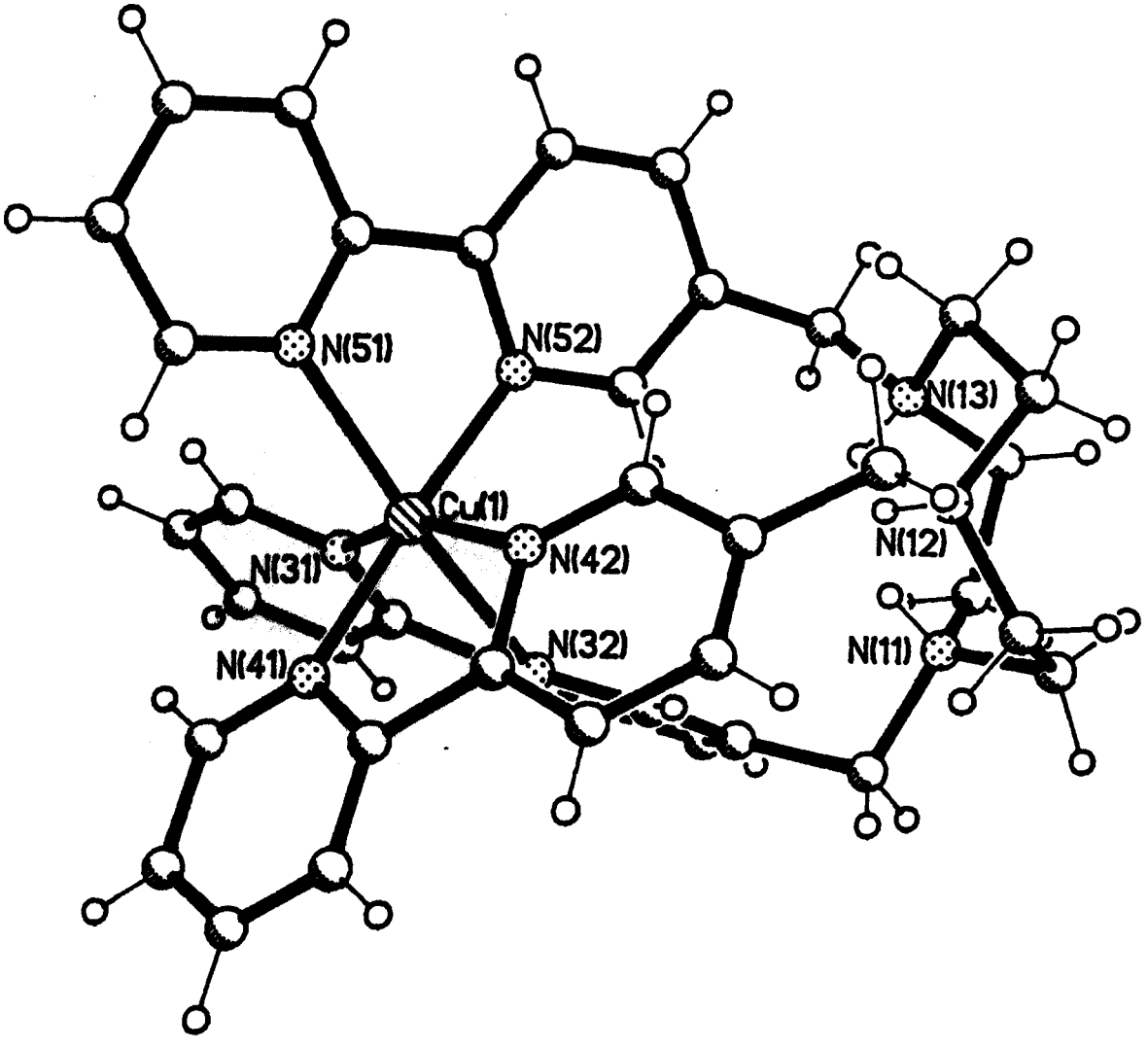

Figure 2.16. The molecular structure of $[Cu^1(L^1H)]^{3+}$.

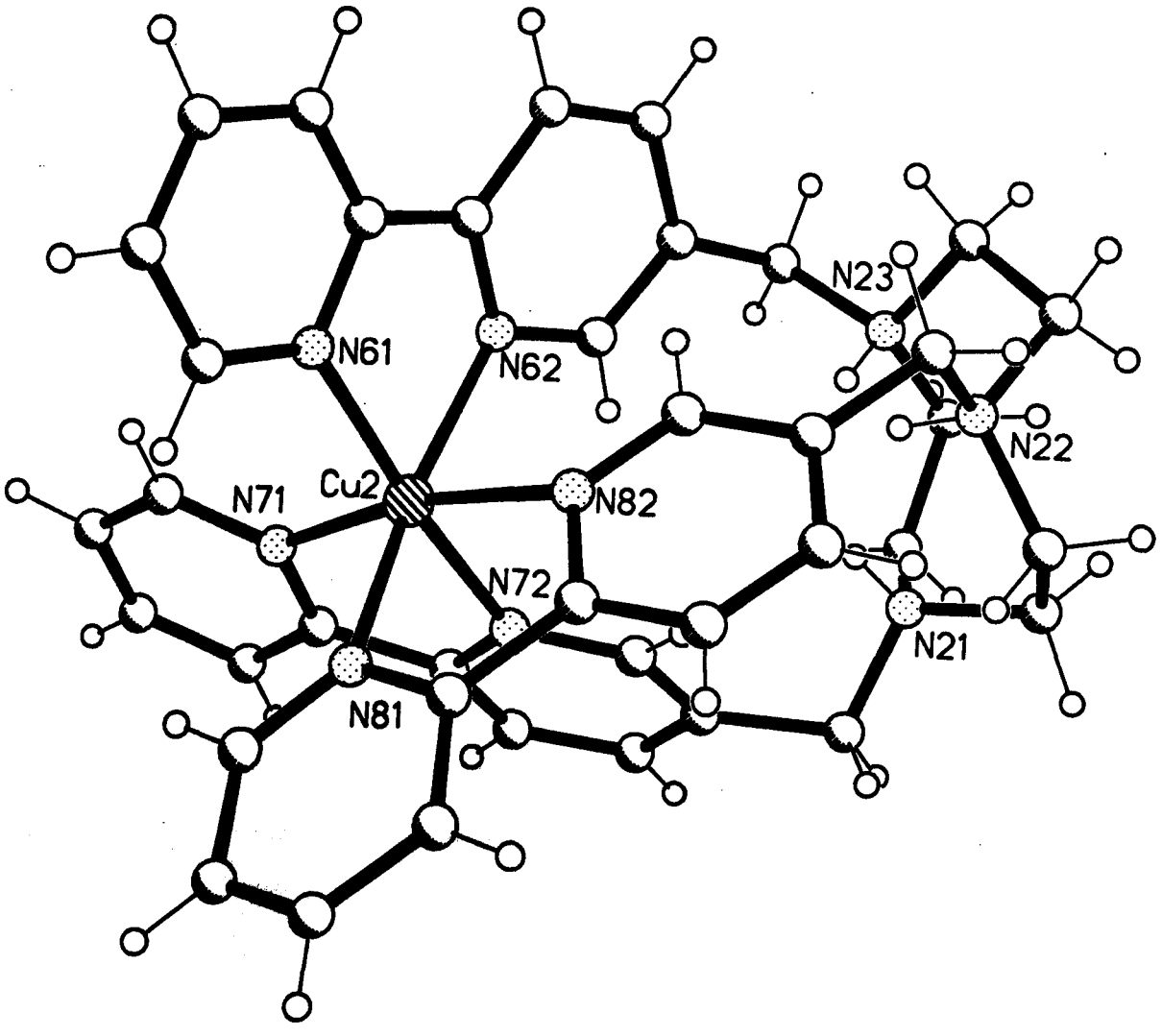

Figure 2.17. The molecular structure of $[Cu^2(L^1H)]^{3+}$.

Cu1 –	Distance / Å	Angle / °				
N31	2.036(11) *2.026(5)*					
N32	2.358(11) *2.450(7)*	74.1(4) *73.9(2)*				
N41	2.024(12) *2.034(8)*	93.6(5) *94.0(3)*	85.6(4) *83.6(3)*			
N42	2.024(12) *2.035(5)*	159.4(4) *165.6(2)*	85.6(4) *92.2(2)*	81.1(5) *80.4(3)*		
N51	2.246(11) *2.226(7)*	100.1(4) *101.6(2)*	169.8(4) *174.8(2)*	103.4(4) *99.5(3)*	100.5(4) *92.4(2)*	
N52	2.027(11) *2.030(8)*	91.9(4) *91.6(3)*	95.2(4) *99.1(3)*	174.5(5) *174.8(2)*	93.5(5) *94.4(3)*	76.4(5) *78.2(3)*
	Cu1	**N31**	**N32**	**N41**	**N42**	**N51**

Table 2.3. Comparison of selected bond lengths and angles in $[Cu^1(L^1H)]^{3+}$ with those in $[Cu(bipy)_3]^{2+}$ (from ref. 126, in *italics*). Standard deviations are in parentheses.

Cu2 –	Distance / Å	Angle / °				
N61	1.977(12)					
N62	2.202(12)	77.0(5)				
N71	2.082(12)	98.2(5)	96.1(4)			
N72	2.047(11)	169.2(5)	92.9(5)	79.0(5)		
N81	2.178(14)	98.3(5)	164.2(4)	99.5(5)	92.4(4)	
N82	2.197(11)	90.9(4)	89.8(4)	170.1(5)	92.7(4)	75.1(5)
	Cu2 –	N61	N62	N71	N72	N81

Table 2.4. Selected bond lengths and angles in $[Cu^2(L^1H)]^{3+}$, standard deviations are in parentheses.

From this data it can be seen that there are four 'short' and two 'long' Cu–N bonds in $[Cu^1(L^1H)]^{3+}$, but three 'short' and three 'long' bonds in $[Cu^2(L^1H)]^{3+}$. $[Cu^1(L^1H)]^{3+}$ shows the type of Jahn–Teller distortion commonly found in six coordinate Cu(II) structures, i.e. elongation along one axis. This type of distortion is found in the X–ray determination of $[Cu(bipy)_3]^{2+}$, selected data are collected in **Table 2.3** for comparison.[126]

As the three bipyridyl–arms in L^1 are anchored at one end by the 9N3 ring, some strain is bound to occur when they are coordinated to a ***single*** metal ion. This strain may contribute to the more unusual distortion found around Cu^2. This strain must also be present in $[Cu^1(L^1H)]^{3+}$ and a twisting can be seen within the bipyridyl arms, most particularly that arm containing N31 and N32 (**Figure 2.16**). Selected torsion angles are given below (**Table 2.5**).

	Angle / °	Atoms
$[Cu^1(L^1H)]^{3+}$	20.33(1.60)	N31–C35–C36–N32
	-2.52(1.58)	N41–C45–C46–N42
	2.34(1.65)	N51–C55–C56–N52
$[Cu^2(L^1H)]^{3+}$	5.99(1.69)	N61–C65–C66–N62
	5.73(1.73)	N71–C75–C76–N72
	4.68(1.69)	N81–C85–C86–N82

Table 2.5. Selected torsion angles in $[Cu^1(L^1H)]^{3+}$and $[Cu^2(L^1H)]^{3+}$.

From simple entropic considerations, L^1 is presumed to chelate more strongly to a metal ion than three 2,2'–bipyridine ligands.

$$[MS_6]^{n+} + 3(bipy) \rightleftharpoons [M(bipy)_3]^{n+} + 6S \qquad \text{Eqn. 2.1}$$

$$[MS_6]^{n+} + L^1 \rightleftharpoons [ML^1]^{n+} + 6S \qquad \text{Eqn. 2.2}$$

The entropy gained in forming $[M(bipy)_3]^{n+}$ (Eqn. 2.1) is expected to be less than that gained in forming $[ML^1]^{n+}$ (Eqn. 2.2). (However, the larger L^1 may lose more 'translational entropy' on complexation than three bipy ligands). An NMR study with Zn(II) confirms that L^1 chelates to the metal ion more strongly than three equivalents of bipy. A solution of $[Zn(L^1H)](PF_6)_3$ in CD_3CN was shaken with three molar equivalents of 2,2'–bipyridine. The proton NMR spectrum of this solution was then obtained. The upfield region of the spectrum remained comparable to that taken previously of $[Zn(L^1H)]^{3+}$, therefore L^1 had not been displaced (either wholly or partially) from the Zn (II) ion by bipy. A solution of $[Zn(bipy)_3]^{2+}$ in CD_3CN was shaken with one equivalent of L^1 and the proton NMR spectrum taken. This also showed no evidence of free L^1 (which has two upfield singlets at 3.69 and 2.84 p.p.m.). The L^1 must therefore have coordinated though at least one pendant–arm to the Zn(II) ions, displacing the bipy ligands. Multiplets attributed to the 9N3 ring

protons can be seen between 3.2 and 2.3 p.p.m., and an AB quartet centred at 3.58 p.p.m. is assigned to the majority of the linking methylene protons. A lower intensity split AB quartet centred at 3.93 p.p.m. can be seen, this is characteristic of $[Zn(L^1H)]^{3+}$.

Aspects of the uv–visible absorption spectra of the Fe, Ru, Co, Ni and Cu complexes are compared with the corresponding $[M(bipy)_3]^{2+}$ analogues in **Table 2.6.** It can be seen that the spectra of some complexes are somewhat different to their bipy analogues.

Coordination entity	λ_{max} / nm (ε / $dm^3\ mol^{-1}\ cm^{-1}$)
$[Fe(L^1H)]^{3+}$	520 (7 140)[a]
$[Fe(bipy)_3]^{2+}$ [120]	522 (8 650)[a]
$[Ru(L^1H)]^{3+}$	468 (9 500)[a]
$[Ru(bipy)_3]^{2+}$ [122]	452 (14 600)[a]
$[Co(L^1H)]^{3+}$	480 (61.0)[b]
$[Co(bipy)_3]^{2+}$	460 (shoulder, ≈130)[b]
$[Co(L^1H)]^{4+}$	445 (shoulder, 252)[b]
$[Co(bipy)_3]^{3+}$ [127]	440 (shoulder, 94)[a]
$[Ni(L^1H)]^{3+}$	528 (21.0), 800 (10.4), 860 (9.6)[b]
$[Ni(bipy)_3]^{2+}$ [128]	521 (12.7), 787 (8.1), 862 (7.3)[c]
$[Cu(L^1H)]^{3+}$	690 (100)[b]
$[Cu(bipy)_3]^{2+}$ [129]	671 (56.2)[c]

[a] measured in H_2O; [b] measured in CH_3CN; [c] measured in CH_3OH/H_2O, 1:3; [d] measured in CH_3NO_2.

Table 2.6. Uv–visible charge transfer and d–d absorption spectra of Ru, Fe, Co, Ni and Cu complexes of L^1 with their bipy analogues.

Experimental

Materials and methods.– 1,4,7–triazacyclononane (9N3) was prepared by the published method.[130] All other chemicals were the best commercially available, and were used without further purification. ^{1}H and ^{13}C NMR spectra were recorded at 250 and 62.89 MHz respectively using a Bruker ACF 250 spectrometer, and at 400 and 100.62 MHz respectively using a Bruker WH 400 instrument. Uv–visible spectra were recorded with a Shimadzu UV–365, and fluorescence spectra were obtained at room temperature, using aerated solutions in quartz cells, with a Perkin–Elmer LS–3 spectrometer. IR Spectra were obtained with a Perkin–Elmer FT–IR 1720 X instrument. Mass spectra were obtained with a Kratos MS80 spectrometer.

*Synthesis of 1,4,7-tris-(2,2'-*bipy*ridyl-5'-ylmethyl)-1,4,7-triazacyclononane*, L^1.–

1,4,7–Triazacyclononane (100 mg, 0.77 mmol), 5–(bromomethyl)–2,2'–bipyridine[6] (580 mg, 2.32 mmol) and Et_3N (252 mg, 2.50 mmol) were refluxed in chlorobenzene (100 cm^3) for 1 h. The solution was then allowed to cool, the resulting white precipitate ($Et_3N.HBr$) removed by filtration, and the solvent evaporated leaving a yellow oil. This was recrystallised from acetonitrile, and the product collected as white needle crystals (Yield 325 mg, 66 %). ^{1}H NMR (250 MHz, $CDCl_3$): δ/p.p.m. 8.65 (m, 6H), 8.35 (t, 6H), 7.80 (m, 6H), 7.30 (m, 3H), 3.69 (s, 6H), 2.84 (s, 12H). ^{13}C NMR (62.89 MHz, $CDCl_3$): δ/p.p.m. (relative populations in parentheses) 156.0 (3), 155.0 (3), 149.8 (3), 149.1 (3), 137.7 (3), 136.8 (3), 123.5 (3), 120.9 (3), 120.6 (6), 60.1 (3), 55.3 (6). Mass spectrum (FAB / NBA): *m/z* 634 (Calc. for L^1H^+, 634).

Synthesis of $[Fe(L^1H)](PF_6)_3$.– $FeSO_4.7H_2O$ (88 mg, 0.32 mmol) was added to a stirred solution of L^1 (200 mg, 0.32 mmol) in CH_3OH (50 cm^3). The solution immediately turned a blood red colour. The solvent was removed on a rotary

evaporator, the residue dissolved in H_2O (5 cm^3) and the solution loaded onto a column of Sephadex SP C-25 cation exchange resin (1 x 10 cm). This was eluted with aqueous 0.1–1.0 mol dm^{-3} NaCl. The main red band, eluted with approximately 0.4 mol dm^{-3} NaCl, was treated with excess NH_4PF_6 to yield a red precipitate which was collected by filtration, recrystallised from $MeOH/H_2O$ (1:1) and dried *in vacuo* over silica gel. Yield 305 mg, 85 %. ^1H NMR (400 MHz, CD_3CN): δ/p.p.m. 8.52 (d, 3H), 8.48 (d, 3H), 8.19 (d, 3H), 8.10 (d, 3H), 7.88 (d, 3H), 7.85 (s, br, 1H), 7.60 (t, 3H), 6.48 (s, 3H), 3.89 (split AB q, 6H), 3.26 to 3.18 (m, 3H), 3.02 to 2.98 (m, 3H), 2.89 to 2.82 (m, 6H). ^{13}C NMR (100.62 MHz, 295 K, $(CD_3)_2SO$): δ/p.p.m. 160.5 (3), 159.9 (3), 157.2 (3), 155.9 (3), 141.2 (3), 140.2 (3), 137.2 (3), 128.8 (3), 125.2 (3), 125.1 (3), 57.6 (3), 50.1 (3), 49.7 (3). Mass spectrum (FAB / NBA): *m/z* 982 (Calc. for $[FeL^1H_2(PF_6)_2]^+$, 982), negative ion spectrum; 145 (PF_6^-). Uv-visible spectrum in H_2O [λ_{max}/nm (ε / dm^3 mol^{-1} cm^{-1})]: 520 (7 140), 359 (5 830), 296 (59 900), 250 (30 400). Found: C, 39.75, H, 3.35, N, 10.60. Calc. for $C_{39}H_{40}F_{18}FeN_9P_3.3H_2O$: C, 39.72, H, 3.93, N, 10.69 %.

Synthesis of $[Cu(L^1H)](ClO_4)_3$.– L^1 (100 mg, 0.16 mmol) in MeOH (10 cm^3) was added to a solution of $Cu(ClO_4).6H_2O$ (48 mg, 0.13 mmol) in H_2O (20 cm^3) at 60 °C. The solution turned blue/green, and was left to cool. Blue crystals suitable for X-ray analysis grew overnight from this solution (data given below), and were collected by filtration. Yield 64 mg, 41 %. Mass spectrum (FAB / NBA): *m/z* 696, (Calc. for $[Cu(L^1)]^+$, 696). Uv-visible spectrum in CH_3CN [λ_{max}/nm (ε / dm^3 mol^{-1} cm^{-1})]: 692 (803), 297 (45 600), 252 (48 400). Found: C, 45.43, H, 3.95, N, 12.18. Calc. for $C_{39}H_{40}$ $Cl_3CuN_9O_{12}.2H_2O$: C, 45.46, H, 4.29, N, 12.21 %. Lattice water can be seen in the IR spectrum and in the crystal structure. It is anticipated that the addition of excess $NaClO_4$ to the blue/green solution obtained after addition of L^1 to Cu(II) would increase the yield.

Crystal data:–

$[C_{39}H_{40}Cu](ClO_4)_3.0.5H_2O$, M = 1005.71, monoclinic, a = 20.135(8), b = 14.907(6), c = 28.772(9) Å, β = 102.86(3) °, U = 8405(6) Å^3, D_c = 1.588 g cm^{-3}, T = 230(2) K, Mo-K_α radiation, λ = 0.71073 Å, space group $P2_{1/n}$, Z = 8, μ = 0.787 mm^{-1}, $F(000)$ = 4 136, crystal size 0.32 x 0.31 x 0.20 mm. Data were collected with a Siemens four circle diffractometer in the ω–2θ mode to a maximum 2θ of 45 °. A gaussian absorption correction was applied and resulted in transmission factors ranging from 0.86 to 0.82. The number of reflections collected was 11 304, of which 10 940 [$R(int)$ = 0.0802] were unique. Refinement was upon F^2 using SHELXL-93;[131] the final cycle involved 10 904 reflections and 1 180 parameters. A disordered model was used for one of the $(ClO_4)^-$ groups and also for the water molecule. The final R factors were $R1 = \sum ||F_0| - |F_c|| / \sum |F_0| = 0.0963$ [for $I > 2\sigma(I)$] and $wR2 = [\sum [w(F_0^2 - F_c^2)^2 / \sum [w(F_0^2)^2]]^{1/2} = 0.3524$ (for all data). The maximum and minimum peaks on a final difference Fourier map corresponded to 0.817 and –0.603 Å^{-3}. The weighting scheme $w = 1/[\sigma^2(F_0^2) + (0.0472\ P)^2 + 26.39P]$ where $P = [\max(F_0^2, 0) + 2F_c^2] / 3$ was shown to be satisfactory.

Atomic coordinates, bond lengths and angles, and thermal parameters have been deposited at the Cambridge Crystallographic Data Centre, and are listed in the Appendix.

Synthesis of $[(Ru_2(L^1)_2H)](PF_6)_5$. – L^1 (128 mg, 0.20 mmol) and $[Ru\{(CH_3)_2SO\}_4Cl_2]$ (97 mg, 0.20 mmol) were refluxed in H_2O (50 cm^3) for 12 h. The orange solution was treated with excess saturated aqueous NH_4PF_6 to yield an orange precipitate which was collected by suction filtration and dried *in vacuo* over silica gel. Yield 141 mg, 64 %. ^{1}H NMR (400 MHz, $(CD_3)_2SO$): δ/p.p.m. 8.79 (d, 4H), 8.76 (d, 4H), 8.66 (d, 2H), 8.57 (s, 2H), 8.36 (d, 4H), 8.22 (m, 12H), 7.93 (t, 2H), 7.75 (m, 6H), 7.65 (s, br, 1H), 7.44 (m, 2H), 6.93 (s, 4H), 4.05 (s, 4H), 4.02

(split AB q, 8H), 3.38 (t, 4H), 3.24 to 2.88 (m, 16H), 2.79 to 2.76 (m, 4H). There is evidence for a small amount of NH_4PF_6 in the ^1H NMR spectrum. ^{13}C NMR (100.62 MHz, $(CD_3)_2SO$): δ/p.p.m. 156.6 (4), 156.5 (4), 155.1 (2), 154.6 (2), 151.7 (4), 151.4 (4), 150.1 (2), 149.0 (2), 139.1 (4), 138.3 (2), 137.9 (4), 137.1 (2), 136.6 (4), 130.9 (2), 128.0 (4), 124.7 (4), 124.3 (4), 124.1 (2), 120.5 (2), 120.3 (2), 56.3 (4), 55.9 (2), 49.3 (4), 49.1 (4), 48.5 (4). Uv–visible spectrum in CH_3CN [λ_{max}/nm (ε / dm^3 mol^{-1} cm^{-1})]: 453 (14 800), 288 (169 000), 250 (80 300). Found: C, 41.55, H, 3.75, N, 11.36. Calc. for $C_{78}H_{79}F_{30}N_{18}P_5Ru.2H_2O$: C, 41.98, H, 3.75, N, 11.30 %. Crystals suitable for X–ray analysis were obtained by slow diffusion of Et_2O into a solution of $[(Ru_2(L^1)_2H)](PF_6)_5$ in CH_3NO_2, data are given below. Curiously, crystals isolated proved to be of the monomeric form. ^1H NMR (400 MHz, $(CD_3)_2SO$): δ/p.p.m. 8.81 (t, 6H), 8.20 (m, 9H), 7.73 (t, 3H), 7.58 (s, br, 1H), 6.90 (s, 3H), 4.01 (split AB q, 6H), 3.35 (m, 3H), 2.97 to 2.86 (m, 9H). ^{13}C NMR (100.62 MHz, $(CD_3)_2SO$): 156.71 (3C), 156.68 (3C), 151.9 (3C), 151.6 (3C), 139.3 (3C), 138.2 (3C), 136.9 (3C), 128.3 (3C), 125.0 (3C), 124.5 (3C), 56.3 (3C), 49.5 (3C), 48.6 (3C). Mass Spectrum (FAB/NBA): *m/z* 1026 (Calc. for $[(Ru(L^1H))(PF_6)_2]^+$, 1026. Uv–visible spectrum in H_2O [λ_{max}/nm (ε / dm^3 mol^{-1} cm^{-1})]: 468 (9500), 432 (8900), 287 (56700), 245 (28700). Found: C, 39.95, H, 3.72, N, 10.74. Calc. for $C_{39}H_{40}F_{18}N_9P_3Ru$: C 40.01, H 3.44, N 10.77 %.

Crystal data:–

$[C_{39}H_{40}Ru](PF_6)_3.(CH_3NO_2)_3$, M = 1353.91, monoclinic, a = 12.596(13), b = 25.81(2), c = 17.417(14) Å, β = 110.65(7) °, U = 8405(6) $Å^3$, D_c = 1.588 g cm^{-3}, T = 230(2) K, Mo-K_α radiation, λ = 0.71073 Å, space group $P2_{1/n}$, Z = 4, μ = 0.509 mm^{-1}, $F(000)$ = 2 736, crystal size 0.49 x 0.34 x 0.28 mm. Data were collected with a Siemens four circle diffractometer in the ω–2θ mode to a maximum 2θ of 45 °. An analytical absorption correction was applied and resulted in transmission factors ranging from 0.89 to 0.85. The number of reflections collected was 7 320, of which 6 954 [$R(int)$ = 0.0802] were unique. Refinement was upon F^2

using SHELXL–93;[131] the final cycle involved 6 941 reflections and 761 parameters. A disordered model was used for one of the $(PF_6)^-$ groups and also for one of the nitromethane molecules. The final *R* factors were $R1 = \sum | |F_o| - |F_c| | / \sum |F_o| = 0.059$ [for $I > 2\sigma(I)$] and $wR2 = [\sum [w(F_o^2 - F_c^2)^2 / \sum [w(F_o^2)^2]]^{½} = 0.1722$ (for all data). The maximum and minimum peaks on a final difference Fourier map corresponded to 0.684 and –0.636 $Å^{-3}$. The weighting scheme $w = 1/[\sigma^2(F_o^2) + (0.0472\ P)^2 + 26.39P]$ where $P = [\max(F_o^2, 0) + 2F_c^2] / 3$ was shown to be satisfactory.

Atomic coordinates, bond lengths and angles, and thermal parameters have been deposited at the Cambridge Crystallographic Data Centre, and are listed in the Appendix.

Synthesis of $[Zn(L^1H)](PF_6)_3$.– A solution of $ZnSO_4.7H_2O$ (68 mg, 0.24 mmol) in H_2O (25 cm^3) was added to a solution of L^1 (150 mg, 0.24 mmol) in acetone / water (1:4) 50 cm^3). The reaction mixture was heated to 60 °C for 30 min. Excess saturated aqueous NH_4PF_6 was added and the product filtered and dried *in vacuo* over silica gel (yield 256 mg, 95 %). ^1H NMR (250 MHz, $(CD_3)_2SO$): δ/p.p.m. 8.58 (d, 3H), 8.55 (d, 3H), 8.45 (d, 3H), 8.35 (t, 3H), 8.27 (d, 3H), 8.13 (br, s, 1H), 7.79 (m, 3H), 6.59 (s, 3H), 3.99 (split AB q, 6H), 3.34 to 3.20 (m, 3H), 3.04 to 2.82 (m, 9H). ^{13}C NMR (100.62 MHz, $(CD_3)_2SO$): 149.5 (3), 148.9 (3), 148.8 (3), 148.7 (3), 143.6 (3), 142.4 (3), 136.1 (3), 127.9 (3), 124.15 (3), 124.10 (3), 56.1 (3), 48.6 (3), 40.0 (3). Mass spectrum (FAB / NBA): *m/z* 990 (Calc. for $[(Zn(L^1H_2)(PF_6)_2]^+$, 990). Uv–visible spectrum in CH_3CN [λ_{max}/nm (ε / $dm^3\ mol^{-1}\ cm^{-1}$)]: 298 (40 500), 248 (35 000). Found: C, 41.06, H, 3.59, N, 10.58. Calc. for $C_{39}H_{40}F_{18}N_9P_3Zn.H_2O$: C 40.62, H 3.67, N 10.93 %.

Synthesis of $[Ni(L^1H)](PF_6)_3$. – L^1 (45 mg, 0.07 mmol) and $NiCl_2.6H_2O$ (17 mg, 0.07 mmol) were stirred in H_2O (50 cm^3). HCl (1 drop, d 1.18) was added and the solution turned pale pink. Treatment with excess saturated aqueous NH_4PF_6 gave a pale pink crystalline precipitate which was collected by filtration and dried *in vacuo* over silica gel. Yield 77 mg, 100 %. Mass spectrum (FAB/NBA): *m/z* 983 (Calc. for $[(Ni(L^1H_2)(PF_6)_2]^+$, 983). Uv–visible spectrum in CH_3CN [λ_{max}/nm (ε / dm^3 mol^{-1} cm^{-1})]: 532 (27.1), 300 (57 300), 252 (51 400). Found: C, 40.84, H, 3.35, N, 10.72. Calc. for $C_{39}H_{40}F_{18}N_9NiP_3.H_2O$: C 40.86, H 3.69, N 11.00 %.

Synthesis of $[Co^{II}(L^1H)](PF_6)_3$– Nitrogen gas was bubbled through a solution of $CoCl_2.6H_2O$ (57 mg, 0.24 mmol) in CH_3CH_2OH (50 cm^3) for 15 min to remove atmospheric O_2. A second solution of L^1 (150 mg, 0.24 mmol) in CH_3CH_2OH (50 cm^3) was treated similarly, then added dropwise to the $CoCl_2.6H_2O$ solution under N_2. The reaction mixture turned yellow. After bubbling with N_2 for a further 15 min excess saturated aqueous NH_4PF_6 was added. A fawn precipitate formed which was filtered off and recrystallised from the minimum volume of hot H_2O. The product was isolated as golden brown crystals, yield 211 mg, 78 %. ^1H NMR (250 MHz, $(CD_3)_2SO$): δ/p.p.m. 108.3 (s, 3H), 100.8 (s, 3H), 83.7 (s, 3H), 76.7 (s, 3H), 46.8 (s, 3H), 14.5 (s, 3H), 9.9 (d, 3H), 7.7 (s, 3H), –2.2 (d, 3H), –3.3 (s, 6H), -3.9 (t, 3H), -16.2 (s, 1H). Mass spectrum (FAB/NBA): *m/z* 984 (Calc. for $[Co(L^1H_2)(PF_6)_2]^+$, 984). Uv–visible spectrum in CH_3CN [λ_{max}/nm (ε / dm^3 mol^{-1} cm^{-1})]: 300 (31 100), 248 (30 100). Found: C, 41.04, H, 3.48, N, 10.93. Calc. for $C_{39}H_{40}CoF_{18}N_9P_3.H_2O$: C 40.85, H 3.69, N 10.99 %.

Synthesis of $[Co^{III}(L^1H)](PF_6)_4$.– $CoCl_2.6H_2O$ (57 mg, 0.24 mmol) and L^1 (150 mg, 0.24 mmol) were heated in H_2O (50 cm^3) to 80 °C. The yellow solution was treated with H_2O_2 (2 cm^3, 30 %) and HCl (2 cm^3, density 1.18) and kept at 80 °C for a further 30 min. The solvent was then evaporated, the residue dissolved in H_2O (5 cm^3) and the solution loaded onto a column of Sephadex SP C–25 cation exchange

resin. This was eluted with aqueous 0.1–1.0 mol dm^{-3} NaCl. The main fraction was eluted with 0.6 mol dm^{-3} NaCl, concentrated using a rotary evaporator and treated with excess saturated aqueous NH_4PF_6. This gave a yellow precipitate which was collected by filtration and dried as described above. Yield 120 mg, 40 %. ^1H NMR (250 MHz, $(CD_3)_2CO$): δ/p.p.m. 8.71 (d, 6H), 8.57 (d, 3H), 8.50 (d, 3H), 7.90 (t, 3H), 7.67 (s, br 1H), 7.49 (d, 3H), 6.10 (s, 3H), 4.02 (split AB q, 6H), 3.29 to 3.17 (m, 3H), 3.09 to 3.02 (m, 3H), 2.92 to 2.78 (m, 6H). ^{13}C NMR (62.89 MHz, $CDCl_3$): δ /p.p.m. 157.2 (3), 156.7 (3), 153.4 (3), 153.2 (3), 146.3 (3), 145.1 (3), 141.8 (3), 132.9 (3), 128.8 (3), 128.2 (3), 57.4 (3), 50.3 (3), 49.9 (3). Mass spectrum (FAB/NBA): *m/z* 983 (Calc. for $[(Co(L^1H)(PF_6)_2]^+$, 983). Uv–visible spectrum in CH_3CN [λ_{max}/nm (ε / dm^3 mol^{-1} cm^{-1})]: 445 (366), 312 (30 800), 250 (49 700), 225 (69 000). Found: C, 35.91, H, 2.92, N, 9.47. Calc. for $C_{39}H_{40}CoF_{24}N_9P_4.H_2O$: C 36.27, H 3.28, N 9.76 %.

CHAPTER 3

Chapter 3

Bipyridyl functionalised Ligands Synthesised From 1,4,7-Triazacyclononane, 1,4,8,11-Tetraazacyclotetradecane and 1,2-Diaminoethane.

Studies of pendant–arm macrocycles and their metal complexes continue to attract significant attention. Cyclam (1,4,8,11–tetraazacyclotetradecane) and 9N3 (1,4,7-triazacyclononane) are two commonly used macrocyclic ligands, and various pendant donor groups have been added to the nitrogen atoms of these macrocycles for increased functionality. 2,2'–Bipyridine (bipy) has been incorporated into macrocyclic structures, both as part of the cyclic framework and as pendant–arm(s). In this chapter, the synthesis of four new polynucleating ligands with pendant bipy arm(s) is described, and some of their complexes with ruthenium(II) are reported. (The synthesis of L^1, together with mononuclear complexes of that ligand is described in Chapter 2).

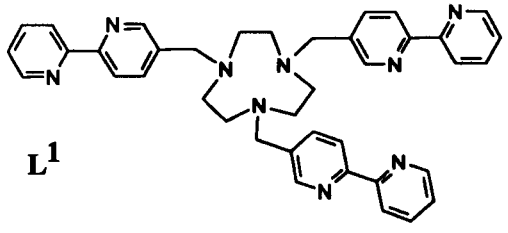

L^1

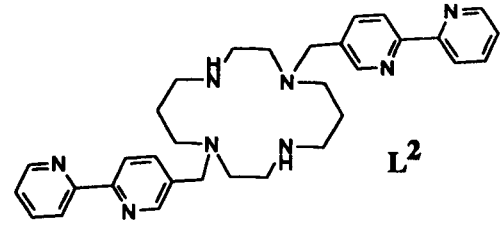

L^2

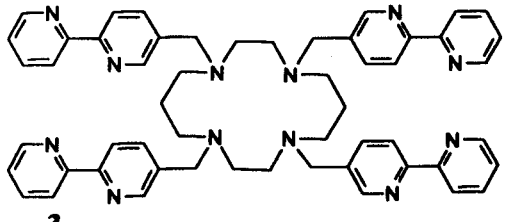

L^3

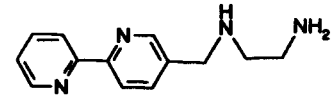

L^4

Reaction of the *N*–pendant bipy arm(s) with *cis*–$[Ru(bipy)_2Cl_2]$ introduces the fluorescent $[Ru(bipy)_3]^{2+}$ group at each pendant arm, to give ligands L^5 – L^8 with up to four attached $[Ru(bipy)_3]^{2+}$ groups. The fluorescence of these groups is affected by subsequent cation complexation (either by protons or transition metals) which permits their use as fluorescent pH and transition metal ion sensors.

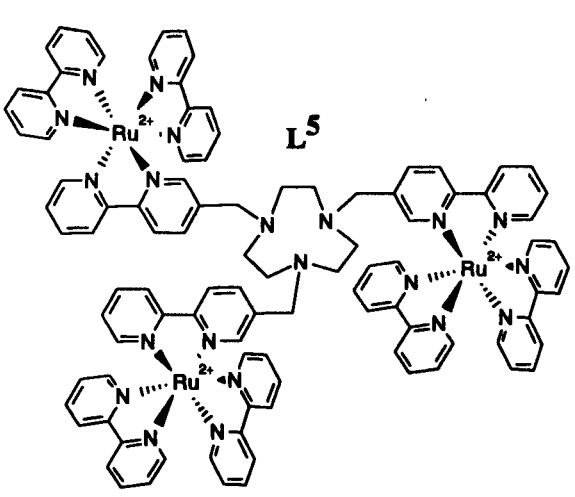

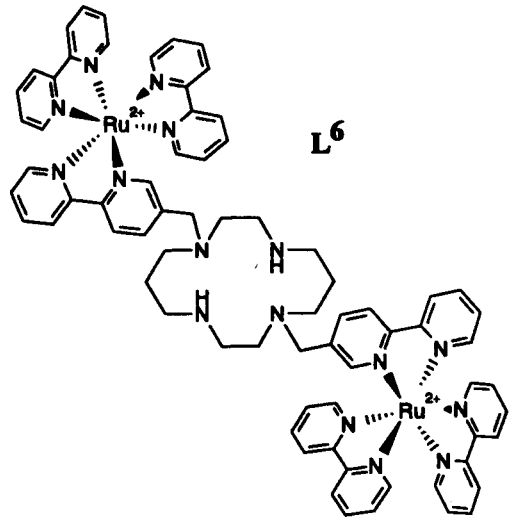

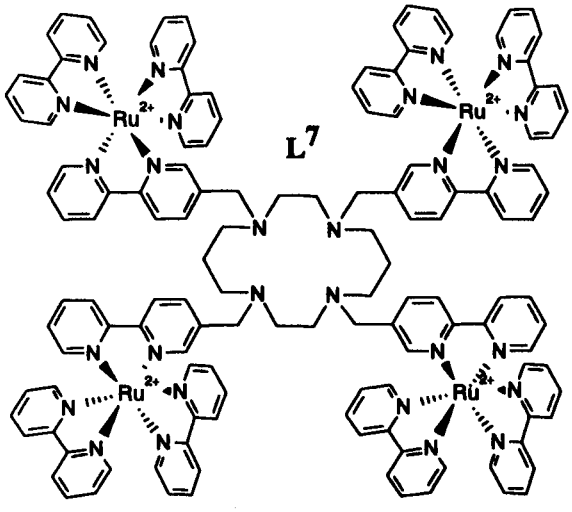

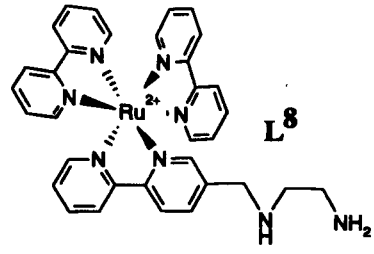

Results and Discussion.

Synthesis.– The synthesis of L^1 is described in Chapter 2. L^2 was obtained from the parent macrocycle cyclam by reaction with 1.5 equivalents of 5–bromomethyl–2,2'–bipyridine. It was characterised by its proton and ^{13}C NMR spectra, and by its CI mass spectrum. It may seem more appropriate to use 2 equivalents of 5–bromomethyl –2,2'–bipyridine rather than 1.5, however the latter quantity was chosen by anology with the work of Parker in which the syntheses of 1,8–disubstituted derivatives of cyclam are described.[132] The formation of 1,8–disubstituted derivatives is more difficult than the formation of mono–, tri– or tetra– derivatives as it requires the selective formation of one of the [1,4], [1,8] or [1,11] derivatives. The three positional isomers of bis–(2',2"–bipyridyl–5'–ylmethyl)–1,4,8,11–tetraazacyclo–tetradecane are shown below (**Figure 3.1**).

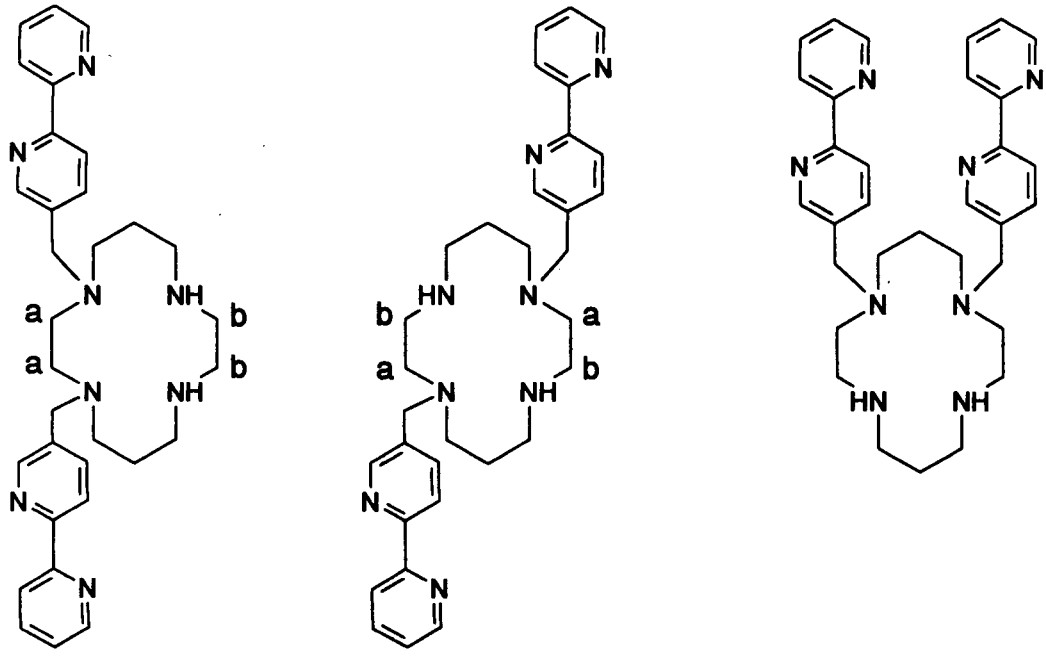

[1,4] **[1,8] (L^2)** **[1,11]**

Figure 3.1. Three isomers of bis–(2',2"–bipyridyl–5'–ylmethyl)–1,4,8,11–tetraazacyclotetradecane.

As expected, the ^{13}C NMR spectrum of L^2 has six upfield (aliphatic) resonances. This means it can be quickly distinguished from the [1,11] isomer, which would be expected to have seven. As with L^2, the [1,4] isomer would have six upfield resonances, so the proton NMR spectrum must be used to distinguish between the two. This can be done easily by examining resonances corresponding to $R^1NCH_2CH_2NR^2$ portions of the macrocyclic ring (**Figure 3.1**); in L^2, $R^1 \neq R^2$ therefore two triplets are observed for H_a and H_b. In the [1,4] isomer, $R^1 = R^2$ so two singlets would be observed for H_a and H_b. Triplets are observed in the proton NMR of L^2, confirming the formation of the desired isomer.

L^3 was readily obtained from reaction of cyclam with an excess of 5–bromomethyl–2,2'–bipyridine in the presence of Et_3N. It was characterised by its proton and ^{13}C NMR spectra, and by a CI mass spectrum. As expected, the ^{13}C spectrum showed ten aromatic and four aliphatic resonances.

L^4 was obtained from reaction of 5–bromomethyl–2,2'–bipyridine and a four–fold excess of 1,2–diaminoethane. Excess 1,2–diaminoethane was used for two reasons, firstly to take up HBr produced in the reaction, and secondly to decrease the chance of two molecules of 5–bromomethyl–2,2'–bipyridine reacting with a single 1,2-diaminoethane molecule. L^4 was also characterised by its proton and ^{13}C NMR spectra, and by a CI mass spectrum.

Ruthenium Complexes.– Reaction of L^1 – L^3 with three, two and four equivalents of *cis*–$[Ru(bipy)_2Cl_2]$ respectively introduced the highly fluorescent $[Ru(bipy)_3]^{2+}$ group at each bipy arm to give the complexes L^5 – L^7. L^4 was stirred with two equivalents of HBr before reaction with one equivalent of *cis*–$[Ru(bipy)_2Cl_2]$, to form the $[Ru(bipy)_3]^{2+}$ group at the bipy site and thus give L^8) Use of neat L^4 gives a side reaction, presumably as the 1,2–diaminoethane (en) attacks the Ru centre. Protonation of the en unit allows the desired reaction to proceed.

The complexes L^5 – L^8 were obtained as red solids, and were characterised by proton and ^{13}C NMR spectra, uv–visible spectra, and CHN analysis. L^8 was also characterised by its FAB mass spectrum. L^5 – L^8 all show fluorescence typical of the parent chromophore $[Ru(bipy)_3]^{2+}$ (λ_{ex} = 450 nm, λ_{em} = 607 nm)[122], and all showed uv–visible spectra characteristic of the $[Ru(bipy)_3]^{2+}$ group. The proton NMR spectra of L^5– L^7 are rather broad, most noticeably in the aliphatic region. This is particularly so when $(CD_3)_2SO$ is used as a solvent.

The proton NMR spectrum of L^5 shows two broad singlets (integrals 2:1) in the upfield region, indicating that all linking methylene protons are equivalent, and all 9N3 protons are equivalent. Like the proton NMR spectrum, the ^{13}C NMR spectrum is broad in the upfield region, with two singlets as expected. The broadening is thought to be caused by slow 'umbrella' inversion at the macrocyclic nitrogen atoms. Umbrella inversion is thought to be hindered due to the difficulty of moving the bulky $[Ru(bipy)_3]^{2+}$ groups through the solvent.

As with the NMR spectra of L^5, upfield resonances in the proton and ^{13}C NMR spectra of L^6 are broad. Like the parent ligand L^2, the ^{13}C NMR spectrum (**Figure 3.2**) shows six resonances for the upfield carbon atoms, indicating that the ten carbon atoms in the cyclam ring split into two sets of five resonances. Two of these resonances overlap at δ 48.3 p.p.m.. Three of these resonances (at δ 55.0, 50.8 and 48.3 p.p.m.) together with one aromatic (downfield) resonance (at δ 137.8 p.p.m.) are noticeably broader than the remaining resonances. The three broad aliphatic (upfield) resonances are attributed to carbon atoms adjacent to the two macrocyclic nitrogen atoms that bear the pendant arms, and it is tentatively suggested that slow 'umbrella' inversion at these nitrogen atoms is responsible for the observed broadening of the spectra. Inversion at the two secondary nitrogen atoms is presumably unrestricted and therefore more rapid.

The proton NMR spectrum of L^6 (**Figure 3.3**) shows four broad resonances for the aliphatic protons. The resonance at δ 3.57 p.p.m., assigned to the four linking methylene protons, is a quartet (^2J = –15.1 Hz). The two protons of each methylene link must therefore be inequivalent due to the intrinsic chirality of the complex.

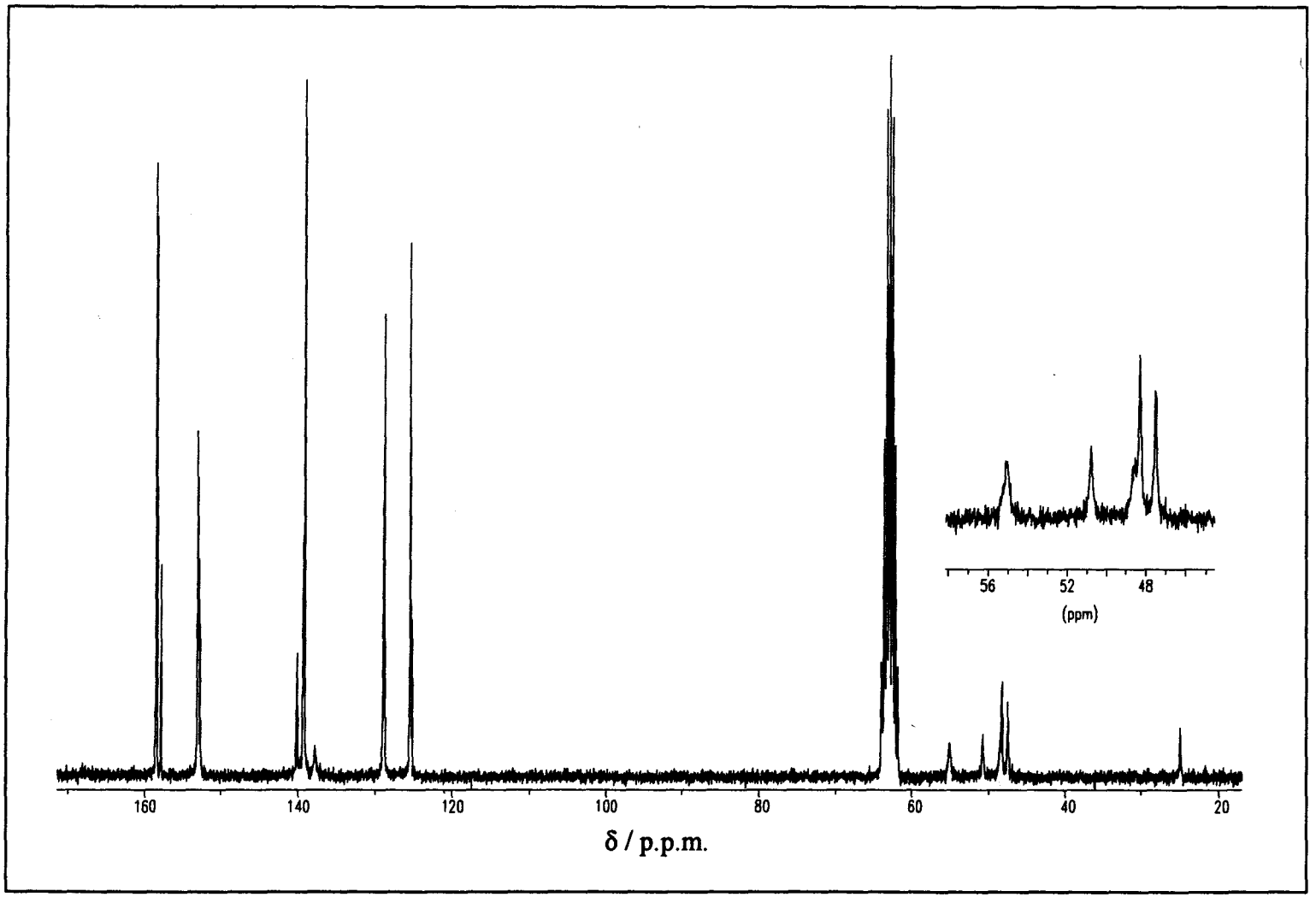

Figure 3.2. ^{13}C NMR Spectrum of L^6 in CD_3NO_2 at 298 K

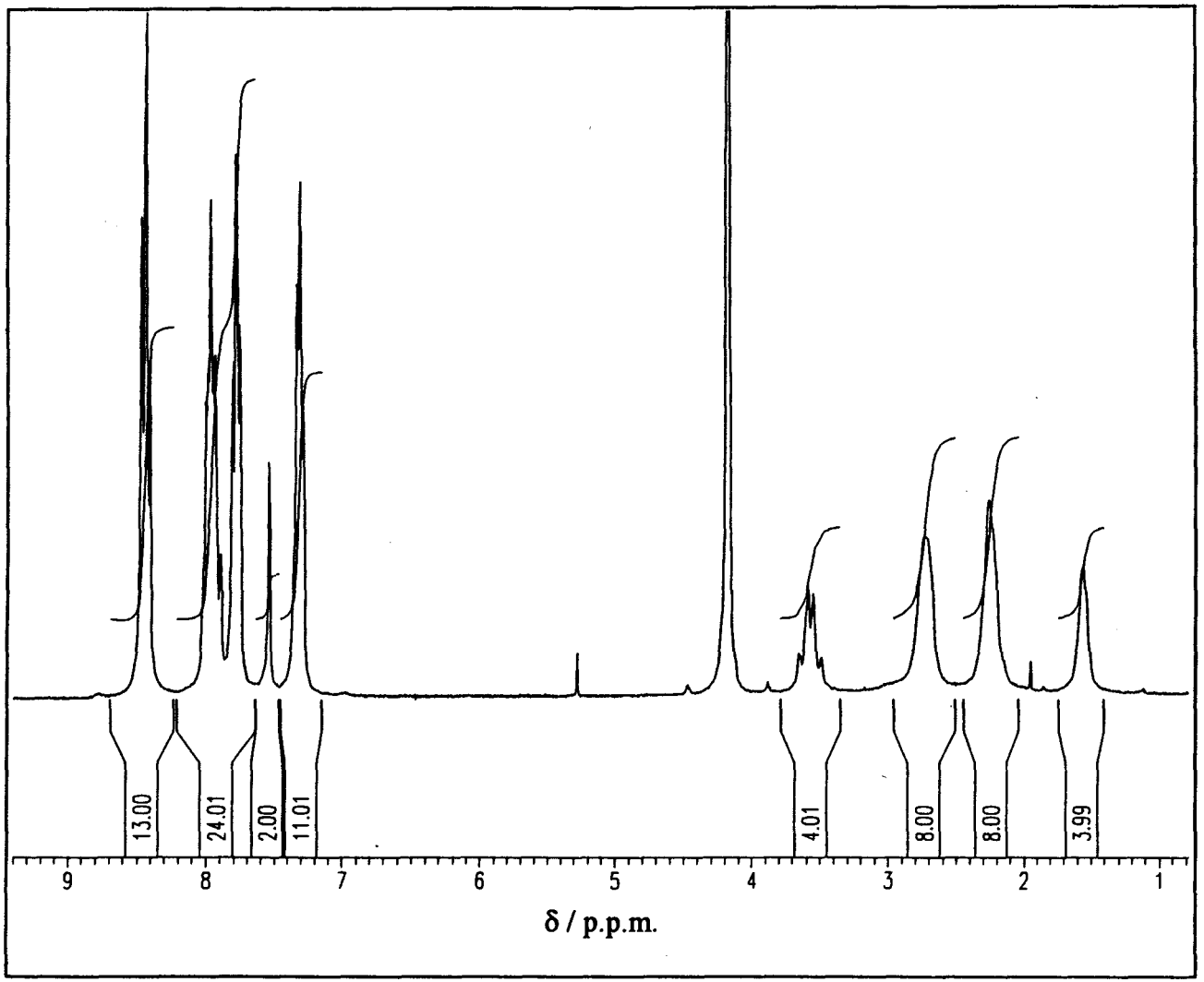

Figure 3.3. Proton NMR Spectrum of L^6 in CD_3NO_2 at 298 K.

CHN analysis suggests L^6 has the formulation $[\{Ru(bipy)_2\}_2H_2L^2](PF_6)_6$, implying that in the solid two protons are associated with the four nitrogen atoms of the cyclam moiety. This is as expected since these protons would be attached to the two secondary nitrogen atoms, as these are the more basic. The proton NMR spectrum in CD_3NO_2 confirms that these protons are also attached in solution; the total integral value of the multiplets from δ = 8.5 to 7.3 p.p.m. is 50, which corresponds to 46 protons from the two $[Ru(bipy)_3]^{2+}$ groups, plus 4 protons from the two NH_2^+ groups in the cyclam rings. The first two pK_a's of L^6 (determined by fluorimetric titration by Mrs A. M. Josceanu) are 10.58 and 6.89 (**Table 3.1**) indicating that the cavity is at least mono-protonated in aqueous solution at neutral pH.

Proton and ^{13}C NMR spectra of L^7 also show broadening, again, particularly noticeable in the upfield (aliphatic) region and attributed to slow umbrella inversion. The ^{13}C NMR spectrum shows four aliphatic resonances, as expected. CHN analysis suggests L^7 has the formulation $[\{Ru(bipy)_2\}_4(L^3H)](ClO_4)_9$, implying that in the solid a single proton is associated with the 4 nitrogen atoms of the macrocyclic ring. Evidence for this proton was also found in solution. A sharp singlet can be seen at δ 5.29 p.p.m. in the proton NMR (**Figure 3.4**). This integrates for a single proton, and suggests that the cyclam cavity is also mono-protonated in CD_3NO_2. In an attempt to remove this proton, two drops of base (dicyclohexylamine) were added to the NMR tube. The solution was shaken and warmed and the spectrum re-taken; however this made little difference to the resonance at δ 5.29 p.p.m.. It is therefore assumed that dicyclohexylamine is insufficiently strong to remove the cyclam bound proton. A stronger base like NaOH was not used as it is insoluble in the NMR solvent (CD_3NO_2). It is suggested that an alternative base such as butyl lithium could be used (under anhydrous conditions). pK_a values for L^7 (determined by Mrs A. M. Josceanu) show the macrocyclic cavity to be mono-protonated in aqueous solution. Variable temperature NMR studies (**Figure 3.5**) shows that as the solution is cooled to 243 K

some structure can be seen from the resonances at δ = 3.25, 2.15 and 2.05 p.p.m. (H_a, H_b and H_c respectively).

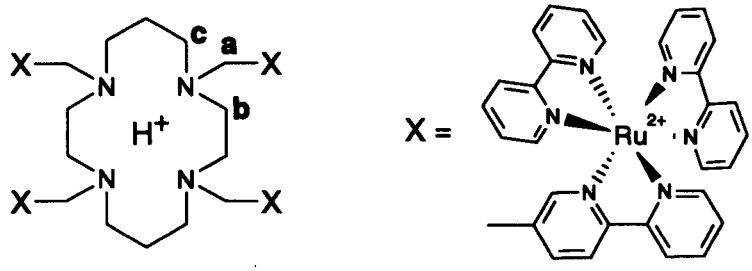

On further cooling (to 233 and then 223 K) the spectrum becomes even broader and the structure is lost. It is suggested that the structure in the proton NMR spectrum arises as L^7 becomes locked in different *N*–conformational isomers, due to slow umbrella inversion as discussed above. In an attempt to obtain a simpler, sharper spectrum, decoupling experiments were performed on the proton spectrum that showed the most structure, i.e. that taken at 243 K. The resonances at δ = 1.21 and 5.29 p.p.m. were irradiated in turn, but this made little difference to the remainder of the spectrum.

The proton NMR spectrum of L^8 was much sharper than those of L^5 – L^8, as might be expected since L^8 is a considerably smaller molecule that has no macrocyclic component. Inversion at the aliphatic nitrogen atoms is not hindered. The methylene bridge protons appear as a singlet (δ 4.19 p.p.m.) and there are two triplets (δ 3.39 and 3.32 p.p.m.) assigned to the NCH_2CH_2N 1,2–diaminoethane moiety. As expected, three upfield (aliphatic) resonances can be seen in the ^{13}C NMR spectrum.

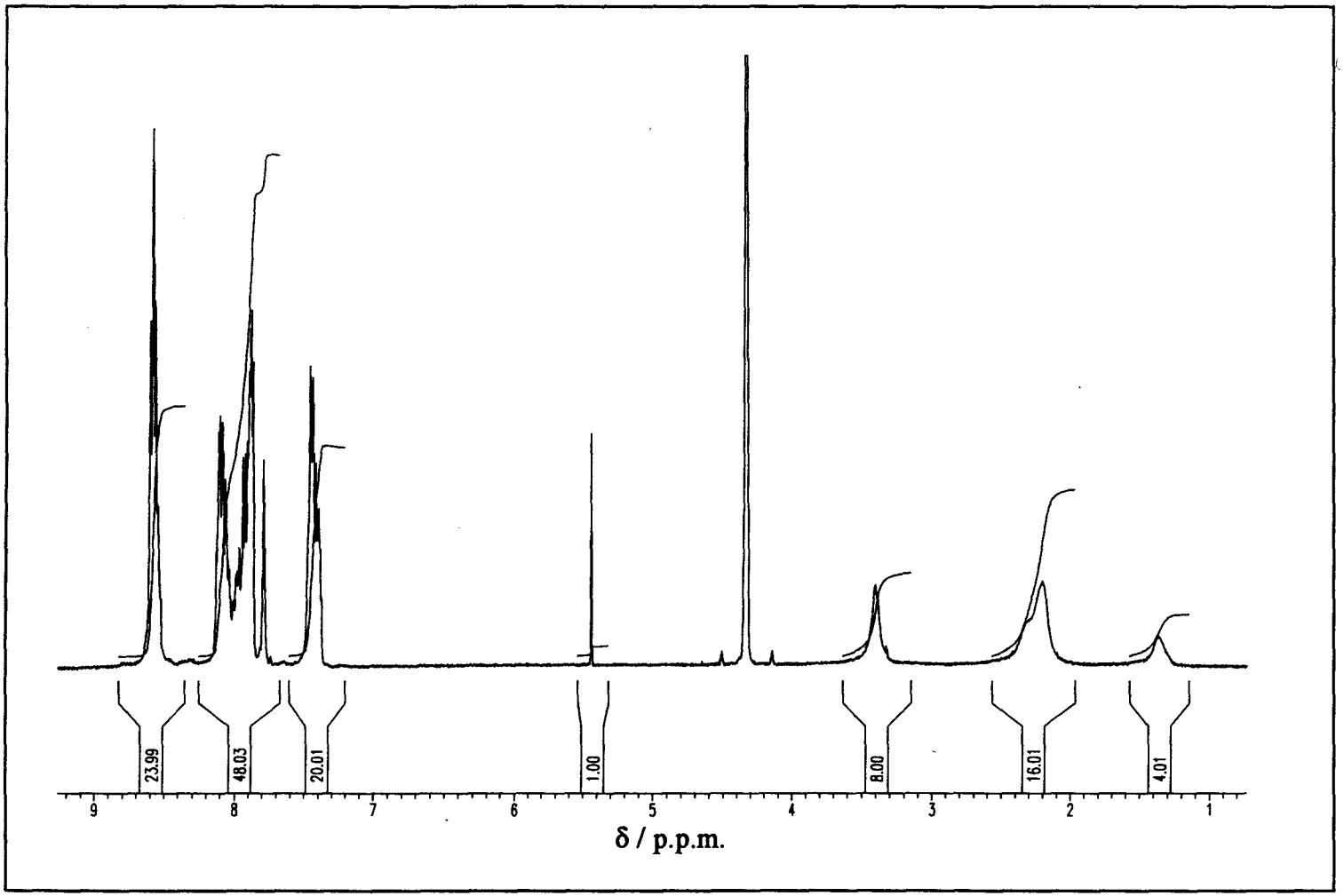

Figure 3.4. Proton NMR Spectrum of L^7 at 298 K in CD_3NO_2.

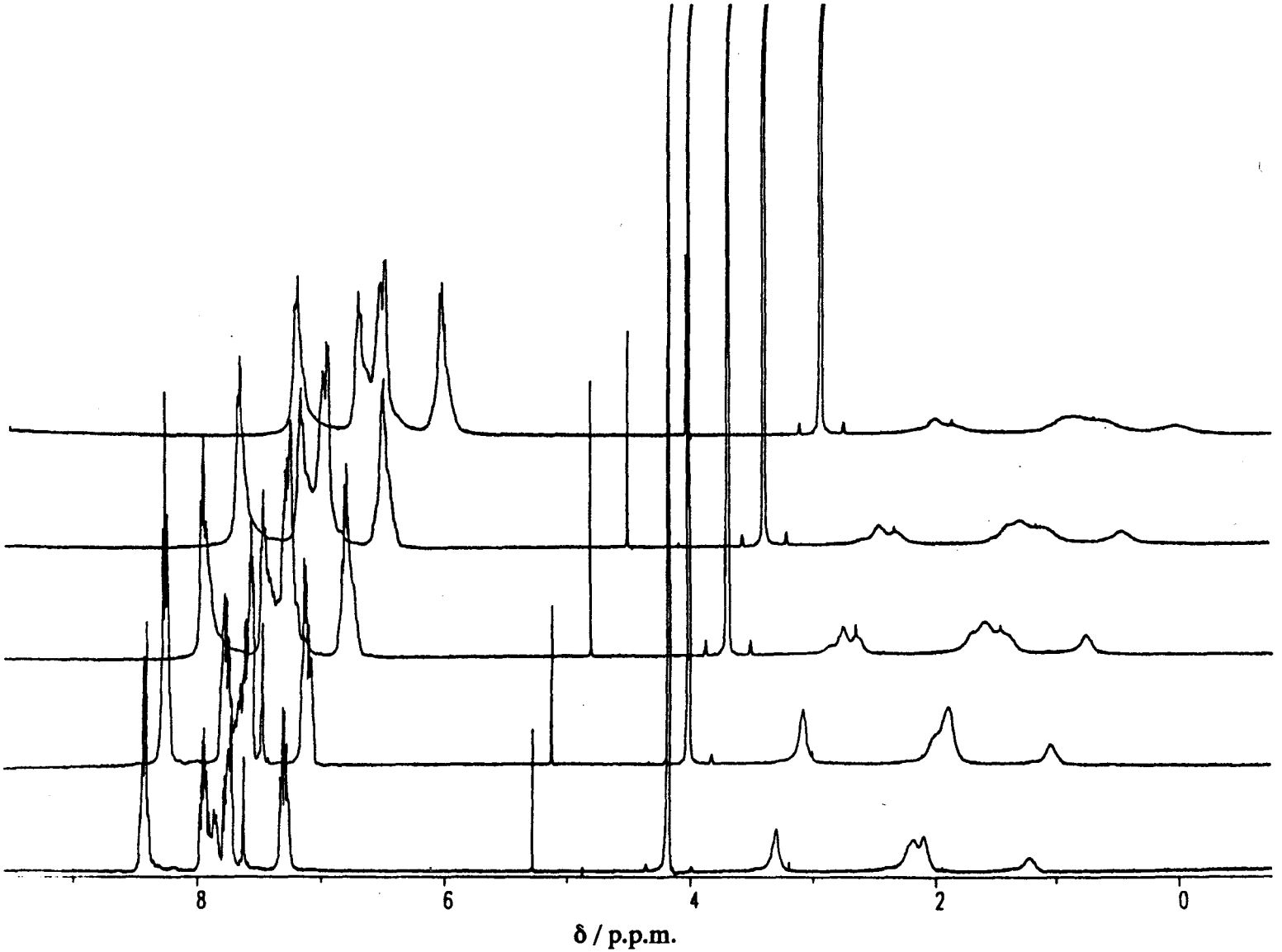

Figure 3.5. Proton NMR Spectra of L^7 in CD_3NO_2 at 343, 298, 243, 233 and 223 K.

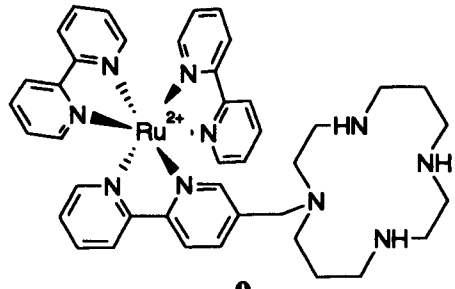

L^9

As with L^9 (Moore et. al[55]) the fluorescence intensity of L^5 – L^8 varies with changes in pH, being greatest at high pH. The change in fluorescence intensity can be used to calculate photo excited state pK_a's. A pH fluorescence titration curve for L^8 is shown in **Figure 3.6**, where the calculated fluorescence curve is compared with the observed data. Data from this titration curve were fitted to Equation 3.1 to give two photo excited state pK_a's.

$$F_{obs} = L_t \frac{F_L + F_{HL}10^{pK_{a1}-pH} + F_{H_2L}10^{pK_{a1}+pK_{a2}-2pH}}{1+10^{pK_{a1}-pH} + F_{H_2L}10^{pK_{a1}+pK_{a2}-2pH}} \qquad \text{Eqn 3.1}$$

where L_t = total concentration of ligand

F_L = molar fluorescence intensity of unprotonated ligand

F_{HL} = molar fluorescence intensity of monoprotonated ligand

F_{H_2L} = molar fluorescence intensity of diprotonated ligand

F_{obs} = observed fluorescence intensity

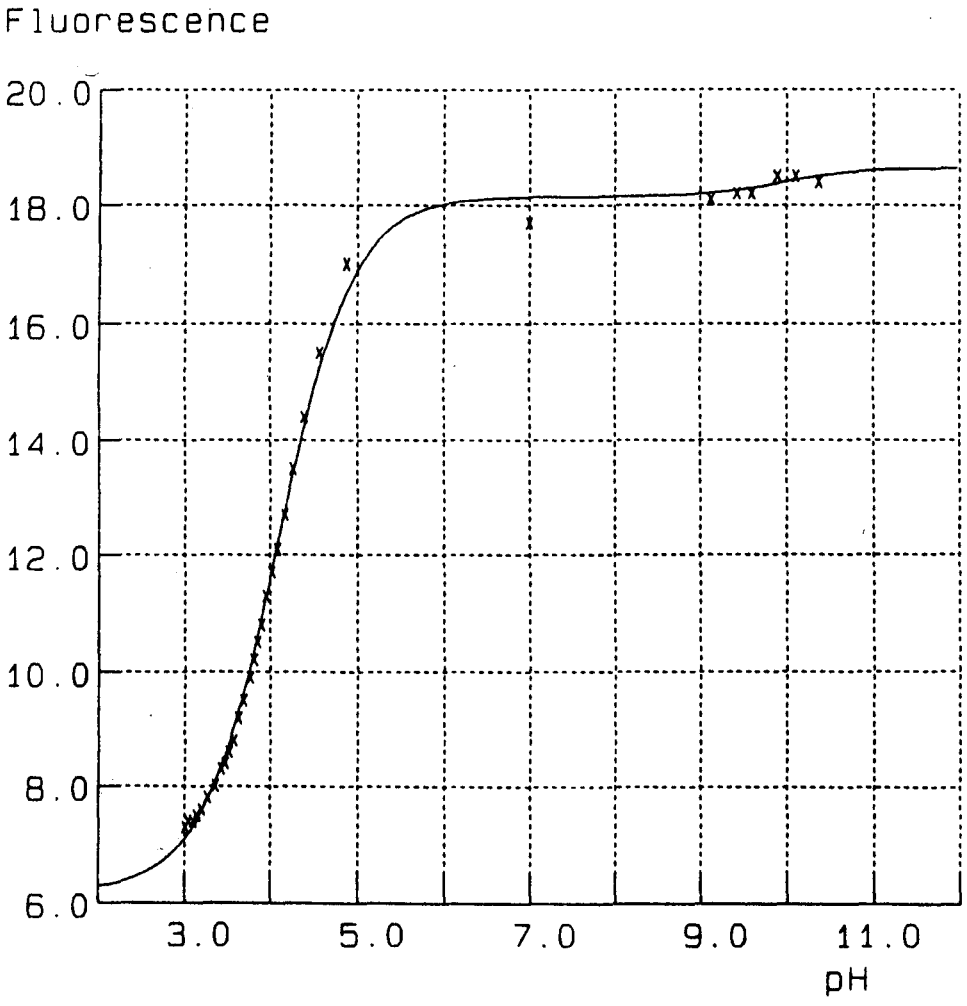

Figure 3.6. A pH fluorescence titration curve for L^8.

The calculated photo excited state pK_a's for L^8 are 10.0 ± 1.2 and 4.08 ± 0.02 (these are compared to the ground state pK_a's of 9.89 ± 0.07 and 7.08 ± 0.03 for 1,2–diaminoethane). It should be stressed that the pK_a's for L^8 are the result of a preliminary investigation only, and further experiments are needed to produce reliable values. Data should be repeated, being recorded at constant temperature and constant ionic strength. As can be seen from **Figure 3.6**, more data is needed between pH 5 and pH 9. The lack of points in this region, and the small fluorescence change on first protonation makes determination of pK_1 inaccurate. It is assumed that the first protonation occurs at the primary nitrogen atom of the 1,2–diaminoethane unit which is fairly remote from the $[Ru(bipy)_3]^{2+}$ group and so the small change in fluorescence intensity observed on pK_1 seems reasonable. It is unsurprising that there is a much greater change in fluorescence intensity on the second protonation, as this occurs closer to the $[Ru(bipy)_3]^{2+}$ group. pK_2 for L^8 is significantly lower than the corresponding value for 1,2–diaminoethane, which reflects the electrostatic repulsion between Ru^{2+} and the incoming proton.

More rigorous pH fluorescence titration curves were measured and analysed for L^5 - L^7 and L^9 by Mrs A. M. Josceanu. As an example of this work, a pH fluorescence titration curve for L^5 is shown in **Figure 3.7.**

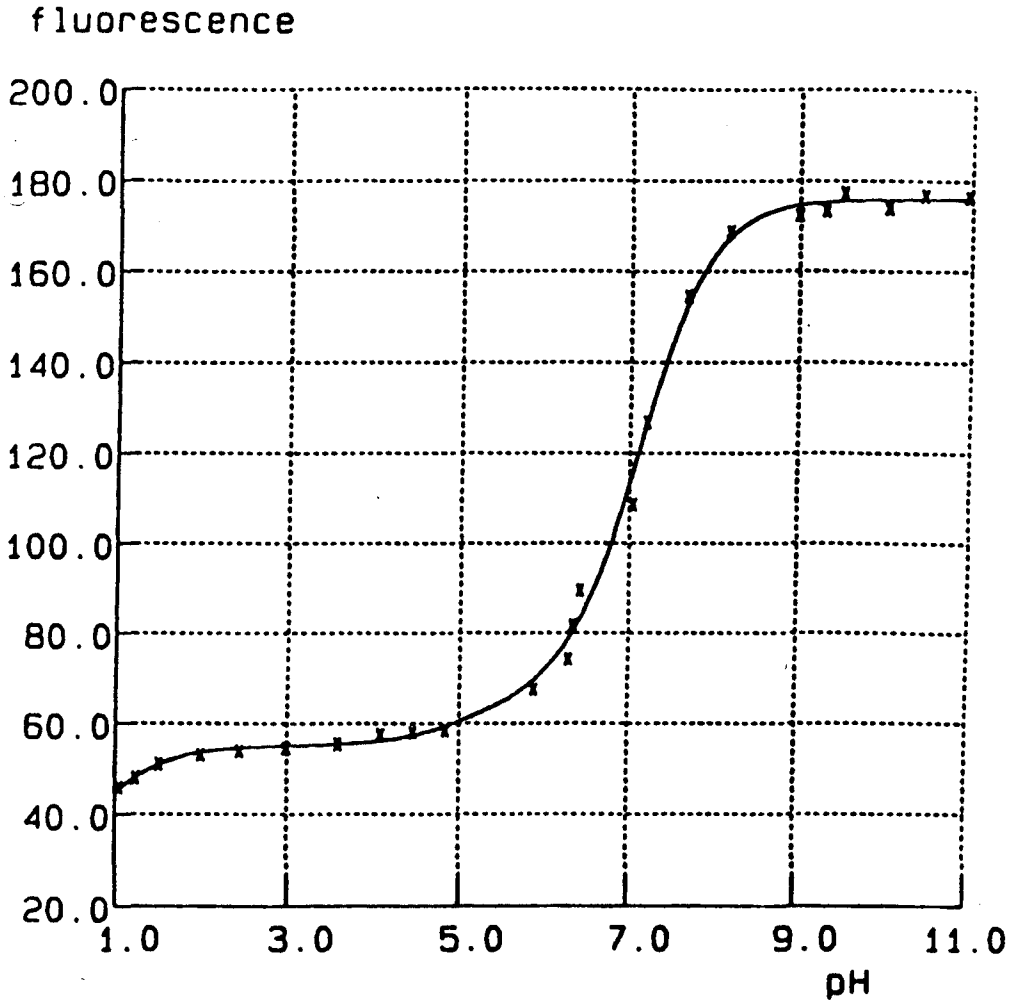

Figure 3.7. A pH fluorescence curve for L^5.

Data from this titration curve were used to calculate three photo excited state pK_a's. Here, the first protonation results in the greatest change in fluorescence. The first photo excited state pK_a for L^5 is 7.14, and the change in fluorescence intensity at around pH 7 can be seen in **Figure 3.7.** It is therefore suggested that L^5 could be useful as a fluorescent sensor at physiological pH, operating at below micromolar concentrations.

pH Fluorescence titration curves were also measured for L^6, L^7 and L^9, and used to calculate photo excited state pK_a's for each ligand. Like L^5, L^7 shows a decrease in fluorescence with lowering of pH. L^6 and L^9 have more complex pH fluorescence titration curves. Lowering the pH causes the fluorescence to decrease, then increase, before decreasing again. It is thought that initial protonation occurs at the nitrogen atoms not bearing pendant arms which gives rise to smaller fluorescence changes. The photo excited state pK_a's are shown in **Table 3.1**, along with the corresponding ground state values for the parent macrocycles cyclam and 9N3.

In addition to lowering the pH, the binding of metal cations to L^5 – L^9 also quenches their fluorescence. Quenching of this fluorescence by cations such as Ni^{2+}, Cu^{2+} and nH^+ has been studied in conjunction with Mrs A. M. Josceanu. A comparison of the fluorescent spectrum of $[Ru(bipy)_3]^{2+}$ (8×10^{-6} mol dm^{-3}) with L^7 (2×10^{-6} mol dm^{-3}) at high pH is shown in **Figure 3.8.** Also shown in **Figure 3.8** is the effect of adding acid, excess Ni^{2+} and Cu^{2+} to L^7. It is thought that the metal cations form 1:1 complexes with L^7. L^7 was heated with a five fold excess of Ni^{2+} to see if a species with more than one metal ion coordinated to the cyclam cavity could be isolated, however the 1:1 complex $[\{Ru(bipy)_2\}_4L^7Ni](ClO_4)_{10}$ was obtained.

The quenching of L^5–L^9 at low pH may appear to be the reverse of the behaviour that is expected. Some luminescent pH sensors containing $[Ru(bipy)_3]^{2+}$ reporters and amine receptors are found to be fluorescent at low pH, the fluorescence being quenched as the pH increases.[83] The quenching is caused by photo electron transfer from the amine site to the $[Ru(bipy)_3]^{2+}$ unit. This does not happen at low pH when the amine is protonated, as the protonated amine is a better electron acceptor than $[Ru(bipy)_3]^{2+}$.[83] Where complexes are found to be more highly fluorescent at high pH, (e.g. for L^5–L^9), the energy required for photo electron transfer is presumably prohibitive, even at high pH. Quenching must therefore be occurring by some other mechanism. It is suggested that on protonation of L^5–L^9, the presence of proximal

positive charges could encourage cleavage of a Ru–N bond to form a five coordinate intermediate, which may coordinate to a solvent molecule to restore six coordination.[83] The complex must thermally return to the original tris(bipy) coordination, as L^5–L^9 are photo stable.

Quenching of the fluorescence by metal cations such as the quenching of L^7 by Ni^{2+} and Cu^{2+} may occur *via* a third mechanism. An energy transfer mechanism may be operating; the excited $[Ru(bipy)_3]^{2+}$ initiating an electronic transition in the attached metal – cyclam unit.[55, 65]

Ligand	Overall Charge	pK_1	pK_2	pK_3	pK_4	Method
cyclam	0	11.5	10.2	1.6	0.9	pH titre
9N3	0	10.4	6.8	<2.5		NMR
L^9	2+	10.24	8.58	4.23 ± 0.31	−0.3 ± 0.8	Fluorescence
L^6	4+	10.58 ± 0.14	6.89 ± 0.24	3.48 ± 0.29	0.57 ± 0.36	Fluorescence
L^5	6+	7.14 ± 0.03	5.04 ± 0.33	0.71 ± 0.31		Fluorescence
L^7	8+	5.92 ± 0.11	4.78 ± 0.06	2.87 ± 0.81	0.50 ± 0.18	Fluorescence

Table 3.1. Comparison of the photo excited state pK_a values of the macrocycles L^5-L^7 and L^9, determined at 25 °C by fluorimetric titration, with the values for the parent macrocycles 9N3 and cyclam. (These values were determined by Mrs A. M. Josceanu).

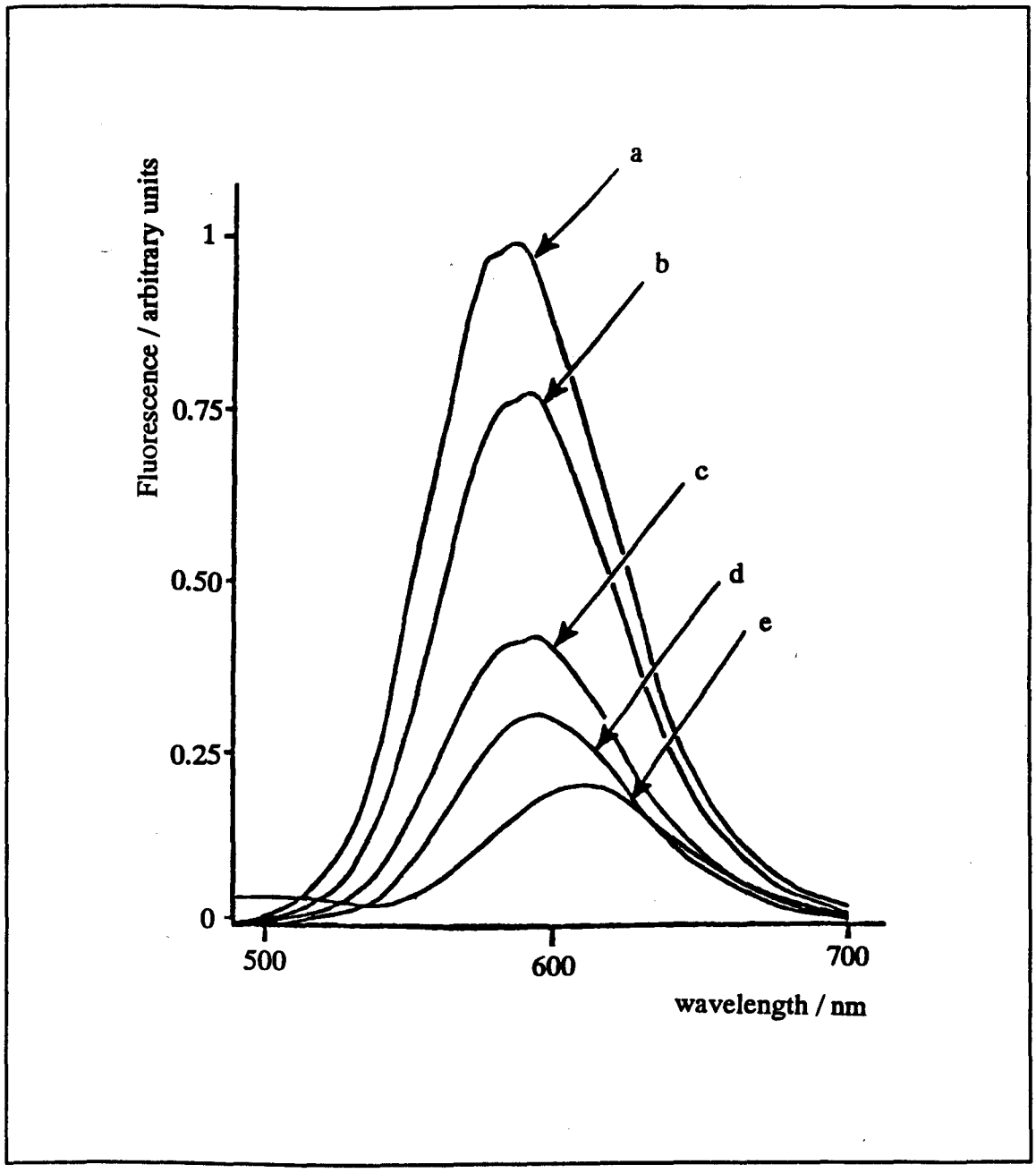

Figure 3.8. A comparison of the fluorescent spectra of L^7; a = $[Ru(bipy)_3]^{2+}$ (8 x 10^{-6} mol dm^{-3}), b = L^7 (2 x 10^{-6} mol dm^{-3}), c = L^7 with excess Ni^{2+}, d = L^7 with excess Cu^{2+}, e = L^7 with acid.

Experimental

Synthesis of 1,4,7-tris(2,2'-bipyridyl-5'-ylmethyl)-1,4,7-triazacyclononane, L^1.– Described in Chapter 2.

Synthesis of 1,8-bis-(2',2"-bipyridyl-5'-ylmethyl)-1,4,8,11-tetraazacyclotetradecane, L^2.– 5–(Bromomethyl)–2,2'–bipyridine (600 mg, 2.4 mmol), 1,4,8,11-tetraazacyclotetradecane (320 mg, 1.6 mmol) and triethylamine (303 mg, 3.0 mmol) were stirred together in chlorobenzene (150 ml) at 0 °C for 8 h. The solution was then filtered and the solvent evaporated from the filtrate. The residue was dissolved in the minimum volume of CH_2Cl_2, loaded onto a column of silica gel and eluted with CH_3OH : CH_2Cl_2 : NH_3 (50:7:1). The solvent was removed from the desired fraction (determined by proton NMR spectroscopy) to leave a white solid. This was recrystallised from the minimum amount of CH_3CN to give L^2 as a white crystalline solid. Yield 205 mg, 32 %. ^1H NMR ($CDCl_3$, 250 MHz): δ/p.p.m. 8.67 (d, 2H), 8.58 (s, 2H), 8.37 (d, 2H), 8.34 (d, 2H), 7.75 (m, 4H), 7.31 (m, 2H), 4.24 (s, br, 2H), 3.84 (s, 4H), 2.95 (t, 4H), 2.77 (m, 8H), 2.60 (t, 4H), 1.97 (qu., 4H). ^{13}C NMR ($CDCl_3$, 62.89 MHz): δ/p.p.m. 155.6 (2C), 155.3 (2C), 150.1 (2C), 149.1 (2C), 138.1 (2C), 136.8 (2C), 132.6 (2C), 123.7 (2C), 120.9 (2C), 120.6 (2C), 55.9 (2C), 50.5 (2C), 49.6 (2C), 47.9 (2C), 47.3 (2C), 24.3 (2C). Mass spectrum (CI / NH_3): *m/z* 537 (Calc. for L^2H^+, 537).

Synthesis of 1,4,8,11-tetra-(2',2"-bipyridyl-5'-ylmethyl)-1,4,8,11-tetraazacyclotetradecane, L^3.– 5–(Bromomethyl)–2,2'–bipyridine (1.01g, 4.1 mmol), 1,4,8,11–tetraazacyclotetradecane (0.20g, 1.0 mmol) and triethylamine (0.50 g, 5 mmol) were stirred at 100 °C in chlorobenzene (200 cm^3) for 1 h. The solution was then filtered and the solvent evaporated. The residue was recrystallised from the minimum quantity of acetonitrile and the product collected as a white crystalline material. Yield 570 mg, 65 %. ^1H NMR (250 MHz, $CDCl_3$): δ/p.p.m. 8.64 (d, 4H), 8.56 (s, 4H), 8.33 (d, 4H),

8.27 (d, 4H), 7.77 (m, 8H), 7.26 (m, 4H), 3.46 (s, 8H), 2.63 (s, 8H), 2.52 (t, 8H), 1.79 m, 4H). ^{13}C NMR (62.89 MHz, $CDCl_3$): δ/p.p.m. 156.1 (4C), 154.9 (4C), 149.6 (4C), 149.0 (4C), 137.4 (4C), 136.7 (4C), 135.4 (4C), 123.4 (4C), 120.9 (4C), 120.5 (4C), 56.2 (4C), 51.3 (4C), 50.5 (4C), 24.3 (2C). Mass spectrum *m/z* (CI / NH_3): 873 (Calc. for L^3H^+, 873).

Synthesis of (2',2"-bipyridyl-5'-ylmethyl)-1,2-diaminoethane, L^4.– A solution of 5-(bromomethyl)–2,2'–bipyridine (420 mg, 1.7 mmol) in chlorobenzene (10 cm^3) was added dropwise to a stirred solution of 1,2–diaminoethane (400 mg, 6.8 mmol) in the same solvent (100 cm^3) at 110 °C. After 1 h the reaction mixture was cooled and the solvent removed. The residue was recrystallised from chloroform to give white needles of L^4. Yield 221 mg, 57 %. ^1H NMR (CD_3OD, 250 MHz): δ/p.p.m. 8.70 (d, 2H), 8.33 (m, 2H), 8.01 (m, 2H), 7.50 (m, 1H), 4.94 (s, 4H), 3.96 (s, 2H), 3.06 (t, 2H), 2.93 (t, 2H). ^{13}C NMR (CD_3OD, 62.89 MHz): δ/p.p.m. 154.6, 153.8, 149.2, 149.1, 138.7, 138.5, 135.9, 125.0, 122.1, 121.9, 50.7, 50.0, 40.5. Mass spectrum (CI / NH_3): *m/z* 229 (Calc. for L^4H^+, 229).

Ruthenium Complexes.

Synthesis of $[\{Ru(bipy)_2\}_3L^1](ClO_4)_6$, L^5. – L^1 (80 mg, 0.13 mmol) and *cis*-$[(bipy)_2RuCl_2].2H_2O$ (197 mg, 0.38 mmol, 3 equiv.) were refluxed in H_2O (100 cm^3) for 5 hours. The solution was then filtered (to remove any unreacted and sparingly soluble *cis*-$[(bipy)_2RuCl_2].2H_2O$) and the solvent volume reduced to approximately 25 cm^3. Dropwise addition of excess aqueous $NaClO_4$ gave an orange precipitate which was collected by suction filtration and dried *in vacuo* over silica gel. The product was obtained as an orange powder, yield 256 mg, 78 %. ^1H NMR (400 MHz, $(CD_3)_2SO$): δ/p.p.m. 8.85 to 8.69 (m, 18H), 8.20 to 7.90 (m, 18H), 8.03 to 7.90 (m, 15H), 7.77 to 7.38 (m, 18H), 4.14 (s, br, 2H), 3.16 (s, 6H), 2.27 to 1.85 (m, 12H). ^{13}C NMR (100.62 MHz, $(CD_3)_2SO$): δ/p.p.m. 156.7 to 156.5, (12C), 155.2

(2C), 151.4 (14C), 150.9 (2C), 149.5 (1C), 140.1 (2C), 138.1 to 137.5 (20C), 128.1 to 127.9 (15C), 24.6 to 124.2 (20C), 120.4 (1C), 120.2 (1C), 58.4 (3C), 54.4 (6C). Uv-visible spectrum in CH_3CN [λ_{max} / nm (ε / dm^3 mol^{-1} cm^{-1})]: 453 (42 500), 288 (249 000), 243 (84 700). Found: C, 47.83, H, 3.59, N, 11.76. Calc. for $C_{99}H_{87}Cl_6N_{21}O_{24}Ru_3$ H_2O: C, 47.77, H, 3.58, N, 11.82 %.

Synthesis of $[\{Ru(bipy)_2\}_2L^2H_2](PF_6)_6$, L^6. – L^2 (100 mg, 0.19 mmol) and *cis*-$[(bipy)_2RuCl_2].2H_2O$ (194 mg, 0.37 mmol) were refluxed in methanol (25 cm^3) for 12 h. The solvent was removed and the deep orange residue dissolved in H_2O (5 cm^3). This was loaded onto a column of Sephadex C–25 cation exchange resin and eluted as described before. The main fraction was eluted with 0.8 mol dm^{-3} NaCl (aq) and was treated with excess saturated aqueous NH_4PF_6 solution. The resulting orange precipitate was collected by filtration recrystallised from hot CH_3OH : H_2O (1:4) and dried *in vacuo* over silica gel. Yield 171 mg, 46 %. ^1H NMR (250 MHz, CD_3NO_2): δ/p.p.m. 8.44 (m, 13H), 7.97 (m, 12H), 7.79 (m,12H), 7.54 (s, 2H), 7.31 (m, 11H), 3.37 (q, br, 4H), 2.73 (s, br, 8H), 2.26 (s, br, 8H), 1.56 (s, br, 4H). ^{13}C NMR (62.89 MHz, CD_3NO_2): δ/p.p.m. 158.6 (2), 158.5 (2), 158.44 (2), 158.40 (2), 157.9 (2), 153.10 (4), 153.07 (4), 152.9 (2), 152.7 (2), 140.2 (2), 139.3 (6), 139.2 (6), 137.8 (2), 55.0 (2), 50.8 (2), 48.3 (2), 47.5 (2), 24.8 (2). Uv–visible spectrum in CH_3CN [λ_{max} / nm (ε / dm^3 mol^{-1} cm^{-1})]: 452 (27 000), 287 (15 900), 248 (53 100). Found C, 39.12, H, 3.39, N, 9.97. Calc for $C_{72}H_{74}F_{36}N_{16}P_6Ru_2$: C, 38.68, H, 3.31, N, 10.03 %.

Synthesis of $[\{Ru(bipy)_2\}_4L^3](ClO_4)_9$, L^7.– L^3 (100 mg, 0.11 mmol) and *cis*-$[(bipy)_2RuCl_2].2H_2O$ (235 mg, 0.45 mmol) were refluxed in H_2O (100 cm^3) overnight and then treated as described above for $[\{Ru(bipy)_2\}_3L^1]^{6+}(ClO_4)_6$. The product was obtained as an orange powder. Yield 260 mg, 69 %. ^1H NMR (400 MHz, CD_3NO_2): δ/p.p.m. 8.43 (m, 24H), 7.95 (m, 20H), 7.85 to 7.71 (m, 24H),

7.64 (s, 4H), 7.29 (m, 20H), 5.29 (s, 1H), 3.25 (s, br, 8H), 215 (s, br, 8H), 2.05 (s, br, 8H), 1.21 (s, br, 4H). ^{13}C NMR (100.62 MHz, $(CD_3)_2SO$): δ/p.p.m. 158.6 (8), 158.5 (8), 157.1 (4), 153.1 (4), 153.0 (4), 152.9 (8), 152.8 (4), 152.4 (4), 142.3 (4), 139.1 (20), 139.0 (4), 128.8 (16), 128.6 (4), 125.5 (20), 125.3 (4), 125.1 (4), 57.0 (4), 52.2 (4), 51.8(4), 24.0 (2). Uv–visible spectrum in H_2O [λ_{max} / nm (ε / dm^3 mol^{-1} cm^{-1})]: 453 (46 000), 285 (283 000), 243 (105 000). Found: C, 47.12, H, 3.96, N, 11.41. Calc. for $C_{134}H_{121}Cl_9N_{28}O_{36}Ru_4$: C, 47.02, H, 3.56, N, 11.46 %.

Synthesis of $[\{Ru(bipy)_2\}_4L^3Ni](ClO_4)_{10}$. – L^7 (50 mg, 0.015 mmol) and $Ni(ClO_4)_2.6H_2O$ (27 mg, 0.075 mmol, a five fold equivalence) were refluxed in CH_3OH / H_2O (1:1, 50 cm^3) for 1 h. Dropwise addition of excess saturated aqueous $NaClO_4$ resulted in the precipitation of $[\{Ru(bipy)_2\}_4L^3Ni](ClO_4)_{10}$ as an orange crystalline solid. Yield 32 mg, 62 %. Found: C, 44.43, H, 3.54, N, 10.45. Calc. for $C_{134}H_{120}Cl_{10}N_{28}NiO_{40}Ru_4.2H_2O$: C, 44.51, H, 3.46, N, 10.85 %.

Synthesis of $[Ru(bipy)_2L^4H](PF_6)_3$, L^8.– 5% HBr (0.4 cm^3, 1.5 mmol) was added to a stirred solution of L^4 (230 mg, 0.75 mmol) and *cis*-$[Ru(bipy)_2Cl_2].2H_2O$ (390 mg, 0.75 mmol). The solution was refluxed in H_2O (50 cm^3) for 5 h, filtered (to remove any unreacted *cis*-$[Ru(bipy)_2Cl_2].2H_2O$) and the solvent evaporated. The deep orange residue was dissolved in H_2O (5 cm^3), loaded onto a column of Sephadex C-25 cation exchange resin and eluted with 0.1 – 1.0 mol dm^{-3} NaCl (aq). The main orange band was eluted with approximately 0.4 mol dm^{-3} NaCl and was treated with excess aqueous NH_4PF_6. The resulting orange precipitate was filtered and dried as described above. Yield 340 mg, 42 %. ^1H NMR (250 MHz, D_2O): δ/p.p.m. 8.54 (m, 6H), 8.16 (d, 1H), 8.02 (m, 6H), 7.76 (m, 5H), 7.35 (m, 5H), 4.19 (s, 2H), 3.39 (t, 2H), 3.32 (t, 2H). ^{13}C NMR (45.28 MHz, D_2O / dioxan): δ/p.p.m. 159.1 (1C), 157.7 (4C), 157.1 (1C), 153.2 (1C), 152.2 (4C), 152.0 (3C), 139.6 (1C), 138.6 (4C), 131.4 (1C), 128.5 (1C), 128.1 (4C), 125.6 (1C), 125.0 (4C), 48.9 (1C), 45.1 (1C), 36.3 (1C). Mass spectrum (FAB / NBA): *m/z* 787 (Calc. for $[\{Ru(bipy)_2L^4\}(PF_6)_2]^+$, 787).

Uv-visible spectrum in CH_3CN [λ_{max} / nm (ε / dm^3 mol^{-1} cm^{-1})]: 452 (14 200), 287 (82 000), 245 (27 500).

*Data for pH Fluorescence titration curve of L^8 (**Figure 3.6**):* – Data were recorded at room temperature in aerated solutions, λ_{ex} 450 nm, λ_{em} 600 nm. Two stock solutions were made up: 2.0 x 10^{-4} mol dm^{-3} L^8 in 2 x 10^{-3} NaOH and 2.0 x 10^{-4} mol dm^{-3} L^8 in 10^{-3} HCl. 10 cm^3 of the acidic solution was then titrated with the basic solution, the pH and fluorescence intensity (arbitary units) being recorded after each addition. The data are shown in **Table 3.2.**

pH	Fluorescence Intensity	pH	Fluorescence Intensity
3.00	7.3	3.89	10.8
3.04	7.4	3.95	11.3
3.10	7.4	4.01	11.7
3.14	7.5	4.08	12.1
3.20	7.6	4.16	12.7
3.27	7.8	4.26	13.5
3.38	8.0	4.39	14.4
3.42	8.3	4.57	15.5
3.46	8.4	4.87	17.0
3.51	8.6	7.00	17.7
3.56	8.8	9.12	18.1
3.62	9.2	9.42	18.2
3.69	9.5	9.59	18.2
3.76	9.9	9.89	18.5
3.80	10.2	10.10	18.5
3.85	10.5	10.37	18.4

Table 3.2. Data for the pH fluorescence titration curve of L^8.

CHAPTER 4

Chapter 4

Preliminary Studies on the Functionalisation of Tet *a* and Tet *b* with 2,2'–Bipyridyl–5'–ylmethyl Pendant Arms, and of Tet *b* with 2–Pyridylmethyl arms.

The tetra–azamacrocyclic ligands tet *a* (meso) and tet *b* (racemic) were first synthesised by Curtis.[133] In this early synthesis, tet *a* and tet *b* were obtained *via* a template reaction using nickel perchlorate. The use of a metal ion has subsequently been shown to be unnecessary. Tet *a* and tet *b* may be obtained in good yield from the reaction of 1,2–diaminoethane monohydrobromide with acetone, followed by reduction with sodium borohydride.[134] There is one previous example of the selective functionalisation of tet *a* and tet *b*. The chemistry of these ligands has been reviewed.[135, 136]

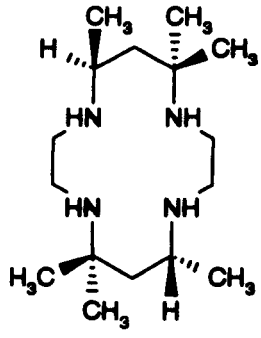

Tet A

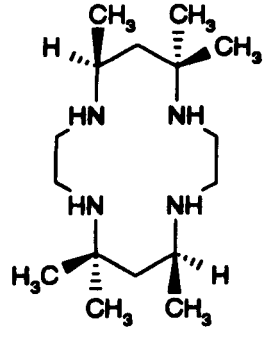

Tet B

Different pendant arms have been added to the nitrogen atoms of the macrocycles cyclam and 9N3, giving new ligands for a variety of applications. Methyl groups attached to the cyclic backbone of tet *a* and tet *b* mean that two of the nitrogen atoms in each macrocycle are more hindered. It was anticipated that steric effects could be used to direct substitution of pendant arms onto the less hindered nitrogen atoms, so

that disubstituted macrocyclic ligands could be synthesised without the problem of positional isomers that is present when forming disubstituted isomers of cyclam.

In this chapter, the synthesis and characterisation of two new ligands L^{10} and L^{11} with two pendant bipyridyl arms is reported, and preliminary investigations into the complexes formed on reaction of these ligands with *cis*-$[Ru(bipy)_2Cl_2]$ (to give L^{12} and L^{13}). Tet *b* was also modified with two pendant 2–pyridylmethyl arms to give L^{14} (time did not permit the analogous modification of tet *a*). The synthesis and characterisation of L^{14} is described. It is anticipated that L^{14} could coordinate to a single metal ion through all six nitrogen atoms, although no complexes of L^{14} have been synthesised to date.

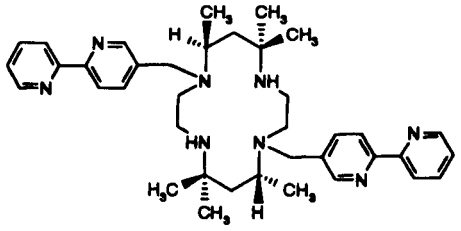

L^{10}

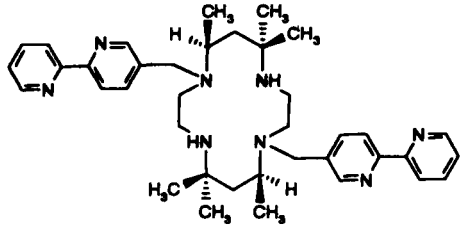

L^{11}

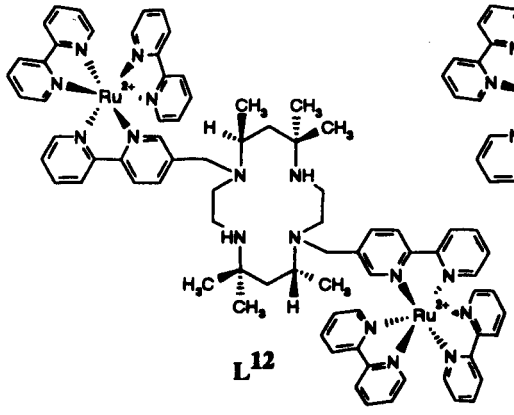

L^{12}

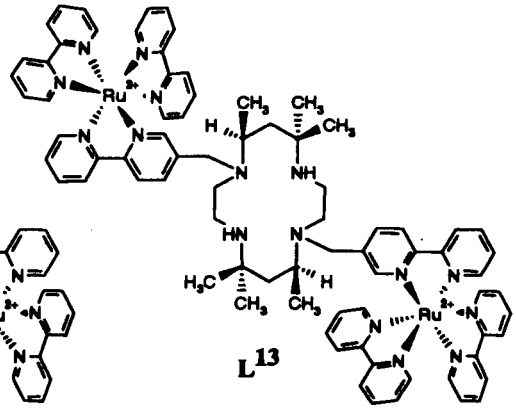

L^{13}

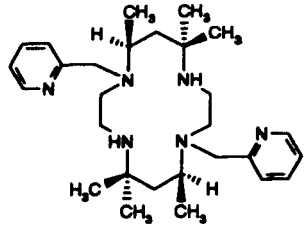

L^{14}

Results and Discussions.

Synthesis.– L^{10} and L^{11} are obtained from the parent macrocycles tet *a* and tet *b* by reaction with two equivalents of 5–bromomethyl–2,2'–bipyridine in the presence of triethylamine. The ligands are characterised by their proton and ^{13}C NMR spectra, by DEPT and NOE difference experiments, and by their CI mass spectra. The ^{13}C NMR spectra show each ligand to have an element of symmetry. In the ^{13}C NMR spectrum of L^{10} in $CDCl_3$, there are ten downfield (aromatic) and nine upfield (aliphatic) resonances, with two overlapping upfield resonances at δ 51.9 p.p.m.. In a DEPT experiment on L^{10}, resonances at δ 156.1, 154.6, 136.4 and 52.4 p.p.m. disappeared, and they are therefore assigned to carbon atoms that have no attached protons. Resonances at δ 50.3, 46.9, 44.5 and 40.3 p.p.m. were inverted (CH_2), and all remaining resonances (δ 150.0, 148.9, 138.6, 136.7, 123.3, 120.8, 120.2, 50.9, 28.8, 24.4 and 13.1 p.p.m.) were unchanged (CH, CH_3).

The four possible positional isomers of bis(bipy) tet *a* are shown in **Figure 4.1.** As the nitrogen atoms at positions 4 and 11 of the macrocyclic ring are less hindered than those at positions 1 and 8, L^{10} is thought to be the most favoured isomer.

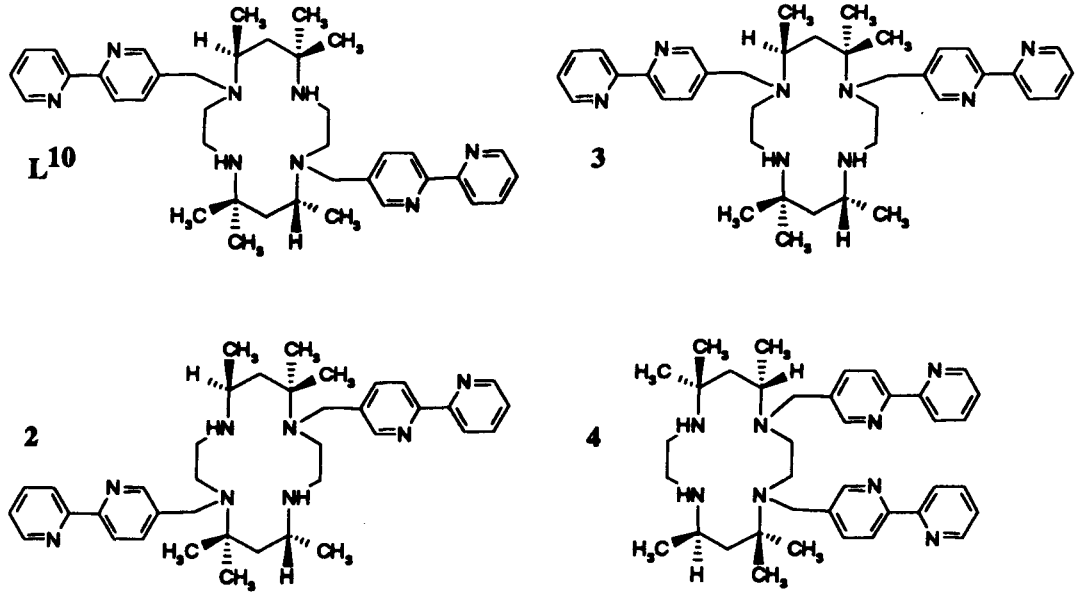

Figure 4.1. The four possible positional isomers of bis(bipy) tet *a*.

L^{10} can be easily distinguished from **3** and **4** as it has nine upfield resonances in the ^{13}C NMR spectrum, **3** and **4** would be expected to have eighteen upfield resonances. NOE difference experiments were performed to help locate the position of the bipy arms on the ring, and thus distinguish L^{10} from **2**. Proximal protons that are established by these experiments include $H_1 - H_i$, $H_i - H_j$ $H_a - H_j$ and $H_2 - H_l$ which confirms the suggestion that L^{10} was the isolated product.

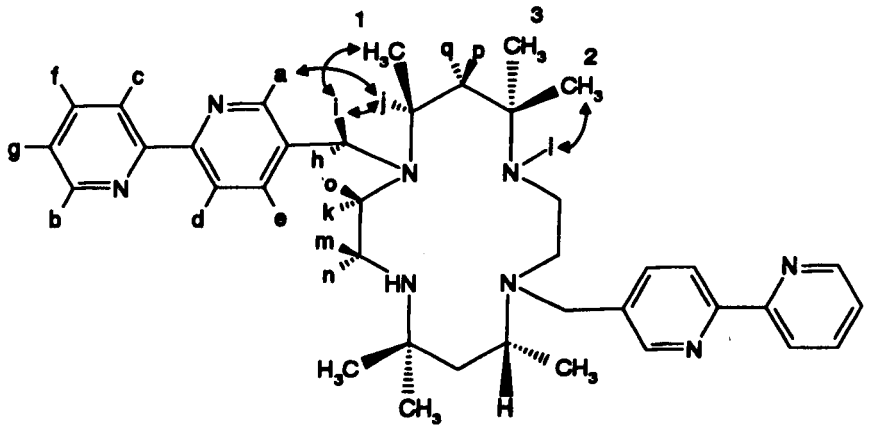

Figure 4.2. L^{10}: Some observed NOE signals. a – q and 1 – 3 are the assignments shown in the NMR spectrum below (Figure 4.3).

The proton NMR spectrum of L^{10} was assigned with the help of a proton carbon correlation, a DEPT spectrum, and NOE difference experiments. From the DEPT spectrum, the four types of carbon atom can be identified (C, CH, CH_2, CH_3). From the proton carbon correlation (**Figure 4.5**), resonances from protons that are attached to the same carbon atom can be identified, i.e. it can be established that p + q, o + k, m + n etc. are attached to the same carbon atom. Protons j can be identified as the only CH protons, and l are absent as they are attached to nitrogen atoms.

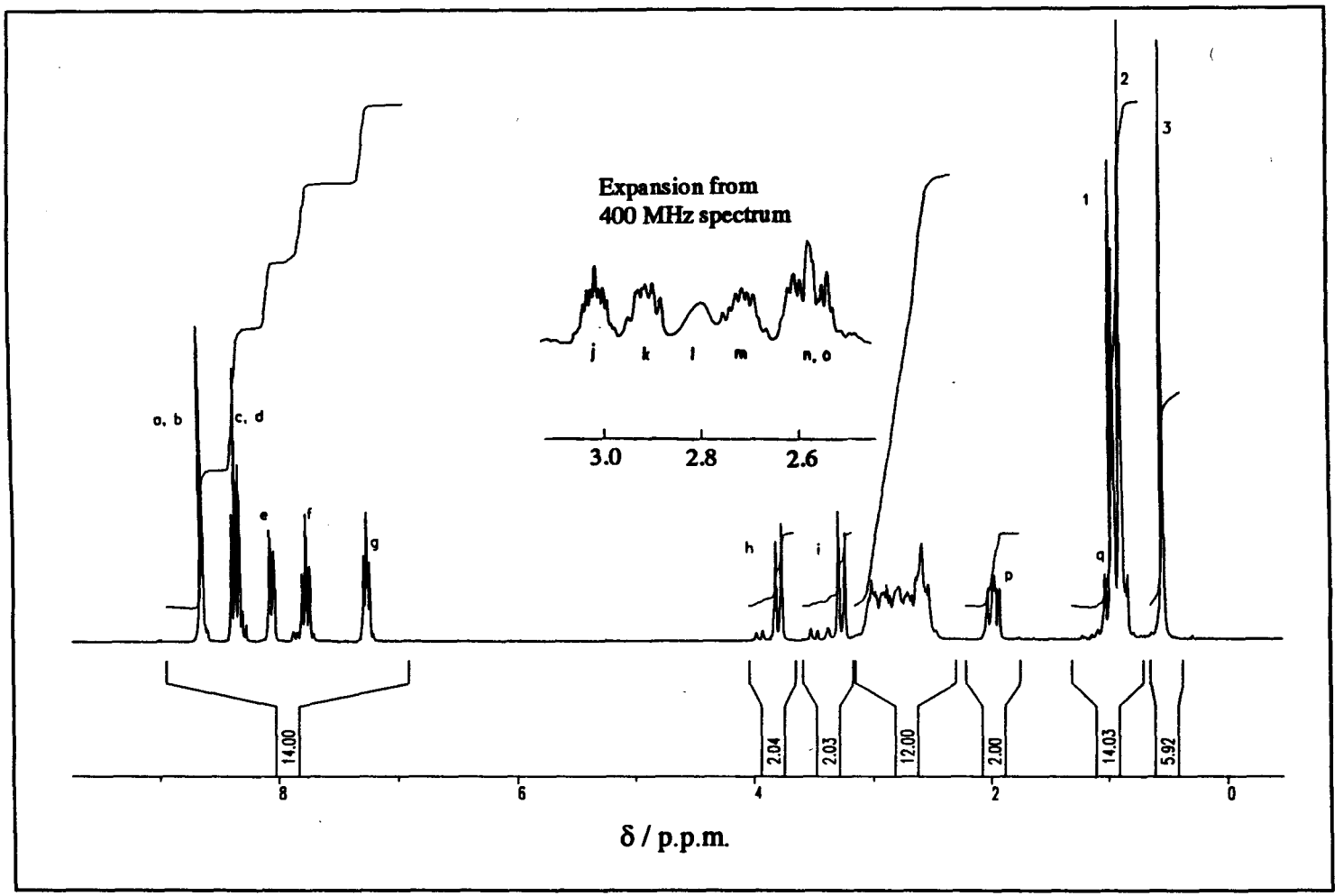

Figure 4.3. Proton NMR Spectrum of L^{10} in $CDCl_3$. Small resonances adjacent to d, f, h and i are attributed to a second *N*–conformational isomer of L^{10}. From the relative integrals, the isomers are present in the ratio 10:1.

In the proton NMR spectrum, an AB quartet centred at 3.52 p.p.m. is assigned to H_h and H_i, the linking methylene protons (**Figure 4.2**). The presence of this quartet shows that these protons are inequivalent, as there is no C_n or S_n axis that equivalences them, they are diastereotopic. Axial and equatorial protons around the macrocyclic backbone are also inequivalent. This is in contrast to the proton NMR spectrum observed for L^2 (cyclam modified with two pendant bipy arms); in the latter case, the spectrum shows the methylene link protons to appear as a singlet (δ 3.46 p.p.m.) and axial and equatorial protons on the macrocyclic framework are also equivalent.

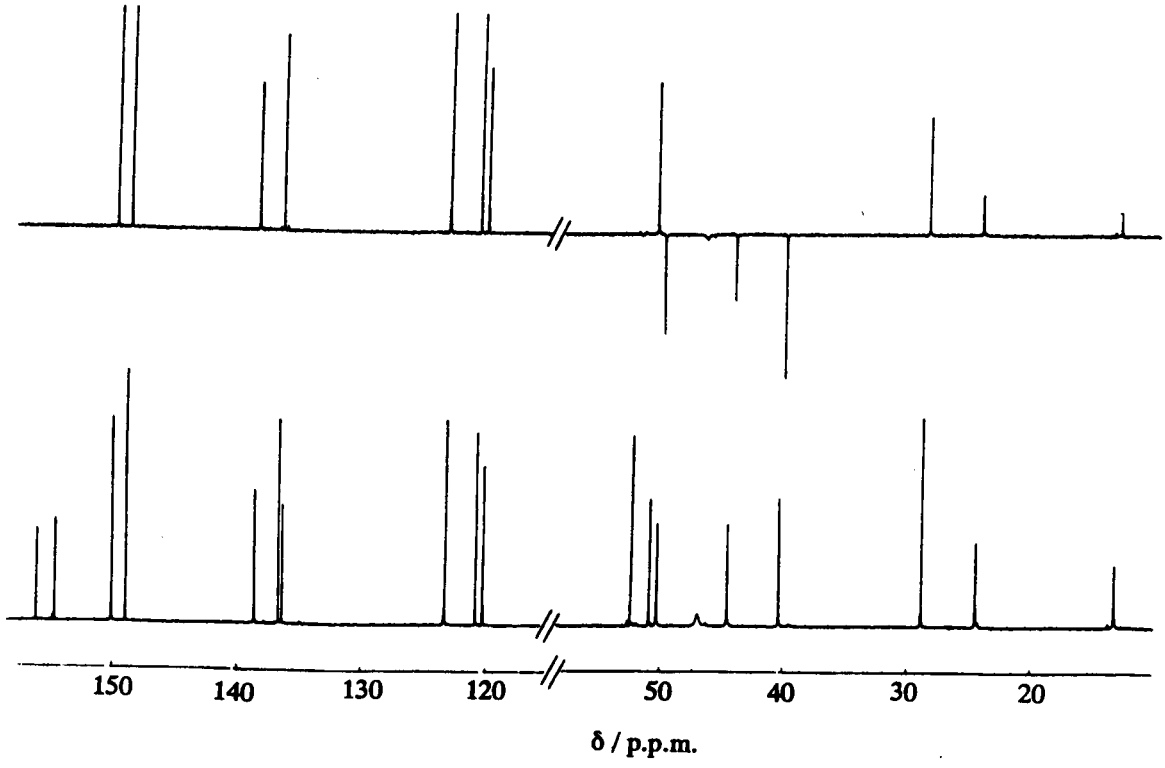

Figure 4.4 Proton decoupled ^{13}C NMR (*lower trace*) and DEPT (*upper trace*) spectra of L^{10} in $CDCl_3$.

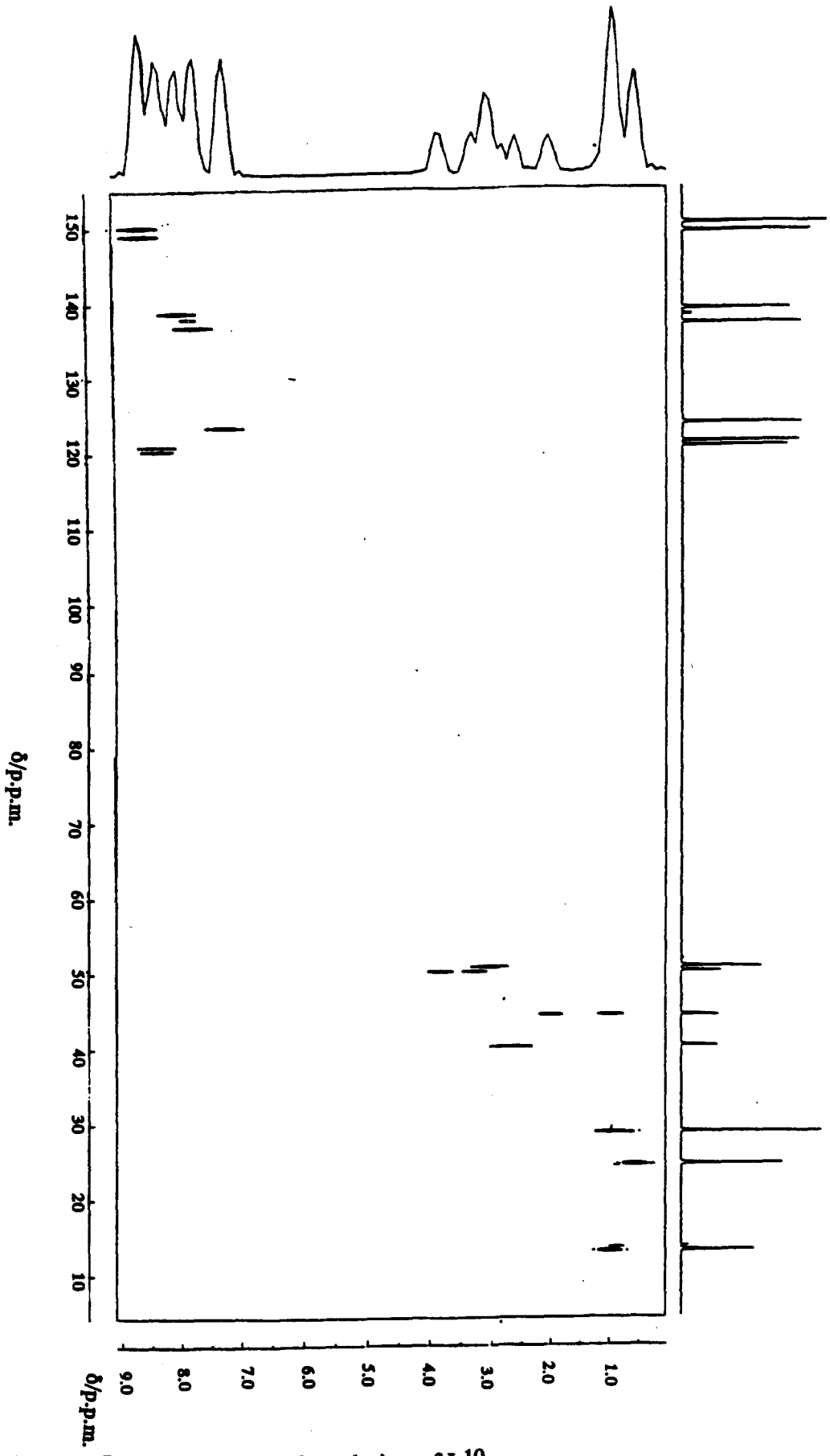

Figure 4.5. Proton Carbon Correlation of L^{10}.

DEPT and NOE difference experiments were also performed on L^{11}. In the DEPT experiment, resonances at δ 155.52, 155.46, 134.2 and 56.5 p.p.m. disappeared (carbon atoms that have no attached protons), resonances at δ 51.9, 47.1, 43.6 and 41.5 p.p.m. were inverted (CH_2), and all remaining resonances (δ 150.3, 149.1, 137.9, 136.9, 123.7, 120.9, 120.6, 51.9, 27.3, 23.9 and 14.4 p.p.m. were unchanged (CH, CH_3).

As with L^{10}, there are four possible positional isomers of L^{11}. Again, two of these isomers can be eliminated from the ^{13}C NMR spectrum, and NOE experiments support the given structure of L^{11}. In particular, $H_h - H_k$, $H_i - H_k$, $H_o - H_a$ and $H_j - H_e$ (**Figure 4.6**) are established as proximal protons which again confirms the positioning of the bipy arms at the less hindered nitrogen atoms. Further NOE signals observed between $H_h - H_2$, $H_o - H_p$, and $H_p - H_h$ would seem to indicate that L^{11} folds in solution, as does the parent macrocycle tet *b*.[163, 164]

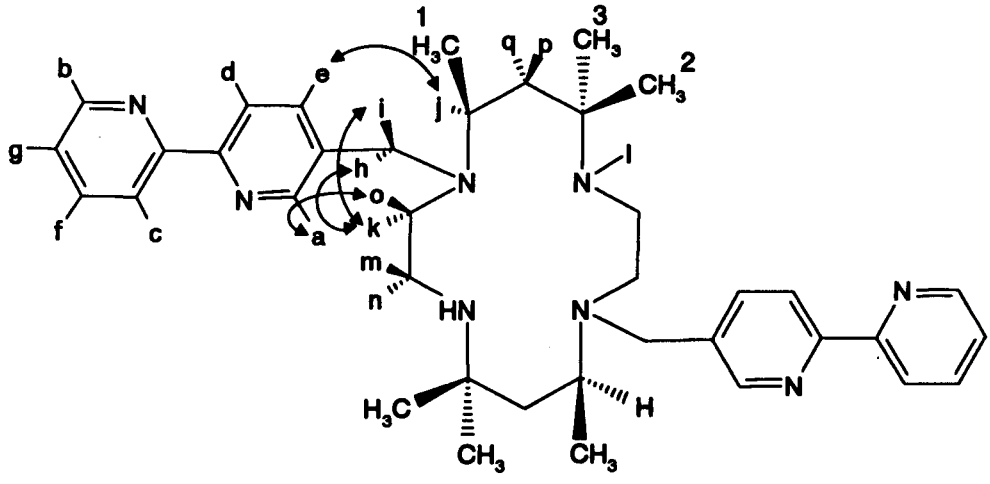

Figure 4.6. Some observed NOE signals and labelling of protons for L^{11}.

The proton NMR spectrum of L^{11} (**Figure 4.7**) shows that umbrella inversion at the macrocyclic nitrogen atoms is slow – methylene link protons, and axial and equatorial macrocyclic protons are inequivalent. This is analogous to the situation discussed above for L^{10}.

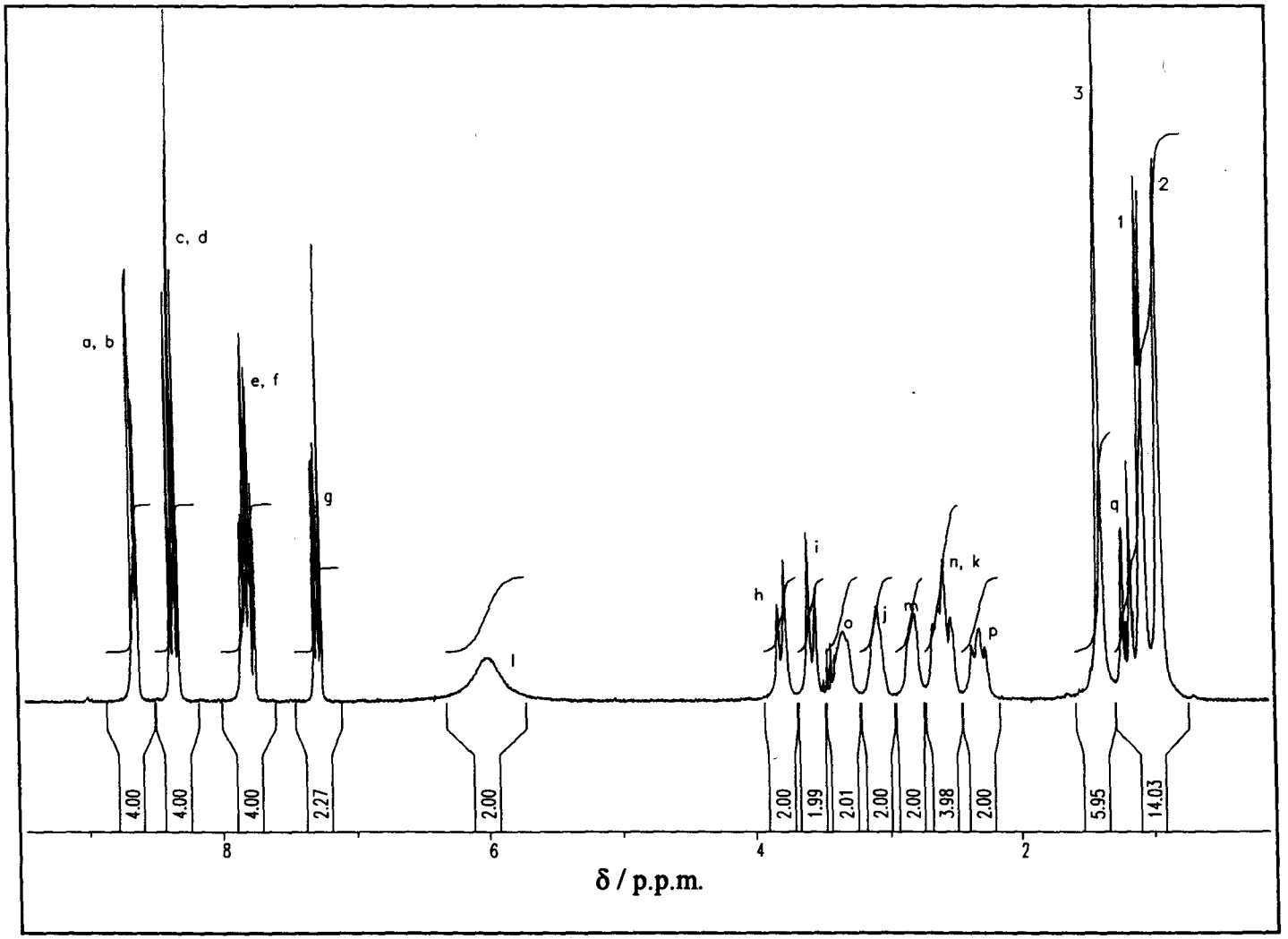

Figure 4.7. Proton NMR Spectrum of L^{11} in $CDCl_3$.

Ruthenium Complexes: – Reaction of L^{10} and L^{11} with two equivalents of *cis*-$[Ru(bipy)_2Cl_2]$ gives L^{12} and L^{13}, which are obtained as red solids. L^{12} and L^{13} are characterised by proton and ^{13}C NMR spectra, uv–visible spectra and elemental analysis. The NMR spectra of L^{12} and L^{13} are broad, particularly in the aliphatic (upfield) region. The related ligands L^5–L^7 (9N3 and cyclam carrying two – four *N*-pendant $[Ru(bipy)_3]^{2+}$ groups) also show broadening in this region. In the case of L^5–L^7, this broadening is attributed to slow umbrella inversion at the macrocyclic nitrogen atoms. With L^{12} and L^{13}, it is thought that another dynamic process must be causing the broadening. In the parent ligands L^{10} and L^{11}, umbrella inversion is slowed to the extent where the aliphatic regions of the proton and ^{13}C NMR spectra are sharp. In the proton NMR spectrum, the linking methylene protons are inequivalent and are seen as a sharp AB quartet (**Figure 4.3** and **4.7**), and axial and equatorial protons about the macrocyclic rings can be distinguished. It is presumed that one preferred conformation of L^{10} and L^{11} is 'frozen out'. It would seem unlikely that addition of bulky $[Ru(bipy)_3]^{2+}$ groups to the pendant bipy arms of L^{10} and L^{11} would cause the umbrella inversion to speed up (and so give rise to broader NMR spectra). Instead, it is postulated that another dynamic process must be present in L^{12} and L^{13} to cause the observed broadening. This could be restricted rotation of the $[Ru(bipy)_3]^{2+}$ units due to interaction of these units with the methyl groups on the backbone of each macrocyclic ring.

The proton and ^{13}C NMR spectra of L^{12} suggest that more than one isomer is present. The parent ligand L^{10} has a single resonance above δ 20 p.p.m., at δ 13.1 p.p.m. This is assigned to C_a and $C_{a'}$ (**Figure 4.8**).

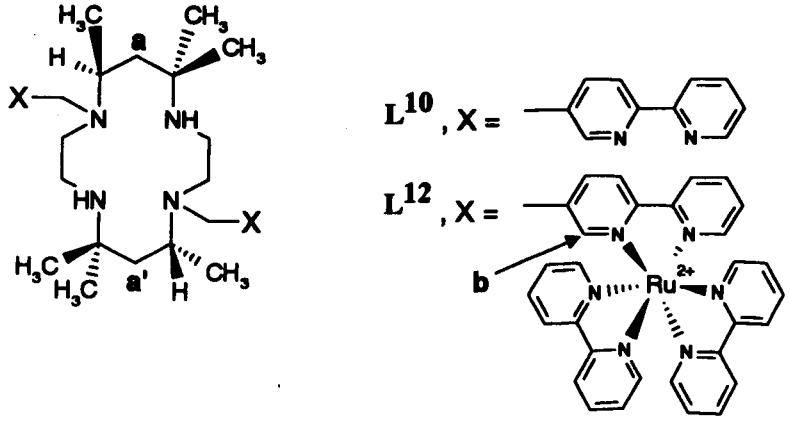

Figure 4.8. L^{10} and L^{12}.

The ^{13}C NMR spectrum of L^{12} shows four resonances upfield from 20 p.p.m., at δ 13.6, 13.3, 12.5 and 12.4 p.p.m. (**Figure 4.10**). It is therefore suggested that umbrella inversion at the tertiary nitrogen atoms of the macrocyclic ring is hindered to such an extent that different *N*–conformational isomers of L^{12} can be seen. **Figure 4.9** shows the nine *N*–conformational isomers of tet *a* with two pendant N–R arms. (This excludes enantiomeric isomers, possible for **2**, **3**, **7**, **8** and **9**).

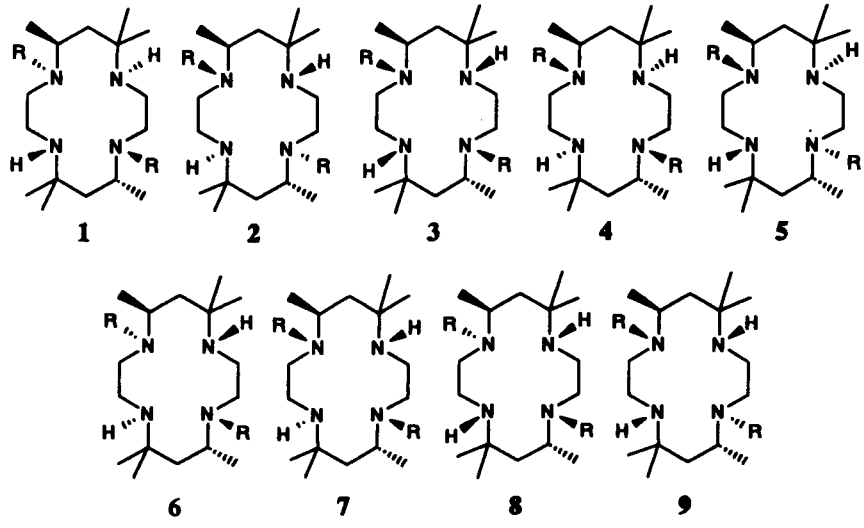

Figure 4.9. The nine *N*–conformational isomers of tet *a* with two pendant N–R arms.

Of the nine isomers possible, three are favoured (isomers **1**, **6** and **8**) because in these isomers the *N*–pendant arms (R) are on the opposite side of the macrocyclic plane to that of the neighbouring C–Me groups. **1** and **6** are centrosymmetric, and so $C_a = C_{a'}$ and only one ^{13}C NMR resonance upfield from δ 20 p.p.m. is expected from either of these isomers. In **8**, $C_a \neq C_{a'}$, so two equal height resonances upfield from δ 20 p.p.m. are expected. Therefore, four resonances upfield from δ 20 p.p.m. are likely for the three favoured isomers, as observed.

Further evidence for isomerism of L^{12} can be seen in the proton NMR spectrum; H_b (**Figure 4.8**) would be expected to appear as a singlet at around δ 7.6 p.p.m. (in the related ligands L^6 and L^7, H_b is at δ 7.54 and 7.64 p.p.m. respectively). In the proton NMR spectrum of L^{12} (**Figure 4.11**), no clear singlet in this region can be seen. Instead, there are two resonances at δ 7.74 and 7.78 p.p.m., both of which seem to be made up of two or more overlapping singlets. The elemental analysis results obtained for L^{12} also indicate a mixture of products. They suggest a formula of $[\{Ru(bipy)_2\}_2L^{10}H_{1.5}](PF_6)_{5.5}$, which could reflect a mixture of products, having either one or two protons associated with the tet *a* ring. This is in contrast to L^{13}, where elemental analysis results support the expected formulation of $[\{Ru(bipy)_2\}_2L^{11}H_2](PF_6)_6$. In the latter case, two protons are associated with the secondary nitrogen atoms of the macrocyclic ring. Recrystallisation of L^{12} from hot CH_3OH/H_2O (1:5) gives a second orange solid, elemental analysis of the recrystallised product also suggests the formulation $[\{Ru(bipy)_2\}_2L^{10}H_{1.5}](PF_6)_{5.5}$. The proton NMR spectrum of the recrystallised product is broader than that of the un–recrystallised material. The two spectra are compared in **Figure 4.11**. The indication is that recrystallisation may be causing isomerisation.

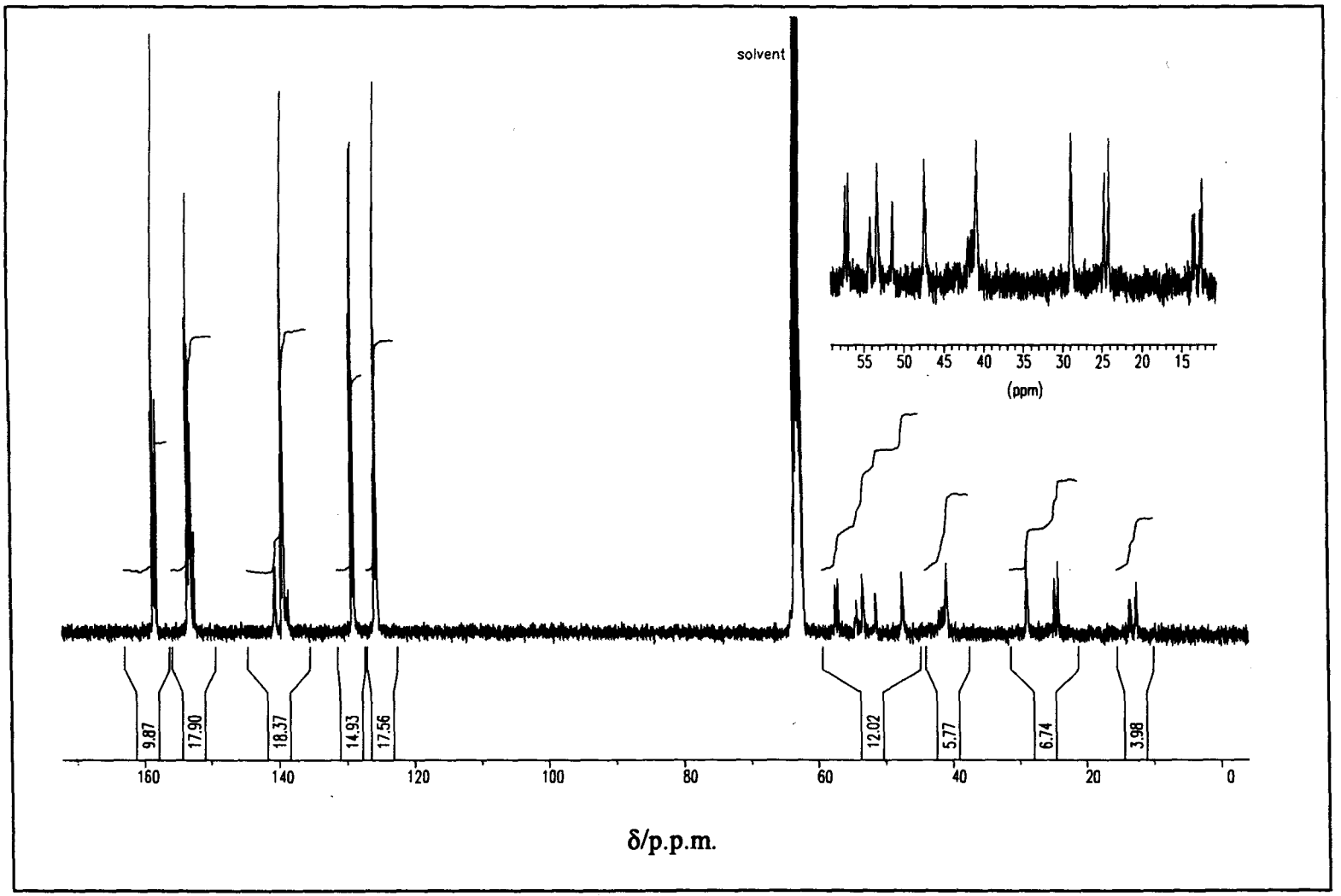

Figure 4.10. ^{13}C NMR Spectrum of L^{12} in CD_3NO_2.

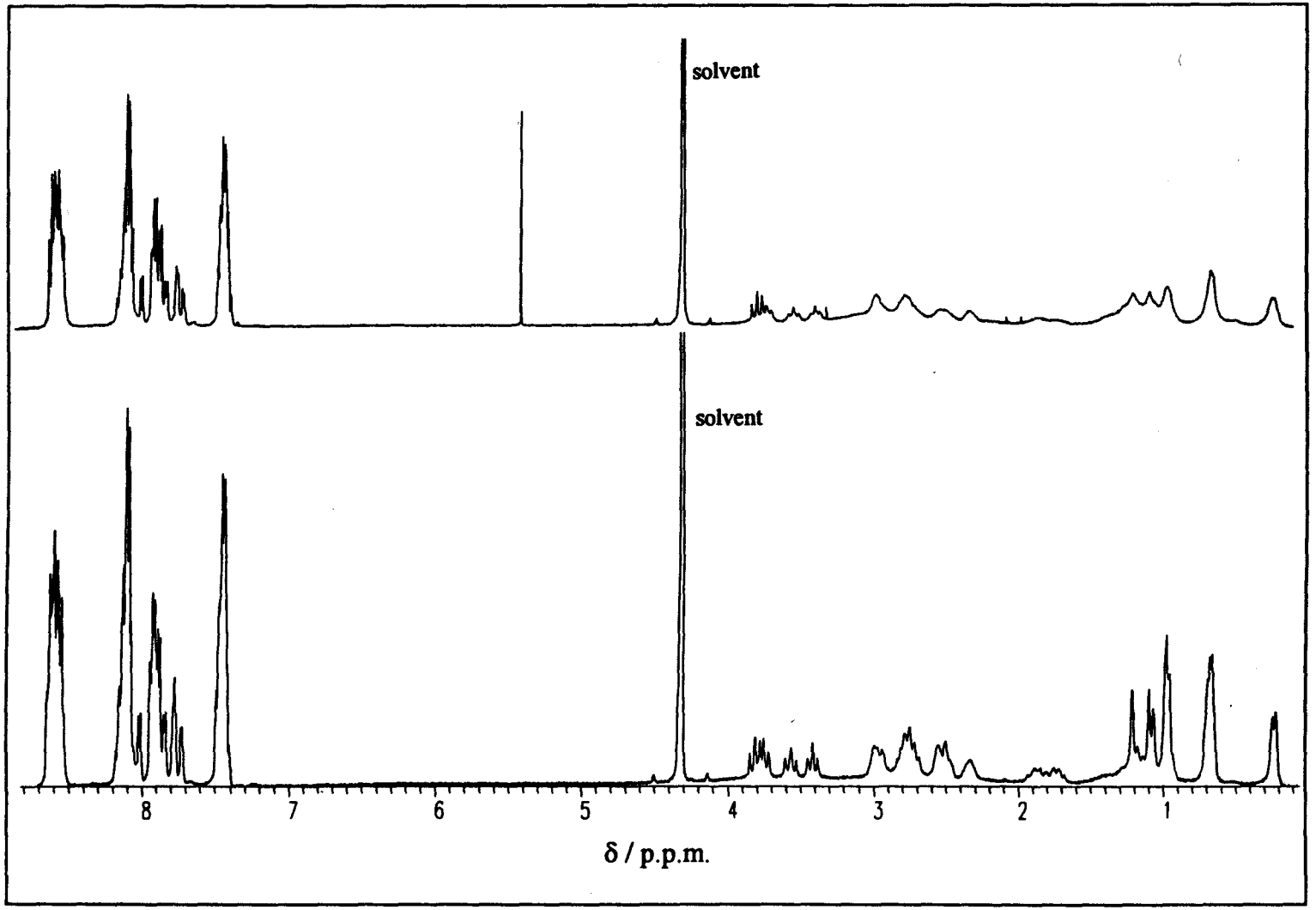

Figure 4.11. Proton NMR Spectra of L^{12} in CD_3NO_2 before (*lower trace*) and after (*upper trace*) recrystallistaion from hot CH_3OH / H_2O.

The proton NMR spectrum of L^{13} is broader than that of L^{12}. This could be caused by greater hindrance to rotation of the $[Ru(bipy)_3]^{2+}$ groups in L^{13} compared to L^{12}, possible if L^{13} adopts a folded geometry in solution. The presence of *N*–conformational isomers can again be detected. In the ^{13}C NMR spectrum of L^{13}, nine upfield (aliphatic) resonances would be expected for a single species, but it can be seen from the ^{13}C NMR spectrum shown in **Figure 4.13** that the number of resonances observed in this region exceeds nine. **Figure 4.12** shows the nine *N*–conformational isomers of tet *b* with two pendant N–R arms. (Excluding enantiomers).

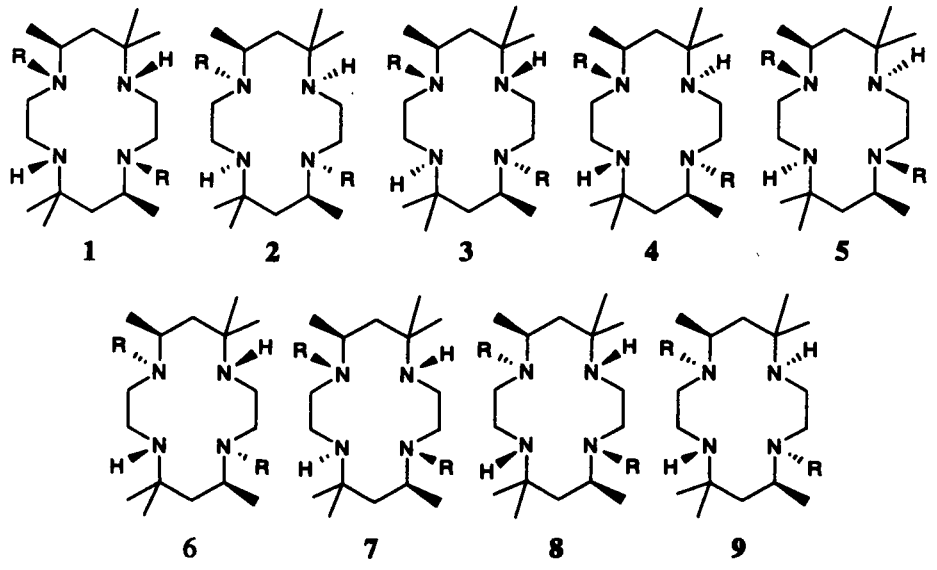

Figure 4.12. The nine *N*–conformational isomers of tet *b* with two pendant N–R arms.

As with the isomers of tet *a*, there are three favoured isomers (**2**, **6** and **9**) out of the nine possible isomers, because in these isomers the *N*–pendant arms (R) are on the opposite side of the macrocyclic plane to that of the neighbouring C–Me groups. In **2** and **6**, $C_a = C_{a'}$ and only one ^{13}C NMR resonance upfield from δ 20 p.p.m. is expected from either of these isomers. In **9**, $C_a \neq C_{a'}$, so two resonances upfield from δ 20 p.p.m. are expected. A total of four resonances upfield from δ 20 p.p.m. is again likely for the three favoured isomers, however the broadness of the ^{13}C NMR spectrum (**Figure 4.13**) makes it difficult to judge how many resonances are present.

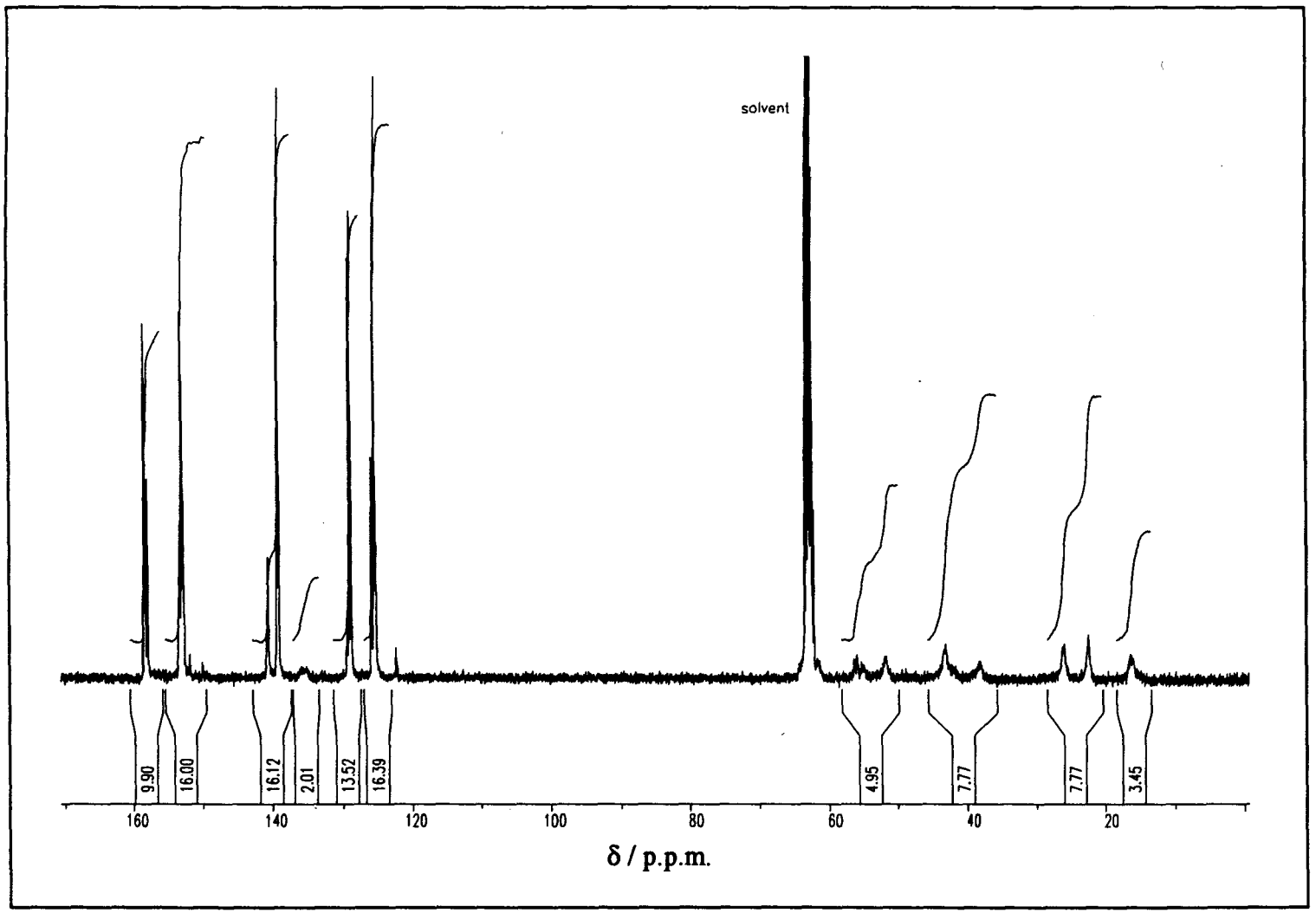

Figure 4.13. ^{13}C NMR Spectrum of L^{13} in CD_3NO_2.

In the uv–visible spectra, both L^{12} and L^{13} show bands at 452 nm (ε = 28 000 and 27 900 $dm^3\ mol^{-1}\ cm^{-1}$ respectively), assigned to the $[Ru(bipy)_3]^{2+}$ groups present in each ligand. L^{12} and L^{13} are fluorescent, having an emission maximum at 607 nm in H_2O when excited at 450 nm. This is typical of $[Ru(bipy)_3]^{2+}$,[122] and together with the uv–visible spectra suggests that any possible steric effects between the $[Ru(bipy)_3]^{2+}$ groups and the tet *a* or *b* moiety do not significantly affect the coordination structure of ruthenium.

L^{14} was prepared by the reaction of tet *b* with 2–chloromethylpyridine hydrochloride in the presence of $NaHCO_3$. Free 2–chloromethylpyridine has a tendency to decompose, so only a small concentration should be present in solution at any one time. This reaction was carried out in refluxing acetonitrile over three days, $NaHCO_3$ being only sparingly soluble in this solvent which allows a low concentration of free 2-chloromethylpyridine to be maintained during the course of the reaction. L^{14} was isolated as a hydrated salt, $C_{28}H_{46}N_6.2HCl.2H_2O$. In the proton NMR spectrum (**Figure 4.14**), a broad singlet at 2.47 p.p.m. is assigned to the two moles of water. An NH^+ proton is associated with each secondary nitrogen atom of the macrocyclic ring. A NOE difference experiment indicates a water molecule is close to one of the protons of each $[NH_2]^+$ group, making the two protons in these groups inequivalent. Two broad triplets at δ 10.14 and 9.55 p.p.m. are assigned to the protons of both $[NH_2]^+$ groups. As with L^{10} and L^{11}, the methylene link protons are inequivalent due to the distereotopic nature of L^{14} (an AB quartet from g and i is observed at δ 3.98 p.p.m; **Figure 4.15**). Axial and equatorial protons around the tet *b* moiety are also inequivalent. The ^{13}C NMR spectrum shows that L^{14} is symmetrical. As expected, there is a total of fourteen resonances. The CI mass spectrum shows a molecular ion at *m/z* 467, assigned to $[C_{28}H_{46}N_6]H^+$.

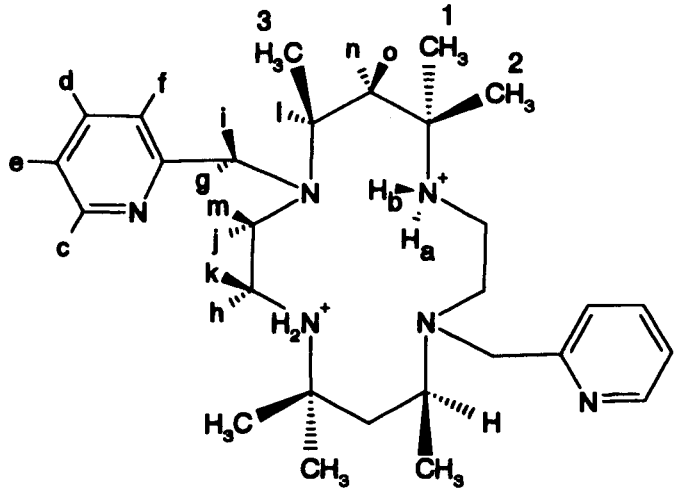

Figure 4.14. $[L^{14}.H_2.2H_2O]^{2+}$; a – o and 1 – 3 are the assignments shown in the proton NMR spectrum (Figure 4.14). The water molecules are omitted for clarity.

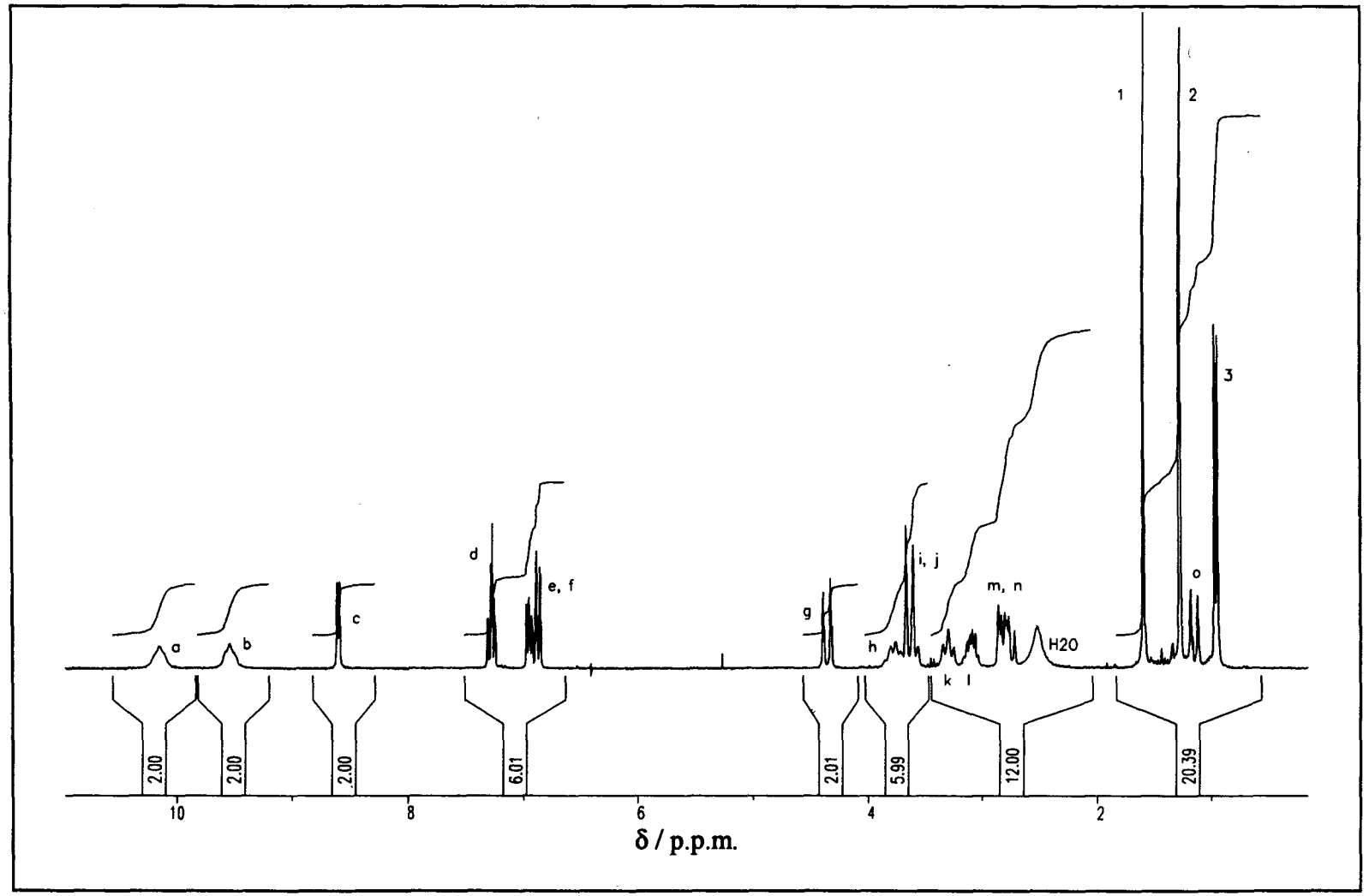

Figure 4.15. Proton NMR Spectrum of $L^{14}.2HCl.2H_2O$ in $CDCl_3$.

Experimental

Synthesis of 5,7,7,12,14,14-hexamethyl-1,4,8,11-tetraazacyclotetradecane, isomers a *and* b *(tet* a *and tet* b*).*– Tet *a*.2H_2O and tet *b*.H_2O were obtained by the literature method.[134] In this synthesis, the reaction of 1,2–diaminoethane monohydrobromide with acetone gives *trans*–[14]–diene dihydrobromide (A.2HBr). Reduction of A with sodium borohydride gives both tet *a*.2H_2O and tet *b*.H_2O which are separated by successive recrystallisations at different pH.

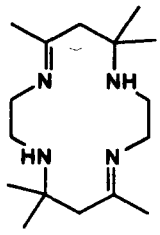

A

Tet *a*.2H_2O was isolated as a white crystalline solid; the melting point was in agreement with literature values[134] (146–147 °C). ^{1}H NMR (250 MHz, $CDCl_3$): δ /p.p.m. 2.79 (m, 6H), 2.50 (t, 2H), 2.25 (t, 2H), 1.36 (m, 4H), 1.05 (s, 6H), 1.04 (s, 6H), 0.96 (d, 6H). ^{13}C NMR (62.89 MHz, $CDCl_3$): δ/p.p.m. 53.0, 51.4, 51.1, 48.0, 42.1, 28.8, 24.1, 21.3.

Like tet *a*.2H_2O, tet *b*.H_2O was isolated as a white crystalline solid; the melting point was in agreement with literature values[134] (102–105 °C). ^{1}H NMR (250 MHz, $CDCl_3$): δ/p.p.m. 2.81 (m, 2H), 2.70 (m, 6H), 2.23 (m, 2H), 1.70 (d of d, 2H), 1.04 (s, 6H), 1.02 (s, 6H), 0.96 (m, 2H), 0.92 (d, 6H). ^{13}C NMR (62.89 MHz, $CDCl_3$): δ /p.p.m. 52.6, 51.4, 47.9, 43.6, 41.1, 29.3, 28.1, 21.1.

Synthesis of 4,11-bis(2,2'-bipyridyl-5'-ylmethyl)-5,7,7,12,14,14-hexamethyl-1,4,8,11-tetraazacyclotetradecane, (L^{10}).– 5,7,7,12,14,14-Hexamethyl-1,4,8,11-tetraazacyclotetradecane, isomer a (tet *a*)[134] dihydrate (0.96 g, 3.0 mmol) 5-bromomethyl–2,2'–bipyridine (1.60 g, 6.4 mmol) and Et_3N (0.66 g, 6.6 mmol) were stirred in C_6H_5Cl (100 cm^3) for 24 h. A white precipitate formed which was removed by filtration and the solvent evaporated. The resultant oily residue was recrystallised from CH_3CN / CH_2Cl_2 (4:1). Yield 0.80 g, 43%. ^{1}H NMR (400 MHz, $CDCl_3$): δ / p.p.m. 8.65 (s,

4H), 8.37 (d, 2H), 8.33 (d, 2H), 8.05 (d, 2H), 7.76 (t, 2H), 7.25 (t, 2H), 3.78 (d, 2H), 3.59 (AB quartet, 4H), 2.90 (m, 2H), 2.79 (s, br, 2H), 2.71 (m, 4H), 1.96 (m, 2H), 0.96 (d, 6H), 0.92 (d, 2H), 0.89 (s, 6H), 0.54 (s, 6H). ^{13}C NMR (100.62 MHz, $CDCl_3$): δ / p.p.m. 156.1 (2), 154.6 (2), 150.2 (2), 148.9 (2), 138.6 (2), 136.7 (2), 136.4 (2), 123.3 (2), 120.8 (2), 120.2 (2), 52.4 (2), 50.9 (2), 50.3 (2), 46.2 (br, 2), 44.5 (2), 40.3 (2), 28.8 (2), 24.4 (2), 13.1 (2). Mass spectrum (CI / NH_3): *m/z* 621 (Calc. for MH^+, 621).

Synthesis of 4,11-bis(2,2'-bipyridyl-5'-ylmethyl)-5,7,7,12,14,14-hexamethyl-1,4,8,11-tetraazacyclotetradecane, (L^{11}).– 5,7,7,12,14,14-Hexamethyl-1,4,8,11-tetraazacyclotetradecane, isomer b (tet *b*)[134] (270 mg, 0.89 mmol), 5–bromomethyl–2,2'-bipyridine (489 mg, 1.96 mmol) and Et_3N (250 mg, 2.47 mmol) were stirred in C_6H_5Cl (50 cm^3) for 24 h. The solution was then filtered and the solvent removed from the filtrate. The resultant oily residue was recrystallised from Et_2O / CH_2Cl_2 (4:1). Yield 280 mg, 51 %. ^1H NMR (400 MHz, $CDCl_3$): δ / p.p.m. 8.68 (s, 2H), 8.66 (d, 2H), 8.38 (d, 2H), 8.35 (d, 2H), 7.83 (d, 2H), 7.79 (t, 2H), 7.30 (m, 2H), 5.28(s, br, 2H), 3.80 (d, 2H), 3.58 (d, 2H), 3.37 (m, 2H), 3.11 (m, 2H), 2.82 (m, 2H), 2.64 (m, 2H), 2.55 (m, 2H), 2.33 (m, 2H), 1.40 (s, 6H), 1.23 (d, 2H), 1.09 (d, 6H), 0.95 (s, 6H). ^{13}C NMR (100.62 MHz, $CDCl_3$): δ / p.p.m. 155.52 (2), 155.46 (2), 150.3 (2), 149.1 (2), 137.9 (2), 136.9 (2), 134.2 (2), 123.7 (2), 120.9 (2), 120.6 (2), 56.5 (2), 51.9 (4), 47.1 (2), 43.6 (2), 41.5 (2), 27.3 (2), 23.9 (2), 14.4 (2). Mass spectrum (CI / NH_3): *m/z* 621 (Calc. for MH^+, 621).

Synthesis of $[\{Ru(bipy)_2\}_2(L^{10}H_{1.5})](PF_6)_{5.5}$, L^{12}. – L^{10} (100 mg, 0.61 mmol) and *cis*-$[Ru(bipy)_2Cl_2].2H_2O$ (177 mg, 0.34 mmol) were refluxed in CH_3OH / H_2O (1:1, 100 cm^3) for 15 h to give a deep orange solution. The solvent was removed and the residue dissolved in H_2O (50 cm^3). The solution was then filtered, and excess saturated aqueous NH_4PF_6 added to the filtrate. This gave an orange precipitate which was collected by suction filtration and recrystallised from hot CH_3OH / H_2O. Yield

320 mg, 86 %. ^{1}H NMR (400 MHz, CD_3NO_2): [Assignment of this spectrum is complicated by (i), broadening, especially in the aliphatic region, and (ii), the presence of at least 4 isomers of L^{12}]. δ / p.p.m. 8.62 (m, 13H), 8.13 (m, 14H), 7.93 (m, 9H), 7.78 (m, 3H), 7.74 (m, 11H), 3.79 (m, br, 3H), 3.57 (t, br, 1H), 3.41 (t, br, 1H), 3.00 (m, br, 2H), 2.80 (m, br, 4H), 2.56 (m, br, 2H), 2.36 (s, br, 1H), 1.80 (m, br, 2H), 1.38 (m, br, 2H), 1.23 (m, br, 3H), 1.11 (m, br, 3H), 0.99 (m, br, 3H), 0.68 (s, br, 6H), 0.26 (m, br, 3H). ^{13}C NMR (100.62 MHz, CD_3NO_2). Due to the presence of four isomers, an estimation of relative populations for each shift is not attempted. δ / p.p.m. 158.6, 158.51, 158.45, 158.3, 158.2, 158.0, 153.5, 153.3, 153.1, 153.04, 152.98, 152.8, 152.4, 140.6, 139.6, 139.4, 139.31, 139.25, 139.22, 138.5, 129.2, 129.0, 128.9, 128.8, 125.8, 125.6, 125.5, 125.4, 125.3, 57.4, 57.0, 55.3, 54.1, 53.2, 51.4, 47.4, 43.4, 40.9, 28.8, 25.4, 24.8, 24.2, 13.5, 13.3, 12.5, 12.4. Uv–visible spectrum in CH_3CN [λ_{max} / nm (ε / dm^3 mol^{-1} cm^{-1})]: 452 (28 000), 288 (162 000), 248 (56400). Found: C, 41.80, H, 3.80, N, 9.84. Calc. for $C_{78}H_{86}F_{24}N_{16}P_4Ru_2.1.5HPF_6$: C, 41.71, H, 3.81, N, 9.98 %.

Synthesis of $[\{Ru(bipy)_2\}_2(L^{11}H_2)](PF_6)_6$, L^{13}. – L^{11} (100 mg, 0.16 mmol) and *cis*-$[Ru(bipy)_2Cl_2].2H_2O$ (177 mg, 0.34 mmol) were treated as described above in the synthesis of L^{12}. Yield 134 mg, 64 %. ^{1}H NMR (250 MHz, CD_3NO_2): δ / p.p.m. 8.47 (m, 13H), 7.97 (m, 13H), 7.75 (m, 13H), 7.31 (m, 11H), 3.48 (s, br, 4H), 3.18 (m, br, 2H), 2.79 (m, br, 4H), 2.56 (s, br, 2H), 2.10 (m, br, 2H), 1.84 (m, br, 2H), 1.23 (m, br, 6H), 1.09 (s, br, 6H), 0.68 (s, br, 2H), 0.02 (s, br, 6H). ^{13}C NMR (100.62 MHz, CD_3NO_2): Again, the presence of more than one isomer and broadening of the spectrum prohibits an estimation of the relative populations. δ / p.p.m. 158.7, 158.44, 158.38, 158.1, 158.04, 157.97, 153.4, 153.3, 153.1, 153.02, 152.98, 152.90, 152.8, 140.8, 140.7, 139.5, 139.4, 139.3, 139.2, 135.7, 129.4, 129.3, 129.13, 129.07, 128.8, 125.9, 125.8, 125.6, 125.5, 125.3, 57.4, 56.9, 54.2, 53.3, 51.4, 51.3, 47.4, 41.9, 41.6, 41.3, 40.8, 28.9, 28.8, 24.7, 24.1, 13.5, 13.3, 12.6, 12.4. Uv–visible spectrum in CH_3CN [λ_{max} / nm (ε / dm^3 mol^{-1} cm^{-1})]: 452 (27 900), 288 (181 000), 248

(63 400). Found: C, 40.54, H, 3.82, N, 9.46. Calc. for $C_{78}H_{86}F_{36}N_{16}P_6Ru_2$: C, 40.39, H, 3.74, N, 9.66 %.

Synthesis of 4,11-bis(2-pyridylmethyl)-5,7,7,12,14,14-hexamethyl-1,4,8,11-tetraazacyclotetradecane, (L^{14}).– 5,7,7,12,14,14-hexamethyl-1,4,8,11-tetraazacyclotetradecane, isomer *b* (tet *b*),[134] (570 mg, 2.0 mmol), 2–chloromethyl–pyridine hydrochloride (660 mg, 4.0 mmol) and $NaHCO_3$(672 mg, 8.0 mmol) were refluxed in acetonitrile (50 cm^3) for 3 days. The solution was then filtered and the filtrate evaporated. The resulting brown oil was dissolved in a solution of CH_2Cl_2 / 40–60 pet. ether from which L^{14} precipitated as its hydrated hydrochloride salt, $L^{14}.2HCl.H_2O$. Yield 412 mg, 37 %. ^1H NMR (400 MHz, $CDCl_3$): δ / p.p.m. 10.14 (t, 2H), 9.55 (t, 2H), 8.59 (d, 2H), 7.27 (t, 2H), 6.94 (t, 2H), 6.86 (d, 2H), 3.98 (AB quartet, 4H), 3.77 (q, br, 4H), 3.60 (m, br, 2H), 3.29 (t, 2H), 3.08 (sextuplet, 2H), 2.79 (m, 4H), 2.47 (s, br, 4H), 1.58 (s, 6H), 1.26 (s, 6H), 1.13 (d, 2H), 0.94 (d, 6H). ^{13}C NMR (100.62 MHz, $CDCl_3$): δ / p.p.m. 156.4 (2), 148.6 (2), 122.9 (2), 122.4 (2), 60.8 (2), 54.2 (2), 51.8 (2), 43.8 (2), 41.5 (2), 37.9 (2), 25.3 (2), 21.1 (2), 12.2 (2). Mass spectrum (CI / NH_3) *m/z* 467 (Calc. for $[C_{28}H_{47}N_6]^+$, 467).

CHAPTER 5

Chapter 5

Two Ligands [1–(2,2'–Bipyridyl–5'–ylmethyl)–1,4,8,11–tetraazacyclotetradecane (L^{15}) and 5,5'–Bis(1,4,8,11–tetra–azacyclotetradecane–1–ylmethyl)–2,2'–bipyridine (L^{16})] Designed for the Synthesis of Polymetallic Complexes.

Bi– and poly–nuclear complexes consisting of two or more metal centres bridged by multidentate ligands have attracted interest in recent years. Such complexes can involve metal–metal interactions, such as energy or electron transfer. L^{15} has been shown to react with an equimolar concentration of different metal ions (M^{2+}) to give mononuclear complexes with the metal ion situated in the macrocyclic cavity (M = Ni, Cu, Zn) or at the pendant arm (M = Fe, Ru).[55] The vacant coordination site can then be used to bind an appropriate second metal ion, and hence to produce polynuclear complexes. In a study of ring size effects among metal complexes with the macrocyclic ligands [13–16]N4,[137, 138] 14N4 (cyclam) was calculated to have the ring size that fits Co^{3+} best. It was anticipated that Co^{3+} could be introduced into the macrocyclic cavity of L^{15}.

Two new complexes of the single pendant arm ligand L^{15} are reported, together with a crystal structure of the mononuclear Co(III) complex *trans*–$[CoCl_2(L^{15}H)](ClO_4)Cl$. In L^{15} (as in L^1 – L^4, Chapter 3) the bipy arm is attached *via* the 5 position, making it sterically impossible for both the cyclam and bipy groups to coordinate simultaneously to a *single* metal ion.[55]

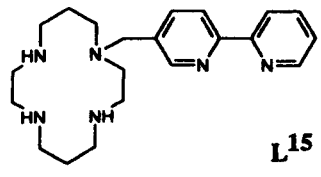

L^{15}

As L^{15} is an unsymmetrical ligand, some of its metal complexes may be formed in two or more isomers. For example, $[Fe(L^{15}H)_3](PF_6)_5$,[55] with an $[Fe(bipy)_3]^{2+}$ core, is isolated as a mixture of both *fac* and *mer* isomers. By using a more symmetrical starting ligand such as L^{16}, this mixture of products can be avoided.

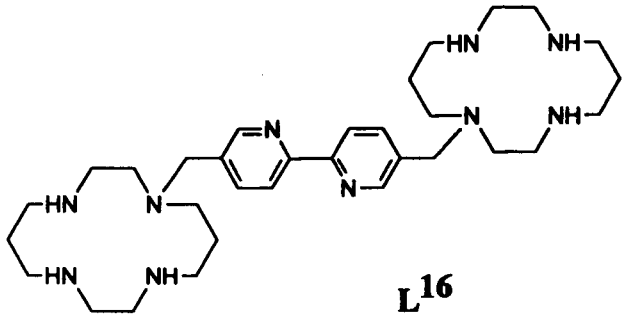

L^{16}

Several bis(tetraazamacrocycles) have been synthesised.[139, 140] These ligands contain two macrocyclic groups joined together by links through the azamacrocyclic nitrogen atoms or by a C–C bond. They have been used to study the formation of binuclear complexes of transition metal ions. Where the metal–metal distance in complexes of these ligands is less than about 9 Å, the magnetic, electrochemical and electronic properties of the binuclear complexes are often different from their mononuclear analogues. Three ligands containing two cyclam units are shown below (**A** – **C**). Unlike L^{16}, these ligands contain only one type of coordination site.

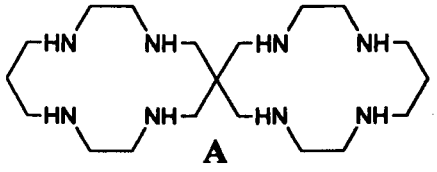

A

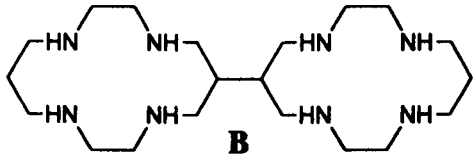

B

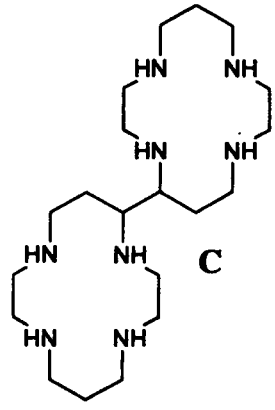

C

In this chapter, the synthesis and characterisation of L^{16} is described. Judicious choice of metal ion enables L^{16} to be used to synthesise mono–, bi– tri– and poly–metallic complexes. Some complexes of L^{16} with Fe(II), Ru(II), Ni(II) and Cu(II) are described.

Results and Discussion.

Synthesis and characterisation of trans–$[CoCl_2(L^{15}H)](ClO_4)Cl$.– Reaction of $CoCl_2.6H_2O$ with L^{15} in the presence of O_2 and HCl followed by the addition of saturated aqueous $NaClO_4$ gave the Co(III) complex *trans*–$[CoCl_2(L^{15}H)](ClO_4)Cl$ as a green solid. Crystals suitable for X–ray analysis were obtained from a hot solution of 0.6 mol dm^{-3} HCl. The crystal structure (**Figure 5.1**) clearly shows the metal ion at the centre of the cyclam cavity, with the bipy arm uncoordinated.

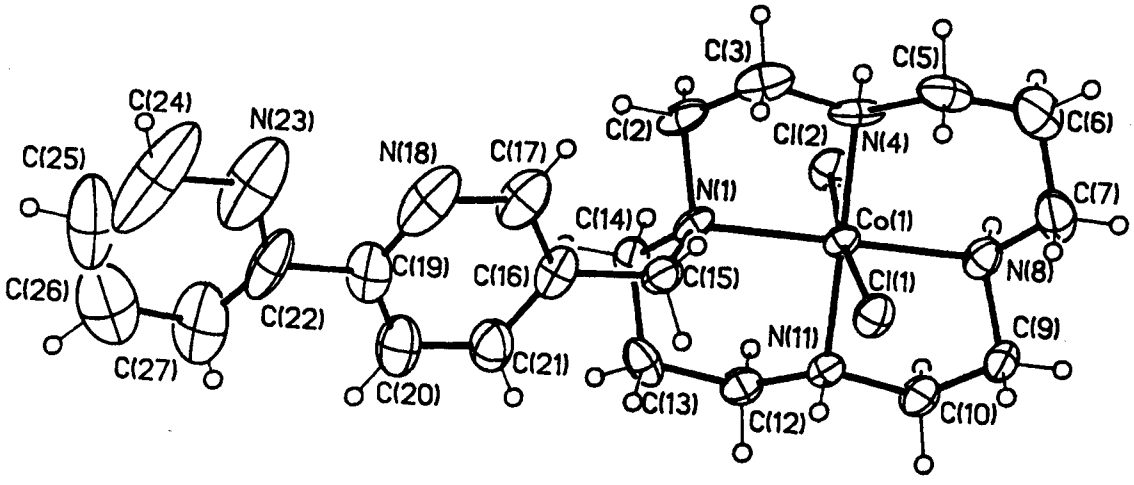

Figure 5.1. X–Ray structure of $[CoCl_2(L^{15}H)](ClO_4)Cl.0.5H_2O$. The anions and H_2O molecules are omitted for clarity.

In $[CoCl_2(L^{15}H)]^{2+}$, the configuration of the cyclam moiety was found to be *RRSS* (the *trans*–III isomer[141]) (**Figure 5.1**). The Co^{3+} ion is coordinated within the N_4 plane of the cyclam cavity. The average cobalt–nitrogen distance to the three secondary amine groups is 1.970 Å, whilst that to the tertiary nitrogen atom (N1) that carries the bipy arm is longer (at 2.068 Å). The Co(III) ion is in a distorted *trans*-octahedral environment, the remaining two coordination sites filled by axial Cl^-

ligands, [Co-Cl(1) = 2.244 Å, Co-Cl(2) = 2.279 Å]. The shorter of these two distances is to the Cl^- ion on the same side of the cyclam ring as the pendant arm.

Co(1) –	Distance / Å	Angle / °				
N1	2.068 (7)					
N4	1.961 (7)	86.4 (3)				
N8	1.975 (7)	179.0 (3)	93.8 (3)			
N11	1.973 (7)	93.5 (3)	177.0 (3)	86.2 (3)		
Cl1	2.244 (3)	94.6 (2)	93.8 (2)	86.4 (2)	89.2 (2)	
Cl2	2.279 (3)	92.5 (2)	86.8 (2)	86.5 (2)	90.2 (3)	172.93 (9)
	Co1	N1	N4	N8	N11	Cl1

Table 5.1. Selected bond lengths and angles in $[CoCl_2(L^{15}H)](ClO_4)Cl$.

The pyridine rings of the bipyridyl pendant arm are essentially coplanar. Their nitrogen atoms are *cis* with respect to the central C–C bond. One of the bipy nitrogen atoms is mono–protonated, and this proton is likely to form a hydrogen bond to the other bipy nitrogen atom making the two bipy N–atoms adopt a *cis*, rather than the more usual *trans* conformation. As a result of protonation, a corresponding Cl^- ion is located in the lattice. From the crystal packing diagrams (**Figure 5.2, 5.3**) $\pi - \pi$ stacking can be detected between the pendant bipyridyl arms. There is hydrogen bonding between one of the Cl^- ions on the cobalt ion and a proton of one secondary amine group (N8). The presence of a proton attached to the bipyridine pendant arm can be detected in the uv–visible spectrum; a solution of bipy at pH 4.40 shows two bands with λ_{max} = 288 and 237 nm, whereas unprotonated bipy in H_2O at pH 7 has two bands at 282 and 235 nm.[158] The observed uv–visible spectrum of $[CoCl_2(L^{15}H)](ClO_4)Cl$ has two bands at 288 and 240 nm, as expected for a protonated species.

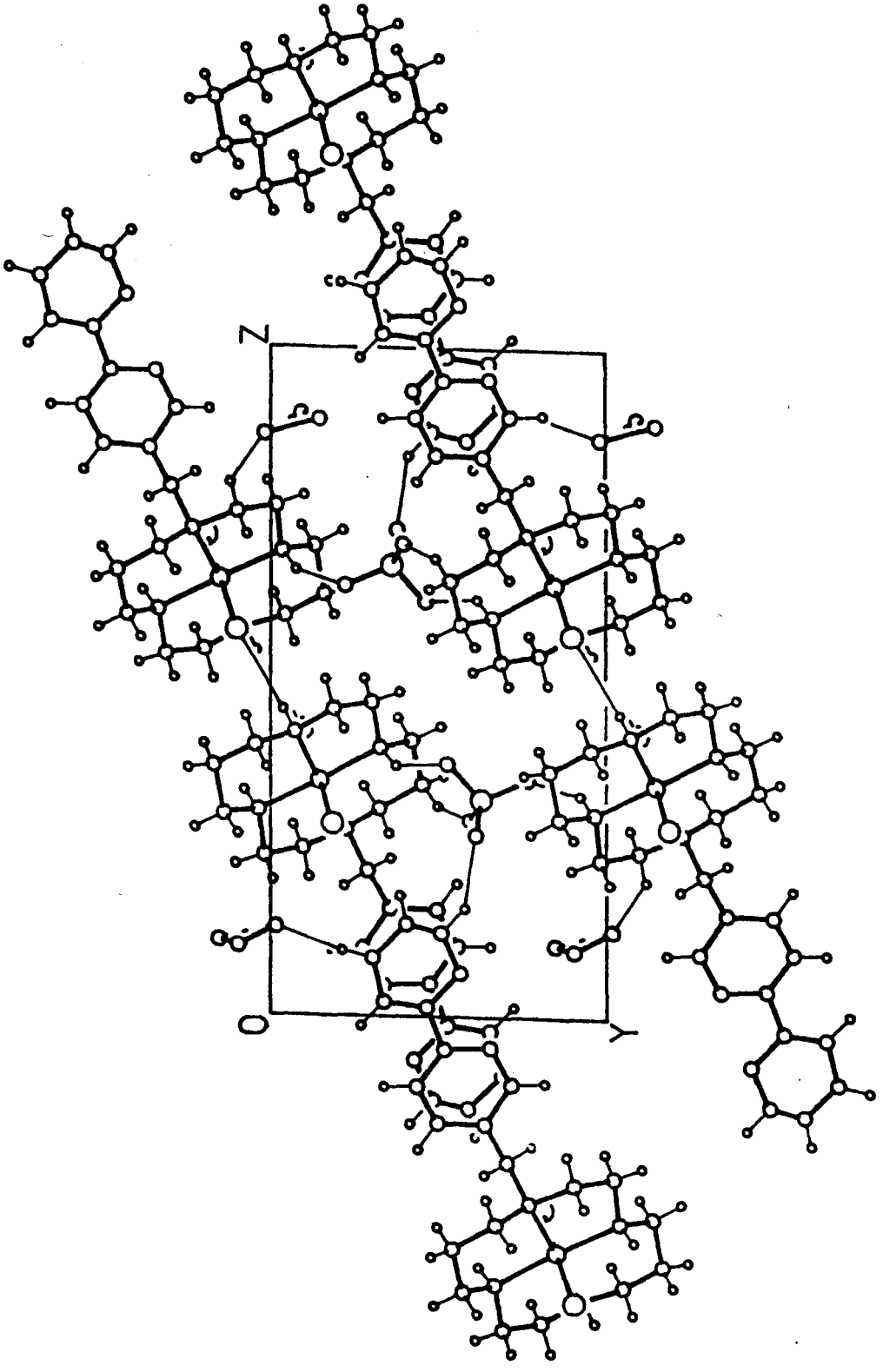

Figure 5.2 Crystal packing diagram of $[CoCl_2(L^{15}H)](ClO_4)Cl.0.5H_2O$.

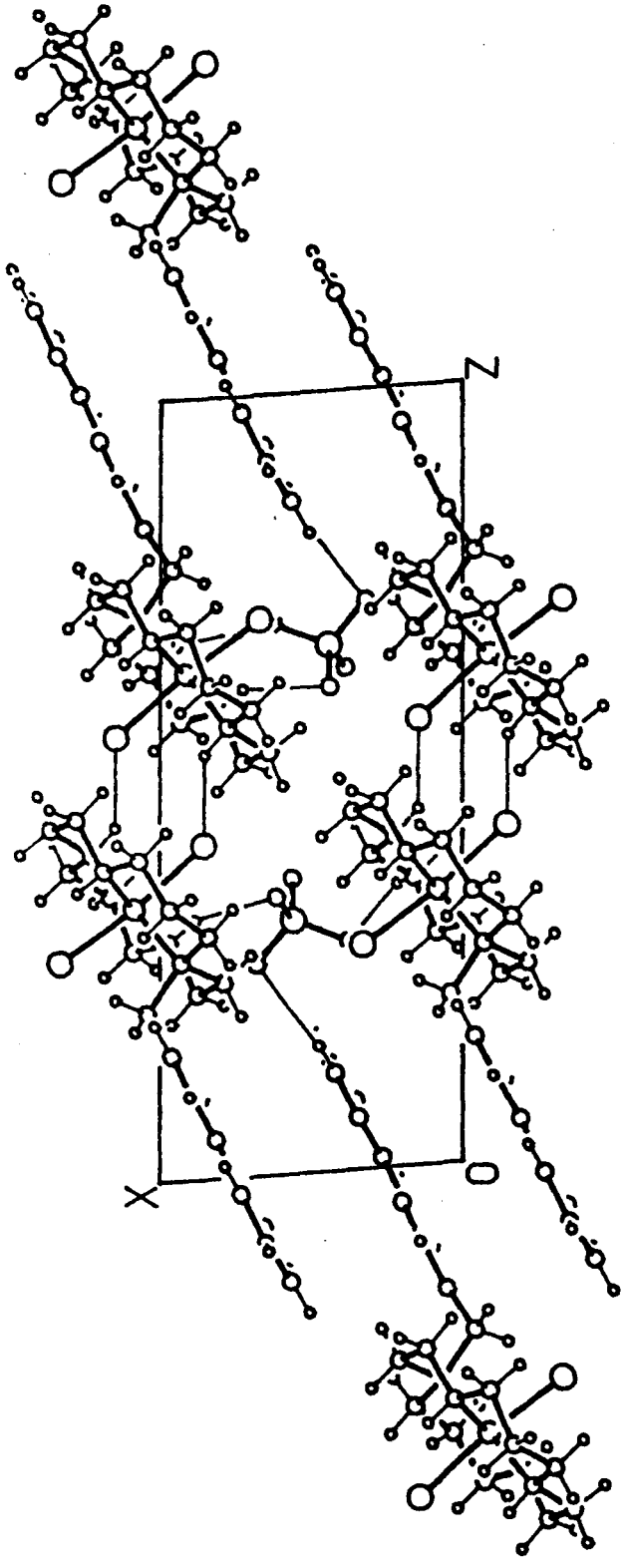

Figure 5.3 Crystal packing diagram of $[CoCl_2(L^{15}H)](ClO_4)Cl.0.5H_2O$.

In addition to the crystal structure, $[CoCl_2(L^{15}H)]^{2+}$ was characterised by its proton and ^{13}C NMR spectra, by a FAB mass spectrum and by its uv–visible spectrum. As the molecule is unsymmetrical, 21 resonances can be seen in the ^{13}C NMR spectrum. As expected, there are many differences between the proton NMR spectrum of $[CoCl_2(L^{15}H)]^{2+}$ and that of L^{15}, particularly in those resonances due to the cyclam ring. In uncomplexed cyclam (and L^{15}), rapid umbrella inversion at the macrocyclic nitrogen atoms means that axial and equatorial protons around the cyclam framework are equivalent on the NMR time scale, as are the two linking methylene group protons in L^{15}. When L^{15} forms a complex with the inert Co(III) ion, the cyclam unit is locked into one configuration. The crystal structure shows this to be the *RRSS* isomer in the solid state. From the proton NMR spectrum, it appears that one configurational isomer persists in solution (presumably the *RRSS* isomer). The resonance assigned to the linking methylene group protons, a singlet in L^{15} (δ = 3.53 p.p.m.) becomes an AB quartet in $[CoCl_2(L^{15}H)]^{2+}$ (δ = 4.14 p.p.m.). Resonances due to the CH_2 protons of the macrocyclic ring in $[CoCl_2(L^{15}H)]^{2+}$ are rather complex. As axial and equatorial protons are inequivalent, and the cyclam unit is unsymmetrical due to the single pendant arm, there are 20 resonances, 14 of which overlap in the region δ 3.05 to 2.35 p.p.m. One NCH_2CH_2N proton shows an unexpected downfield shift and can be seen as a quartet at δ 3.44 p.p.m. One of the four $NCH_2CH_2CH_2N$ protons also shows an unexpected downfield shift; these protons appear as two quintuplets (δ 1.73 and 1.52 p.p.m.) in L^{15}, however in the complex one is shifted to within the main multiplet from δ 3.05 to 2.35 p.p.m. Two protons adjacent to nitrogen atoms in the macrocyclic ring show unexpected upfield shifts, appearing upfield of 2.05 p.p.m.. To help with the assignment, a proton – 2D correlation spectrum (COSY) was taken (**Figure 5.4**).

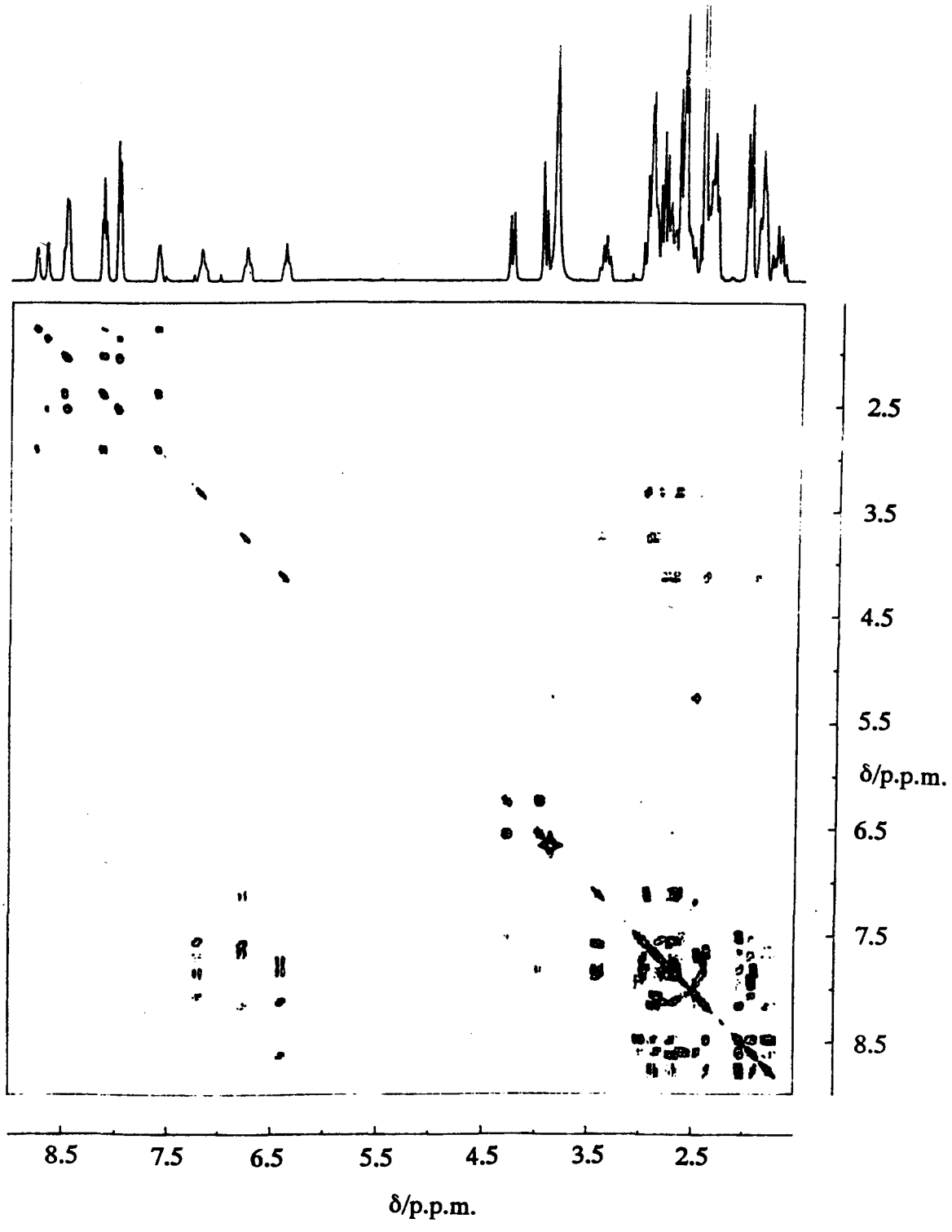

Figure 5.4. Proton – 2D Correlation Spectrum (COSY) at 303 K in $(CD_3)_2SO$, used in the partial assignment of the proton NMR spectrum of $[CoCl_2(L^{15}H)]^{2+}$. The 1–D proton NMR spectrum is shown along the top of the COSY spectrum.

The uv–visible spectrum in 3 mol dm^{-3} HCl shows four bands. Two of these at λ_{max} = 258 nm (ε = 25 300 dm^3 mol^{-1} cm^{-1}) and λ_{max} = 294 nm (ε = 23 200 dm^3 mol^{-1} cm^{-1}) are attributed to the bipy groups of the macrocyclic ligand. The remaining two bands are at λ_{max} = 480 nm (shoulder) (ε = 47 dm^3 mol^{-1} cm^{-1}) and λ_{max} = 638 nm (ε = 34.3 dm^3 mol^{-1} cm^{-1}). The band at 480 nm appears as a shoulder, partially swamped by a ligand band. These values are compared to literature values[142] for $[CoCl_2cyclam]^+$, λ_{max} = 385 nm (ε = 56 dm^3 mol^{-1} cm^{-1}), λ_{max} = 450 nm (ε = 31 dm^3 mol^{-1} cm^{-1}) and λ_{max} = 635 nm (ε = 43 dm^3 mol^{-1} cm^{-1}). It is assumed that a third band in $[CoCl_2(L^{15}H)]^{2+}$ at around 385 nm is swamped by the high intensity ligand band.

Synthesis and characterisation of $[(bipy)_2RuL^{15}CoCl_2](PF_6)_3$.– Reaction of $[CoCl_2(L^{15}H)](ClO_4)Cl$ with *cis*–$[Ru(bipy)_2Cl_2]$ in ethanol–water gave the binuclear species $[(bipy)_2RuL^{15}CoCl_2]^{3+}$ which was isolated as the hexafluorophosphate salt by the addition of excess saturated aqueous NH_4PF_6. The same product could also be obtained by first reacting L^{15} with *cis*–$[Ru(bipy)_2Cl_2]$ and then adding $CoCl_2$ in the presence of O_2 and HCl (**Scheme 5.1**). These findings are similar to previous work, where $[Ru(bipy)_2L^{15}]^{2+}$ reacts further with several divalent metal ions (M^{2+}) to give binuclear species of the type $[(bipy)_2Ru(L^{15}M)]^{4+}$.[55]

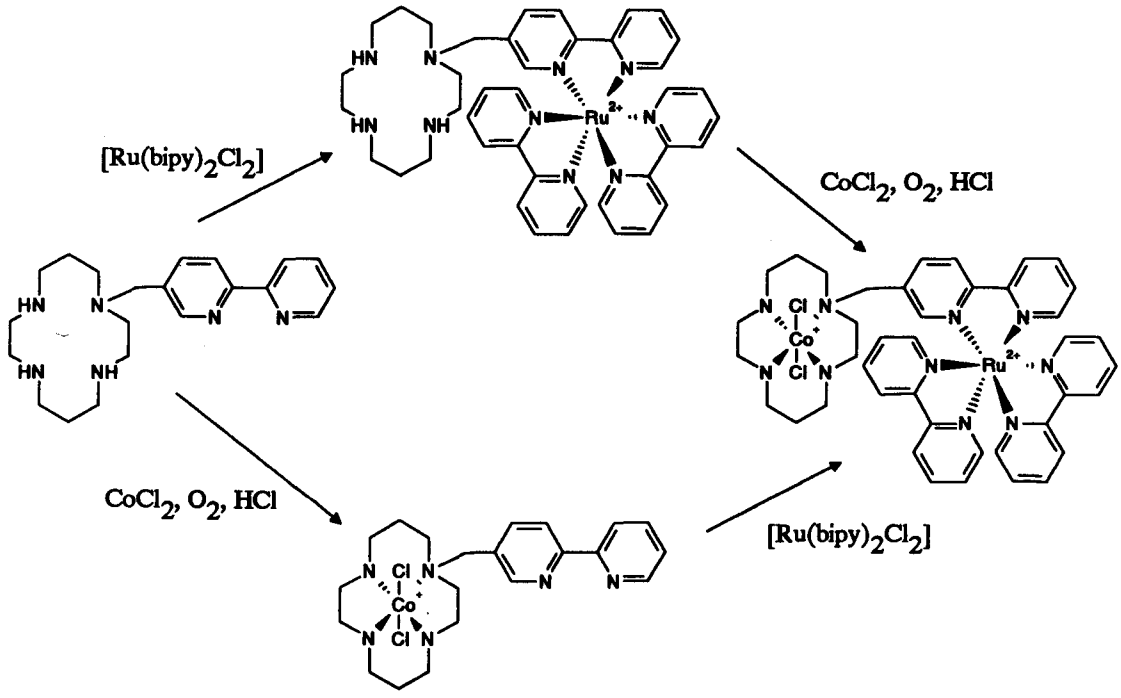

Scheme 5.1. Two routes to $[(bipy)_2RuL^{15}CoCl_2](PF_6)_3$.

$[(bipy)_2RuL^{15}CoCl_2](PF_6)_3$ was characterised by elemental analysis, its proton and ^{13}C NMR spectra, a FAB mass spectrum and its uv–visible spectrum. The ^{13}C NMR spectrum illustrates the lack of symmetry. All 11 aliphatic resonances can clearly be seen. Most of the 30 aromatic resonances can also be seen, although two coincide at δ 158.5 p.p.m., three coincide at δ 139.3 p.p.m. and a further two coincide at δ 125.5 p.p.m.. Upfield resonances in the proton NMR spectrum indicate axial and equatorial protons in the cyclam moiety are inequivalent, as in $[CoCl_2(L^{15}H)]^{2+}$. An AB quartet is again observed for the linking methylene protons. The uv–visible spectrum is characteristic of the $[Ru(bipy)_3]^{2+}$ chromophore. $[(bipy)_2RuL^{15}CoCl_2](PF_6)_3$ shows a band at 453 nm (ε = 11 300 dm^3 mol^{-1} cm^{-1}) which is attributed to the Ru – bipy MLCT transition. This is compared to a band at 453 nm (ε = 14 600 dm^3 mol^{-1} cm^{-1}) for $[Ru(bipy)_3]^{2+}$ itself.[122] Therefore, the $Ru(bipy)_3]^{2+}$ moiety in $[(bipy)_2RuL^{15}CoCl_2]^{3+}$ is little affected by the attached $[CoCl_2(cyclam)]^+$. No absorption bands due to the $[CoCl_2cyclam]^+$ group were recorded as there was insufficient material to make up a strong enough solution.

$[(bipy)_2RuL^{15}CoCl_2](PF_6)_3$ is fluorescent, the emission maximum in H_2O being 612 nm on excitation at 450 nm. This is only slightly shifted from an emission maximum of 607 nm for $[Ru(bipy)_3]^{2+}$ itself,[122] a further indication that a substituent in the 5'–position of bipy has little affect on the coordination structure of Ru^{2+}. However, the relative emission intensity of $[(bipy)_2RuL^{15}CoCl_2](PF_6)_3$ is reduced in comparison to the parent fluorophore, being only one third of that of $[Ru(bipy)_3]^{2+}$. External addition of 100 equivalents of $[CoCl_2(cyclam)]Cl$ did not significantly quench the emission at from the excited state of $[Ru(bipy)_3]^{2+}$, showing that the quenching is caused by the covalently linked $[Co(cyclam)]^+$ group.

Synthesis.– L^{16} is obtained in good yield from the reaction of 5,5'–dibromomethyl–2,2'–bipyridine with a large excess of cyclam. Separation of L^{16} from the excess cyclam can usually be achieved by recrystallisation from acetonitrile (cyclam being less soluble in this solvent than the desired product), although occasionally NMR spectra of L^{16} obtained in this way show evidence of cyclam contamination. If this is so, purification of L^{16} is achieved by the formation, separation and subsequent demetallation of the Cu(II) complexes. An impure sample of L^{16} is stirred with aqueous Cu^{2+}, the resultant Cu–cyclam and Cu–L^{16} complexes are then separated by cation exchange chromatography. The Cu^{2+} ions can subsequently be removed from complexes of L^{16} by stirring with excess Na_2S. A black precipitate of CuS is formed which can be removed by filtration. L^{16} is characterised by its proton and ^{13}C NMR spectra, and by a FAB mass spectrum.

Metal Complexes of L^{16}.– Reaction of L^{16} with one equivalent of *cis*-$[Ru(bipy)_2Cl_2]$ gave, after work up, $[Ru(bipy)_2L^{16}H_4]^{6+}$ which was isolated as its hexafluorophosphate salt by the addition of excess saturated aqueous NH_4PF_6. $[Ru(bipy)_2L^{16}H_4](PF_6)_6$ was characterised by CHN analysis, proton and ^{13}C NMR

spectra and by a FAB mass spectrum. All are consistent with the postulated structure shown in **Figure 5.5.**

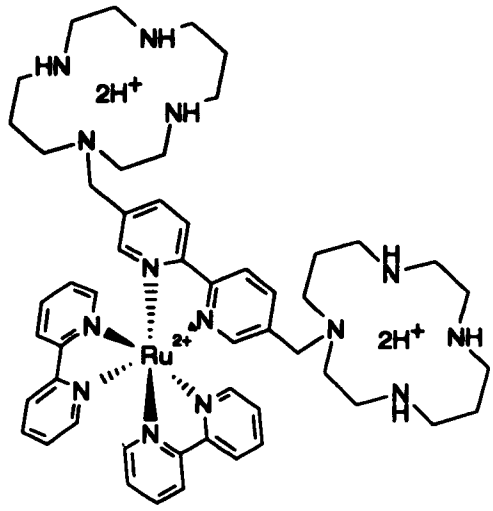

Figure 5.5. Postulated structure of $[Ru(bipy)_2(L^{16}H_4)]^{6+}$.

The proton and ^{13}C NMR spectra show $[Ru(bipy)_2(L^{16}H_4)]^{6+}$ to have a plane of symmetry. In the ^{13}C NMR spectrum, fifteen downfield resonances are observed, assigned to the $[Ru(bipy)_3]^{2+}$ group, while the presence of eleven upfield resonances indicates both cyclam rings are equivalent. A singlet (δ 3.75 p.p.m.) is observed in the proton NMR spectrum for the four protons of the linking methylene groups, indicating that umbrella inversion at the nitrogen atoms of each cyclam ring is rapid. Axial and equatorial protons around the macrocyclic rings are also equivalent. The uv–visible spectrum of $[Ru(bipy)_2L^{16}H_4](PF_6)_6$ has a band with λ_{max} = 452 nm (ε = 13 800 dm^3 mol^{-1} cm^{-1}) in acetonitrile, which is characteristic of the $[Ru(bipy)_3]^{2+}$ group. The latter has a corresponding band at λ_{max} = 452 nm (ε = 13 000 dm^3 mol^{-1} cm^{-1}) in the same solvent.[143] $[Ru(bipy)_2L^{16}H_4](PF_6)_6$ is fluorescent, having an emission maximum at 618 nm in acetonitrile, the intensity of this emission is compared with that of $[Ru(bipy)_3]^{2+}$ in **Table 5.2.** Again, the fluorescence is characteristic of $[Ru(bipy)_3]^{2+}$ which has an emission maximum at 615 nm on excitation at 450 nm in the same solvent.[143] The FAB mass spectrum of $[Ru(bipy)_2L^{16}H_4](PF_6)_6$ exhibits a daughter ion peak at *m/z* 1140 assigned to [M+1] based on $([Ru(bipy)_2L^{16}H(PF_6))]^+$.

$[Ru(bipy)_2L^{16}H_4]^{6+}$ can be used to synthesise other polymetallic systems. The reaction of $[Ru(bipy)_2L^{16}H_4](PF_6)_6$ with 2.2 equivalents of $Ni(ClO_4)_2.6H_2O$, followed by the addition of excess aqueous $NaClO_4$, introduced Ni^{2+} into both macrocyclic cavities to give $[Ru(bipy)_2L^{16}Ni_2](ClO_4)_6$. This was characterised by elemental analysis, and by proton and ^{13}C NMR spectra. The proton NMR spectrum of $[Ru(bipy)_2L^{16}Ni_2](ClO_4)_6$ is similar to, although slightly broader than that of $[Ru(bipy)_2L^{16}H_4](PF_6)_6$. Axial and equatorial macrocyclic protons are again equivalent, as are the linking methylene protons, indicating that umbrella inversion at the cyclam nitrogen atoms is rapid. This may indicate that the Ni–cyclam units are labile, with Ni(II) ions coordinated out of the plane of each cyclam ring. This is in contrast to complexes containing the $[CoCl_2cyclam]^+$ moiety, discussed above. Both proton and ^{13}C NMR spectra of $[Ru(bipy)_2(L^{16}Ni_2)](ClO_4)_6$ show it to have a plane of symmetry like the parent complex $[Ru(bipy)_2(L^{16}H_4)](PF_6)_6$. The uv–visible spectrum of $[Ru(bipy)_2(L^{16}Ni_2)](ClO_4)_6$ is characteristic of the $[Ru(bipy)_3]^{2+}$ moiety. The high intensity MLCT band characteristic of this group (λ_{max} = 452 nm) swamps bands due to the $[Nicyclam]^{2+}$ units. $[Ru(bipy)_2(L^{16}Ni_2)](ClO_4)_6$ is slightly fluorescent, with an emission maximum at 618 nm in acetonitrile (λ_{ex} = 452 nm). The relative intensity of the fluorescence of $[Ru(bipy)_2(L^{16}Ni_2)]^{6+}$ is compared to that of $[Ru(bipy)_3]^{2+}$ in **Table 5.2.**

$[Ru(bipy)_2(L^{16}Cu_2)](ClO_4)_6$ was synthesised from the reaction of $[Ru(bipy)_2(L^{16}H_4)](PF_6)_6$ and Cu^{2+} by the method used to obtain $[Ru(bipy)_2(L^{16}Ni_2)]^{6+}$. The proposed structure is also analogous to that postulated for the Ru–Ni complex. As expected, $[Ru(bipy)_2(L^{16}Cu_2)](ClO_4)_6$ has uv–visible and fluorescence spectra characteristic of the $[Ru(bipy)_3]^{2+}$ group. A comparison of this data is given in **Table 5.2.** It can be seen that the presence of cations in cyclam cavities intra–molecularly linked to $[Ru(bipy)_3]^{2+}$ significantly quenches the fluorescence of that group. This is in line with other work discussed in Chapter 3, where the fluorescence intensity of L^7 in the presence of excess H^+, Ni^{2+} and Cu^{2+} is

compared with that of $[Ru(bipy)_3]^{2+}$. In both cases, Cu^{2+} is seen to quench the fluorescence intensity more efficiently than Ni^{2+}.

	Uv–visible spectra[a]	Fluorescence[c]	
	λ_{max} / nm (ε / dm^3 mol^{-1} cm^{-1})	emission max	Relative intensity[b]
$[Ru(bipy)_2(L^{16}H_4)]^{6+}$	452 (13 800)	618[a] 607[b]	100
$[Ru(bipy)_2(L^{16}Ni_2)]^{6+}$	452 (14 300)	618[a] 607[b]	14
$[Ru(bipy)_2(L^{16}Cu_2)]^{6+}$	452 (12 300)	620[a] 607[b]	1
$[Ru(bipy)_3]^{2+}$ [d]	452 (13 000)	615[a] 607[b]	370

[a] CH_3CN, [b] H_2O, [c] λ_{ex} = 450 nm, [d] ref 143

Table 5.2. Uv–visible and fluorescence spectroscopy data for ruthenium complexes of L^{16}.

Reaction of L^{16} with two equivalents of Cu^{2+} in ethanol gave two species, a bimetallic and a pentametallic complex. Addition of Cu^{2+} to a refluxing ethanolic solution of L^{16} resulted in the immediate formation of a deep purple colour. A purple solid isolated from this solution was separated into three fractions by cation exchange chromatography. The relative yields of each fraction are 1:40:10, all fractions were treated with excess aqueous $NaClO_4$. Fraction 1, eluted with 0.4 mol dm^{-3} NaCl was found to contain $[Cu(cyclam)]^{2+}$. The second fraction, eluted with 0.8 mol dm^{-3} NaCl, was $[Cu_2L^{16}](ClO_4)_4$, the major product. A FAB mass spectrum exhibits a peak at *m/z* = 453, assigned to $[(Cu_2L^{16})(ClO_4)_2]^{2+}$. The uv–visible spectrum in acetonitrile has a band at λ_{max} = 522 nm (ε = 265 dm^3 mol^{-1} cm^{-1}). This is compared to bands in the uv–visible spectra of $[Cucyclam]^{2+}$ (λ_{max} = 504 nm (ε = 76 dm^3 mol^{-1} cm^{-1})) and $[CuL^{15}]^{2+}$ (λ_{max} = 512 nm (ε = 105 dm^3 mol^{-1} cm^{-1})) [144] in the same solvent. It is postulated that a Cu(II) ion occupies each cyclam cavity in L^{16}, leaving the bipy group free.

A third very slow moving fraction was eluted with 1.5 mol dm^{-3} NaCl. CHN analysis suggests the formulation $[Cu_5(L^{16})_2](ClO_4)_{10}$ which is supported by ICP metal analysis ($[Cu_5(L^{16})_2](ClO_4)_{10}$ requires Cu 12.9 %, found, 13.0 %). The proposed structure of $[Cu_5(L^{16})_2]^{10+}$ is shown below (**Figure 5.6**).

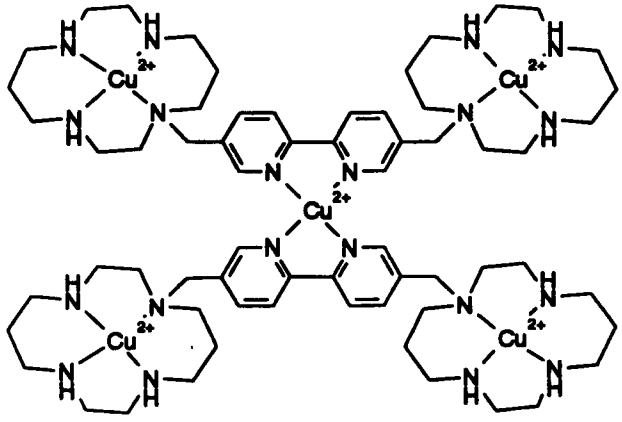

Figure 5.6. Proposed structure of $[Cu_5(L^{16})_2]^{10+}$.

The uv–visible spectrum shows a band with λ_{max} = 570 nm (ε = 671 dm^3 mol^{-1} cm^{-1}), indicating some difference in the environment of each $[Cu(cyclam)]^{2+}$ moiety, The difference in the visible spectra indicates that the $[Cu(cyclam)]^{2+}$ groups probably do not have the same macrocyclic conformation as that found in $[Cu(cyclam)]^{2+}$ itself.

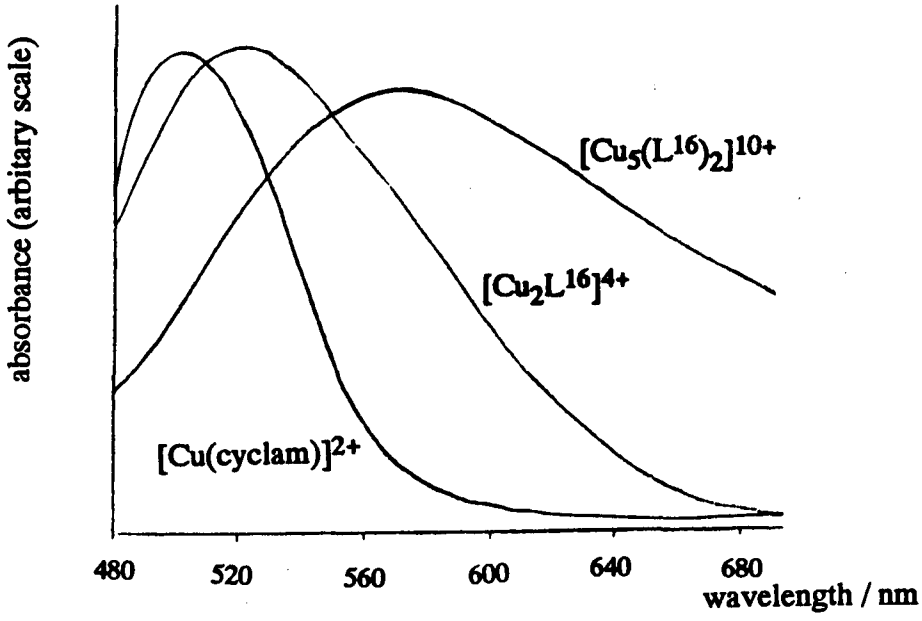

Figure 5.7. Visible spectra of $[Cu(cyclam)]^{2+}$ (2 x 10^{-2} mol dm^{-3}), $[Cu_2L^{16}]^{4+}$ (6 x 10^{-2} mol dm^{-3}) and $[Cu_5(L^{16})_2]^{10+}$ (2 x 10^{-3} mol dm^{-3}) in acetonitrile.

The diamagnetic (low-spin) $[Fe(L^{16}{}_3H_8)](PF_6)_{10}$ was isolated from the reaction of Fe^{2+} with three equivalents of L^{16}, and was characterised by proton and ^{13}C NMR spectra, and by elemental analysis. The Fe(II) ion is six coordinate, being coordinated to the three bipy groups of the L^{16} ligands.

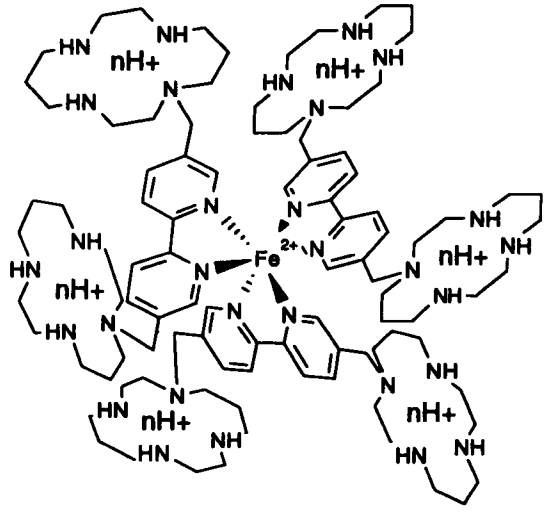

Figure 5.8. Proposed structure of $[Fe(L^{16}{}_3H_8)]^{10+}$ (n = 1 or 2).

The ^{13}C NMR spectra shows the three L^{16} ligands to be equivalent. Five downfield and eleven upfield resonances are observed, showing the symmetry of L^{16} to be retained on complexation. The room temperature proton NMR spectrum is broad; this broadening is attributed to slow tumbling of the large $[Fe(L^{16}{}_3H_8)](PF_6)_{10}$ molecules in the viscous $(CD_3)_2SO$ solution. A sharper spectrum is obtained at 378 K. $[Fe(L^{16}{}_3H_8)]^{10+}$ contains six cyclam cavities and a resonance at δ 2.50 p.p.m. (integral 8H) in the 378 K proton NMR spectrum is assigned to NH^+ protons bound to the cyclam units. Previous work (e.g. the isolation of $[Ru(bipy)_2(L^{16}H_4)]^{6+}$ from 1:1 CH_3OH / H_2O) suggests that two protons are expected to be associated with each cyclam cavity; however, it seems reasonable that the high concentration of charge in $[Fe(L^{16}{}_3H_8)]^{10+}$ lowers this number. It appears that eight is an average value for the number of protons bound in each complex cation. Lower intensity resonances very close to the main resonances (and at approximately one fifth of the intensity of the larger group) can be seen in the 378 K proton NMR spectrum. These are attributed to conformational isomers of $[Fe(L^{16}{}_3H_8)](PF_6)_{10}$. A band with λ_{max} = 520 nm (ε =

2 090 dm^3 mol^{-1} cm^{-1}) is observed in the uv–visible spectrum of $[Fe(L^{16}{}_3H_8)](PF_6)_{10}$. This is characteristic of $[Fe(bipy)_3]^{2+}$, although at a much reduced intensity [for $[Fe(bipy)_3]^{2+}$, λ_{max} = 522 nm (ε = 8 650 dm^3 mol^{-1} cm^{-1}].[120]

Experimental.

Synthesis of 5,5'-dibromomethyl-2,2'-bipyridine .– 5,5'-Dimethyl-2,2'-bipyridine[147] (460 mg, 2.5 mmol) and *N*–bromosuccinimide (890 mg, 5 mmol) were heated at 65°C in CCl_4 (100 cm^3) under a tungsten lamp until the *N*-bromosuccinimide (which is denser than CCl_4) had been converted to succinimide (which floats on the solvent surface). The mixture was then filtered whilst hot and the solvent volume reduced by 50 %. The desired product crystallised on cooling, and was collected by suction filtration. It was washed with a little ice cold CH_2Cl_2 and air dried. Yield 550 mg, 64 %. ^1H NMR (250 MHz, $CDCl_3$): δ/p.p.m. 8.69 (s, 2H), 8.40 (d, 2H), 7.86 (d, 2H), 4.54 (s, 4H). ^{13}C NMR ($CDCl_3$, 62.90 MHz): δ/p.p.m. 149.3, 137.5, 133.8, 121.1, 120.1, 29.5. Mass spectrum (FAB / NBA): *m/z* 343 (Calc. for MH^+, 343).

Syntheses of L^{16}.– 5,5'–dibromomethyl–2,2'–bipyridine (1.03 g, 3 mmol) was added in small portions to a hot, vigorously stirred solution of cyclam (4.08 g, 20 mmol) in chlorobenzene (300 cm^3) at 110 °C, addition taking approximately 2 h. The solution was maintained at 110 °C for a further hour after addition was complete, then filtered hot (to remove cyclam.2HBr). The solvent volume was reduced to 150 cm^3 and the solution cooled. This allowed excess cyclam to crystallise, which was then removed by filtration. The remaining solvent was evaporated, and the product obtained as a white solid which was recrystallised from the minimum volume of hot CH_3CN. Yield 1.38 g, 79 %. ^1H NMR ($CDCl_3$, 250 MHz): δ/p.p.m. 8.53 (s, 2H), 8.26 (d, 2H), 7.79 (d, 2H), 3.60 (s, 4H), 2.78 to 2.43 (m, 38H) 1.82 (qu, 4H), 1.61 (qu, 4H). ^{13}C NMR ($CDCl_3$, 62.90 MHz): δ/p.p.m. 154.9, 149.7, 137.6, 133.9, 120.4, 54.8, 54.2, 53.2, 50.6, 49.2, 49.0, 48.7, 47.7, 47.1, 28.2, 26.0. Mass spectrum (FAB / NBA): *m/z* 581 (Calc. for MH^+ 581).

N.B. Occasionally NMR spectra of L^{16} show evidence of cyclam contamination which crystallises out with the desired product. In this case L^{16} may be purified by

forming the Cu(II) complexes of the mixture of cyclam and L^{16}. A solution of impure L^{16} in CH_3OH was stirred with excess saturated aqueous $CuSO_4$. The solution turned deep purple. The solvent was removed and the resultant purple solid dissolved in H_2O (5 cm^3) and loaded onto a column of Sephadex–C25 cation exchange resin. The column was eluted with 0.1–1.0 mol dm^{-3} NaCl. $[Cu(cyclam)]^{2+}$ was eluted with 0.3 mol dm^{-3} NaCl, and the major fraction containing $[L^{16}Cu_2]^{4+}$ with 0.8 mol dm^{-3} NaCl. This fraction was stirred with excess aqueous Na_2S to give a black precipitate of CuS which was removed by filtration. The filtrate was made strongly alkaline (pH >10) with aqueous NaOH, and was then extracted with several portions of CH_2Cl_2. The organic extracts were combined, dried over anhydrous $MgSO_4$ and filtered. Evaporation of the filtrate yielded pure L^{16} as a white solid.

Synthesis of $[CoCl_2(L^{15}H)](ClO_4)Cl$.– The synthesis is based on that of *trans*–$[CoCl_2(cyclam)]$.[142] A solution of $CoCl_2.6H_2O$ (65 mg, 0.27 mmol) in CH_3OH (15 cm^3) was added dropwise to a solution of L^{15} (100 mg, 0.27 mmol)[55] in CH_3OH (15 cm^3). In the presence of O_2, the solution turns brown. HCl (1 cm^3) was added and air was bubbled through the solution for 1h. The solvent was then removed. The resulting green solid was dissolved in H_2O (10 cm^3) and treated with saturated aqueous $NaClO_4$ until precipitation ceased. The precipitate was collected by suction filtration and dried *in vacuo* over silica gel. Yield 90 mg, 54 %. The proton NMR spectrum of this solid is rather broad, probably due to the presence of a small amount of Co(II). Crystals suitable for X–ray crystallography were grown from a solution of HCl (0.6 mol dm^{-3}). NMR spectra of the crystalline material are sharp. ^1H NMR (400 MHz, $(CD_3)_2SO$): δ / p.p.m. 8.78 (d, 1H), 8.69 (s, 1H), 8.54 (d, 1H), 8.50 (d, 1H), 8.19 (t, 1H), 8.03 (d, 1H), 7.66 (t, 1H), 7.25 (t, br, 1H), 6.83 (t, br, 1H), 6.45 (t, br, 1H), 4.14 (AB quartet, 2H), 3.44 (q, 1H), 3.05 to 2.35 (m, 14H), 2.05 (d, 1H), 1.92 (m, 2H), 1.76 (q, 1H). ^{13}C NMR (100.62 MHz, $(CD_3)_2SO$): δ / p.p.m. 153.2, 152.7, 152.3, 148.2, 142.1, 139.7, 128.8, 125.4, 121.7, 120.9, 56.0, 53.5, 53.4, 53.0, 52.2, 51.1, 49.1, 47.8, 47.3, 27.3, 24.3. Mass spectrum *m/z* (FAB / NBA): 497 (Calc. for

$[C_{21}H_{32}N_6CoCl_2]^+$, 497). Uv–visible spectrum in 0.5 mol dm^{-3} HCl [λ_{max} / nm (ε / dm^3 mol^{-1} cm^{-1})]: 258 (25 300), 294 (23 200), 480 (shoulder) (47), 638 (34.3). Found: C, 36.98, H, 5.20 N, 11.97 . Calc. for $[C_{21}H_{33}N_6CoCl_2](ClO_4)Cl.2.5H_2O$, C, 37.11, H, 5.71, N, 12.37 %. It appears that the crystal chosen for X–ray analysis has lost 2 molecules of water.

Crystal data.– $[CoCl_2(L^{15}H)](ClO_4)Cl.0.5H_2O.$, M = 643.3, Triclinic, space group P1, a = 7.634(4), b = 9.879(5), c = 18.951(9) Å, α = 91.74(4), β = 92.58(4), γ = 105.21(4) °, U = 1388.3 $Å^3$, (at 290 K, a = 7.626(5), b = 9.942(6), c = 18.965(11) Å, α = 91.82(5), β = 92.66(5), γ = 104.77(5) °, U = 1388.3 $Å^3$], Z = 2, D_c = 1.56 g cm^{-3}, Mo–K_α radiation, λ = 0.71069 Å, μ(Mo–K_α) = 0.96 mm^{-1}, T = 200 K, R = 0.088 for 2806 unique reflections.

Experimental.– Crystals were obtained from 50%HCl.

Character: weakly diffracting green plates. Data were collected with a Siemens R3m four circle diffractometer in ω-2θ mode. The data from an initial collection at room temperature proved too weak for satisfactory refinement, though the structure could be solved. For a second attempt, a fresh crystal was therefore held at 200K with an Oxford Cryosystems Cryostream Cooler; the data were improved in quality though still of low intensity. Maximum 2θ was 50° with scan range ± 0.75°(ω) around the $K_{\alpha1}$-$K_{\alpha2}$ angles, scan speed 2-15°(ω) min^{-1}, depending on the intensity of a 2s pre–scan; backgrounds were measured at each end of the scan for 0.25 of the scan time. hkl ranges were: 0/9; -10/10; -20/20. Three standard reflections were monitored every 200 reflections, and showed no decrease during data collection. Unit cell dimensions and standard deviations were obtained by least-squares fit to 15 reflections (20 < 2θ < 22°). The 5879 reflections were processed using profile analysis to give 5454 unique reflections (R_{int} = 0.108), of which 2806 were considered observed (I/σ(I) ≥ 2.0). These were corrected for Lorentz, polarization and absorption effects (by the Gaussian method); minimum and maximum transmission factors were 0.86 and 0.94.

Crystal dimensions were 0.25 x 0.25 x 0.10 mm. There were no systematic reflection conditions: Space group $P\bar{1}$ was initially selected and shown to be correct by the successful refinement.

The structure was solved by direct methods using SHELXTL (TREF) using the room temperature data set; refinement on the low temperature data was started from the room temperature coordinates. Several additional peaks were located which were initially modelled as two full and two fractional occupancy (0.25) oxygen atoms of water molecules. Replacement of each of the two full oxygen atoms by a 0.5 occupancy chloride ion was investigated; from the refinement, these alternatives are indistinguishable although the latter is preferred on chemical considerations. Although none of the residual peaks are large, several remain in the region of these Cl/O atoms, indicating additional disorder in this area. The nitrogen positions in the bipyridyl rings were assigned from thermal parameter behaviour on refinement, but cannot be considered conclusive. Anisotropic temperature factors were used for all non-H atoms (apart from the partial occupancy oxygens). Hydrogen atoms were given fixed isotropic temperature factors, U = 0.08 $Å^2$; they were inserted at calculated positions and not refined. Final refinement was on F by least squares methods refining 342 parameters. Largest positive and negative peaks on a final difference Fourier synthesis were of height ±0.95 el. $Å^{-3}$. The weighting scheme was calc $w=1/[\sigma^2(Fo^2) +(0.1375P)^2]$ where $P=(Fo^2+2Fc^2)/3$. Goodness-of-fit on F^2 was 0.997, R1[for 2806 reflections with $I>2\sigma(I)$] = 0.0865, wR2 = 0.2653. The number of parameters refined was 342. Largest difference peak and hole were +/- 0.95 e.$Å^{-3}$.

R for all reflections = 0.171; the comparatively high R-values are understandable in the light of the weak diffraction. Maximum shift/error in final cycle 0.72. Computing with SHELXTL PLUS (Sheldrick, 1986) on a DEC Microvax-II and final refinement using SHELXL 93 (Sheldrick, 1994) on a PC486.[145] Scattering factors in the analytical form and anomalous dispersion factors taken from International Tables

(1974) (stored in the program).[146] Final atomic coordinates, bond lengths and angles are given in the Appendix (**Tables A.9 – A.12**).

Synthesis of $[(bipy)_2RuL^{15}CoCl_2](PF_6)_3$.– $[CoCl_2(L^{15}H)](ClO_4)Cl$ (40 mg, 0.07 mmol) and *cis*–$[Ru(bipy)_2Cl_2]$ (35 mg, 0.07 mmol) were refluxed in a solution of CH_3CH_2OH / H_2O (1:1, 20 cm^3) overnight. The solution was filtered, the solvent removed and the resulting dark orange filtrate treated with excess aqueous NH_4PF_6 to give a brown/orange precipitate. This was collected by suction filtration, and recrystallised from H_2O. The recrystallised product was dried *in vacuo* over silica gel. Yield 58 mg, 64 %. ^1H NMR (250 MHz, CD_3NO_2): δ / p.p.m. 8.45 (m, 6H), 7.96 (m, 5H), 7.77 (m, 6H), 7.49 (s, 1H), 7.30 (m, 5H), 7.03 (s, br, 1H), 5.68 (s, br, 1H), 5.30 (s, br, 1H), 3.62 (AB quartet, 2H), (s, 2H), 3.25 (m, 4H), 2.85 (m, 4H), 2.50 to 1.65 (m, 12H). ^{13}C NMR (100.62 MHz, CD_3NO_2): δ / p.p.m. 158.7 (1), 158.6 (1), 158.5 (2), 158.3 (1), 158.1 (1), 153.3 (1), 153.2 (1), 153.1 (1), 153.04 (1), 153.01 (1), 152.8 (1), 141.5 (1), 139.5 (1), 139.4 (1), 139.3 (3), 133.1 (1), 129.2 (1), 129.1 (1), 129.0 (1), 128.92 (1), 128.87 (1), 125.8 (1), 125.5 (3), 125.5 (1), 125.3 (1), 52.5 (1), 52.0 (1), 51.7 (1), 51.1 (1), 50.3 (1), 50.1 (1), 49.5 (1), 46.3 (1), 45.9 (1), 25.9 (1), 22.6 (1). Mass spectrum *m/z* (FAB / NBA): 1073, (Calc. for $[\{(bipy)_2RuL^{15}CoCl_2.H_2O\}(PF_6)]^+$, 1073. Uv–visible spectrum in CH_3CN [λ_{max} / nm (ε / dm^3 mol^{-1} cm^{-1})]: 453 (11 300), 287 (84 100), 243 (28 000). Found: C, 36.08, H, 3.40, N, 9.80 %. Calc for $C_{41}H_{48}Cl_2CoF_{18}N_{10}P_3Ru.H_2O$: C, 36.09, H, 3.69, N, 10.26 %.

Synthesis of $[Ru(bipy)_2L^{16}H_4](PF_6)_6$.– *Cis*–$[Ru(bipy)_2Cl_2].2H_2O$ (100 mg, 0.2 mmol) and L^{16} (112 mg, 0.2 mmol) were refluxed overnight in EtOH : H_2O (1:1, 50 cm^3). The solution became deep orange in colour. The solvent was removed, the residue dissolved in H_2O (5 cm^3) and loaded onto a column of Sephadex–C25 cation exchange resin (1 x 10 cm). The column was eluted with 0.1–1.0 mol dm^{-3} NaCl, the main fraction being eluted with 0.6 mol dm^{-3} solution. This fraction was treated with

excess saturated aqueous NH_4PF_6 to yield an orange precipitate. The precipitate was collected by suction filtration and dried *in vacuo* over silica gel. Yield 213 mg, 59 %. ^1H NMR (250 MHz, CD_3NO_2): δ/p.p.m. 8.46 (2 x d, 6H), 8.02 (d, 2H), 7.96 (d, 2H), 7.79 (m, 6H), 7.50 (s, 2H), 7.32 (m, 4H), 6.75 (s, br, 6H), 3.75 (s, 4H), 3.20 (m, 16H), 2.89 (m, 8H), 2.47 (m, 8H), 2.30 (m, 4H), 1.83 (qu, 4H), 1.70 (qu, 4H). ^{13}C NMR (CD_3NO_2, 62.90 MHz): δ/p.p.m. 158.4 (2C), 158.2 (4C), 153.3 (2C), 153.2 (2C), 153.0 (2C), 141.6 (2C), 139.6 (2C), 139.5 (2C), 133.4 (2C), 129.1 (4C), 125.6 (6C), 52.4 (2C), 52.0 (2C), 51.5 (2C), 51.0 (2C), 50.2 (2C), 50.0 (2C), 49.4 (2C), 46.2 (2C), 45.9 (2C), 25.7 (2C), 22.5 (2C). Mass spectrum (FAB / NBA): 1140 (Calc. for $[\{Ru(bipy)_2L^{16}H\}PF_6]^+$, 1140. Uv–visible spectrum in MeCN [λ_{max}/nm (ε / dm^3 mol^{-1} cm^{-1})]: 452 (13 800), 287 (79 800), 248 (29 900). Found C, 33.40, H, 4.09, N, 10.20. Calc. for $C_{52}H_{76}F_{36}N_{14}P_6Ru$: C, 33.43, H, 4.10, N, 10.50 %.

Synthesis of $[Ru(bipy)_2L^{16}Ni_2](ClO_4)_6$.– $[Ru(bipy)_2L^{16}H_4](PF_6)_2.4PF_6$ (100 mg, 0.05 mmol) and $Ni(ClO_4)_2.6H_2O$ (40 mg, 0.11 mmol) were stirred in CH_3OH (100 cm^3) for 0.5 h at 60 °C. The solvent was then removed, the red–brown residue dissolved in H_2O and treated with excess aqueous $NaClO_4$. The resulting precipitate was collected by suction filtration and dried *in vacuo* over silica gel. Yield 61 mg, 74%. ^1H NMR (400 MHz, $(CD_3)_2SO$): δ/p.p.m. 8.83 (2 x d, 6H), 8.18 (t, 4H), 8.02 (d, 2H), 7.78 (t, 4H), 7.55 (m, 4H), 7.36 (s, 2H), 6.81 (s, br, 6H), 3.64 (s, 4H), 3.06 (m, 8H), 2.98 (m, 8H), 2.72 (m, 8H), 2.28 (m, 4H), 2.16 (m, 4H), 1.75 (qu, 4H), 1.55 (qu, 4H). ^{13}C NMR ($(CD_3)_2SO$, 100.62 MHz): δ/p.p.m. 156.5 (4C), 155.6 (2C), 151.6 (2C), 151.4 (2C), 151.2 (2C), 139.8 (2C), 138.2 (4C), 133.8 (2C), 128.1 (4C), 124.5 (4C), 124.2 (2C), 49.0 (2C), 48.5 (2C), 48.1 (2C), 47.6 (2C), 47.5 (2C), 45.2 (2C), 43.8 (2C), 43.5 (2C), 43.1 (2C), 24.9 (2C), 21.8 (2C). Uv–visible spectrum in MeCN [λ_{max}/nm (ε / dm^3 mol^{-1} cm^{-1})]: 452 (14 300), 287 (88 300), 246 (33 000). Found C, 36.30, H, 4.53, N, 11.21. Calc. for $C_{52}H_{72}Cl_6N_{14}Ni_2O_{24}.H_2O$ Ru: C, 36.18, H, 4.32, N, 11.36 %.

Synthesis of $[Ru(bipy)_2L^{16}Cu_2](ClO_4)_6$.– $[Ru(bipy)_2L^{16}H_4](PF_6)_6$ (214 mg, 0.11 mmol) and $CuSO_4.5H_2O$ (60 mg, 0.24 mmol) were refluxed in CH_3OH (50 cm^3) for 1 h. The solvent was removed, leaving a rust coloured solid which was dissolved in approximately 25 cm^3 H_2O and treated with excess saturated aqueous $NaClO_4$. A brown precipitate formed which was collected by suction filtration and dried *in vacuo* over silica gel. Yield 138 mg, 73 %. Found C, 36.98, H, 4.31, N, 11.22. Calc. for $C_{52}H_{72}Cl_6Cu_2N_{14}O_{24}Ru$: C, 36.35, H, 4.22, N, 11.41 %. Uv–visible spectrum in MeCN [λ_{max}/nm (ε / dm^3 mol^{-1} cm^{-1})]: 452 (12 300), 288 (92 600), 248 (36 800).

Synthesis of $[Cu_2L^{16}](ClO_4)_4$ and $[Cu_5L^{16}{}_2](ClO_4)_{10}$.– A stirred solution of L^{16} (150 mg, 0.26 mmol) in EtOH (50 cm^3) was heated to reflux. A solution of $Cu(ClO_4)_2.6H_2O$ (193 mg, 0.52 mmol) in H_2O (20 cm^3) was then added dropwise. The resulting purple precipitate was collected by filtration, dissolved in water (5 cm^3) and loaded onto a column of Sephadex–C25 cation exchange resin. This was eluted with aqueous NaCl (0.1–1.5 mol dm^{-3}) as described above. Three bands were observed with the relative yields 1:40:10. They were eluted with 0.4, 0.8 and 1.5 mol dm^{-3} NaCl respectively. The major product, eluted with 0.8 mol dm^{-3} was treated with excess aqueous saturated $NaClO_4$ to give a purple precipitate. This was collected by suction filtration and dried *in vacuo* over silica gel. Yield 175 mg, 61 %. Mass spectrum (FAB / NBA): *m/z* = 453. (Calc. for $[(Cu_2L^{16})(ClO_4)_2]^{2+}$, 453). Uv-visible spectrum in MeCN [λ_{max}/nm (ε / dm^3 mol^{-1} cm^{-1})]: 522 (265), 290 (20 700), 244 (16 600). Found C, 34.16, H, 5.15, N, 11.80. Calc. for $C_{32}H_{56}Cl_4Cu_2N_{10}O_{16}.H_2O$: C, 34.19, H, 5.16, N, 12.47 %. The fraction eluted with 1.5 mol dm^{-3} NaCl was also treated with aqueous NH_4PF_6, filtered and dried as described above. Yield 48 mg, 15 %. Uv-visible spectrum in MeCN [λ_{max}/nm (ε / dm^3 mol^{-1} cm^{-1})]: 570 (671), 295 (14 900), 255 (13 900). Found C, 31.14, H, 4.76, N, 11.22, Cu, 13.0 %. Calc. for $C_{64}H_{112}Cl_{10}Cu_5N_{20}O_{40}$: C, 31.07, H, 4.56, N, 11.32, Cu, 12.9 %.

Synthesis of $[Fe(L^{16}{}_3H_8)](PF_6)_{10}$.– L^{16} (500 mg, 0.86 mmol) and $FeSO_4.7H_2O$ (80 mg, 0.29 mmol) were stirred together in CH_3OH / H_2O (100 cm^3, 1:1). The solution turned a deep red colour. Excess saturated aqueous NH_4PF_6 was added, and the resulting red precipitate removed by suction filtration, and dried *in vacuo* over silica gel. Yield 554 mg, 59 %. ^1H NMR (400 MHz, $(CD_3)_2SO$, 378 K): δ/p.p.m. 8.60 (s, 6H), 8.40 (d, 6H), 7.84 (d, 6H), 3.78 (s, 12H), 3.08 (m, 48H), 2.91 (s, br, 12H), 2.85 (m, 24H), 2.66 (m, 24H), 2.58 (s, br, 6H), 2.50 (s, 8H), 1.91 (qu, 12H), 1.78 (qu, 12H). ^{13}C NMR (100.62 MHz, $(CD_3)_2SO$, 378 K): δ/p.p.m. 154.3, 149.8, 138.0, 137.9, 131.6, 52.5, 50.9, 50.0, 48.0, 47.6, 45.7, 45.2, 44.6, 44.5, 24.4, 22.6. Uv-visible spectrum in MeCN [λ_{max}/nm (ε / dm^3 mol^{-1} cm^{-1})]: 520 (2 090), 292 (78 600), 248 (52 100). Found: C, 36.06, H, 5.27, N, 12.56. Calc. for $C_{96}H_{176}N_{30}P_{10}F_{60}Fe$: C, 35.40, H, 5.41, N, 12.91 %.

CHAPTER 6

Chapter 6

The Macrocycle 1,4,7–Triazacyclononane (9N3) Modified with *N*–pendant 2,2':6',2"-Terpyridyl–5–yl–methyl and Pyridyl–3–ylmethyl Groups.

The possibility of obtaining stable luminescent complexes of lanthanide ions has attracted growing attention in recent years.[107] The use of lanthanide complexes as luminescent labels in immunology, more specifically fluoroimmunoassay, is of special interest. This involves the labelling of samples with fluorescent species and the measuring of the luminescence. It has the advantages over radioimmunoassay of being less dangerous and less expensive, although it is hindered by lower sensitivity. The search is on for long-lived strongly luminescent species that are stable and water soluble.

Lanthanide ions lack intense metal centred absorption bands, so the luminescence of the metal is obtained by the 'antenna effect'; light is absorbed by coordinated ligands and transferred to the metal ion. Lanthanide ions often form relatively weak complexes, so to form more stable complexes, preorganised multidentate ligands are used which surround the metal ion. Some examples of these are given in Chapter 1, Section 1.11. 2,2':6',2"–Terpyridine (terpy) is well suited for terdentate coordination to large ions like the lanthanides, for which coordination numbers of 7, 8 and 9 are common. It was with this in mind that the potentially nonadentate ligand L^{17}, containing three terpyridyl arms, was synthesised.

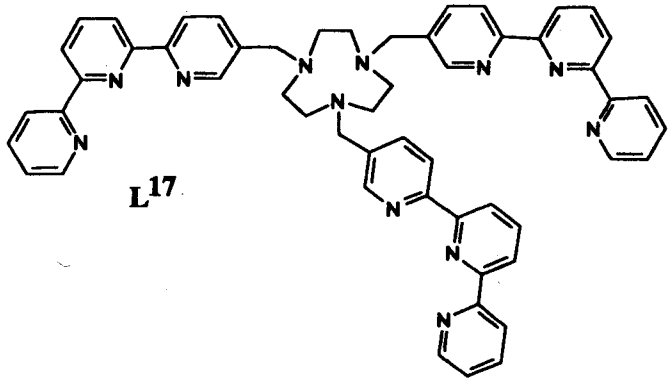

L^{17}

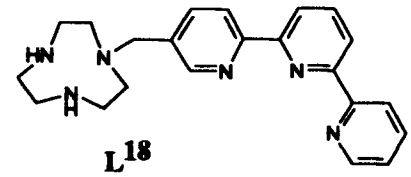

L^{18}

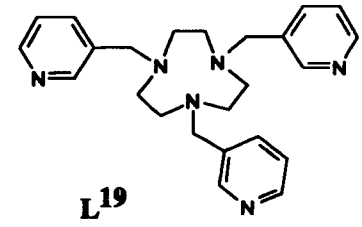

L^{19}

L^{17} has been isolated and two of its complexes with the lanthanide ions Eu^{3+} and La^{3+} have been investigated. L^{17} is analogous to L^{1}, but has three terpy pendant arms instead of 2,2'-bipyridyl (bipy) arms. A mode of coordination similar to that of L^{1} was anticipated.

L^{18}, which bears a single terpy arm, has also been isolated and its complex with Fe(II) investigated. L^{18} has two different types of terdentate coordination site. The 9N3 moiety is facially coordinating and the terpy arm is meridionally coordinating. With Fe(II) it was expected that the terpy arm would be the favoured coordination position.

The macrocycle 9N3 was also functionalised with three pyridylmethyl arms to give L^{19}. Although L^{19} contains six potentially donating nitrogen atoms, it is thought that only three of these will be able to coordinate simultaneously to a single metal ion. A complex of L^{19} with Zn(II) has been investigated.

A number of azamacrocycles *N*–functionalised with 2–pyridylmethyl groups are now known. These include the ligands **A** – **C**.[148–151] In addition, similar systems based on mixed donor macrocycles have been reported.[39, 152–155] In all but one of these ligands, the pendant arms are attached *via* the 2 position of the pyridine ring, the exception being a mixed oxygen nitrogen donor macrocycle, carrying pyridylmethyl arms attached *via* the 4 position.[153]

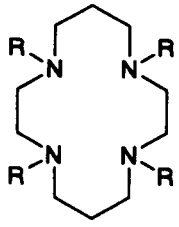

A

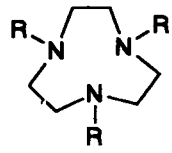

B

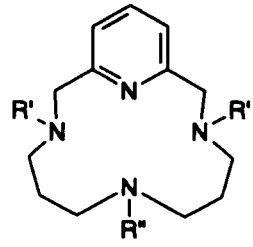

C R' = R, R" = H

D R' = $PhCH_2$, R" = R

E R' = R" = R

R = 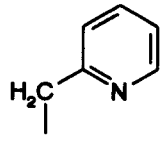

A – **D** coordinate readily to transition metal ions, forming complexes where the metal ion is bound to macrocyclic and pendant arm nitrogen atoms simultaneously.[148–152, 156] The Cu(II) and Ni(II) complexes of **A** are binuclear, in which the macrocycle coordinates to two metal ions in an 'exo' fashion.[148]

Results and Discussion.

Studies of L^{17}.– The potentially nonadentate macrocycle L^{17}, analogous to L^1 but with three 2,2':6',2"-terpyridine (terpy) pendant arms, was isolated in good yield from the parent macrocycle 1,4,7–triazacyclononane (9N3) by reaction with three equivalents of 5-bromomethyl-2,2':6',2"-terpyridine in chlorobenzene containing triethylamine. L^{17} is characterised by its proton and ^{13}C NMR spectra, and by a FAB mass spectrum. In the ^{13}C NMR spectrum, all of the carbon atoms of the 9N3 ring are equivalent, as are the three methylene carbon atoms of the pendant arms. There are 15 aromatic carbon resonances, with three overlapping at δ 155.2 p.p.m.

L^{17} reacts with equimolar amounts of Eu(III) and La(III) in methanol to give mononuclear complexes of the type $[M(L^{17}H)]^{4+}$ (M = Eu, La), isolated as the hexafluorophosphate salts. Elemental analyses confirm the formula given. The X–ray crystal structure of the related complex $[Eu(terpy)_3](ClO_4)_3$ [157] shows the metal ion to be nine coordinate with a tricapped trigonal prismatic arrangement. By analogy with previous studies of L^1 it was anticipated that the cations $[M(L^{17}H)]^{4+}$ would have a structure similar to that shown in **Figure 6.1.**

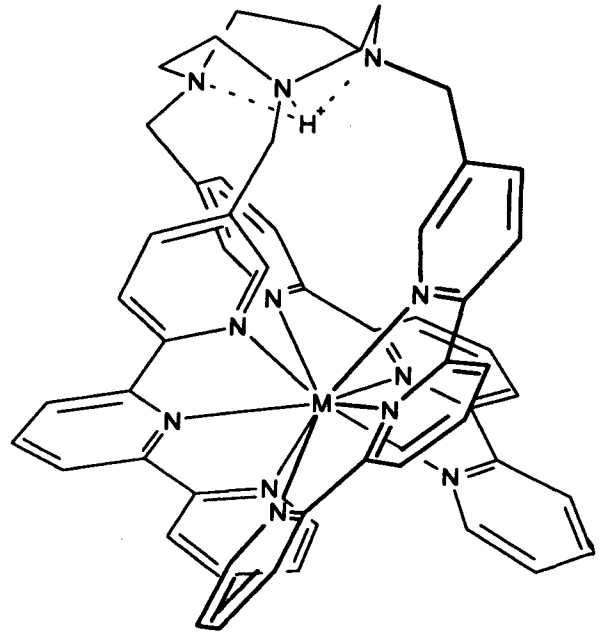

Figure 6.1. Proposed structure of $[M(L^{17}H)]^{4+}$ ($M = Eu^{3+}, La^{3+}$).

$[Eu(L^{17}H)](PF_6)_4$ is obtained as a cream coloured crystalline solid. The uv–visible spectrum in acetonitrile shows three bands at λ_{max} = 322 nm (ε = 43 400 dm^3 mol^{-1} cm^{-1}), 290 (53 200) and 234 (81 800). Earlier work on the uv–visible spectra of metal chelates of terpy[158] with various metal ions report three bands, with λ_{max} in the regions 340 to 320, 285 to 270 and 235 to 220 nm. The uv–visible spectra of the metal chelates are similar to that of terpy in acidic solution (325 (18 500), 285 (20 000), 230 (18 000)), where the terpy is believed to be in a *cis-cis* conformation, and distinct from that in basic solution (λ_{max} = 285 and 235) where the ligand adopts a *trans-trans* conformation.[158]

$[Eu(L^{17}H)](PF_6)_4$ is fluorescent, having an emission spectrum comparable to that of the related complex $[Eu(terpy)_3](ClO_4)_3$. Excitation of a 10^{-4} mol dm^{-3} solution of $[Eu(L^{17}H)](PF_6)_4$ at 355 nm results in three bands at 590, 615 and 712 nm, attributed to Eu(III) transitions. The relative intensity of these bands can be changed by altering the excitation wavelength. For example, exciting at 360 nm instead of 355 nm enhances the band at 712 nm with respect to those at 615 and 590 nm. Excitation of $[Eu(terpy)_3](ClO_4)_3$ (a 10^{-2} mol dm^{-3} solution in acetonitrile) at 370 nm resulted in three sharp Eu(III) transition bands, at 595, 620 and 700 nm.[159] The presence of structured emission from the Eu^{3+} ion shows that energy transfer from the ligand to the metal ion must take place. The metal ion is thought to be encapsulated by L^{17}, and protected from interaction with solvent molecules. It is known that water coordinates readily to Eu^{3+}, and that coordinated water molecules provide efficient non–radiative decay pathways.[107] $[Eu(L^{17}H)](PF_6)_4$ is only sparingly soluble in H_2O, but is strongly fluorescent in this solvent. It is thought that the solubility in H_2O could be increased by exchanging the PF_6^- anion for a simpler anion such as Cl^-. A solution of $[Eu(L^{17}H)](PF_6)_4$ in H_2O / CH_3OH (1:1, 10^{-6} mol dm^{-3}), is also strongly fluorescent.

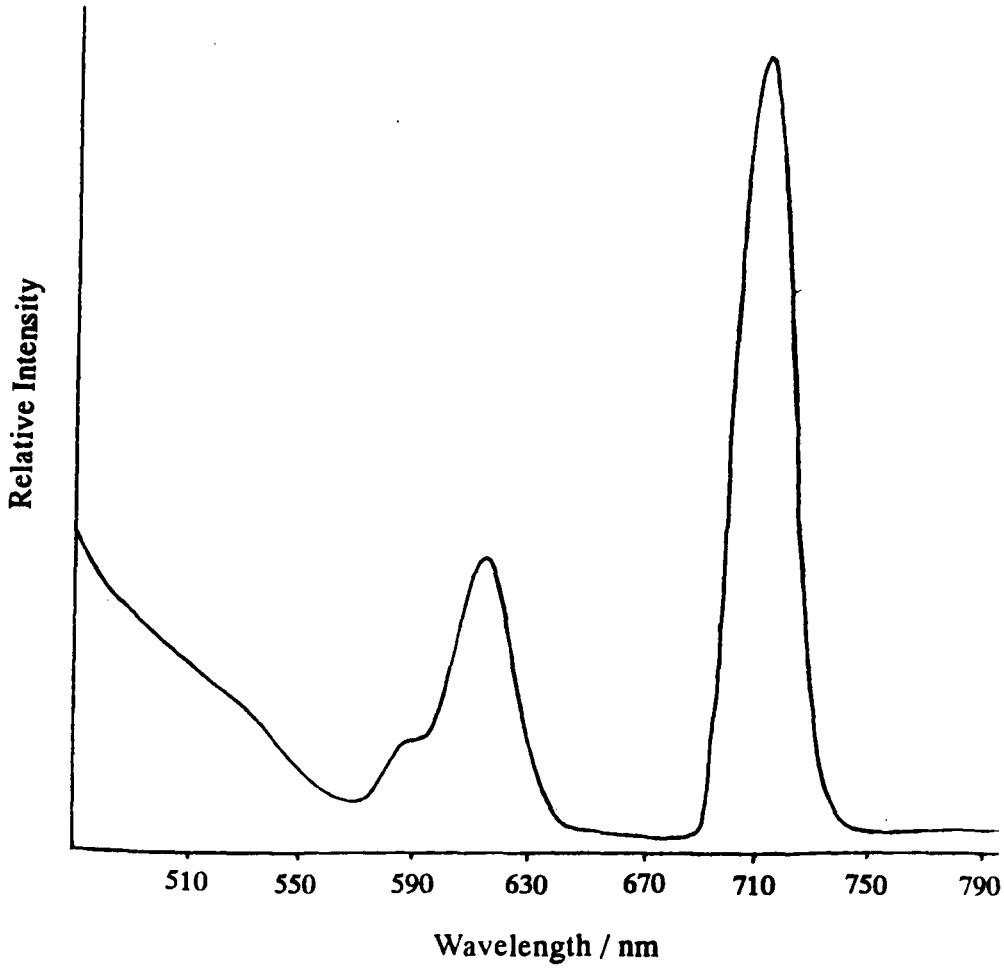

Figure 6.2. Fluorescence emission spectrum of 10^{-4} mol dm^{-3} $[Eu(L^{17}H)](PF_6)_4$ in acetonitrile. λ_{ex} = 355 nm.

The proton NMR spectrum of $[Eu(L^{17}H)](PF_6)_4$ (**Figures 6.4** and **6.5**) taken in CD_3CN is consistent with the presence of a single unsymmetrical species. The X-ray structure of $[Eu(terpy)_3]^{3+}$ shows a distortion from D_3 to C_2 symmetry, explained by distortion of the terpy ligands which makes them non-planar.[157] In addition, there is evidence for the existence of an on-off equilibrium of the pyridine rings in CH_3CN solution (discussed below) which may be expected to further reduce the symmetry. In an unsymmetrical species, each of the 49 protons of $[EuL^{17}H](PF_6)_4$ may be expected to have a different proton NMR chemical shift. 49 Resonances can indeed be identified in the proton NMR, although some resonances coincide. The integral values were used to establish the relative populations. **Figure 6.3** shows the expected splitting pattern of each resonance in an unsymmetrical species. The expected proton NMR spectrum would, therefore, consist of 3 x s, 24 x d, 9 x t, 12 x m and 1 x s (broad). The observed spectrum consists of 3 x s (sharp), 3 x s (broad), 21 x d (sharp), 2 x d (broad), 6 x t (sharp), 2 x t (broad) and 12 x m. It is thought that fine structure has been lost from the 'missing' triplet and doublet, possibly due to fluxional motion, which would account for the two 'extra' broad singlets. In this way the experimental observations would be in keeping with the expected splitting patterns. A proton NMR spectrum was taken at 243 K, but is no sharper than the room temperature spectrum.

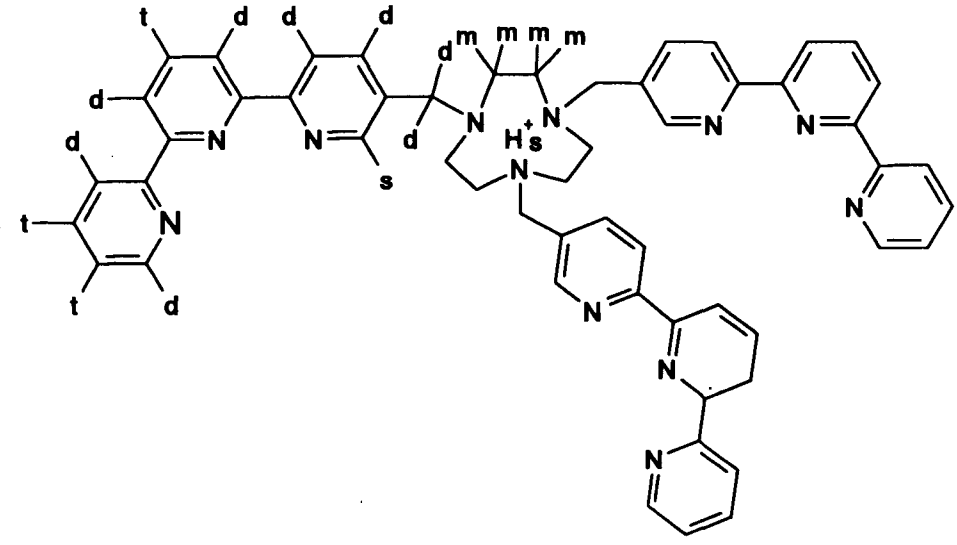

Figure 6.3. Expected splitting pattern (s = singlet, d = doublet, m = multiplet) for the proton NMR spectrum of an unsymmetrical molecule of $[Eu(L^{17}H)](PF_6)_4$. Labels on the remaining two-thirds of the molecule, plus additional elements, have been omitted for clarity.

The proton NMR spectrum of $[Eu(terpy)_3]^{3+}$ in CD_3CN has been studied as part of a report which suggests that CH_3CN solutions of $[Eu(terpy)_3]^{3+}$ exhibit a conformational equilibrium of the ligands, giving rise to $[Eu(terpy)_3]^{3+}$ complexes that are 7, 8 or 9 coordinate in terpy nitrogens.[159] The proton NMR spectrum showed three types of resonances which were attributed to three isomers of $[Eu(terpy)_3]^{3+}$. The authors assigned the most intense resonances (δ 15.3, 6.9, 6.1, 5.2 and 2.5 p.p.m.) to protons in the predominant tridentate form of terpy. Smaller resonances between 7.2 and 9.5 p.p.m. that are only slightly shifted from those in free terpy were assigned to protons on pyridine moieties not nitrogen coordinated to europium, and smaller shifted resonances were assigned to the coordinated parts of mono- or bi-dentate terpy ligands. A similar on-off equilibrium of the pyridine rings in $[Eu(L^{17}H)](PF_6)_4$ would help explain the observed broadening of some resonances, and the lack of symmetry.

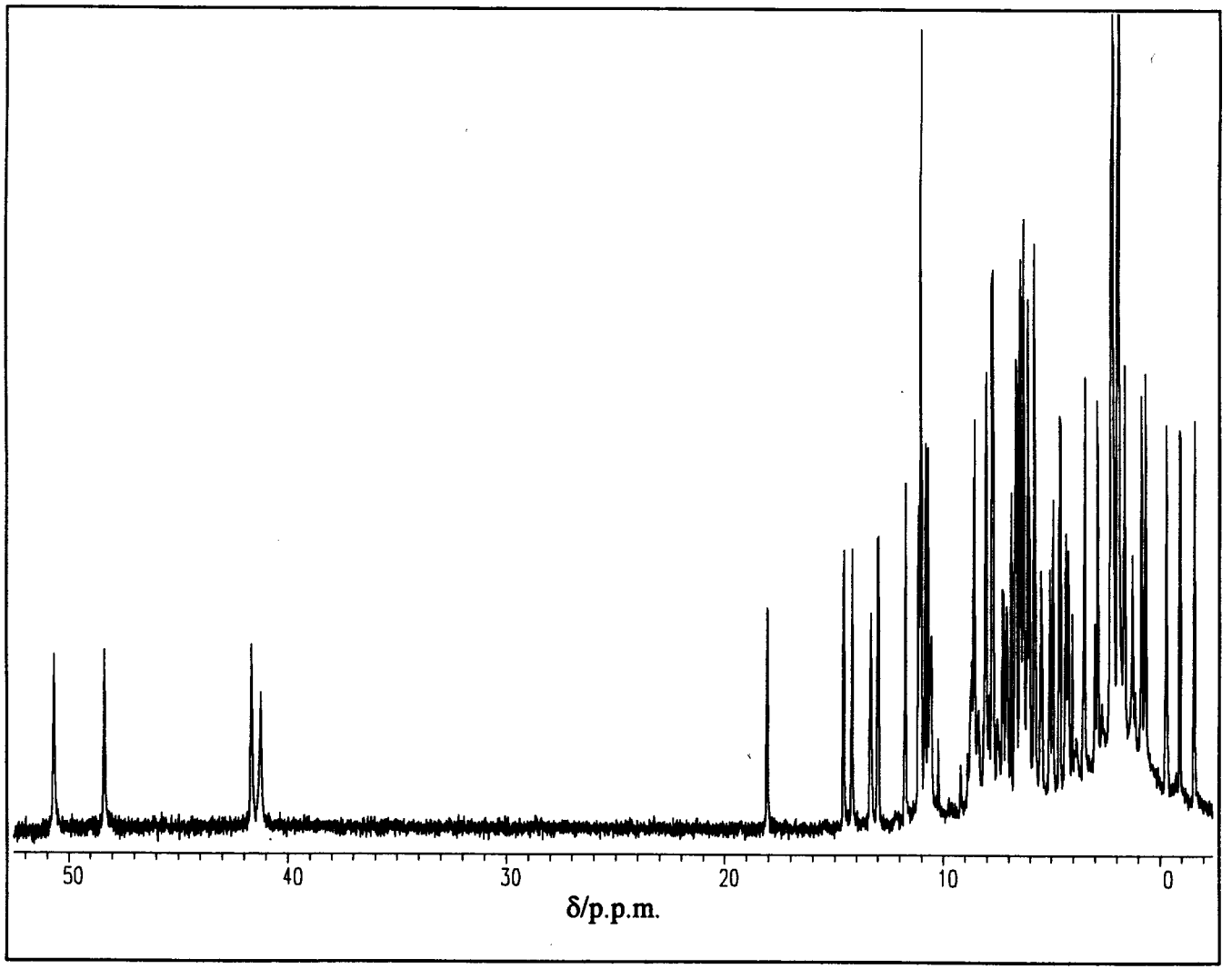

Figure 6.4. Proton NMR Spectrum of $[Eu(L^{17}H)](PF_6)_3$ in CD_3CN at 298 K.

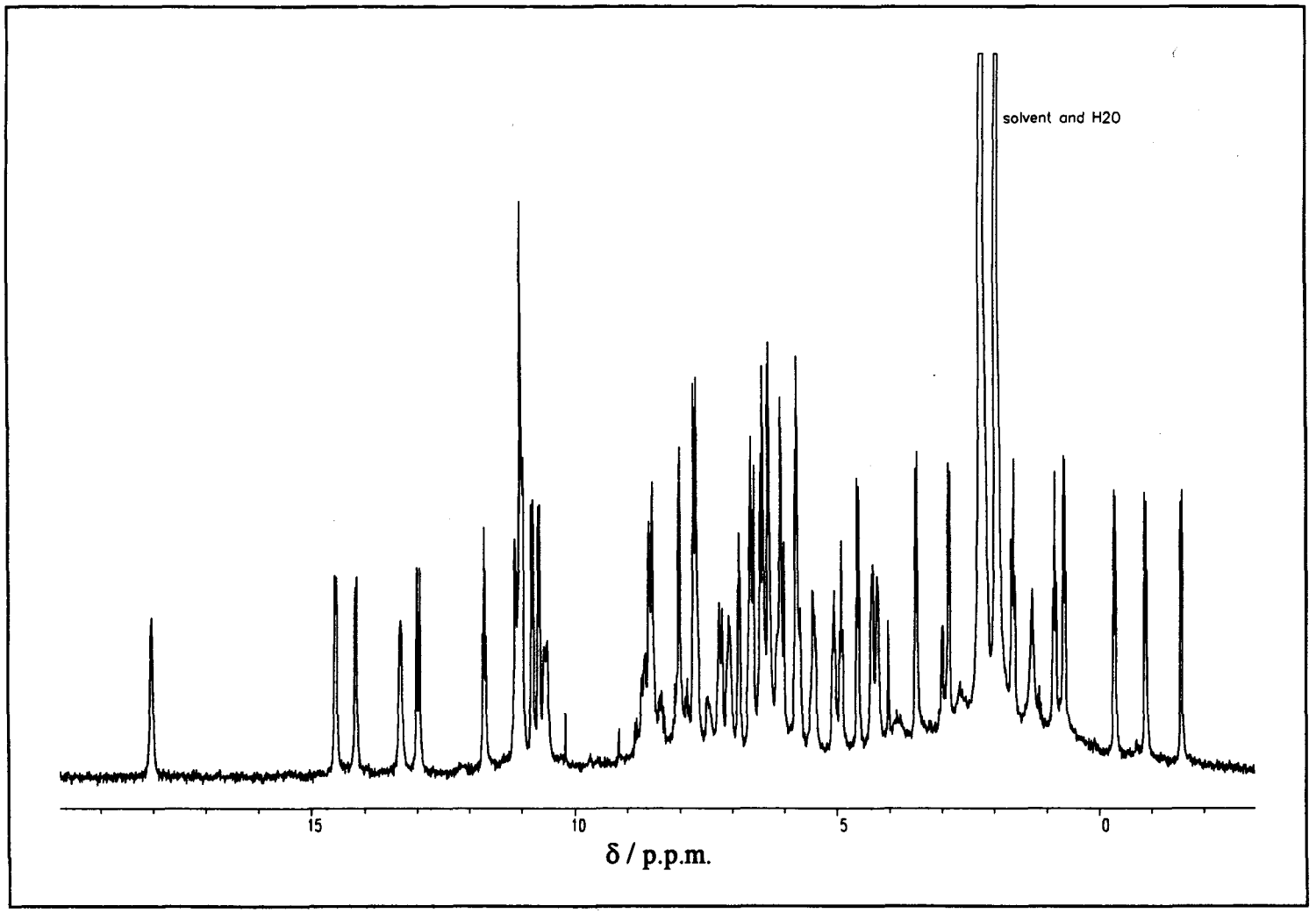

Figure 6.4. Expansion of part of the proton NMR Spectrum of $[Eu(L^{17}H)](PF_6)_3$ in CD_3CN at 298 K.

$[La(L^{17}H)](PF_6)_4$ is obtained as a white crystalline solid. The proton and ^{13}C NMR spectra show a high degree of symmetry. In the ^{13}C NMR spectrum, the presence of 15 downfield resonances, each with a relative population of three, (two coincide at δ 154.4 p.p.m., and a second pair coincide at δ 121.0 p.p.m.) indicates that the three terpy arms are equivalent. There are just two upfield resonances, one at δ 55.9 p.p.m. (relative area three, assigned to the linking methylene carbon atoms) and the other at δ 49.2 p.p.m. (relative area six, assigned to the 9N3 ring carbon atoms). The proton NMR spectrum also indicates that all terpy arms are equivalent, as are the six bipyCH_2 protons and the twelve protons of 9N3 . This is rather surprising, as complexation of all three pendant arms to a single metal ion should make the linking methylene protons split into two groups of three protons (by analogy with the proton NMR spectra of complexes of L^1). Similarly, axial and equatorial protons about the 9N3 ring become inequivalent. The lack of splitting in the aliphatic protons could indicate that the complex is labile. A rapid on–off equilibrium of one of the pendant arms from the La^{3+} ion, or some twist process within the molecule could allow these protons to become equivalent on the NMR time scale. Re–recording the proton NMR spectrum at 243 K had little effect on the upfield resonances.

As with $[Eu(L^{17}H)](PF_6)_4$, elemental analysis suggests that one mole of HPF_6 is bound to each L^{17}. The single proton is likely to be associated with the three nitrogen atoms of the 9N3 ring. The related ligand L^1 also forms metal complexes where the additional proton is trapped in the cavity formed between 9N3 ring and metal ion (Chapter 2). In complexes of L^1 the trapped proton can be seen as a broad singlet in the proton NMR spectra, in the region 7.58 to 8.13 p.p.m. The proton is tightly bound in the cavity, since attempts to remove it from the complex $[Ru(L^1H)]^{3+}$ at high pH failed. A very broad resonance (at δ ≈ 9.6 p.p.m.) is seen in the proton NMR spectrum of $[La(L^{17}H)](PF_6)_4$ at 298 K, which is attributed to the single proton attached to the nitrogen atoms of the 9N3 ring. At 243 K, this resonance is considerably sharper, and is shifted to δ 9.4 p.p.m.

The uv–visible spectrum shows two distinct bands at λ_{max} = 284 nm (ε = 59 000 $dm^3\ mol^{-1}\ cm^{-1}$) and λ_{max} = 238 nm (ε = 66 200 $dm^3\ mol^{-1}\ cm^{-1}$), plus one shoulder at λ_{max} = 310 nm (ε = 41 700 $dm^3\ mol^{-1}\ cm^{-1}$).

Studies of L^{18}.– L^{18}, which has two independent terdentate binding sites, was synthesised from the reaction of 5-bromomethyl-2,2':6',2"-terpyridine with a five fold excess of 9N3, and characterised by proton and ^{13}C NMR spectra, and by a CI mass spectrum. The ^{13}C NMR spectrum shows the expected 19 resonances. The proton NMR spectrum shows that the CH protons of the 9N3 ring split into three groups, each of integral four, two triplets and a singlet.

The reaction of L^{18} with $FeSO_4.7H_2O$ in methanol results in the formation of an intensely purple solution. After column chromatography, the complex $[Fe(L^{18}H)_2]^{4+}$ was isolated from the reaction mixture as its hexafluorophosphate salt by addition of aqueous NH_4PF_6. The FAB mass spectrum shows a peak at 1241, assigned to $[Fe(L^{18}H_2)(PF_6)_3]^+$. The uv–visible spectrum of $[Fe(L^{18}H)_2](PF_6)_4$ shows a MLCT band with λ_{max} = 553 nm (ε = 8350 $dm^3\ mol^{-1}\ cm^{-1}$), which is characteristic of the $[Fe(terpy)_2]^{3+}$ unit (λ_{max} = 552, ε = 11 900 $dm^3\ mol^{-1}\ cm^{-1}$).[160] The Fe^{2+} ion is low spin, and diamagnetic. Complexation with Fe^{2+} leaves the 9N3 group essentially free for coordination to a second metal ion or with protons. (Elemental analysis, the mass spectrum and the proton NMR spectrum show there to be two protons, one associated with each of the two 9N3 rings. The proton NMR spectrum shows only one type of L^{18} in $[Fe(L^{18}H)_2](PF_6)_4$, indicating that the two ligands in each molecule are equivalent. In the terpy moiety, H_a and H_b show upfield shifts of 1.7 and 1.6 p.p.m. respectively due to complexation. Shifts of a similar magnitude are observed for the analogous protons on complexation of terpy and pyterpy [4'–(4'''–pyridyl)–2,2':6',2"–terpyridine] with Fe^{2+}.[160] It is

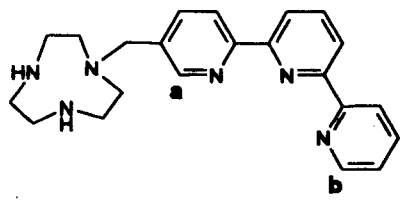

thought that these *ortho* protons are oriented towards the metal ion, where they are shielded by the electron density of the metal t_{2g} electrons and the π electrons of the other L^{18}. The ^{13}C NMR spectrum also shows just one type of L^{18} ligand. As in the free ligand, there are three types of 9N3 carbon atoms, one methylene link and 15 terpy carbon atoms (with two resonances coinciding at 154.3 p.p.m., and a second two coinciding at 125.0 p.p.m.).

Studies of L^{19}.– L^{19}, analogous to L^1 but with three 3–pyridylmethyl pendant arms, was prepared by the reaction of 9N3.3HBr with three equivalents of 3–chloromethylpyridine (3–picolyl chloride hydrochloride) and excess aqueous NaOH. As free 3–chloromethylpyridine has a tendency to decompose, the reaction was carried out at 0 °C and the aqueous NaOH added dropwise over 8 h. In this way only a low concentration of free 3-chloromethylpyridine is present in solution during the course of the reaction. L^{19} was isolated as a reddish oil of reasonable purity.

The pyridylmethyl pendant arms in L^{19} are attached *via* the 3 position of the pyridine ring. This makes L^{19} significantly different from its isomer **B**. **B** forms complexes of the type $[ML]^{2+}$ (M = Mn(II), Fe(II), Co(II), Ni(II), Cu(II), Ru(II) and Pd(II)), where it coordinates though all six nitrogen atoms.[149, 150] It is thought that steric strain within L^{19} would prevent the formation of analogous 1:1 complexes.

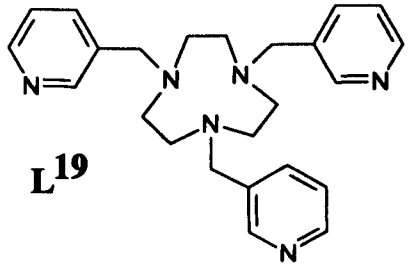

L^{19}

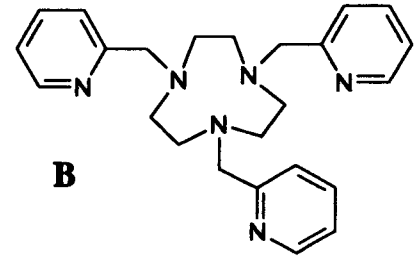

B

In a reaction of L^{19} with a six coordinate metal ion, coodination of the 9N3 moiety (necessarily to one face of the metal ion) would leave the second face free. It may be initially assumed that this could then be occupied either by the 9N3 or by the three pyridine groups of a second molecule of L^{19}, however the coordination of two

molecules of L^{19} to a single Zn^{2+} ion through both 9N3 units can be discounted for steric reasons. Coordination of the second L^{19} in this case would have to be through three pyridyl arms. A second possibility would be the formation of complexes also of the type $[ML^{19}_2]^{2+}$, where each L^{19} is coordinated through its three pyridylmethyl arms. In each case, three nitrogen donor atoms of each L^{19} molecule remain uncoordinated, so the possibility of forming polymeric structures cannot be discounted.

Reaction of two equivalents of L^{19} with $ZnSO_4.7H_2O$ in methanol, followed by addition of excess saturated aqueous NH_4PF_6 gives an off white precipitate. NMR spectra show this crude product to be a mixture of species. Careful recrystallisation by allowing diethyl ether to diffuse slowly into a solution of the crude product in nitromethane gives a white crystalline solid and a brown oil. The oil is thought to be a mixture of species, probably of a polymeric nature. Elemental analysis suggests the solid has the formulation $[Zn(L^{19}H)_2](PF_6)_4$, and the proposed structure of this material is shown below (**Figure 6.6**). As mentioned above, coordination of two 9N3 faces to one Zn ion is thought to be impossible, for steric reasons. Coordination of one 9N3 face and three pyridyl arms of the second L^{19} is not consistent with the elemental analysis result which suggests that a proton is bound to each 9N3 ring.

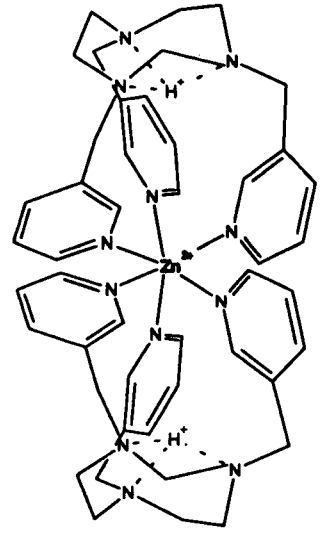

Figure 6.6. Proposed structure of $[Zn(L^{19}H)_2](PF_6)_4$.

Proton and ^{13}C NMR spectra suggest this compound has a high degree of symmetry. In the ^{13}C NMR spectrum, five downfield resonances are observed, indicating that all pyridyl arms are equivalent. There are two upfield resonances, showing all linking methylene protons to be equivalent, and all twelve 9N3 protons are equivalent. As discussed above, for the upfield resonances in the NMR spectra of $[La(L^{17}H)](PF_6)_4$, this high degree of symmetry is surprising, and is again attributed to the lability of the complex or fluxional motion such as a twist process occurring within the molecule. No resonance is observed for the proton believed to be associated with the nitrogen atoms of each 9N3 ring. It is postulated that H–D exchange occurs between these two protons and the CD_3NO_2 solution, presumably allowed by the lability of the complex.

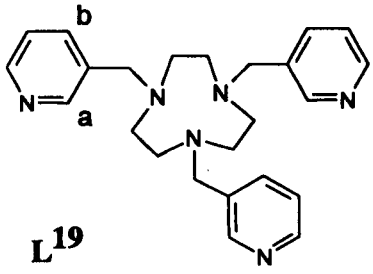

L^{19}

H_a shows an upfield shift of 0.67 p.p.m. on complexation. It is thought that in the complex, H_a lies above the plane of another pyridine ring, or is directed towards the electron density of the metal ion. This supports the argument that L^{19} coordinates to Zn(II) through the pyridine arms. If L^{19} were coordinated through the 9N3 face, then either no upfield shift for H_a would be expected, or an equal upfield shift for H_a and H_b would be anticipated. The low yield of $[Zn(L^{19}H)_2](PF_6)_4$ (38 %) could probably be improved by mono–protonating each L^{19} before reaction with Zn. It is likely that this would introduce a proton into each 9N3 ring, thereby reducing the possibility of this moiety subsequently reacting with Zn^{2+}. This should reduce the number of species formed on reaction with Zn(II).

Experimental

Synthesis of 5-Methyl-2,2':6',2''-terpyridine (**Scheme 6.1**).

The preparation (which was developed with Dr. S. C. Rawle) is based on the literature synthesis of terpyridine,[161] the only difference is that 2-bromo-5-methylpyridine is used in place of 2-bromo-pyridine. This is prepared from 2-amino-5-methylpyridine following a literature method.[162] References concerning the synthesis of intermediates **2**, **3** and **4** can be found in ref. 161.

Synthesis of 2-bromo-5-methylpyridine (**1**).– 2–amino–5–methylpyridine (3.0 g, 27.8 mmol) was dissolved in 48 % HBr (40 cm^3) and cooled to –10 °C in an ice/salt bath. Bromine (6 cm^3) was added dropwise with vigorous stirring, followed by a solution of $NaNO_2$ (6 g) in water (20 cm^3). The temperature was maintained below 5 °C throughout the additions. After stirring for 30 min below 5 °C, aqueous NaOH was added until the orange colour disappeared and a brown oil separated. The mixture was extracted with several portions of CH_2Cl_2 (which may float on the very dense aqueous layer); the combined organic extracts were dried with anhydrous $MgSO_4$ and the solvent removed to leave a brown oil which crystallised on cooling. The oil may be purified by distillation *in vacuo* (0.1 mm pressure), or alternatively it may be recrystallised from warm 40–60 petroleum ether. Yield 3.97 g, 83 %. Mass spectrum (EI) *m/z* 171/173 (Calc. for M^+ (^{79}Br and ^{81}Br), 171/173). ^1H NMR (250 MHz, $CDCl_3$): δ/p.p.m. 8.22 (s, 1H), 7.38 (s, 2H), 2.31 (s, 3H).

Synthesis of ethyl-β -pyrollidino-propionate (**2**).– Equimolar quantities of ethyl acrylate and pyrollidine were mixed together with stirring, whereupon the mixture refluxes spontaneously. After stirring for 4 h, the product was distilled under reduced pressure (120 °C at 14 mm Hg); small amounts of unreacted starting material were removed in the initial forerun. Yield 90 %. ^1H NMR (250 MHz, $CDCl_3$): δ/p.p.m. 4.13 (q, 2H), 2.74 (2 x t, 2H), 2.49 (m, 4H), 1.74 (m, 4H), 1.22 (t, 3H).

Synthesis of 1-oxo-1-[2-{5-methyl}-pyridyl]-3-[N-pyrollidino]propane, oxalate salt (3).$(CO_2H)_2$– N–butyllithium (23 cm^3 of 1.6 mol dm^{-3} solution in hexane, 36.8 mmol) was added to dry, degassed THF (60 cm^3) at –78 °C under N_2. A solution of 1 (5.95 g, 34.6 mmol) in THF (30 cm^3) was added dropwise, keeping the temperature below –70 °C. The reaction mixture became brown–orange, and was stirred for 15 min after the addition was complete. The mixture was stirred for 1 h at –70 °C and then allowed to warm up to room temperature slowly. HCl (50 cm^3, 2 mol dm^{-3}) was added, and most of the THF removed on a rotary evaporator. The aqueous solution was basified with NaOH, upon which a brown oil separates which is then extracted with ether. The combined ethereal extracts were dried ($MgSO_4$) and the solvent removed. The residual brown oil was dissolved in acetone (50 cm^3), and a solution of oxalic acid (5 g) in acetone (50 cm^3) was added. On cooling, a white solid precipitated which was collected by filtration and recrystallised from acetone / water (4:1) at –20 °C. Yield 5.1 g, 50 %. Mass spectrum (EI) *m/z* = 218 (Calc. for $[C_{13}H_{19}N_2O]^+$, 218). ^1H NMR (250 MHz, $(CD_3)_2SO$): δ/p.p.m. 8.69 (s, 1H), 7.99 (m, 2H), 3.74 (t, 2H), 3.55 (t, 2H), 3.40 (m, 4H), 2.40 (s, 3H), 1.92 (m, 4H).

Synthesis of 'pyridacyl pyridinium iodide' (4).– 2–Acetyl pyridine (6.05 g, 50 mmol) was added dropwise to a stirred solution of iodine (12.69 g, 50 mmol) in dry pyridine (60 cm^3). The mixture was refluxed for 1 h and allowed to cool slowly to room temperature. The reaction flask was then cooled further in ice, upon which a thick black precipitate appeared. The precipitate was collected by filtration and washed with ether/ethanol (9:1). The black solid was redissolved in boiling methanol (200 cm^3) to which a little activated charcoal had been added. After refluxing for 5 min, the black mixture was filtered hot through a celite pad to give a clear yellow solution. On cooling, golden yellow crystals precipitated which were collected by filtration and dried. Yield 9.8 g, 60 %.

Synthesis of 5-Methyl-2,2':6',2''-terpyridine (**5**).– A mixture of **3** (3.06 g, 10 mmol), **4** (3.26 g, 10 mmol) and ammonium acetate (4 g, a large excess) in methanol / water (2:1, 100 cm^3) was heated to reflux overnight to give a clear, dark brown solution. The solution was concentrated on a rotary evaporator until a precipitate appeared, the flask was then chilled in an ice bath. The product was collected as an off–white crystalline solid, and washed thoroughly with water to remove any ammonium oxalate which may also have precipitated. Further purification may be affected by recrystallisation from ethanol / water (1:1). Mass spectrum (CI / NH_3) 248 (Calc. for MH^+, 248). ^1H NMR (250 MHz, $CDCl_3$): δ/p.p.m. 8.70 (d, 1H), 8.61 (d, 1H), 8.52 (s, 1H), 8.50 (d, 1H), 8.41 (d, 1H), 7.94 (t, 1H), 7.85 (t, 1H), 7.66 (d, 1H), 7.33 (m, 1H). ^{13}C NMR (400 MHz, $CDCl_3$); 156.2, 155.4, 155.1, 153.6, 149.5, 149.0, 137.7, 137.3, 136.7, 133.1, 123.6, 121.0, 120.6 (2C), 120.5, 18.3.

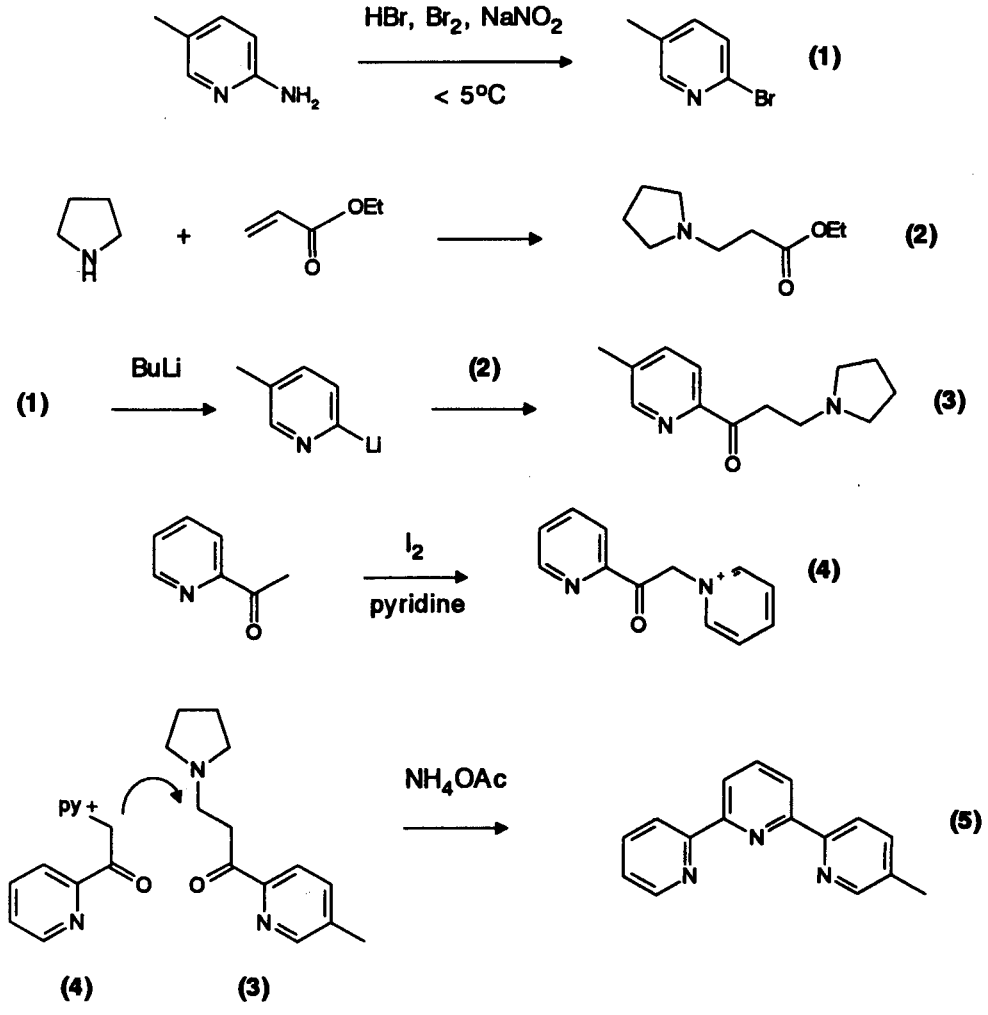

Scheme 6.1. Synthesis of 5-Methyl-2,2':6',2''-terpyridine (5).

Synthesis of 5-Bromomethyl-2,2',6',2''-terpyridine.– 5–Methyl–2,2',6',2''–terpyridine (494 mg, 2.0 mmol) and *N*–bromosuccinimide (356 mg, 2.0 mmol) were refluxed in CCl_4 (100 cm^3) under N_2 in strong light until reaction had occurred (about 1 h). Completion of the reaction could be determined by the disappearance of *N*-bromosuccinimide (which is denser than CCl_4) and its replacement by succinimide (which floats). The succinimide was filtered off, the solvent evaporated and the residue recrystallised from diethyl ether. Yield 420 mg, 64 %. ^1H NMR (250 MHz, $CDCl_3$): δ/p.p.m. 8.70 (d, 2H), 8.59 (d, 2H), 8.45 (m, 2H), 7.96 (t, 1H), 7.86 (t, 2H), 7.39 (m, 1H), 4.55 (s, 2H). ^{13}C NMR (62.90 MHz, $CDCl_3$): δ/p.p.m. (relative populations in parentheses) 156.0 (2), 155.2 (1), 149.1 (2), 149.0 (1), 137.9 (1), 137.4 (1), 136.9 (1), 133.6 (1), 123.7 (1), 121.1 (3), 29.6 (1). Mass spectrum (CI / NH_3): *m/z* 327 (Calc. for L^1H^+, 327).

Synthesis of 1,4,7-tris-(2,2':6',2''-terpyridyl-5'-ylmethyl)-1,4,7-triazacyclononane, L^{17}. – 5–Bromomethyl–2,2':6',2''–terpyridine (480 mg, 1.47 mmol), 9N3 (63 mg, 0.49 mmol) and Et_3N (125 mg, 1.70 mmol) were stirred in chlorobenzene (75 cm^3) at room temperature overnight. The resultant white of precipitate $Et_3NH^+Br^-$ was filtered off and the solvent removed from the filtrate. The residue was dissolved in CH_2Cl_2 and loaded onto a silica gel column (particle size 0.040–0.063 mm). This was washed with CH_2Cl_2 / CH_3OH / NH_3 (50:7:1). The desired product was eluted with 10 to 15 % CH_3OH. The solvent was removed from the desired fraction (which was identified by ^1H NMR) and the product dissolved in CH_2Cl_2. This solution was dried over anhydrous $MgSO_4$, and filtered to give L^{17} as a white crystalline solid. Yield 279 mg, 66 %. ^1H NMR (250 MHz, $CDCl_3$): δ/p.p.m. 8.64 (d, 3H), 8.61 (s, 3H), 8.55 (d, 6H), 8.39 (d, 6H), 7.88 (t, 3H), 7.86 (d, br, 3H), 7.76 (t, 3H), 7.26 (t, 3H), 3.72 (s, 6H), 2.88 (s, 12H). ^{13}C NMR (62.90 MHz, $CDCl_3$): δ/p.p.m. 156.1 (3), 155.2 (9), 155.0 (3), 149.7 (3), 149.0 (3), 137.8 (3), 137.6 (3), 136.7 (3), 135.6 (3), 123.6 (3), 121.0 (3), 120.8 (3), 120.7 (3), 60.2 (3), 55.5 (6). Uv-visible spectrum in CH_3CN [λ_{max} /nm

(ε / dm^3 mol^{-1} cm^{-1})]: 326 (50 700), 286 (66 000), 238 (66 700). Mass spectrum (FAB / NBA): *m/z* 865 (Calc. for MH^+, 865).

Synthesis of $[Eu(L^{17}H)](PF_6)_4$.– A solution of $Eu(NO_3)_2.6H_2O$ (70 mg, 0.16 mmol) in methanol (50 cm^3) was added to a hot (60 °C), stirred solution of L^{17} (136 mg, 0.16 mmol) in the same solvent (50 cm^3). The solution was refluxed for 3 h after addition was complete. A solution of excess saturated NH_4PF_6 in methanol was then added. On cooling, a fine buff coloured precipitate appeared. This was collected by suction filtration and dried *in vacuo* over silica gel. The product was then recrystallised by allowing diethyl ether to diffuse slowly into a concentrated solution of nitromethane. Yield 150 mg, 66%. ^1H NMR (250 MHz, CD_3NO_2): δ/p.p.m. 50.61 (s, 1H), 48.32 (s, 1H), 41.61 (s, 1H), 41.21 (s, br, 1H), 18.03 (s, br, 1H), 14.52 (d, 1H), 14.14 (d, 1H), 13.31 (s, br, 1H), 12.96 (d, 1H), 11.71 (t, 1H), 11.01 (m, 3H), 10.79 (d, 1H), 10.67 (d, 1H), 10.51 (d, 1H), 8.69 (d, br, 1H), 8.55 (d, 1H), 8.35 (m, 1H), 8.02 (d, 1H), 7.71 (d, 2H), 7.23 (d, 1H), 7.05 (m, 1H), 6.87 (t, 1H), 6.60 (m, 1H), 6.58 (d, 1H), 6.41 (m, 2H), 6.30 (d, 1H), 6.07 (m, 2H), 5.76 (m, 2H), 5.45 (t, br, 1H), 5.06 (t, 1H), 4.92 (t, 1H), 4.60 (d, 1H), 4.32 (d, 1H), 4.25 (d, 1H), 3.49 (d, 1H), 2.87 (d, 1H), 1.65 (t, 1H), 1.28 (t, br, 1H), 0.85 (t, 1H), 0.68 (d, 1H), –0.28 (d, 1H), –0.88 (d, 1H), –1.55 (d, 1H). Mass spectrum (FAB / NBA) 1077 (Calc. for the daughter ion $[EuL^1F_2]^+$, 1077). Uv–visible spectrum in CH_3CN [λ_{max} / nm (ε / dm^3 mol^{-1} cm^{-1})]: 322 (43 400), 290 (53 200), 234 (81 800). Found C, 38.76, H, 3.24, N, 12.03. Calc. for $C_{54}H_{49}EuF_{24}N_{12}P_4.3CH_3NO_2$.C, 38.44, H, 3.28, N, 11.80 %.

Synthesis of $[La(L^{17}H)](PF_6)_4$.– A solution of $LaCl_3$ (17 mg, 0.07 mmol) in methanol (10 cm^3) was added to a hot (60 °C), stirred solution of L^{17} (57 mg, 0.07 mmol) in the same solvent (25 cm^3). The solution was refluxed for 3 h after addition was complete. A solution of excess saturated NH_4PF_6 in methanol was then added. On cooling, a fine off–white precipitate appeared, which was collected by suction filtration and dried *in vacuo* over silica gel. Yield 60 mg, 60%. ^1H NMR (250 MHz, (CD_3NO_2): δ

/p.p.m. 9.6 (s, very br, 1H), 8.57 (d, 3H), 8.54 (d, 3H), 8.37 (d, 3H), 8.34 (d, 3H), 8.26 (d, 3H), 8.16 (d, 3H), 8.07 (t, 3H), 7.92 (t, 3H), 7.74 (d, 3H), 7.56 (t, 3H), 4.07 (s, 6H), 3.06 (m, 12H). ^{13}C NMR (100.62 MHz, $CDCl_3$): δ/p.p.m. 154.8 (3), 154.5 (3), 154.4 (6), 150.4 (3), 149.0 (3), 138.9 (3), 138.5 (3), 138.0 (3), 131.5 (3), 124.6 (3), 121.0 (6), 120.9 (3), 120.8 (3), 55.9 (3), 49.2 (6). Uv–visible spectrum in CH_3CN [λ_{max} / nm (ε / dm^3 mol^{-1} cm^{-1})]: 310 (shoulder, ~ 41 300), 284 (56 900), 238 (65 300). Found C, 41.06, H, 3.69, N, 10.25. Calc. for $C_{54}H_{49}F_{24}LaN_{12}P_4$ C, 40.93, H, 3.12, N, 10.61 %.

Synthesis of 2,2':6',2''-terpyridyl-5-ylmethyl)-1,4,7-triazacyclononane, L^{18}. 5-Bromomethyl–2,2',6',2''–terpyridine (250 mg, 0.77 mmol), was added dropwise in C_6H_5Cl (15 cm^3) to a stirred solution of 9N3 (495 mg, 3.83 mmol, a 5 fold excess) in the same solvent (100 cm^3) at 100 °C. The temperature was maintained at 100 °C for 1 h after addition was complete. The solution was filtered and the solvent removed from the filtrate to leave a yellow oil. This was loaded onto a column of silica gel (particle size 0.040–0.063 mm) and eluted with CH_2Cl_2 / CH_3OH / NH_3 (50 : 7 : 1). Fractions containing the desired product (identified by ^1H NMR) were combined, and the solvent removed. The residual oil was dissolved in CH_2Cl_2 (50 cm^3) and dried over anhydrous $MgSO_4$. After filtration, the solvent was removed to leave the desired product as a light yellow oil which solidified on standing. Yield 293 mg, 38 %. ^1H NMR (400 MHz, $CDCl_3$): δ/p.p.m. 8.69 (d, 1H), 8.63 (d, 1H), 8.61 (d, 1H), 8.58 (d, 1H), 8.44 (d, 1H), 8.41 (d, 1H), 7.95 (t, 1H), 7.87 (d, 1H), 7.86 (t, 1H), 7.33 (m, 1H), 3.90 (s, 2H), 3.07 (s, 4H), 2.91 (t, 4H) 2.79 (t, 4H). ^{13}C NMR (100.62 MHz, $CDCl_3$): δ/p.p.m. 156.0, 155.3, 155.2, 155.0, 149.4, 149.0, 137.8, 137.5, 136.7, 136.4, 123.6, 121.0, 120.8, 120.76, 120.74, 58.4, 52.2 (2), 46.0 (2), 45.8 (2). Mass spectrum (CI / NH_3) *m/z* 375 (Calc. MH^+ 375).

Synthesis of $[Fe(L^{18}H)_2](PF_6)_4$.– A solution of $FeSO_4.7H_2O$ (32 mg, 0.12 mmol) in CH_3OH (20 cm^3) was added dropwise to a solution of L^{18} (90 mg, 0.23 mmol) in the

same solvent (30 cm^3) at 50 °C. The resulting purple solution was refluxed for 1 h. The solvent was evaporated and the residue dissolved in H_2O (5 cm^3), loaded onto a column of Sephadex C–25 cation exchange resin and eluted with 0.1 – 1.0 mol dm^{-3} NaCl. The main band was eluted with approximately 0.6 mol dm^{-3} NaCl and treated with excess saturated aqueous NH_4PF_6 solution. The resulting purple precipitate was collected by suction filtration and dried *in vacuo* over silica gel. Yield 119 mg, 73 %. ^1H NMR (250 MHz, CD_3NO_2): δ/p.p.m. 8.82 (d, 4H), 8.61 (d, 2H), 8.38 (d, 2H), 8.35 (d, 4H), 7.88 (d, 2H), 7.77 (t, 2H), 7.03 (d, 2H), 6.98 (s, 2H), 6.96 (t, 2H), 3.39 (s, 4H), 3.28 (s, br, 2H), 2.88 (s, 8H), 2.57 (t, 8H), 2.31 (t, 8H) 1.95 (s, br, 4H). ^{13}C NMR (100.62 MHz, CD_3NO_2): δ/p.p.m. 161.9 (2), 161.5 (2), 159.1 (2), 154.5 (2), 154.3 (4), 142.1 (2), 140.3 (2), 139.8 (2), 136.6 (2), 128.7 (2), 125.0 (4), 124.9 (2), 124.8 (2), 55.6 (2), 47.6 (4), 44.9 (4), 43.8(4). Mass spectrum (FAB / NBA): *m/z* 1241. Calc. for $[(Fe(L^{18})_2H_2(PF_6)_3]^+$, 1241. Uv–visible spectrum in CH_3CN [λ_{max} / nm (ε / dm^3 mol^{-1} cm^{-1})]: 553 (8 350), 500 (shoulder) (4 740), 370 (shoulder) 4 150), 325 (43 200), 275 (31 800). Found C, 37.19, H, 3.84, N, 11.44. Calc. for $C_{44}H_{54}F_{24}FeN_{12}P_4.2H_2O$ C, 37.15, H, 4.11, N, 11.81 %.

Synthesis of 1,4,7-Tris(3-pyridylmethyl)-1,4,7-triazacyclononane, L^{19}.– 3–Chloro–methylpyridine hydrochloride (4.167 g, 25 mmol) and 9N3.3HBr (3.124g, 8.47 mmol) were dissolved in H_2O (100 cm^3). The solution was cooled in an ice bath, and a solution of NaOH (3.20 g, 80 mmol) in H_2O (100 cm^3) was added dropwise over 8 h. The solvent was then removed and the residue extracted with CH_2Cl_2. The organic extracts were combined, dried over anhydrous $MgSO_4$ and filtered. The solvent was removed from the filtrate to leave the product as a red oil. Yield 2.21 g, 65 %. ^1H NMR (250 MHz, $CDCl_3$): δ / p.p.m. 8.45 (d, 3H), 8.39 (d, 3H), 7.54 (m, 3H), 7.15 (m, 3H), 3.51 (s, 6H), 2.69 (s, 12H). ^{13}C NMR (69.90 MHz, $CDCl_3$): δ / p.p.m. 150.2 (3), 148.2 (3), 136.5 (3), 135.3 (3), 123.1 (3), 60.2 (3), 55.3 (6). Mass spectrum (CI / NH_3) *m/z* 403 (Calc. MH^+ 403).

Synthesis of $[Zn(L^{19}H)_2](PF_6)_4$.– A solution of $ZnSO_4.7H_2O$ (100 mg, 0.35 mmol) in H_2O (50 cm^3) was added dropwise to a refluxing solution of L^{19} (279 mg, 0.69 mmol) in methanol (100 cm^3). The mixture was kept at reflux for 0.5 h after addition was complete. Excess saturated aqueous NH_4PF_6 was then added and the solvent volume reduced to approx. 50 cm^3. On cooling, an off–white precipitate formed which was removed by suction filtration and recrystallised from CH_3NO_2/ Et_2O (by allowing Et_2O to diffuse into a solution of the crude product in CH_3NO_2) to give a brown oil and a white crystalline solid. The solid was carefully separated from the oil, washed with a little Et_2O and dried *in vacuo* over silica gel. Yield 195 mg, 38 %. ^1H NMR (250 MHz, CD_3NO_2): δ/p.p.m. 8.46 (d, 6H), 7.93 (d, 6H), 7.78 (s, 6H), 7.57 (t, 6H), 3.93 (s, 12H), 2.99 (s, 24 H). ^{13}C NMR (62.89 MHz, CD_3NO_2): δ/p.p.m. 150.5 (6), 150.2 (6), 143.3 (6), 135.0 (6), 127.8 (6), 58.3 (6), 50.4 (12). Found: C, 39.60, H, 4.36, N, 11.48. Calc. for $C_{48}H_{62}F_{24}N_{12}P_4Zn$, C, 39.70, H, 4.30, N, 11.57 %.

Conclusions and Future Work.

Synthesis of azamacrocycles with N-pendant pyridylmethyl, bipyridylmethyl and terpyridylmethyl arms:– The preparation of the fully N–alkylated azamacrocycles L^1, L^3, L^{17} and L^{19} is readily achieved by direct alkylation of the parent macrocycles 9N3 and cyclam with an excess of the requisite alkylating agent, $ArCH_2X$ (X = Cl, Br; Ar = py, bipy, terpy) in the presence of a base. Mono N–alkylation of 9N3 with $terpyCH_2$ and of cyclam with $bipyCH_2$ to give L^9 and L^{18} respectively is achieved by reaction of the alkylating agent with an excess of macrocycle. Steric effects are thought to control the selective alkylation of tet *a* and tet *b*, to give L^{10} and L^{11}.

Complexes:– Reacting the N–pendant bipy CH_2 groups in L^1–L^3, L^{10}, L^{11} and L^{16} with *cis*–$[Ru(bipy)_2Cl_2]$ gives fluorescent ligands with uncomplexed (or protonated) macrocyclic cavities, and up to four attached $[Ru(bipy)_3]^{2+}$ groups. These ligands have potential for use as fluorescent pH or transition metal ion sensors; binding proton(s) or a transition metal ion(s) in the macrocyclic cavity significantly quenches the fluorescence of the $[Ru(bipy)_3]^{2+}$ groups. That based on 1,4,7–triazacyclononane (9N3) with three attached $[Ru(bipy)_3]^{2+}$ groups has a first photoexcited state pK_a of 7.1, and thus may be useful as a fluorescent sensor for physiological pH at below micromolar concentrations. This is being pursued by Mrs A. M. Josceanu, and will be discussed in her thesis. The potentially nonadentate ligand L^{17}, based on the macrocycle 9N3 with three N–pendant $terpyCH_2$ arms forms a strongly fluorescent complex with Eu^{3+}, $[Eu(L^{17}H)](PF_6)_4$. The persistent coordination of Eu^{3+} to L^{17} in solution is shown by proton NMR and luminescence measurements. The sexidentate ligand L^{18} contains two independent terdentate coordination sites. As the 9N3 moiety is facially coordinating, and the terpy arm meridonally coordinating, L^{18} can be expected to give rise to a degree of self assembly in polynuclear structures with six coordinate metal ions. This is illustrated schematically in **Figure 7.1.** Suitable metal ions would discriminate between the facially coordinating macrocycle (9N3) and the

meridonally coordinating pendant arm (terpy). The degree of aggregation could be controlled with 'end–stopping' groups. For example, $[Mo(CO)_3]$ could be used to block the 9N3 moiety, and $[Ru(terpy)]^{2+}$ to block the terpy arm. With L^{18}, the possibility of forming *cis* or *trans* isomers exists at metal centres coordinated to 9N3 groups, although this could be overcome by linking the terpy arm to the 9N3 *via* the 4'–position of the terpy, to form a ligand such as **A**.

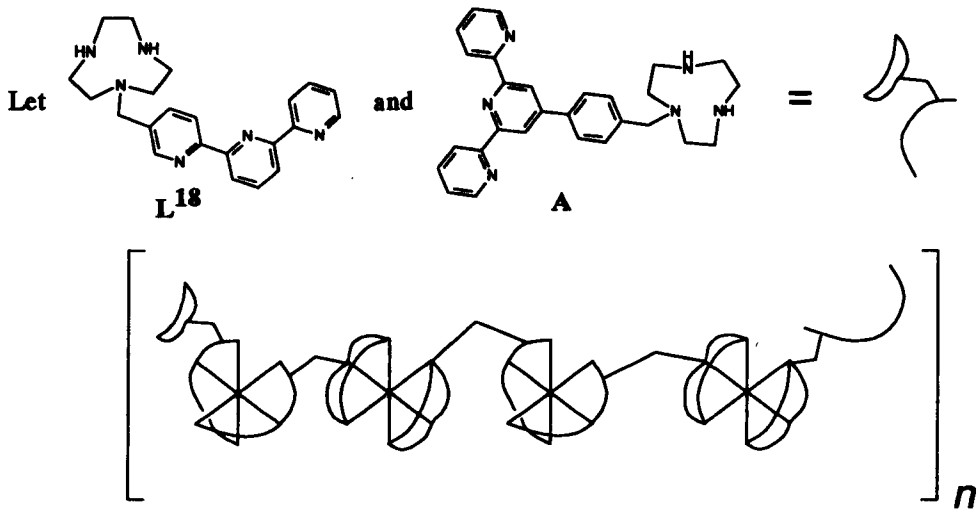

Figure 7.1. Sketch of the formation of polynuclear complexes by facially and meridonally coordinating macrocyclic ligands.

Further work is required on the functionalisation of the macrocycles tet *a* and tet *b* with *N*–pendant pyridyl and bipyridyl arms. Reaction of L^{10} and L^{11} (tet *a* and tet *b* functionalised with two *N*–pendant 2,2'–bipyridyl–5'–ylmethyl arms) with two equivalents of *cis*–$[Ru(bipy)_3]^{2+}$ gives ligands (L^{12} and L^{13}) carrying two pendant $[Ru(bipy)_3]^{2+}$ groups. L^{12} and L^{13} are isolated as a mixture of diastereoisomers. Prolonged heating of solutions of L^{12} and L^{13} could help to determine whether the conformational isomers are inter convertible, and whether there is a preferred conformational isomer for each ligand. It is anticipated that the *N*–functionalisation of tet *a* and tet *b* with 2–pyridylmethyl arms will give hexadentate ligands. These ligands may adopt different geometries on complexation with a six coordinate metal ion. Tet *a* does not easily adopt a folded geometry and so is likely to form *trans* complexes, but tet *b* folds readily and so may coordinate *cis* to a metal ion.

Appendix
Crystallographic Data

$[Ru(L^1H)](PF_6)_3$.– Synthesis and characterisation discussed in Chapter 2.

Table A.1. Crystal data and structure refinement for $[Ru(L^1H)](PF_6)_3.(CH_3NO_2)_3$

Identification	pipruab
Empirical formula	$C_{42}H_{49}F_{18}N_{12}O_6P_3Ru$
Formula weight	1353.91
Temperature	220(2) K
Wavelength	0.71073 A
Crystal system	Monoclinic
Space group	P2(1)/n
Unit cell dimensions	a = 12.596(13) A $\alpha = 90°$
	b = 25.81(2) A $\beta = 110.65(7)°$
	c = 17.417(14) A $\gamma = 90°$
Volume	5299(8) A^3
Z	2
Density (calculated)	1.697 Mg/m^3
Absorption coefficient	0.509 mm^{-1}
F(000)	2736
Crystal size	0.49 x 0.34 x 0.28 mm
Θ range for data collection	2.01 to 22.55°
Index ranges	$0 \le h \le 13, 0 \le k \le 27, -18 \le l \le 17$
Reflections collected	7320
Independent reflections	6954 [R(int) = 0.0421]
Absorption correction	Analytical
Max. and min. transmission	0.89 and 0.85

Refinement method	Full-matrix least-squares on F^2
Data / restraints / parameters	6941 / 186 / 761
Goodness-of-fit on F^2	1.033
Final R indices [I>2sigma(I)]	R1 = 0.0590, wR2 = 0.1261
R indices (all data)	R1 = 0.0974, wR2 = 0.1733
Largest diff. peak and hole	0.684 and -0.636 $e.A^{-3}$

Table A.2. Atomic coordinates (x 10^4) and equivalent isotropic displacement parameters ($Å^2$ x 10^3) for $[Ru(L^1H)](PF_6)_3.(CH_3NO_2)_3$

U(eq) is defined as one third of the trace of the orthogonalized Uij tensor.

	x	y	z	U(eq)
Ru(1)	2463(1)	1451(1)	7132(1)	29(1)
P(1)	2643(2)	1040(1)	2340(1)	44(1)
P(2)	8149(2)	1952(1)	4771(1)	59(1)
P(3)	7543(2)	578(1)	863(2)	60(1)
F(11)	2238(5)	647(2)	1607(3)	75(2)
F(12)	3056(6)	1440(2)	3055(3)	98(2)
F(13)	3036(8)	557(3)	2917(4)	100(4)
F(14)	3842(8)	1046(4)	2261(9)	138(6)
F(15)	1481(6)	997(3)	2452(6)	93(3)
F(16)	2281(13)	1514(3)	1776(4)	139(6)
F(13')	3755(24)	803(13)	2830(17)	66(10)
F(14')	3127(24)	1325(11)	1785(14)	41(8)
F(15')	2082(29)	779(11)	2857(16)	56(10)
F(16')	1491(20)	1288(12)	1810(17)	59(10)
F(21)	9459(4)	1864(2)	5218(3)	76(2)
F(22)	8070(6)	1472(2)	4224(4)	123(3)
F(23)	6844(4)	2065(3)	4322(3)	98(2)
F(24)	8269(5)	2454(2)	5312(3)	87(2)
F(25)	7897(5)	1631(3)	5436(4)	108(2)
F(26)	8395(5)	2296(2)	4108(3)	92(2)
F(31)	7059(6)	984(2)	1334(4)	105(2)
F(32)	8711(6)	808(3)	1241(7)	197(5)
F(33)	7954(7)	175(3)	387(5)	143(3)
F(34)	6302(5)	360(2)	511(4)	100(2)
F(35)	7254(7)	955(2)	123(4)	121(3)
F(36)	7767(5)	178(2)	1565(4)	110(2)

N(1)	-1249(5)	1889(2)	8073(4)	41(2)
N(2)	298(5)	1469(2)	9467(3)	38(1)
N(3)	-868(5)	768(2)	8287(4)	44(2)
N(11)	3457(5)	2086(2)	7206(3)	32(1)
N(12)	1335(4)	2038(2)	7056(3)	28(1)
N(21)	3750(4)	924(2)	7433(4)	30(1)
N(22)	2850(4)	1396(2)	8369(3)	27(1)
N(31)	1978(5)	1368(2)	5886(3)	36(2)
N(32)	1240(4)	898(2)	6911(3)	30(1)
N(4)	5378(7)	1532(4)	5431(5)	78(3)
N(5)	6336(8)	2008(3)	9624(6)	77(3)
N(6)	7240(10)	364(4)	3764(7)	95(3)
O(41)	5760(7)	1339(4)	6079(5)	127(3)
O(42)	5032(9)	1956(4)	5297(7)	137(4)
O(51)	7250(8)	2197(3)	9934(8)	141(4)
O(52)	5997(9)	1799(5)	8979(5)	148(4)
O(61)	8120(9)	203(4)	3901(7)	163(5)
O(62)	6728(12)	319(5)	4218(7)	168(5)
C(1)	-968(6)	2183(3)	8818(4)	46(2)
C(2)	-562(7)	1842(3)	9564(5)	49(2)
C(3)	167(7)	933(3)	9724(5)	50(2)
C(4)	-882(6)	689(3)	9113(5)	51(2)
C(5)	-1913(6)	997(3)	7708(5)	49(2)
C(6)	-2188(6)	1519(3)	7956(5)	48(2)
C(11)	4526(6)	2094(3)	7221(5)	45(2)
C(12)	5095(7)	2548(4)	7210(5)	56(2)
C(13)	4580(7)	2999(3)	7203(5)	57(2)
C(14)	3495(7)	3005(3)	7192(5)	52(2)
C(15)	2950(6)	2547(3)	7191(4)	34(2)
C(16)	1781(6)	2512(3)	7181(4)	32(2)
C(17)	1179(7)	2918(3)	7322(5)	49(2)
C(18)	137(7)	2841(3)	7377(5)	49(2)
C(19)	-327(6)	2351(3)	7254(4)	35(2)
C(110)	294(5)	1970(3)	7081(4)	30(2)
C(111)	-1430(6)	2214(3)	7350(5)	44(2)
C(21)	4239(6)	719(3)	6936(5)	38(2)
C(22)	5135(6)	387(3)	7203(6)	47(2)
C(23)	5550(7)	253(3)	8012(6)	53(2)
C(24)	5070(6)	450(3)	8531(5)	43(2)
C(25)	4162(6)	787(3)	8231(4)	33(2)
C(26)	3590(6)	1017(3)	8740(4)	33(2)
C(27)	3734(6)	866(3)	9527(4)	39(2)
C(28)	3069(6)	1069(3)	9912(4)	41(2)
C(29)	2292(6)	1450(3)	9535(4)	32(2)
C(210)	2255(5)	1609(3)	8782(4)	32(2)
C(211)	1470(6)	1684(3)	9875(4)	39(2)
C(31)	2421(7)	1616(3)	5398(5)	45(2)
C(32)	2069(8)	1523(4)	4580(5)	65(3)
C(33)	1220(9)	1173(4)	4235(5)	68(3)
C(34)	751(7)	923(3)	4725(5)	52(2)
C(35)	1142(6)	1030(3)	5550(4)	35(2)

C(36)	669(6)	787(3)	6111(5)	38(2)
C(37)	-304(6)	497(3)	5886(5)	47(2)
C(38)	-727(6)	318(3)	6467(5)	49(2)
C(39)	-144(6)	423(3)	7269(5)	39(2)
C(310)	846(6)	701(3)	7463(4)	32(2)
C(311)	-554(6)	297(3)	7952(5)	44(2)
C(41)	5250(10)	1210(5)	4728(7)	121(5)
C(51)	5612(8)	2008(4)	10095(6)	79(3)
C(61)	6809(22)	642(6)	3009(11)	125(10)
C(61')	6512(28)	667(16)	3178(17)	121(26)

Table A.3. Selected bond lengths [Å] and angles [deg] for $[Ru(L^1H)](PF_6)_3.(CH_3NO_2)_3$

Ru(1)-N(32)	2.035(6)
Ru(1)-N(21)	2.038(5)
Ru(1)-N(11)	2.039(6)
Ru(1)-N(22)	2.039(6)
Ru(1)-N(31)	2.048(6)
Ru(1)-N(12)	2.050(5)
N(32)-Ru(1)-N(21)	93.5(2)
N(32)-Ru(1)-N(11)	169.4(2)
N(21)-Ru(1)-N(11)	96.0(2)
N(32)-Ru(1)-N(22)	92.0(2)
N(21)-Ru(1)-N(22)	79.0(2)
N(11)-Ru(1)-N(22)	94.4(2)
N(32)-Ru(1)-N(31)	78.6(2)
N(21)-Ru(1)-N(31)	96.7(2)
N(11)-Ru(1)-N(31)	95.6(2)
N(22)-Ru(1)-N(31)	169.5(2)
N(32)-Ru(1)-N(12)	92.6(2)
N(21)-Ru(1)-N(12)	168.7(2)
N(11)-Ru(1)-N(12)	78.8(2)
N(22)-Ru(1)-N(12)	91.3(2)
N(31)-Ru(1)-N(12)	93.9(2)

Table A.4. Bond lengths [Å] and angles [deg] for $[Ru(L^1H)](PF_6)_3.(CH_3NO_2)_3$

Ru(1)-N(32)	2.035(6)
Ru(1)-N(21)	2.038(5)
Ru(1)-N(11)	2.039(6)
Ru(1)-N(22)	2.039(6)
Ru(1)-N(31)	2.048(6)
Ru(1)-N(12)	2.050(5)
P(1)-F(15')	1.49(2)
P(1)-F(13')	1.49(2)
P(1)-F(14')	1.50(2)
P(1)-F(16)	1.535(7)
P(1)-F(15)	1.547(6)
P(1)-F(16')	1.56(2)
P(1)-F(12)	1.558(5)
P(1)-F(14)	1.565(7)
P(1)-F(13)	1.568(7)
P(1)-F(11)	1.570(5)
P(2)-F(22)	1.545(6)
P(2)-F(25)	1.547(6)
P(2)-F(26)	1.571(6)
P(2)-F(21)	1.574(5)
P(2)-F(24)	1.578(5)
P(2)-F(23)	1.579(5)
P(3)-F(32)	1.505(7)
P(3)-F(33)	1.531(6)
P(3)-F(36)	1.548(6)
P(3)-F(35)	1.553(6)
P(3)-F(34)	1.569(6)
P(3)-F(31)	1.580(6)
N(1)-C(1)	1.436(9)
N(1)-C(111)	1.462(9)
N(1)-C(6)	1.478(9)
N(2)-C(3)	1.482(9)
N(2)-C(211)	1.501(9)
N(2)-C(2)	1.502(9)
N(3)-C(4)	1.459(9)
N(3)-C(311)	1.463(9)
N(3)-C(5)	1.470(9)
N(11)-C(11)	1.338(9)
N(11)-C(15)	1.346(8)
N(12)-C(16)	1.332(8)
N(12)-C(110)	1.339(8)
N(21)-C(21)	1.337(8)
N(21)-C(25)	1.349(9)
N(22)-C(210)	1.328(8)
N(22)-C(26)	1.348(8)
N(31)-C(31)	1.333(9)
N(31)-C(35)	1.334(9)

N(32)-C(310)	1.329(8)
N(32)-C(36)	1.354(9)
N(4)-O(41)	1.169(9)
N(4)-O(42)	1.173(10)
N(4)-C(41)	1.442(12)
N(5)-O(52)	1.182(10)
N(5)-O(51)	1.190(10)
N(5)-C(51)	1.426(11)
N(6)-O(61)	1.128(12)
N(6)-O(62)	1.189(13)
N(6)-C(61')	1.35(2)
N(6)-C(61)	1.43(2)
C(1)-C(2)	1.502(10)
C(3)-C(4)	1.510(11)
C(5)-C(6)	1.494(10)
C(11)-C(12)	1.379(10)
C(12)-C(13)	1.329(11)
C(13)-C(14)	1.360(11)
C(14)-C(15)	1.368(10)
C(15)-C(16)	1.469(10)
C(16)-C(17)	1.367(10)
C(17)-C(18)	1.363(11)
C(18)-C(19)	1.377(10)
C(19)-C(110)	1.355(9)
C(19)-C(111)	1.501(10)
C(21)-C(22)	1.362(10)
C(22)-C(23)	1.362(11)
C(23)-C(24)	1.352(10)
C(24)-C(25)	1.384(9)
C(25)-C(26)	1.451(9)
C(26)-C(27)	1.374(10)
C(27)-C(28)	1.350(10)
C(28)-C(29)	1.379(10)
C(29)-C(210)	1.358(9)
C(29)-C(211)	1.490(9)
C(31)-C(32)	1.356(11)
C(32)-C(33)	1.366(13)
C(33)-C(34)	1.359(12)
C(34)-C(35)	1.373(10)
C(35)-C(36)	1.453(10)
C(36)-C(37)	1.370(10)
C(37)-C(38)	1.380(11)
C(38)-C(39)	1.357(10)
C(39)-C(310)	1.374(9)
C(39)-C(311)	1.489(10)

N(32)-Ru(1)-N(21)	93.5(2)
N(32)-Ru(1)-N(11)	169.4(2)
N(21)-Ru(1)-N(11)	96.0(2)
N(32)-Ru(1)-N(22)	92.0(2)
N(21)-Ru(1)-N(22)	79.0(2)

N(11)-Ru(1)-N(22)	94.4(2)
N(32)-Ru(1)-N(31)	78.6(2)
N(21)-Ru(1)-N(31)	96.7(2)
N(11)-Ru(1)-N(31)	95.6(2)
N(22)-Ru(1)-N(31)	169.5(2)
N(32)-Ru(1)-N(12)	92.6(2)
N(21)-Ru(1)-N(12)	168.7(2)
N(11)-Ru(1)-N(12)	78.8(2)
N(22)-Ru(1)-N(12)	91.3(2)
N(31)-Ru(1)-N(12)	93.9(2)
F(15')-P(1)-F(13')	91(2)
F(15')-P(1)-F(14')	176(2)
F(13')-P(1)-F(14')	93(2)
F(16)-P(1)-F(15)	93.3(7)
F(15')-P(1)-F(16')	90(2)
F(13')-P(1)-F(16')	178(2)
F(14')-P(1)-F(16')	86(2)
F(15')-P(1)-F(12)	85.0(10)
F(13')-P(1)-F(12)	80.4(11)
F(14')-P(1)-F(12)	95.4(10)
F(16)-P(1)-F(12)	85.6(4)
F(15)-P(1)-F(12)	90.7(4)
F(16')-P(1)-F(12)	100.5(11)
F(16)-P(1)-F(14)	90.8(7)
F(15)-P(1)-F(14)	175.9(6)
F(12)-P(1)-F(14)	90.2(4)
F(16)-P(1)-F(13)	178.9(7)
F(15)-P(1)-F(13)	87.8(5)
F(12)-P(1)-F(13)	94.2(4)
F(14)-P(1)-F(13)	88.1(6)
F(15')-P(1)-F(11)	96.5(10)
F(13')-P(1)-F(11)	99.8(11)
F(14')-P(1)-F(11)	83.2(9)
F(16)-P(1)-F(11)	93.2(4)
F(15)-P(1)-F(11)	90.3(4)
F(16')-P(1)-F(11)	79.3(10)
F(12)-P(1)-F(11)	178.5(3)
F(14)-P(1)-F(11)	88.9(4)
F(13)-P(1)-F(11)	86.9(4)
F(22)-P(2)-F(25)	92.6(4)
F(22)-P(2)-F(26)	89.3(4)
F(25)-P(2)-F(26)	178.0(4)
F(22)-P(2)-F(21)	91.0(3)
F(25)-P(2)-F(21)	90.4(3)
F(26)-P(2)-F(21)	90.1(3)
F(22)-P(2)-F(24)	177.4(4)
F(25)-P(2)-F(24)	89.7(4)
F(26)-P(2)-F(24)	88.4(3)
F(21)-P(2)-F(24)	87.7(3)
F(22)-P(2)-F(23)	90.8(4)
F(25)-P(2)-F(23)	90.9(3)

F(26)-P(2)-F(23)	88.5(3)
F(21)-P(2)-F(23)	177.7(4)
F(24)-P(2)-F(23)	90.4(3)
F(32)-P(3)-F(33)	92.3(5)
F(32)-P(3)-F(36)	92.3(5)
F(33)-P(3)-F(36)	88.4(4)
F(32)-P(3)-F(35)	91.3(5)
F(33)-P(3)-F(35)	90.1(4)
F(36)-P(3)-F(35)	176.1(4)
F(32)-P(3)-F(34)	176.2(5)
F(33)-P(3)-F(34)	91.4(4)
F(36)-P(3)-F(34)	87.0(4)
F(35)-P(3)-F(34)	89.4(4)
F(32)-P(3)-F(31)	90.5(4)
F(33)-P(3)-F(31)	177.2(4)
F(36)-P(3)-F(31)	91.6(4)
F(35)-P(3)-F(31)	89.7(3)
F(34)-P(3)-F(31)	85.8(4)
C(1)-N(1)-C(111)	112.9(6)
C(1)-N(1)-C(6)	113.3(6)
C(111)-N(1)-C(6)	112.2(6)
C(3)-N(2)-C(211)	113.4(6)
C(3)-N(2)-C(2)	113.8(6)
C(211)-N(2)-C(2)	109.7(6)
C(4)-N(3)-C(311)	112.1(6)
C(4)-N(3)-C(5)	114.4(6)
C(311)-N(3)-C(5)	111.3(6)
C(11)-N(11)-C(15)	117.0(6)
C(11)-N(11)-Ru(1)	127.3(5)
C(15)-N(11)-Ru(1)	115.6(5)
C(16)-N(12)-C(110)	118.5(6)
C(16)-N(12)-Ru(1)	115.2(4)
C(110)-N(12)-Ru(1)	124.4(5)
C(21)-N(21)-C(25)	117.8(6)
C(21)-N(21)-Ru(1)	127.1(5)
C(25)-N(21)-Ru(1)	115.0(4)
C(210)-N(22)-C(26)	118.0(6)
C(210)-N(22)-Ru(1)	125.0(5)
C(26)-N(22)-Ru(1)	115.0(4)
C(31)-N(31)-C(35)	118.5(6)
C(31)-N(31)-Ru(1)	126.1(5)
C(35)-N(31)-Ru(1)	115.4(5)
C(310)-N(32)-C(36)	117.7(6)
C(310)-N(32)-Ru(1)	125.6(5)
C(36)-N(32)-Ru(1)	115.8(5)
O(41)-N(4)-O(42)	126.0(12)
O(41)-N(4)-C(41)	117.4(11)
O(42)-N(4)-C(41)	116.5(10)
O(52)-N(5)-O(51)	125.9(11)
O(52)-N(5)-C(51)	117.1(10)
O(51)-N(5)-C(51)	116.9(10)

O(61)-N(6)-O(62)	123(2)
O(61)-N(6)-C(61')	137(2)
O(62)-N(6)-C(61')	100(2)
O(61)-N(6)-C(61)	114(2)
O(62)-N(6)-C(61)	123(2)
N(1)-C(1)-C(2)	111.9(7)
C(1)-C(2)-N(2)	108.5(6)
N(2)-C(3)-C(4)	109.7(6)
N(3)-C(4)-C(3)	109.0(6)
N(3)-C(5)-C(6)	114.0(6)
N(1)-C(6)-C(5)	111.5(6)
N(11)-C(11)-C(12)	122.5(7)
C(13)-C(12)-C(11)	119.3(8)
C(12)-C(13)-C(14)	119.7(8)
C(13)-C(14)-C(15)	119.3(8)
N(11)-C(15)-C(14)	122.1(7)
N(11)-C(15)-C(16)	114.4(6)
C(14)-C(15)-C(16)	123.6(7)
N(12)-C(16)-C(17)	120.3(7)
N(12)-C(16)-C(15)	115.0(6)
C(17)-C(16)-C(15)	124.7(7)
C(18)-C(17)-C(16)	120.7(7)
C(17)-C(18)-C(19)	119.3(7)
C(110)-C(19)-C(18)	117.1(7)
C(110)-C(19)-C(111)	118.8(7)
C(18)-C(19)-C(111)	124.0(7)
N(12)-C(110)-C(19)	124.1(7)
N(1)-C(111)-C(19)	111.3(6)
N(21)-C(21)-C(22)	122.9(7)
C(23)-C(22)-C(21)	118.8(7)
C(24)-C(23)-C(22)	119.9(7)
C(23)-C(24)-C(25)	119.3(8)
N(21)-C(25)-C(24)	121.3(7)
N(21)-C(25)-C(26)	115.3(6)
C(24)-C(25)-C(26)	123.3(7)
N(22)-C(26)-C(27)	120.5(6)
N(22)-C(26)-C(25)	114.4(6)
C(27)-C(26)-C(25)	125.0(7)
C(28)-C(27)-C(26)	120.0(7)
C(27)-C(28)-C(29)	120.0(7)
C(210)-C(29)-C(28)	116.9(7)
C(210)-C(29)-C(211)	118.0(7)
C(28)-C(29)-C(211)	125.1(6)
N(22)-C(210)-C(29)	124.3(7)
C(29)-C(211)-N(2)	111.6(6)
N(31)-C(31)-C(32)	122.0(8)
C(31)-C(32)-C(33)	119.7(8)
C(34)-C(33)-C(32)	118.8(8)
C(33)-C(34)-C(35)	119.2(8)
N(31)-C(35)-C(34)	121.8(7)
N(31)-C(35)-C(36)	115.7(6)

C(34)-C(35)-C(36)	122.5(7)
N(32)-C(36)-C(37)	120.5(7)
N(32)-C(36)-C(35)	113.9(6)
C(37)-C(36)-C(35)	125.5(7)
C(36)-C(37)-C(38)	120.7(7)
C(39)-C(38)-C(37)	118.7(7)
C(38)-C(39)-C(310)	118.1(7)
C(38)-C(39)-C(311)	124.3(7)
C(310)-C(39)-C(311)	117.3(7)
N(32)-C(310)-C(39)	124.1(7)
N(3)-C(311)-C(39)	110.8(6)

$[Cu(L^1H)](ClO_4)_3$.– Synthesis and characterisation discussed in Chapter 2.

Table A.5. Crystal data and structure refinement for $[Cu(L^1H)](ClO_4)_3.0.5H_2O$

Identification code	cupipab
Empirical formula	$C_{39}H_{41}Cl_3CuN_9O_{12.50}$
Formula weight	1005.71
Temperature	230(2) K
Wavelength	0.71073 Å
Crystal system	Monoclinic
Space group	P2(1)/n
Unit cell dimensions	a = 20.135(8) Å $\alpha = 90°$
	b = 14.907(6) Å $\beta = 102.86(3)°$
	c = 28.722(9) Å $\gamma = 90°$
Volume	8405(6) $Å^3$
Z	8
Density (calculated)	1.588 Mg/m^3
Absorption coefficient	0.787 mm^{-1}
F(000)	4136
Crystal size	0.32 x 0.31 x 0.20 mm
Θ range for data collection	2.07 to 22.56°
Index ranges	$0 \le h \le 21$, $0 \le k \le 16$, $-30 \le l \le 30$
Reflections collected	11304
Independent reflections	10940 [R(int) = 0.0802]
Absorption correction	Gaussian
Max. and min. transmission	0.859 and 0.819
Refinement method	Full-matrix least-squares on F^2
Data / restraints / parameters	10904 / 268 / 1180
Goodness-of-fit on F^2	1.044

Final R indices [I>2sigma(I)]	R1 = 0.0963, wR2 = 0.2438
R indices (all data)	R1 = 0.1955, wR2 = 0.3524
Largest diff. peak and hole	0.817 and -0.603 e.A^{-3}

Table A.6. Atomic coordinates (x 10^4) and equivalent isotropic displacement parameters ($Å^2$ x 10^3) for $[Cu(L^1H)](ClO_4)_3.0.5H_2O$. U(eq) is defined as one third of the trace of the orthogonalized Uij tensor.

	x	y	z	U(eq)
Cu(1)	9693(1)	8045(1)	1274(1)	48(1)
Cu(2)	3312(1)	4503(1)	770(1)	49(1)
Cl(1)	9351(2)	4206(3)	526(2)	71(1)
Cl(2)	3693(3)	9070(4))	2294(2)	98(2)
Cl(3)	5953(2)	8493(3)	996(2)	71(1)
Cl(4)	2876(2)	8533(3)	-39(2)	62(1)
Cl(5)	1860(2)	1192(3)	1510(2)	63(1)
Cl(6)	6830(7)	4000(9)	1903(4)	83(4)
Cl(6')	6896(8)	3597(11)	1984(5)	110(6)
N(11)	9257(6)	11890(8)	1465(4)	55(3)
N(12)	9496(7)	11154(8)	2374(4)	64(4)
N(13)	8177(7)	10958(9)	1700(4)	64(4)
N(21)	5249(6)	1906(8)	683(4)	56(3)
N(22)	4152(6)	835(7)	805(4)	51(3)
N(23)	4942(6)	1510(8)	1627(4)	54(3)
N(31)	9267(5)	7775(7)	576(4)	42(3)
N(32)	9760(5)	9390(8)	855(4)	46(3)
N(41)	10653(6)	7816(7)	1197(4)	54(3)
N(42)	10209(6)	8715(7)	1855(4)	51(3)
N(51)	9429(6)	6779(7)	1616(4)	51(3)
N(52)	8772(5)	8318(8)	1415(4)	47(3)
N(61)	2492(6)	4578(7)	1040(5)	53(3)
N(62)	3634(6)	3824(7)	1465(4)	50(3)
N(71)	3732(6)	5747(8)	999(5)	59(3)
N(72)	4256(6)	4388(8)	621(4)	52(3)
N(81)	2838(6)	4833(9)	33(5)	62(4)
N(82)	2971(5)	3210(8)	433(4)	47(3)
O(11)	9694(9)	3546(10)	346(6)	168(7)
O(12)	9306(10)	3966(9)	977(5)	177(9)
O(13)	9789(7)	4977(10)	589(8))	191(9)
O(14)	8785(7)	4467(14)	229(6)	204(10)
O(21)	3583(12)	9154(11)	1809(5)	223(11)

O(22)	3708(7)	9922(9)	2495(5)	119(5)
O(23)	4257(8)	8670(11)	2482(10)	320(18)
O(24)	3115(8)	8627(13)	2346(6)	195(8)
O(31)	6406(5)	9149(7)	879(4)	85(3)
O(32)	5293(5)	8597(7)	699(4)	80(3)
O(33)	6199(7)	7642(8)	939(7)	176(9)
O(34)	5879(6)	8624(13)	1467(4)	152(7)
O(41)	2427(6)	9237(9)	-102(6)	152(7)
O(42)	3423(7)	8684(10)	318(6)	167(8)
O(43)	2527(10)	7789(10)	81(7)	191(8)
O(44)	3036(8)	8316(15)	-462(5)	205(10)
O(51)	2187(6)	1739(9)	1231(4)	105(4)
O(52)	1470(7)	514(9)	1231(5)	124(5)
O(53)	2337(7)	842(10)	1877(5)	162(7)
O(54)	1397(7)	1716(10)	1686(6)	149(6)
O(61)	6822(8)	3541(9)	1495(4)	132(5)
O(62)	6335(6)	3815(9)	2152(5)	112(4)
O(63)	7451(7)	4091(13)	2196(5)	170(7)
O(64)	6674(15)	4912(13)	1736(9)	174(12)
O(64')	7031(15)	2696(14)	2137(9)	168(12)
O(71)	2326(23)	6118(32)	2027(14)	233(23)
O(72)	2791(40)	6828(56)	2125(25)	186(42)
C(11)	9536(10)	12490(11)	852(6)	81(5)
C(12)	9917(9)	11916(10)	2289(6)	74(5)
C(13)	8846(9)	11393(11)	2514(6)	70(5)
C(14)	8252(9)	10882(12)	2229(6)	75(5)
C(15)	8049(8)	11896(10)	1523(7)	75(5)
C(16)	8553(7)	12130(11)	1210(6)	64(4)
C(21)	5173(8)	972(11)	481(6)	66(5)
C(22)	4432(8)	681(10)	380(5)	61(4)
C(23)	4425(9)	182(11)	1207(6)	74(5)
C(24)	4569(9)	682(10)	1673(5)	69(5)
C(25)	5625(8)	1398(11)	1534(5)	66(4)
C(26)	5753(8)	1970(11)	1136(6)	66(4)
C(31)	9116(6)	6930(10)	425(5)	49(4)
C(32)	8888(7)	6668(11)	-39(6)	60(4)
C(33)	8806(8)	7366(13)	-372(6)	69(5)
C(34)	8952(7)	8218(12)	-228(5)	61(4)
C(35)	9177(6)	8404(9)	242(5)	43(3)
C(36)	9344(6)	9328(10)	417(5)	49(4)
C(37)	9079(7)	10085(10)	156(5)	58(4)
C(38)	9217(8)	10924(11)	372(6)	63(4)
C(39)	9614(7)	10976(10)	839(5)	51(4)
C(310)	9877(7)	10200(9)	1057(5)	49(4)
C(311)	9738(7)	7365(10)	830(5)	56(4)
C(42)	11477(10)	7440(12)	748(7)	79(6)
C(43)	11940(8)	7963(13)	1070(9)	87(7)
C(44)	11764(8)	8384(12)	1428(7)	66(5)
C(45)	11132(7)	8318(10)	1475(5)	51(4)
C(46)	10885(7)	8806(9)	1851(5)	50(4)
C(47)	11276(8)	9430(10)	2162(6)	63(4)

C(48)	10971(9)	9939(10)	2448(5)	61(4)
C(49)	10286(8)	9876(10)	2436(5)	58(4)
C(410)	9929(8)	9220(9)	2147(5)	48(4)
C(411)	9899(8)	10477(10)	2696(5)	60(4)
C(51)	9806(8)	6043(9)	1710(5)	57(4)
C(52)	9591(10)	5291(11)	1932(5)	72(5)
C(53)	8975(11)	5352(11)	2059(6)	80(6)
C(54)	8587(9)	6102(11)	1972(5)	68(5)
C(55)	8836(8)	6836(9)	1745(5)	50(4)
C(56)	8473(7)	7683(10)	1647(4)	46(4)
C(57)	7880(7)	7924(12)	1788(5)	62(4)
C(58)	7595(7)	8744(11)	1735(5)	53(4)
C(59)	7898(7)	9391(10)	1514(5)	49(4)
C(510)	8484(7)	9138(10)	1348(5)	51(4)
C(511)	7665(8)	10336(11)	1431(6)	69(5)
C(61)	1927(8)	5027(11)	830(6)	63(4)
C(62)	1324(9)	4967(11)	973(7)	72(5)
C(63)	1310(11)	4446(13)	1345(8)	95(7)
C(64)	1887(10)	4006(12)	1567(7)	82(6)
C(65)	2466(8)	4053(10)	1430(6)	53(4)
C(66)	3093(8)	3610(10)	1641(5)	51(4)
C(67)	3139(8)	2920(11)	1987(5)	58(4)
C(68)	3718(9)	2458(11)	2120(6)	66(5)
C(69)	4293(8)	2661(10)	1930(5)	51(4)
C(610)	4231(8)	3358(9)	1624(5)	53(4)
C(611)	4936(8)	2146(11)	2032(5)	62(4)
C(71)	3443(7)	6390(11)	1214(5)	63(4)
C(72)	3772(9)	7186(11)	1358(6)	75(5)
C(73)	4389(9)	7316(10)	1272(7)	74(5)
C(74)	4711(8)	6679(10)	1065(5)	62(4)
C(75)	4359(7)	5875(9)	936(5)	50(4)
C(76)	4690(7)	5095(10)	744(5)	52(4)
C(77)	5339(7)	5006(11)	718(5)	60(4)
C(78)	5591(7)	4222(11)	589(6)	62(4)
C(79)	5164(7)	3511(11)	475(5)	53(4)
C(710)	4487(6)	3622(10)	474(5)	49(4)
C(711)	5376(8)	2566(10)	339(6)	62(4)
C(81)	2776(7)	5650(10)	-146(7)	67(5)
C(82)	2576(7)	5818(11)	-637(8)	73(5)
C(83)	2432(9)	5108(14)	-923(7)	89(6)
C(84)	2483(8)	4247(12)	-752(7)	77(5)
C(85)	2677(7)	4121(11)	-263(6)	42(3)
C(87)	2684(7)	2426(10)	-293(5)	54(4)
C(88)	2848(7)	1646(11)	-81(6)	60(4)
C(89)	3097(6)	1630(9)	414(5)	44(3)
C(810)	3115(7)	2445(11)	647(6)	56(4)
C(811)	3378(8)	824(10)	703(5)	59(4)

Table A.7. Selected bond lengths [Å] and angles [deg] for $[Cu(L^1H)](ClO_4)_3.0.5H_2O$.

Cu(1)-N(41)	2.024(12)
Cu(1)-N(42)	2.024(12)
Cu(1)-N(52)	2.026(11)
Cu(1)-N(31)	2.036(11)
Cu(1)-N(51)	2.246(11)
Cu(1)-N(32)	2.358(11)
Cu(2)-N(61)	1.977(12)
Cu(2)-N(72)	2.047(11)
Cu(2)-N(71)	2.083(12)
Cu(2)-N(81)	2.178(14)
Cu(2)-N(82)	2.197(11)
Cu(2)-N(62)	2.202(12)
N(41)-Cu(1)-N(42)	81.1(5)
N(41)-Cu(1)-N(52)	174.5(5)
N(42)-Cu(1)-N(52)	93.5(5)
N(41)-Cu(1)-N(31)	93.6(5)
N(42)-Cu(1)-N(31)	159.4(4)
N(52)-Cu(1)-N(31)	91.9(4)
N(41)-Cu(1)-N(51)	103.4(4)
N(42)-Cu(1)-N(51)	100.5(4)
N(52)-Cu(1)-N(51)	76.4(5)
N(31)-Cu(1)-N(51)	100.1(4)
N(41)-Cu(1)-N(32)	85.6(4)
N(42)-Cu(1)-N(32)	85.6(4)
N(52)-Cu(1)-N(32)	95.2(4)
N(51)-Cu(1)-N(32)	169.8(4)
N(61)-Cu(2)-N(72)	169.2(5)
N(61)-Cu(2)-N(71)	98.2(5)
N(72)-Cu(2)-N(71)	79.0(5)
N(61)-Cu(2)-N(81)	98.3(5)
N(72)-Cu(2)-N(81)	92.4(4)
N(71)-Cu(2)-N(81)	99.5(5)
N(61)-Cu(2)-N(82)	90.9(4)
N(72)-Cu(2)-N(82)	92.7(4)
N(71)-Cu(2)-N(82)	170.1(5)
N(81)-Cu(2)-N(82)	75.1(5)
N(61)-Cu(2)-N(62)	76.9(5)
N(72)-Cu(2)-N(62)	92.9(5)
N(71)-Cu(2)-N(62)	96.1(4)
N(81)-Cu(2)-N(62)	164.2(4)
N(82)-Cu(2)-N(62)	89.8(4)

Table A.8. Bond lengths [Å] and angles [deg] for $[Cu(L^1H)](ClO_4)_3.0.5H_2O$.

Cu(1)-N(41)	2.024(12)
Cu(1)-N(42)	2.024(12)
Cu(1)-N(52)	2.026(11)
Cu(1)-N(31)	2.036(11)
Cu(1)-N(51)	2.246(11)
Cu(1)-N(32)	2.358(11)
Cu(2)-N(61)	1.977(12)
Cu(2)-N(72)	2.047(11)
Cu(2)-N(71)	2.083(12)
Cu(2)-N(81)	2.178(14)
Cu(2)-N(82)	2.197(11)
Cu(2)-N(62)	2.202(12)
Cl(1)-O(14)	1.322(13)
Cl(1)-O(12)	1.365(13)
Cl(1)-O(11)	1.370(12)
Cl(1)-O(13)	1.436(13)
Cl(2)-O(23)	1.289(13)
Cl(2)-O(21)	1.369(14)
Cl(2)-O(24)	1.375(13)
Cl(2)-O(22)	1.392(13)
Cl(3)-O(33)	1.384(12)
Cl(3)-O(34)	1.408(12)
Cl(3)-O(32)	1.418(10)
Cl(3)-O(31)	1.427(10)
Cl(4)-O(42)	1.345(11)
Cl(4)-O(44)	1.362(13)
Cl(4)-O(41)	1.372(11)
Cl(4)-O(43)	1.396(13)
Cl(5)-O(53)	1.362(11)
Cl(5)-O(54)	1.394(11)
Cl(5)-O(51)	1.405(11)
Cl(5)-O(52)	1.414(11)
Cl(6)-O(63)	1.35(2)
Cl(6)-O(61)	1.35(2)
Cl(6)-O(62)	1.38(2)
Cl(6)-O(64)	1.45(2)
Cl(6')-O(62)	1.36(2)
Cl(6')-O(61)	1.38(2)
Cl(6')-O(64')	1.42(2)
N(11)-C(11)	1.44(2)
N(11)-C(16)	1.49(2)
N(11)-C(311)	1.53(2)
N(12)-C(12)	1.47(2)
N(12)-C(411)	1.48(2)
N(12)-C(13)	1.50(2)
N(13)-C(511)	1.47(2)
N(13)-C(15)	1.49(2)
N(13)-C(14)	1.50(2)

N(21)-C(711)	1.46(2)
N(21)-C(26)	1.46(2)
N(21)-C(21)	1.50(2)
N(22)-C(22)	1.47(2)
N(22)-C(23)	1.52(2)
N(22)-C(811)	1.52(2)
N(23)-C(25)	1.47(2)
N(23)-C(24)	1.47(2)
N(23)-C(611)	1.50(2)
N(31)-C(35)	1.33(2)
N(31)-C(31)	1.34(2)
N(32)-C(310)	1.34(2)
N(32)-C(36)	1.35(2)
N(41)-C(45)	1.34(2)
N(41)-C(41)	1.37(2)
N(42)-C(410)	1.34(2)
N(42)-C(46)	1.37(2)
N(51)-C(51)	1.33(2)
N(51)-C(55)	1.33(2)
N(52)-C(510)	1.35(2)
N(52)-C(56)	1.37(2)
N(61)-C(61)	1.34(2)
N(61)-C(65)	1.38(2)
N(62)-C(66)	1.34(2)
N(62)-C(610)	1.38(2)
N(71)-C(75)	1.33(2)
N(71)-C(71)	1.34(2)
N(72)-C(710)	1.36(2)
N(81)-C(81)	1.32(2)
N(81)-C(85)	1.35(2)
N(82)-C(810)	1.30(2)
N(82)-C(86)	1.33(2)
C(11)-C(12)	1.57(2)
C(13)-C(14)	1.50(2)
C(15)-C(16)	1.54(2)
C(21)-C(22)	1.52(2)
C(23)-C(24)	1.50(2)
C(25)-C(26)	1.50(2)
C(31)-C(32)	1.37(2)
C(32)-C(33)	1.40(2)
C(33)-C(34)	1.35(2)
C(34)-C(35)	1.35(2)
C(35)-C(36)	1.48(2)
C(36)-C(37)	1.39(2)
C(37)-C(38)	1.40(2)
C(38)-C(39)	1.40(2)
C(39)-C(310)	1.36(2)
C(39)-C(311)	1.51(2)
C(41)-C(42)	1.37(2)
C(42)-C(43)	1.40(2)
C(43)-C(44)	1.32(2)

C(44)-C(45)	1.31(2)
C(45)-C(46)	1.48(2)
C(46)-C(47)	1.41(2)
C(47)-C(48)	1.36(2)
C(48)-C(49)	1.37(2)
C(49)-C(410)	1.38(2)
C(49)-C(411)	1.49(2)
C(51)-C(52)	1.40(2)
C(52)-C(53)	1.37(2)
C(53)-C(54)	1.36(2)
C(54)-C(55)	1.42(2)
C(55)-C(56)	1.46(2)
C(56)-C(57)	1.39(2)
C(57)-C(58)	1.34(2)
C(58)-C(59)	1.37(2)
C(59)-C(510)	1.42(2)
C(59)-C(511)	1.49(2)
C(61)-C(62)	1.37(2)
C(62)-C(63)	1.33(2)
C(63)-C(64)	1.36(3)
C(64)-C(65)	1.32(2)
C(65)-C(66)	1.43(2)
C(66)-C(67)	1.42(2)
C(67)-C(68)	1.34(2)
C(68)-C(69)	1.42(2)
C(69)-C(610)	1.35(2)
C(69)-C(611)	1.48(2)
C(71)-C(72)	1.38(2)
C(72)-C(73)	1.33(2)
C(73)-C(74)	1.36(2)
C(74)-C(75)	1.40(2)
C(75)-C(76)	1.50(2)
C(76)-C(77)	1.33(2)
C(77)-C(78)	1.36(2)
C(78)-C(79)	1.36(2)
C(79)-C(710)	1.37(2)
C(79)-C(711)	1.55(2)
C(82)-C(83)	1.33(2)
C(83)-C(84)	1.37(2)
C(84)-C(85)	1.39(2)
C(85)-C(86)	1.47(2)
C(86)-C(87)	1.39(2)
C(87)-C(88)	1.32(2)
C(88)-C(89)	1.40(2)
C(89)-C(810)	1.38(2)
C(89)-C(811)	1.50(2)
N(41)-Cu(1)-N(42)	81.1(5)
N(41)-Cu(1)-N(52)	174.5(5)
N(42)-Cu(1)-N(52)	93.5(5)
N(41)-Cu(1)-N(31)	93.6(5)
N(42)-Cu(1)-N(31)	159.4(4)

N(52)-Cu(1)-N(31)	91.9(4)
N(41)-Cu(1)-N(51)	103.4(4)
N(42)-Cu(1)-N(51)	100.5(4)
N(52)-Cu(1)-N(51)	76.4(5)
N(31)-Cu(1)-N(51)	100.1(4)
N(41)-Cu(1)-N(32)	85.6(4)
N(42)-Cu(1)-N(32)	85.6(4)
N(52)-Cu(1)-N(32)	95.2(4)
N(31)-Cu(1)-N(32)	74.1(4)
N(51)-Cu(1)-N(32)	169.8(4)
N(61)-Cu(2)-N(72)	169.2(5)
N(61)-Cu(2)-N(71)	98.2(5)
N(72)-Cu(2)-N(71)	79.0(5)
N(61)-Cu(2)-N(81)	98.3(5)
N(72)-Cu(2)-N(81)	92.4(4)
N(71)-Cu(2)-N(81)	99.5(5)
N(61)-Cu(2)-N(82)	90.9(4)
N(72)-Cu(2)-N(82)	92.7(4)
N(71)-Cu(2)-N(82)	170.1(5)
N(81)-Cu(2)-N(82)	75.1(5)
N(61)-Cu(2)-N(62)	76.9(5)
N(72)-Cu(2)-N(62)	92.9(5)
N(71)-Cu(2)-N(62)	96.1(4)
N(81)-Cu(2)-N(62)	164.2(4)
N(82)-Cu(2)-N(62)	89.8(4)
O(14)-Cl(1)-O(12)	117.4(11)
O(14)-Cl(1)-O(11)	113.8(11)
O(12)-Cl(1)-O(11)	108.4(9)
O(14)-Cl(1)-O(13)	105.2(10)
O(12)-Cl(1)-O(13)	105.0(10)
O(11)-Cl(1)-O(13)	105.9(10)
O(23)-Cl(2)-O(21)	113.4(13)
O(23)-Cl(2)-O(24)	114.9(13)
O(21)-Cl(2)-O(24)	101.9(10)
O(23)-Cl(2)-O(22)	108.2(10)
O(21)-Cl(2)-O(22)	108.8(9)
O(24)-Cl(2)-O(22)	109.5(10)
O(33)-Cl(3)-O(32)	109.9(9)
O(34)-Cl(3)-O(32)	106.0(7)
O(33)-Cl(3)-O(31)	109.7(7)
O(34)-Cl(3)-O(31)	110.0(8)
O(32)-Cl(3)-O(31)	110.3(7)
O(42)-Cl(4)-O(44)	113.8(10)
O(42)-Cl(4)-O(41)	112.1(8)
O(44)-Cl(4)-O(41)	110.1(10)
O(42)-Cl(4)-O(43)	108.5(11)
O(44)-Cl(4)-O(43)	105.2(11)
O(41)-Cl(4)-O(43)	106.7(9)
O(53)-Cl(5)-O(54)	110.2(10)
O(53)-Cl(5)-O(51)	109.0(8)
O(54)-Cl(5)-O(51)	108.5(9)

O(53)-Cl(5)-O(52)	111.8(8)
O(54)-Cl(5)-O(52)	105.9(8)
O(51)-Cl(5)-O(52)	111.3(8)
O(63)-Cl(6)-O(61)	114.9(12)
O(63)-Cl(6)-O(62)	111.9(11)
O(61)-Cl(6)-O(62)	118.5(12)
O(63)-Cl(6)-O(64)	102.4(14)
O(61)-Cl(6)-O(64)	103.2(13)
O(62)-Cl(6)-O(64)	103.4(13)
O(62)-Cl(6')-O(63)	112.0(13)
O(62)-Cl(6')-O(61)	117.6(13)
O(63)-Cl(6')-O(61)	112.3(13)
O(62)-Cl(6')-O(64')	103.5(14)
O(63)-Cl(6')-O(64')	106.9(14)
O(61)-Cl(6')-O(64')	103.1(14)
C(11)-N(11)-C(16)	113.3(13)
C(11)-N(11)-C(311)	109.5(12)
C(16)-N(11)-C(311)	111.3(11)
C(12)-N(12)-C(411)	112.0(12)
C(12)-N(12)-C(13)	115.5(13)
C(411)-N(12)-C(13)	112.5(12)
C(511)-N(13)-C(15)	111.4(12)
C(511)-N(13)-C(14)	112.8(13)
C(15)-N(13)-C(14)	112.9(13)
C(711)-N(21)-C(26)	111.5(12)
C(711)-N(21)-C(21)	112.5(12)
C(26)-N(21)-C(21)	113.3(12)
C(22)-N(22)-C(23)	112.9(11)
C(22)-N(22)-C(811)	113.8(11)
C(23)-N(22)-C(811)	108.8(12)
C(25)-N(23)-C(24)	116.1(12)
C(25)-N(23)-C(611)	112.5(12)
C(24)-N(23)-C(611)	111.6(11)
C(35)-N(31)-C(31)	116.3(12)
C(35)-N(31)-Cu(1)	122.2(9)
C(31)-N(31)-Cu(1)	121.3(9)
C(310)-N(32)-C(36)	118.6(12)
C(310)-N(32)-Cu(1)	124.9(9)
C(36)-N(32)-Cu(1)	108.8(9)
C(45)-N(41)-C(41)	117.1(13)
C(45)-N(41)-Cu(1)	114.9(11)
C(41)-N(41)-Cu(1)	126.4(10)
C(410)-N(42)-C(46)	120.5(12)
C(410)-N(42)-Cu(1)	125.7(10)
C(46)-N(42)-Cu(1)	111.7(10)
C(51)-N(51)-C(55)	120.3(13)
C(51)-N(51)-Cu(1)	127.1(11)
C(55)-N(51)-Cu(1)	112.5(9)
C(510)-N(52)-C(56)	118.4(12)
C(510)-N(52)-Cu(1)	122.5(9)
C(56)-N(52)-Cu(1)	118.6(9)

C(61)-N(61)-C(65)	117.8(13)
C(61)-N(61)-Cu(2)	123.4(11)
C(65)-N(61)-Cu(2)	118.2(10)
C(66)-N(62)-C(610)	118.6(13)
C(66)-N(62)-Cu(2)	110.7(9)
C(610)-N(62)-Cu(2)	126.3(10)
C(75)-N(71)-C(71)	118.9(13)
C(75)-N(71)-Cu(2)	114.6(10)
C(71)-N(71)-Cu(2)	126.4(10)
C(710)-N(72)-C(76)	119.7(12)
C(710)-N(72)-Cu(2)	122.9(9)
C(76)-N(72)-Cu(2)	116.8(10)
C(81)-N(81)-C(85)	120(2)
C(81)-N(81)-Cu(2)	124.8(12)
C(85)-N(81)-Cu(2)	115.1(11)
C(810)-N(82)-C(86)	119.1(12)
C(810)-N(82)-Cu(2)	123.2(10)
C(86)-N(82)-Cu(2)	115.0(9)
N(11)-C(11)-C(12)	108.4(12)
N(12)-C(12)-C(11)	110.9(13)
N(12)-C(13)-C(14)	111.8(13)
N(13)-C(14)-C(13)	113.8(14)
N(13)-C(15)-C(16)	109.1(13)
N(11)-C(16)-C(15)	109.8(12)
N(21)-C(21)-C(22)	110.5(11)
N(22)-C(22)-C(21)	109.8(12)
C(24)-C(23)-N(22)	109.0(12)
N(23)-C(24)-C(23)	113.8(12)
N(21)-C(26)-C(25)	116.0(13)
N(31)-C(31)-C(32)	125.9(14)
C(31)-C(32)-C(33)	115(2)
C(34)-C(33)-C(32)	120(2)
C(33)-C(34)-C(35)	120(2)
N(31)-C(35)-C(34)	122.6(14)
N(31)-C(35)-C(36)	115.3(12)
C(34)-C(35)-C(36)	122.1(14)
N(32)-C(36)-C(37)	122.0(14)
N(32)-C(36)-C(35)	115.4(12)
C(37)-C(36)-C(35)	122.6(13)
C(36)-C(37)-C(38)	118.1(14)
C(37)-C(38)-C(39)	119.3(14)
C(310)-C(39)-C(38)	118.1(14)
C(310)-C(39)-C(311)	118.6(13)
C(38)-C(39)-C(311)	123.2(13)
N(32)-C(310)-C(39)	123.7(13)
C(39)-C(311)-N(11)	109.4(12)
N(41)-C(41)-C(42)	121(2)
C(41)-C(42)-C(43)	117(2)
C(44)-C(43)-C(42)	122(2)
C(45)-C(44)-C(43)	119(2)
C(44)-C(45)-N(41)	124(2)

C(44)-C(45)-C(46)	122(2)
N(41)-C(45)-C(46)	113.4(13)
N(42)-C(46)-C(47)	118(2)
N(42)-C(46)-C(45)	117.1(13)
C(47)-C(46)-C(45)	123.9(14)
C(48)-C(47)-C(46)	119(2)
C(47)-C(48)-C(49)	122.1(14)
C(48)-C(49)-C(410)	117(2)
C(48)-C(49)-C(411)	125.4(14)
C(410)-C(49)-C(411)	118(2)
N(42)-C(410)-C(49)	123(2)
N(12)-C(411)-C(49)	111.6(12)
N(51)-C(51)-C(52)	122(2)
C(53)-C(52)-C(51)	117(2)
C(54)-C(53)-C(52)	122(2)
C(53)-C(54)-C(55)	120.7(14)
N(51)-C(55)-C(56)	116.4(13)
C(54)-C(55)-C(56)	123(2)
N(52)-C(56)-C(57)	117.4(14)
N(52)-C(56)-C(55)	116.0(13)
C(57)-C(56)-C(55)	126.5(14)
C(58)-C(57)-C(56)	125(2)
C(57)-C(58)-C(59)	118.0(14)
C(58)-C(59)-C(510)	117.2(14)
C(58)-C(59)-C(511)	125.8(14)
C(510)-C(59)-C(511)	117.0(14)
N(52)-C(510)-C(59)	123.8(13)
N(13)-C(511)-C(59)	110.7(13)
N(61)-C(61)-C(62)	124(2)
C(63)-C(62)-C(61)	117(2)
C(62)-C(63)-C(64)	120(2)
C(65)-C(64)-C(63)	124(2)
C(64)-C(65)-N(61)	118(2)
C(64)-C(65)-C(66)	127(2)
N(61)-C(65)-C(66)	114.7(14)
N(62)-C(66)-C(67)	120.5(14)
N(62)-C(66)-C(65)	116.3(14)
C(67)-C(66)-C(65)	123(2)
C(68)-C(67)-C(66)	119(2)
C(67)-C(68)-C(69)	117(2)
C(610)-C(69)-C(611)	119(2)
C(68)-C(69)-C(611)	124(2)
C(69)-C(610)-N(62)	123.4(14)
C(69)-C(611)-N(23)	109.5(11)
N(71)-C(71)-C(72)	122(2)
C(73)-C(72)-C(71)	118(2)
C(72)-C(73)-C(74)	122(2)
C(73)-C(74)-C(75)	117(2)
N(71)-C(75)-C(74)	121.9(14)
N(71)-C(75)-C(76)	116.7(12)
C(74)-C(75)-C(76)	121.3(13)

C(77)-C(76)-N(72)	119.1(14)
N(72)-C(76)-C(75)	112.5(12)
C(76)-C(77)-C(78)	122(2)
C(79)-C(78)-C(77)	118.9(14)
C(78)-C(79)-C(710)	119(2)
C(78)-C(79)-C(711)	125.3(13)
C(710)-C(79)-C(711)	116.0(14)
N(72)-C(710)-C(79)	121.2(14)
N(21)-C(711)-C(79)	110.3(12)
N(81)-C(81)-C(82)	122(2)
C(83)-C(82)-C(81)	117(2)
C(82)-C(83)-C(84)	122(2)
C(83)-C(84)-C(85)	118(2)
N(81)-C(85)-C(84)	120(2)
N(81)-C(85)-C(86)	116.7(14)
C(84)-C(85)-C(86)	123(2)
N(82)-C(86)-C(87)	119.1(13)
N(82)-C(86)-C(85)	116.3(12)
C(87)-C(86)-C(85)	124.5(13)
C(88)-C(87)-C(86)	121.9(14)
C(87)-C(88)-C(89)	118.7(14)
C(810)-C(89)-C(88)	116.2(13)
C(810)-C(89)-C(811)	118.0(12)
C(88)-C(89)-C(811)	125.6(13)
N(82)-C(810)-C(89)	124.4(14)
C(89)-C(811)-N(22)	110.0(11)

$[CoCl_2(L^{15}H)](ClO_4)Cl.0.5H_2O$.- Synthesis and characterisation discussed in Chapter 5.

Table A.9. Atomic coordinates (x 10^4) and equivalent isotropic displacement parameters ($Å^2$ x 10^3) for $[CoCl_2(L^{15}H)](ClO_4)Cl.0.5H_2O$.. U(eq) is defined as one third of the trace of the orthogonalized Uij tensor.

	x	y	z	U(eq)
Co(1)	834.9(14)	1491.0(12)	3514.2(6)	24(1)
Cl(1)	3298(3)	1884(2)	2869.0(11)	34(1)
Cl(2)	-1462(3)	990(2)	4271.7(11)	33(1)
Cl(3)	4426(3)	3672(3)	6748.4(13)	44(1)
O(1)	3199(8)	3827(8)	7280(4)	52(2)
O(2)	4382(11)	4672(9)	6208(4)	72(3)
O(3)	3875(11)	2284(8)	6439(4)	73(2)
O(4)	6246(9)	4000(10)	7069(4)	76(3)
N(1)	-694(8)	2279(7)	2785(3)	29(2)
C(2)	-2117(12)	995(10)	2499(5)	41(2)
C(3)	-1228(13)	-174(11)	2379(5)	43(2)
N(4)	-287(9)	-355(7)	3051(4)	33(2)
C(5)	853(13)	-1360(10)	2966(5)	45(2)
C(6)	1650(14)	-1651(11)	3675(6)	59(3)
C(7)	3060(13)	-418(10)	4013(5)	45(2)
N(8)	2262(9)	739(7)	4223(3)	32(2)
C(9)	3648(12)	1934(10)	4585(5)	39(2)
C(10)	2781(12)	3079(10)	4688(4)	39(2)
N(11)	1858(9)	3331(7)	4013(4)	31(2)
C(12)	664(12)	4253(9)	4126(4)	36(2)
C(13)	-332(12)	4581(9)	3474(5)	38(2)
C(14)	-1610(11)	3301(9)	3105(4)	32(2)
C(15)	410(11)	2934(10)	2176(4)	37(2)
C(16)	-527(11)	3589(11)	1615(4)	37(2)
C(17)	-1352(14)	2799(13)	1015(5)	53(3)
N(18)	-2034(12)	3401(14)	462(4)	69(3)
C(19)	-1894(15)	4780(15)	492(6)	57(3)
C(20)	-1076(14)	5597(13)	1059(5)	53(3)
C(21)	-404(13)	5018(12)	1605(5)	49(3)
C(22)	-2668(14)	5323(17)	-130(6)	66(4)
N(23)	-3452(14)	4376(17)	-668(5)	101(5)
C(24)	-4219(18)	4770(28)	-1238(7)	129(9)
C(25)	-4311(21)	5964(25)	-1343(10)	112(9)
C(26)	-3509(20)	6991(22)	-849(10)	109(7)
C(27)	-2715(18)	6589(19)	-220(8)	90(5)
Cl(01)+	5712(19)	935(10)	9003(6)	148(5)

Cl(02)+	282(16)	-601(10)	710(4)	126(4)
O(003)++	7043(72)	1678(58)	8944(26)	117(16)
O(004)++	5642(63)	-110(53)	8681(25)	112(14)

+ Occupancy 0.5 ++ Occupancy 0.25

Table A.10. Bond lengths [Å] and angles [deg] for $[CoCl_2(L^{15}H)](ClO_4)Cl.0.5H_2O$..

Co(1)-N(4)	1.961(7)
Co(1)-N(11)	1.973(7)
Co(1)-N(8)	1.975(7)
Co(1)-N(1)	2.068(7)
Co(1)-Cl(1)	2.244(3)
Co(1)-Cl(2)	2.279(3)
Cl(3)-O(3)	1.424(8)
Cl(3)-O(1)	1.438(7)
Cl(3)-O(4)	1.442(7)
Cl(3)-O(2)	1.450(8)
N(1)-C(14)	1.499(11)
N(1)-C(2)	1.505(10)
N(1)-C(15)	1.519(10)
C(2)-C(3)	1.502(14)
C(3)-N(4)	1.473(11)
N(4)-C(5)	1.491(11)
C(5)-C(6)	1.517(14)
C(6)-C(7)	1.502(14)
C(7)-N(8)	1.482(12)
N(8)-C(9)	1.487(11)
C(9)-C(10)	1.466(13)
C(10)-N(11)	1.493(10)
N(11)-C(12)	1.465(11)
C(12)-C(13)	1.510(11)
C(13)-C(14)	1.509(12)
C(15)-C(16)	1.509(12)
C(16)-C(17)	1.387(13)
C(16)-C(21)	1.391(14)
C(17)-N(18)	1.369(13)
N(18)-C(19)	1.34(2)
C(19)-C(20)	1.35(2)
C(19)-C(22)	1.47(2)
C(20)-C(21)	1.343(13)
C(22)-C(27)	1.28(2)
C(22)-N(23)	1.37(2)
N(23)-C(24)	1.32(2)
C(24)-C(25)	1.22(3)
C(25)-C(26)	1.36(3)
C(26)-C(27)	1.43(2)

N(4)-Co(1)-N(11)	177.0(3)
N(4)-Co(1)-N(8)	93.8(3)
N(11)-Co(1)-N(8)	86.2(3)
N(4)-Co(1)-N(1)	86.4(3)
N(11)-Co(1)-N(1)	93.5(3)
N(8)-Co(1)-N(1)	179.0(3)
N(4)-Co(1)-Cl(1)	93.8(2)
N(11)-Co(1)-Cl(1)	89.2(2)
N(8)-Co(1)-Cl(1)	86.4(2)
N(1)-Co(1)-Cl(1)	94.6(2)
N(4)-Co(1)-Cl(2)	86.8(2)
N(11)-Co(1)-Cl(2)	90.2(2)
N(8)-Co(1)-Cl(2)	86.5(2)
N(1)-Co(1)-Cl(2)	92.5(2)
Cl(1)-Co(1)-Cl(2)	172.93(9)
O(3)-Cl(3)-O(1)	109.7(4)
O(3)-Cl(3)-O(4)	112.0(5)
O(1)-Cl(3)-O(4)	108.8(4)
O(3)-Cl(3)-O(2)	109.4(5)
O(1)-Cl(3)-O(2)	108.8(5)
O(4)-Cl(3)-O(2)	108.1(5)
C(14)-N(1)-C(2)	109.2(6)
C(14)-N(1)-C(15)	109.9(7)
C(2)-N(1)-C(15)	108.3(6)
C(14)-N(1)-Co(1)	113.4(5)
C(2)-N(1)-Co(1)	103.5(5)
C(15)-N(1)-Co(1)	112.2(5)
C(3)-C(2)-N(1)	108.7(7)
C(3)-N(4)-C(5)	111.8(7)
C(3)-N(4)-Co(1)	109.4(6)
C(5)-N(4)-Co(1)	118.5(5)
N(4)-C(5)-C(6)	111.0(8)
C(7)-C(6)-C(5)	114.0(9)
N(8)-C(7)-C(6)	111.7(8)
C(7)-N(8)-C(9)	111.6(7)
C(7)-N(8)-Co(1)	119.5(6)
C(9)-N(8)-Co(1)	108.6(5)
C(10)-C(9)-N(8)	107.1(7)
C(9)-C(10)-N(11)	110.3(7)
C(12)-N(11)-C(10)	111.7(7)
C(12)-N(11)-Co(1)	118.7(5)
C(10)-N(11)-Co(1)	107.5(5)
N(11)-C(12)-C(13)	116.0(7)
C(14)-C(13)-C(12)	113.5(7)
N(1)-C(14)-C(13)	114.6(7)
C(16)-C(15)-N(1)	117.8(7)
C(17)-C(16)-C(21)	115.6(9)
C(17)-C(16)-C(15)	120.0(10)
C(21)-C(16)-C(15)	123.8(8)
N(18)-C(17)-C(16)	121.4(11)
C(19)-N(18)-C(17)	119.9(10)

N(18)-C(19)-C(20)	121.0(10)
N(18)-C(19)-C(22)	115.6(13)
C(20)-C(19)-C(22)	123.4(13)
C(21)-C(20)-C(19)	119.6(12)
C(20)-C(21)-C(16)	122.5(11)
C(27)-C(22)-N(23)	115.7(13)
C(27)-C(22)-C(19)	127(2)
N(23)-C(22)-C(19)	117.2(14)
C(24)-N(23)-C(22)	121(2)
C(25)-C(24)-N(23)	126(2)
C(24)-C(25)-C(26)	118(2)
C(25)-C(26)-C(27)	118(2)
C(22)-C(27)-C(26)	122(2)

Table A.11. Anisotropic displacement parameters ($A^2 \times 10^3$) for $[CoCl_2(L^{15}H)](ClO_4)Cl.0.5H_2O$.. The anisotropic displacement factor exponent takes the form: $-2\,pi^2\,[\,h^2\,a^{*2}\,U11 + ... + 2\,h\,k\,a^*\,b^*\,U12\,]$

	U11	U22	U33	U23	U13	U12
Co(1)	19(1)	30(1)	22(1)	2(1)	2(1)	3(1)
Cl(1)	25(1)	45(1)	32(1)	5(1)	6(1)	7(1)
Cl(2)	24(1)	43(1)	29(1)	8(1)	8(1)	5(1)
Cl(3)	32(1)	47(2)	42(1)	-5(1)	1(1)	-6(1)
O(1)	33(4)	69(5)	50(4)	3(4)	6(3)	8(3)
O(2)	80(6)	70(6)	46(4)	8(4)	6(4)	-18(4)
O(3)	61(5)	55(5)	85(6)	-23(4)	9(4)	-13(4)
O(4)	27(4)	114(7)	75(6)	-32(5)	-5(4)	6(4)
N(1)	17(3)	35(4)	31(4)	2(3)	-1(3)	1(3)
C(2)	31(5)	53(6)	27(5)	-2(4)	-3(4)	-7(4)
C(3)	37(5)	54(6)	31(5)	-5(5)	4(4)	-2(5)
N(4)	27(4)	35(4)	31(4)	-12(3)	6(3)	-3(3)
C(5)	39(5)	31(5)	62(7)	-4(5)	12(5)	4(4)
C(6)	51(7)	47(7)	85(9)	13(6)	21(6)	21(5)
C(7)	40(5)	49(6)	52(6)	15(5)	4(5)	21(5)
N(8)	26(4)	41(4)	27(4)	8(3)	0(3)	7(3)
C(9)	29(5)	49(6)	38(5)	13(4)	-10(4)	9(4)
C(10)	35(5)	47(6)	28(5)	1(4)	-13(4)	0(4)
N(11)	26(4)	36(4)	28(4)	2(3)	-4(3)	4(3)
C(12)	39(5)	36(5)	30(5)	-4(4)	-5(4)	7(4)
C(13)	44(5)	33(5)	41(5)	8(4)	5(4)	15(4)
C(14)	22(4)	42(5)	32(5)	11(4)	5(4)	4(4)
C(15)	28(5)	48(6)	32(5)	7(4)	-2(4)	6(4)

C(16)	25(4)	67(7)	20(4)	5(4)	9(4)	13(4)
C(17)	48(6)	84(8)	24(5)	3(5)	-1(4)	13(6)
N(18)	53(6)	135(11)	17(4)	17(5)	0(4)	17(6)
C(19)	40(6)	90(10)	49(7)	38(7)	24(5)	26(6)
C(20)	49(6)	77(8)	38(6)	19(6)	7(5)	25(6)
C(21)	43(6)	64(7)	45(6)	20(5)	5(5)	19(5)
C(22)	36(6)	135(13)	28(6)	27(7)	5(5)	23(7)
N(23)	60(7)	206(15)	45(6)	29(8)	17(5)	43(8)
C(24)	40(8)	310(31)	37(8)	37(13)	5(6)	43(13)
C(25)	49(9)	212(24)	102(14)	114(15)	38(9)	65(12)
C(26)	56(10)	160(19)	123(15)	78(14)	38(10)	39(11)
C(27)	65(9)	130(14)	84(10)	63(10)	35(8)	29(9)
Cl(01)	210(13)	80(6)	130(8)	-35(6)	-73(8)	13(7)
Cl(02)	221(11)	103(7)	64(5)	6(4)	46(6)	53(7)

Table A.12. Hydrogen coordinates (x 10^4) and isotropic displacement parameters (A^2 x 10^3) for $[CoCl_2(L^{15}H)](ClO_4)Cl.0.5H_2O$...

	x	y	z	U(eq)
H(2B)	-2692(12)	1193(10)	2068(5)	80
H(2C)	-3033(12)	709(10)	2835(5)	80
H(3B)	-369(13)	84(11)	2020(5)	80
H(3C)	-2113(13)	-1020(11)	2221(5)	80
H(4A)	-1171(9)	-775(7)	3331(4)	80
H(5A)	1829(13)	-962(10)	2670(5)	80
H(5B)	131(13)	-2210(10)	2734(5)	80
H(6A)	2199(14)	-2407(11)	3608(6)	80
H(6B)	680(14)	-1946(11)	3988(6)	80
H(7A)	3986(13)	-82(10)	3687(5)	80
H(7B)	3626(13)	-702(10)	4425(5)	80
H(8A)	1484(9)	400(7)	4558(3)	80
H(9A)	4658(12)	2224(10)	4290(5)	80
H(9B)	4090(12)	1675(10)	5029(5)	80
H(10A)	3683(12)	3916(10)	4846(4)	80
H(10B)	1908(12)	2845(10)	5044(4)	80
H(11A)	2744(9)	3801(7)	3746(4)	80
H(12A)	1403(12)	5115(9)	4340(4)	80
H(12B)	-211(12)	3837(9)	4458(4)	80
H(13A)	539(12)	5037(9)	3149(5)	80
H(13B)	-1038(12)	5211(9)	3602(5)	80
H(14A)	-2433(11)	2824(9)	3440(4)	80
H(14B)	-2321(11)	3580(9)	2734(4)	80
H(15A)	823(11)	2211(10)	1944(4)	80

H(15B)	1468(11)	3624(10)	2367(4)	80
H(17A)	-1426(14)	1820(13)	988(5)	80
H(20A)	-991(14)	6551(13)	1069(5)	80
H(21A)	178(13)	5597(12)	2008(5)	80
H(23)	-3447(14)	3511(17)	-636(5)	80
H(24A)	-4752(18)	4075(28)	-1603(7)	80
H(25A)	-4913(21)	6166(25)	-1767(10)	80
H(26A)	-3574(20)	7916(22)	-953(10)	80
H(27A)	-2195(18)	7248(19)	125(8)	80

References

1. L. F. Lindoy, "The Chemistry of Macrocyclic Ligand Complexes", Cambridge University Press, Cambridge, U. K., 1989.
2. *"Coordination Chemistry of Macrocyclic Compounds"*, Ed. G. A. Melson, pp 145–217, Plenum Press, New York, 1979.
3. T. A. Kaden, *Top. Curr. Chem.*, 1984, **121**, 154.
4. N. F. Curtis, *Coord. Chem. Rev.*, 1968, **3**, 3.
5. A. Luttringhaus, *Ann. Chem.*, 1937, **528**, 181.
6. C. J. Pedersen, *J. Am. Chem. Soc.*, 1967, **89**, 2495.
7. C. J. Pedersen, *Aldrichim. Acta*, 1971, **4**, 1.
8. J.–M. Lehn, *Struct. Bonding*, 1973, **16**, 1.
9. J.–M. Lehn, *Acc. Chem. Res.*, 1978, **11**, 49.
10. I. I. Creaser, J. MacB. Harrowfield, A. J. Herlt, A. M. Sargeson, J. Springborg, *J. Am. Chem. Soc.*, 1977, **99**, 3181.
11. A. M. Sargeson, J. Springborg, *Pure Appl. Chem.*, 1984, **56**, 1603.
12. C. O. Dietrich–Buchecker, J.–P. Sauvage, *Chem. Rev.*, 1987, **87**, 795 and ref. therein.
13. C. O. Dietrich–Buchecker, J.–P. Sauvage, *Angew. Chem. Int. Ed. Engl.*, 1989, **28**, 189.
14. P. R. Ashton, D. Philp, N. Spencer, J. F. Stoddart, *J. Chem. Soc., Chem. Commun.*, 1992, 1124.
15. P. R. Ashton, D. Philp, N. Spencer, J. F. Stoddart, D. J. Williams, *J. Chem. Soc., Chem. Commun.*, 1994, 181.
16. P. R. Ashton, M. R. Johnston, J. F. Stoddart, M. S. Tolley, J. W. Wheeler, *J. Chem. Soc., Chem. Commun.*, 1992, 1128.
17. J.–C. Chambron, V. Heitz, J.–P. Sauvage, *J. Chem. Soc., Chem. Commun.*, 1992, 1131.
18. M. R. Wasielewski, *Chem. Rev.*, 1992, **92**, 435.

19. E. Kimura, *Prog. Inorg. Chem.*, 1994, **41**, 443.

20. M. Murru, D. Parker, G. Williams, A. Beeby, *J. Chem. Soc., Chem. Commun.*, 1993, 1116. K. D. Pulukkody, T. J. Norman, D. Parker, L. Royle, C. J. Broan, *J. Chem. Soc., Perkin Trans 2.*, 1993, 605.

21. D. Parker, *Chem. Soc. Rev.*, 1990, **19**, 271

22. P. D. Beer, O. Kocian, R. J. Mortimer, C. Ridgway, *J. Chem. Soc., Dalton Trans.*, 1993, 2629.

23. E. Kimura, S. Wada, M. Shionoya, Y. Okazaki, *Inorg. Chem.*, 1994, **33**, 770.

24. F. Abba, G. De Santis, L. Fabbrizzi, M. Licchelli, A. M. M. Lanfredi, P. Pallavicini, A. Poggi, F. Ugozzoli, *Inorg. Chem.*, 1994, **33**, 1366.

25. E. Fujita, B. S. Brunschwig, T. Ogata, S. Yanagida, *Coord. Chem. Rev.*, 1994, **132**, 195.

26. D. F. Cabbiness, D. W. Margerum, *J. Am. Chem. Soc.*, 1969, **91**, 6540.

27. R. D. Hancock, A. E. Martell, *Comments Inorg. Chem.*, 1988, **6**, nos. 5 & 6, 237.

28. L. F. Lindoy, "*The Chemistry of Macrocyclic Ligand Complexes*", Chapter 6 & 7, Cambridge University Press, Cambridge, U. K., 1989.

29. A. E. Martell, R. D. Hancock, R. J. Motekaitis, *Coord. Chem. Rev.*, 1994, **133**, 39.

30. B. Dietrich, J.–M. Lehn, J.–P. Sauvage, *Tet. Lett.*, 1969, **34**, 2885.

31. D. J. Cram, T. Kaneda, R. C. Helgeson, S. B. Brown, C. B. Knobler, E. Haverick, K. N. Trueblood, *J. Am. Chem. Soc.*, 1985, **107**, 3645.

32. E. J. Billo, *Inorg. Chem.*, 1984, **23**, 236.

33. D. K. Cabbiness, D. W. Margerum, *J. Am. Chem. Soc.*, year, **92**, 2151.

34. J. D. Lamb, R. M. Izatt, J. J. Christensen. D. J. Eatough, in "*Coordination Chemistry of Macrocyclic Compounds*", Ed. G. A. Melson, pp 145–217, Plenum Press, New York, 1979.

35. R. D. Hancock, *Prog. Inorg. Chem.*, 1989, **37**, 187.

36. V. J. Thöm, C. C. Fox, J. C. A. Boeyens, R. D. Hancock, *J. Am. Chem. Soc.*, 1984, **106**, 5947.

37. D. K. Lavallee, *Coord. Chem. Rev.*, 1985, **61**, 55.

38. P. D. Beer, *Chem. Soc. Rev.*, 1989, **18**, 409.

39. L. F. Lindoy, B. W. Skelton, S. V. Smith, A. H. White, *Aust. J. Chem.*, 1993, **46**, 363.

40. P. V. Bernhardt, G. A. Lawrance, *Coord. Chem. Rev.*, 1990, **104**, 297.

41. P. V. Bernhardt, P. Comba, *J. Chem. Soc., Chem. Commun.*, 1993, 113.

42. R. Ziessel, M. Maestri, L. Prodi, V. Balzani, A. van Dorsselaer, *Inorg. Chem.* 1993, **32**, 1237.

43. G. W. Gokel, *Chem. Soc. Revs.*, 1992, **21**, 39.

44. D. Funkemeier, R. Mattes, *J. Chem. Soc., Dalton Trans.*, 1993, 1313.

45. N. W. Alcock, F. McLaren, P. Moore, G. A. Pike, S. M. Roe, *J. Chem. Soc., Chem. Commun.*, 1989, 629.

46. R. Ziessel, J.–M. Lehn, *Helv. Chim. Acta.*, 1990, **73**, 1149.

47. R. Ziessel, M.–T. Youinou, *Angew. Chem. Int. Ed. Engl.* 1993, **32**, 877.

48. E. Kimura, M. Haruta, T. Koike, M. Shionoya, K. Takenouchi, Y. Iitaka, *Inorg. Chem.*, 1993, **32**, 2779.

49. A. Bencini, A. Bianchi, P. Paoletti, P. Paoli, *Coord. Chem. Revs.*, 1992, **120**, 51.

50. L. R. Gahan, G. A. Lawrance, A. M. Sargeson, *Aust. J. Chem.*, 1982, **35**, 1119.

51. C. M. Madeyski, J. P. Michael, R. D. Hancock, *Inorg. Chem.*, 1984, **23**, 1487.

52. S. C. Rawle, A. J. Clarke, P. Moore, N. W. Alcock, *J. Chem. Soc., Dalton Trans.* 1992, 2755.

53. N. W. Alcock, A. C. Benniston, S. J. Grant, H. A. A. Omar, P. Moore, *J. Chem. Soc., Chem. Commun.*, 1991, 1573.

54. R. M. Izatt, X. Zhang, H. An, C. Y. Zhu, J. S. Bradshaw, *Inorg. Chem.*, 1994, **33**, 1007.

55. S. C. Rawle, P. Moore, N. W. Alcock, *J. Chem. Soc., Chem. Commun.*, 1992, 684.

56. E. C. Constable, *Advances in Inorg. Chem.*, 1989, **34**, 1.

57. E. C. Constable, *Advances in Inorg. Chem.*, 1986, **30**, 69.

58. K. Kalyanasundaram, *Coord. Chem. Rev.* 1982, **46**, 159.

59. R. A. Krause, *Struct. Bonding*, 1987, **67**, 1.

60. A. Juris, V. Balzani, F. Barigelletti, S. Campagna, P. Belser, A. von Zelewsky, *Coord. Chem. Rev.* 1988, **84**, 85.

61. E. W. Abel, K. G. Orrel, A. G. Osborne, H. U. Pain, V. Sik, *J. Chem. Soc., Dalton Trans.*, 1994, 111 and refs. therein.

62. G. R. Newkome, S. Pappalardo, V. K. Gupta, F. R. Fronczek, *J. Org. Chem.*, 1983, **48**, 4848.

63. G. R. Newcome, D. C. Hager, G. E. Kiefer, *J. Org. Chem.*, 1986, **51**, 850.

64. E. C. Constable, J. M. Holmes, *Polyhedron*, 1988, **7**, 2531.

65. X. H. Bu, Y. T. Chen, M. Shionoya, E. Kimura, *Polyhedron*, 1994, **13**, 325.

66. N. Sabbitini, M. Guardigli, I. Manet, F. Bolletta, R. Ziessel, *Inorg. Chem.*, 1994, **33**, 955.

67. R. A. Bissell, A. P. de Silva, H. Q. N. Gunaratne, P. L. M. Lynch, G. E. M. Maguire, K. R. A. S. Sandanayake, *Chem. Soc. Revs.*, 1992, **21**, 187.

68. C. Lin, D. B. Rorabacher, G. A. Cayley, D. W. Margerum, *Inorg, Chem.*, 1975, **14**, 919.

69. P. D. Beer, O. Kocian, R. Mortimer, C. Ridgeway, *J Chem. Soc., Faraday Trans.*, 1993, 333.

70. G. L. Closs, L. T. Calcaterra, N. J. Green, K. W. Penfield, J. R. Muller, *J. Phys. Chem.*, 1986, **90**, 3673.

71. E. Kimura, S. Wada, M. Shionoya, T. Takahashi, Y. Iitaka, *J Chem. Soc., Chem. Commun.*, 1990, 397; E. Fujita, S. J. Milder, B. S. Brunschwig, *Inorg. Chem.*, 1992, **31**, 2079.

72. R. H. Fabian, D. M. Klassen, R. W. Soutag, *Inorg. Chem.*, 1980, **19**, 1977.

73. E. Krausz, J. Ferguson, *Prog. Inorg. Chem.*, 1989, **37**, 293.

74. A. von Zelewsky, P. Belser, P. Hayoz, R. Dux, X. Hua, A. Suckling, H. Stoeckli–Evans, *Coord. Chem. Rev.*, 1994, **132**, 75.

75. J. N. Demas, G. A. Crosby, *J. Mol. Spectrosc.*, 1968, **26**, 72.

76. C. M. Elliot, R. A. Freitag, D. D. Blaney, *J. Am. Chem. Soc.*, 1985, **107**, 4647.

77. L. F. Cooley, C. E. L. Headford, C. M. Elliot, D. F. Kelly, *J. Am. Chem. Soc.*, 1988, **110**, 6673.

78. P. D. Beer, O. Kocian, R. J. Mortimer, C. Ridgway, *J. Chem. Soc., Chem. Commun.*, 1991, 1460.

79. P. D. Beer, C. A. P. Dickson, N. Fletcher, A. J. Goulde, A. Grieve, J. Hodacova, T. Wear, *J. Chem. Soc., Chem. Commun.*, 1993, 828.

80. A. P. de Silva, R. A. D. D. Rupasinghe, *J. Chem. Soc., Chem. Commun.*, 1985, 1669.

81. A. P. de Silva, S. A. de Silva, A. S. Dissanayake, K. R. A. S. Sandanayake, *J. Chem. Soc., Chem. Commun.*, 1989, 1054.

82. R. Grigg, W. D. J. A. Norbert, *J. Chem. Soc., Chem. Commun.*, 1992, 1298.

83. R. Grigg, W. D. J. A. Norbert, *J. Chem. Soc., Chem. Commun.*, 1992, 1300.

84. R. Grigg, J. M. Holmes, S. K. Jones, W. D. J. A Norbert, *J. Chem. Soc., Chem. Commun.*, 1994, 185.

85. M. Beley, J.–P. Collin, R. Ruppert, J.–P. Sauvage, *J. Chem. Soc., Chem. Commun.*, 1984, 1315.

86. M. Beley, J.–P. Collin, R. Ruppert, J.–P. Sauvage, *J. Am. Chem. Soc.*, 1986, **108**, 7461.

87. J. L. Grant, K. Goswanu, L. O. Spreer, J. W. Otvos, M. Calvin, *J. Chem. Soc., Dalton Trans.*, 1987, 2105.

88. E. Kimura, X. Bu, M. Shionoya, T. Takahashi, Y. Iitata, *Inorg. Chem.*, 1992, **31**, 4542.

89. B. Durham, J. V. Caspar, J. K. Nagle, T. J. Meyer, *J. Am Chem. Soc.*, 1982, **104**, 4803.

90. S. Tachiyashiki, H. Ikezawa, K. Mizumachi, *Inorg. Chem.*, 1994, **33**, 623.

91. S. Tachiyashiki, K. Mizumachi, *Coord. Chem. Rev.*, 1994, **132**, 113.

92. F. Barigelletti, L. de Cola, V. Balzani, P. Belser, A. von Zelewsky, F. Vogtle, F. Ebmeyer, S. Grammenudi, *J. Am. Chem. Soc.*, 1988, **110**, 7210.

93. F. Barigelletti, L. de Cola, V. Balzani, P. Belser, A. von Zelewsky, F. Vogtle, F. Ebmeyer, S. Grammenudi, *J. Am. Chem. Soc.*, 1989, **111**, 4662.

94. J. C. Rodriguez–Ubis, B. Alpha, D. Plancherel, J.–M. Lehn, *Helv. Chim. Acta.*, 1984, **67**, 2264.

95. J.–M. Lehn, R, Ziessel, *J. Chem. Soc., Chem. Commun.*, 1987, 1292

96. V. Balzani, E. Berghmans, J. –M. Lehn, N. Sabbatini, R. Terörde, R. Ziessel, *Helv. Chim. Acta.*, 1990, **73**, 2083.

97. R. K. Beeston, S. L. Larson, M. C. Fitzgerald, *Inorg. Chem.*, 1989, **28**, 4187.

98. L. Prodi, M. Maestri, R. Ziessel, V. Balzani, *Inorg. Chem.*, 1991, **30**, 3798.

99. J.–P. Sauvage, J.–P. Collin, J.–C. Chambron, S. Guillerez, C. Coudret, V. Balzani, F. Barigelletti, L. de Cola, L. Flamigni, *Chem. Rev.*, 1994, **94**, 993.

100. E. C. Constable, A. J. Edwards, R. Martinez–Máñez, P. R. Raithby, A. M. W. C. Thompson, *J. Chem. Soc., Dalton trans.*, 1994, 645.

101. J.–P. Sauvage, M. Ward, *Inorg. Chem.*, 1991, **30**, 3869.

102. M. Beley, J.–P. Collin, J.–P. Sauvage, H. Surihara, F. Heisel, A. Miehé, *J. Chem. Soc., Dalton Trans.*, 1991, 3157.

103. E. C. Constable, A. M. W. C. Thompson, N. Armaroli, V. Balzani, M. Maestri, *Polyhedron*, 1992, **11**, 2707.

104. L. M. Vogler, C. Franco, W. Jones, K. J. Brewer, *Inorg. Chim. Acta.*, 1994, **221**, 55.

105. J.–P. Collin, S. Guillerez, J.–P. Sauvage, F. Barigelletti, L. de Cola, L. Flamigni, V. Balzani, *Inorg. Chem.*, 1991, **30**, 4230.

106. M. Beley, S. Chodorowski, J.–P. Collin, J.–P. Sauvage, L. Flamigni, F. Barigelletti, *Inorg. Chem.*, 1994, **33**, 2543.

107. N. Sabbatini, M. Guardigli, J.–M. Lehn, *Coord. Chem. Rev.*, 1993, **123**, 201.

108. B. Alpha, J.–M. Lehn, G. Mathis, *Angew. Chem. Int. Ed. Engl.* 1987, **26**, 266.

109. B. Alpha, V. Balzani, J.–M. Lehn, S. Perathoner, N. Sabbatini, *Angew. Chem. Int. Ed. Engl.* 1987, **26**, 1266.

110. V. Balzani, J.–M. Lehn, J. Van Loosdrecht, A. Mecati, N. Sabbatini, R. Ziessel, *Angew. Chem. Int. Ed. Engl.* 1991, **30**, 190.

111. J.–M. Jehn, M. Pietraszkiewicz, J. Karpiuk, *Helv. Chim. Acta.*, 1990, **73**, 107.

112. R. Ziessel, M. Maestri, L. Prodi, V. Balzani, A. van Dorsselaer, *Inorg. Chem.*, 1993, **32**, 1237.

113. C. Piguet, B. Bocquet, E. Müller, A. F. Williams, *Helv. Chim. Acta.*, 1989, **72**, 323.

114. C. A. Bessel, R. F. See, D. L. Jameson, M. R. Churchill, K. J. Takeuchi, *J. Chem. Soc., Dalton Trans.*, 1993, 1563.

115. C. G. Bochet, C. Piguet, A. F. Williams, *Helv. Chim. Acta.*, 1993, **76**, 372.

116. C. Piguet, A. F. Williams, G. Bernardinelli, E. Moret, J.–C. G, Bünzli, *Helv. Chim. Acta.*, 1992, **75**, 1697.

117. G. Bernardelli, C. Piguet, A. F. Williams, *Angew. Chem. Int. Ed. Engl.*, 1992, **31**, 1622.

118. C. Piguet, A. F. Williams, G. Bernardelli, J.–C. G. Bünzli, *Inorg. Chem.*, 1993, **32**, 4139.

119. C. Piguet, B. Bocquet, G. Hopfgartner, *Helv. Chim. Acta*, 1994, **77**, 931.

120. W. W. Brandt, F. P. Dwyer, E. C. Gyarfas, *Chem. Rev.*, 1954, **54**, 959.

121. G. Orellana, C. A. Ibara, J. Santoro, *Inorg. Chem.*, 1988, **27**, 1025.

122. C. T. Lin, W. Böettcher, M. Chou, C. Creutz, N. Sutin, *J. Am. Chem. Soc.*, 1976, **98**, 6536.

123. M. Biner, H.–B. Bürghi, A. Ludi, C. Röhr, *J. Am. Chem. Soc.*, 1992, **114**, 5197.

124. D. P. Rillema, D. S. Jones, C. Woods, H. A. Levy, *Inorg. Chem.*, 1992, **31**, 2935.

125. J. Harrowfield, A. N. Soboler, *Aust. J. Chem.*, 1994, **47**, 763.

126. O. P. Anderson, *J. Chem. Soc., Dalton Trans.*, 1972, 2597.

127. R. R. Ruminsky, J. D. Petersen, *Inorg. Chim. Acta.*, 1984, **88**, 63.

128. R. D. Hancock, G. J. McDougall, *J. Chem. Soc., Dalton Trans.*, 1977, 67.

129. R. A. Palmer, T. S. Piper, *Inorg. Chem.*, 1966, **5**, 864.

130. M. Briellmann, S. Kaderli, C. J. Meyer, A. D. Zuberbühler, *Helv. Chim. Acta.*, 1987, **70**, 680.

131. G. M. Sheldrick, 'SHELXL–93. Program for Crystal Structure Refinement,' University of Göttingen, Germany, 1994.

132. I. M. Helps, D. Parker, J. R. Morphy, J. Chapman, *Tetrahedron*, 1989, **45**, No. 1, pp 219.

133. N. F. Curtis, *J. Chem. Soc.*, 1964, 2644.

134. R. W. Hay, G. A. Lawrance, N. F. Curtis, *J. Chem. Soc., Perkin Trans I*, 1975, 591.

135. L. F. Lindoy, D. H. Busch, *Prep. Inorg. Reactions*, 1971, **6**, 1.

136. N. F. Curtis, *Coord. Chem. Rev.*, 1968, **3**, 3. X. Jide, N. Shisheng, L. Yujuan, *Inorg. Chem.*, 1988, **27**, 4651, and ibid, *Inorg. Chim. Acta.*, 1986, 14, 61.

137. Y. Hung, L. Y. Martin, S. C. Jackels, A. M. Tait, D. H. Busch, *J. Am. Chem. Soc.*, 1977, **99**, 4029.

138. D. H. Busch, *Acc. Chem. Res.*, 1978, **11**, 392.

139. A. Bencini, A. Bianchi, P. Paoletti, *Coord. Chem. Rev.*,1992, **120**, 51.

140. P. V. Bernhardt, G. A. Lawrance, *Coord. Chem. Rev.*, 1990, **104**, 297.

141. B. Bosnich, C. K. Poon, M. L. Tobe, *Inorg. Chem.*, 1965, **4**, 1106.

142. B. Boswnich, C. K. Poon, M. L. Tobe, *Inorg. Chem.*, 1965, **4**, 1102.

143. A. Juris, V. Balzani, P. Belser, A. von Zelewsky, *Helv. Chim. Acta.*,1981, **64**, 2175.

144. P. Moore, S. C. Rawle, unpublished results.

145. G. M. Sheldrick, SHELXTL PLUS user's manual, 1986, Nicolet Instr. Co., Madison, Wis. USA, and G. M. Sheldrick, *J. Appl. Cryst.*, 1994, in press.

146. International Tables for X-ray Crystallography (1974), Vol.IV. Birmingham: Kynoch Press. (Present distributor Kluwer Academic Publishers, Dordrecht).

147. G. M. Badger, W. H. F. Sasse, *J. Chem. Soc.* 1956, 617, and W. H. F. Sasse, 1959, 3046.

148. N. W. Alcock, K. P. Balakrishnan, P. Moore, *J. Chem. Soc., Dalton Trans.*, 1986, 1743.

149. L. Christiansen, D. N. Hendrickson, H. Toftland, S. R. Wilson, C.-L. Xie, *Inorg. Chem.*, 1986, **25**, 2813.

150. K. Wieghardt, E. Schöfmann, B. Nuber, *Inorg. Chem.*, 1986, **25**, 4877.

151. K. P. Balakrishnan, H. A. A. Omar, P. Moore, N. W. Alcock, G. A. Pike, *J. Chem. Soc., Dalton Trans.*, 1986, 1743.

152. K. V. Damu, M. S. Shaikjee, J. P. Michael, A. S. Howard, R. D. Hancock, *Inorg. Chem.*, 1986, **25**, 3879.

153. H. Tsukube, K. Yamashita, T. Iwachido, M. Zenki, *Tet. Lett.*, 1988, **29**, 569.

154. H. Tsukube, K. Yamashita, T. Iwachido, M. Zenki, *J. Chem. Soc., Perkin Trans. 1*, 1991, 1661.

155. R. Bhula, P. Osvath, D. C. Weatherburn, *Coord. Chem. Rev.*,1988, **91**, 89.

156. G. Vuckovic, E. Asato, N. Matsumoto, S. Kida, *Inorg. Chim. Acta.*, 1990, **171**, 45.

157. G. H. Frost, F. A. Hart, C. A. Heath, M. B. Hursthouse, *J. Chem. Soc., Chem. Commun.*, 1969, 1421.

158. K. Nakamoto, *J. Phys. Chem.*, 1960, **64**, 1420.

159. R. D. Chapman, R. T. Loda, J. P. Riehl, R. W. Schwartz, *Inorg. Chem.*, 1984, **23**, 1652.

160. E. C. Constable, A. M. W. C. Thompson, *J. Chem. Soc., Dalton Trans.*, 1992, 2947.

161. E. C. Constable, M. D. Ward, *Inorg. Chim. Acta*, 1988, **141**, 201.

162. L. C. Craig, *J. Am. Chem. Soc.*, 1934, **56**, 231.

163. R. W. Hay, I. Fraser, *J. Chem. Soc., Dalton Trans.*, 1989, 2183.

164. R. W. Hay, M. P. Pujari, R. Bembi, B. Jeragh, P. R. Norman. *Transition Met. Chem.*, 1989, **14**, 393.